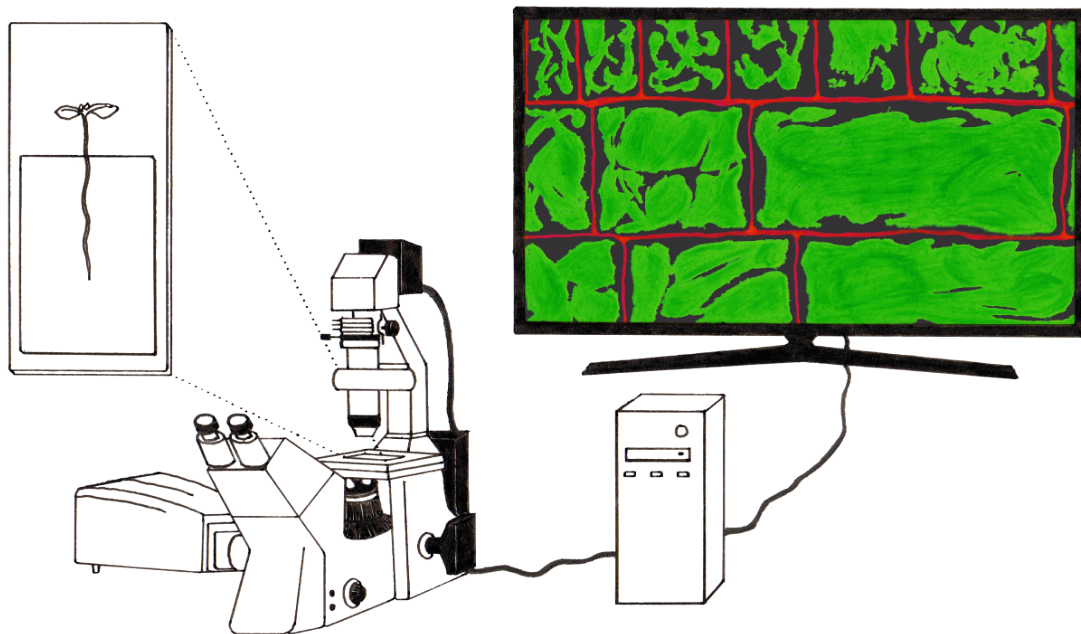

Characterization of the vacuole-cytoskeleton relationship in *Arabidopsis thaliana*

vom Fachbereich Biologie
der Rheinland-Pfälzischen Technischen Universität Kaiserslautern-Landau
zur Verleihung des akademischen Grades „Doktor der Naturwissenschaften“ genehmigte

Dissertation



vorgelegt von
M.Sc. Sabrina Kaiser

Wissenschaftliche Aussprache: 12.12.2024

Berichterstattende:

PD Dr. David Scheuring

Prof. Dr. Stefanie Müller-Schüssele

Kaiserslautern im Jahr 2024

D 386

Table of contents

1	Introduction	4
1.1	The endomembrane system	4
1.2	The plant vacuole	6
1.2.1	Trafficking to the vacuole	8
1.3	Auxin – a growth regulating plant hormone	12
1.4	The actin cytoskeleton	14
1.5	Connecting organelles with the cytoskeleton: Networked proteins.....	16
1.6	Aims and structure of this thesis	18
2	Overview of included articles	19
2.1	Article 1: “NET4 Modulates the Compactness of Vacuoles in <i>Arabidopsis thaliana</i> ”	19
2.2	Article 2: “Vacuolar occupancy is crucial for cell elongation and growth regardless of the underlying mechanism”	22
2.3	Article 3: “Networked proteins redundantly interact with VAP27 and RABG3 to regulate membrane tethering at the vacuole and beyond”	24
2.4	Article 4: “To Lead or to Follow: Contribution of the Plant Vacuole to Cell Growth”	28
3	Closing discussion and future prospects	29
3.1	The different events of cell elongation and the importance of the vacuole.....	29
3.2	Vacuole dynamics: fission and fusion	33
3.3	Membrane contact sites and their potential function	37
3.4	Other putative NET4 and NET3 functions.....	41
3.5	Final remarks.....	43
4	Summary	45
5	Zusammenfassung	46
6	Abbreviations	48
7	References	50
8	Curriculum Vitae	61
9	Acknowledgements	63
10	Declaration of Originality	65
11	Declaration of personal contribution	66
12	Declaration of used tools and assistance	69
13	Full articles for this cumulative thesis	70
13.1	Article 1	70
13.2	Article 2	87
13.3	Article 3	91
13.4	Article 4	141

1 Introduction

Cells are the universal building blocks of life. Their number and size is important for the overall growth of a multicellular organism. Especially in sessile plants, directed growth is a vital skill, allowing them to explore their environment for reaching necessary resources. The more a plant grows and the more matter it produces for its leaves or root network, the better it can generate sugar via photosynthesis or find and take up available nutrients and water from the soil, respectively. Other than animal cells, plant cells can exceed its original size tremendously. Despite being surrounded by rigid cell walls, young root meristem cells increase their volume up to 100-fold during maturation (Veytsman and Cosgrove, 1998). Notably, cell elongation plays a considerable role for rapid tissue increase in plants, being more efficient than producing high amounts of small cells via cell division. Nonetheless, growth always comes with costs, so these processes need to be tightly regulated and adapted to all kind of conditions. Such regulatory mechanisms rely on intracellular events. Therefore, to understand growth regulatory dynamics, it is important to investigate the course of events within a cell on the molecular level.

1.1 The endomembrane system

Like all eukaryotic cells, plant cells consist of several distinct compartments that are surrounded by membranes composed of defined varieties of lipid species and integral or membrane associated proteins. With few exceptions, including plastids and mitochondria, these organelles belong to the so-called “endomembrane system”, which was first described in 1974 (Morré and Mollenhauer, 1974; Fujimoto and Ueda, 2012). Within this system, organelles are linked via membrane trafficking and transport of soluble macromolecules in form of transport vesicles or compartment maturation. In plants, this involves the endoplasmic reticulum (ER) including the nuclear envelope (NE), the Golgi apparatus, the *trans*-Golgi network (TGN)/early endosome (EE), the multivesicular body (MVB)/late endosome (LE), the vacuole as well as the plasma membrane (PM) (Morita and Shimada, 2014; Pizarro and Norambuena, 2014). Among all anterograde and retrograde trafficking between different compartments, there are well-characterized major trafficking pathways that can be grouped into biosynthetic and endocytic routes (Aniento et al., 2022). In *Arabidopsis thaliana* (hereafter referred to as *Arabidopsis*), over 17 % of the products from gene expression show signals for entering the endomembrane system (The Arabidopsis Genome Initiative, 2000). The starting point for the biosynthetic routes is the ER. Here, newly synthesized proteins are recognized as transport cargo before passing Golgi and being sorted for delivery to the TGN. This organelle then represents the intersection dividing cargo for either secretory transport to the PM or vacuolar transport. Endocytic trafficking, on the other hand, starts at the PM. From here, cargo is transported to the TGN, connecting the routes for outward and inward trafficking at this

compartment. Incoming cargo is then also sorted for further transport to the vacuole or recycling to the PM (Aniento et al., 2022) (Fig. 1).

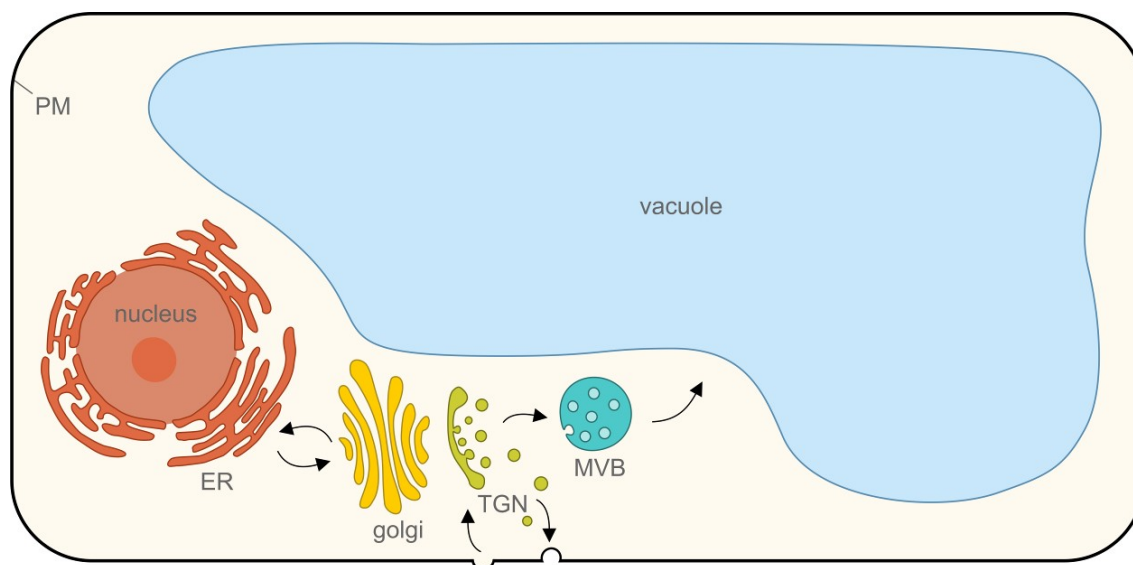


Figure 1: The plant endomembrane trafficking pathways. Trafficking within the biosynthetic pathway starts at the endoplasmic reticulum (ER) and passes the Golgi apparatus before entering the *trans*-Golgi network (TGN). From there, cargo is divided for either further transport to the multivesicular body (MVB) destined for the vacuole or secretion at the plasma membrane (PM). Cargo uptake for the endocytic pathway starts at the PM and bypasses the TGN to either be recycled or transported to the final destination, the vacuole.

In general, vesicle transport between two membranes involves several steps to happen subsequently. At first, soluble cargo and membrane regions for formation and shedding of transport vesicles from the donor membrane need to be selected. Detached vesicles are then transferred to the target membrane until tethering followed by fusion of vesicle membrane with the target membrane occurs and soluble cargo is released into the destined compartment (Fujimoto and Ueda, 2012). To ensure specificity during transport and to maintain the individual identity of each organelle, these steps are governed by a number of regulatory and interacting proteins. Among them are different coat proteins and adaptors, GTP-binding proteins, tethering factors, receptors and more (Rothman, 2002; Aniento et al., 2022).

Apart from these proteins, different lipid species also play a regulatory role during trafficking. This includes phosphoinositides (phosphatidylinositol phosphates/PIPs), a group of low abundant anionic phospholipids, generated via phosphorylation of phosphatidylinositol (PI). In plants, five different phosphoinositides have been found: the monophosphate phosphoinositides PI(3)P, PI(4)P, and PI(5)P as well as the biphosphate phosphoinositides PI(3,5)P₂ and PI(4,5)P₂. These are incorporated in different amounts to the compartments of the endomembrane system and can be modified at certain compartments via enzyme-mediated phosphorylation or dephosphorylation, thereby contributing to membrane identity throughout trafficking. For instance, membranes of MVBs in *Arabidopsis* root epidermal cells

can be enriched in PI(3)P or PI(3,5)P₂, while the tonoplast seems to harbor PI(3)P at a lower extent. On the other hand, PI(4,5)P₂ and PI(4)P can be found at the PM, and the latter in lower concentrations at the TGN (Simon et al., 2014; Hirano et al., 2017; Noack and Jaillais, 2017). These PIP level dynamics as well as the proper action of trafficking relevant proteins are of great importance, since correct movement of molecules along the endomembrane system as well as structurally and functionally intact organelles are crucial for plant viability, growth and development. For example, mutants lacking the TGN-localized protein KEEP ON GOING (KEG), which is necessary for the regulation of various post-Golgi trafficking events, exhibit severe growth defects and are lethal at seedling state. Notably, these defects seem to be mainly based on defective cell expansion and are accompanied with disrupted vacuole structures (Gu and Innes, 2012). As another example, it has been shown that PI(3,5)P₂ to PI3P hydrolyzing phosphatases (SAC2-5), which are localized at the tonoplast, are relevant for vacuole morphology. While higher order mutants exhibited several small vacuolar compartments, overexpression of SAC resulted in untypically large vacuoles, and these changes were also accompanied by growth and developmental defects (Nováková et al., 2014). Based on observations like these, the question arises, which specific roles the vacuole can take on and how its action contributes to the plant.

1.2 The plant vacuole

The term vacuole was originally used in 1841 to describe areas of protozoan cells that were believed to be empty (Dujardin, 1841), before it was also adopted to plant cells (Schleiden, 1842). By now, it is clear that vacuoles are by no means empty spaces. Instead, they can be seen as multi-tools with a variety of different functions. This includes storage of proteins, ions and many secondary metabolites like anthocyanin, alkaloids, glycosides or organic acids, as well as the degradation of various compounds, homeostasis of pH, and maintenance of turgor pressure (Wink, 1993; Marty, 1999). Certain functions can be fulfilled only at specific tissues or specialized cells. In guard cells, for example, drastic changes of vacuolar morphology facilitate the mechanic opening or closing of stomata in order to regulate the plant's water household and gas exchange in response to environmental conditions. Interestingly, it has been shown that perception of certain pathogens can trigger stomatal closure and hinder pathogen entry (Melotto et al., 2006; Andrés et al., 2014; Hawkins et al., 2023), demonstrating one of many examples how vacuoles can also take part in plant defense.

Dependent on their major functions, plant vacuoles can be grouped into two commonly accepted main classes: protein storage vacuoles (PSV) and lytic vacuoles (LV). PSVs are present during germination and store important minerals and proteins to serve as energy supply for the seedling. In Arabidopsis, they are formed from existing embryonic vacuoles

during embryogenesis (Feeney et al., 2018) and it has been shown for root tip cells of *Nicotiana tabacum* that PSVs transit into LVs after all stored compounds have been depleted (Zheng and Staehelin, 2011). In contrast, LVs are common in nearly all vegetative tissues and stages of the life cycle. They resemble mammalian lysosomes by fulfilling lytic or degradative functions (Marty, 1999). Beside other luminal contents, further differences can be found in the composition of the vacuolar membrane (tonoplast). Both vacuole types seem to harbor different isoforms of tonoplast intrinsic proteins (TIPs), which have a general function as water channels. While the two isoforms TIP2;1 or δ -TIP and TIP3;1 or α -TIP are usually localized at the tonoplast of PSV, the membrane of the LV consists of the isoform TIP1;1 or γ -TIP (Jauh et al., 1999; Gattolin et al., 2010). Labeling of TIPs as well as detection of specific luminal proteins or pH helped to show that different vacuole types can exist even within the same cell. However, this seems to be limited to specific plants, tissues and developmental stages or to happen only under exceptional circumstances, while in most cases only one vacuole type is present at a time (Frigerio et al., 2008). In root cells of *Arabidopsis* seedlings, the model cell types for most of the thesis, this is the LV (Fig. 2).

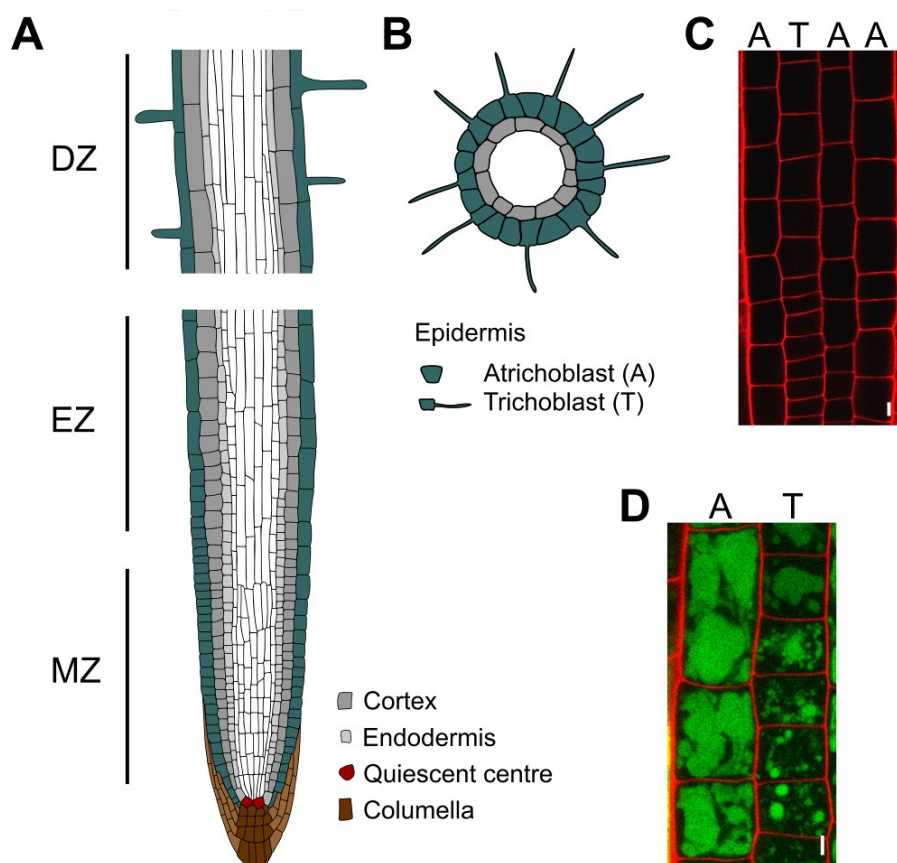


Figure 2: The cellular organization of a root in *Arabidopsis*. Around the central vascular tissue (white), different cell types (depicted in different colors) are arranged in cell files, which build single-celled concentric layers. A, Longitudinal section through the root. Distinct developmental zones can be separated; including the meristematic zone (MZ), the elongation zone (EZ) and the differentiation zone (DZ). Most cell division takes place in the apical

or early meristem at the root tip and gets less within the basal or late meristem near the elongation zone. From there, cell elongation begins in the elongation zone. A small area between meristem and elongation zone can also be referred to as "transition zone". Cell differentiation starts in the differentiation zone. B, Cross section of the differentiation zone. Epidermis cells can be divided in atrichoblast (A) and root hair developing trichoblast (T) cells. C, Cell wall staining with propidium iodide (red) for epidermis cells of the meristem zone. D, Additional staining of the vacuolar lumen with BCECF-AM (green). Trichoblast cells can be recognized as the smaller cells harboring smaller vacuoles compared to neighboring atrichoblast cells. Trichoblast cell files are always separated by one or more atrichoblast cell file(s). Scale bars: 5 μ m. A, to C, was provided by PD Dr. David Scheuring and modified.

In general, the LV is the biggest organelle of plant cells. However, its size and shape can vary drastically, in particular within developing cells of the root meristem. A vacuole from a young cell of the early meristem zone exhibits a rather tubular network-like form and takes up around 30 % of the cell. A bigger, more mature cell of the late elongation zone, on the other hand, harbors a vacuole that shows a fully inflated balloon-like structure and occupies up to 90 % of the cellular space (Dünser et al., 2019). During vacuolar inflation, a high amount of water influx via TIP1;1 water channels must be accompanied by synthesis and delivery of new membrane material. Until now, there is an ongoing debate about the origin or main membrane source of the LV, which involves two opposing models. One model proposes that post-Golgi trafficking serves as source material for the vacuole and includes homotypic MVB fusion to first form smaller, and then larger vacuoles. This theory is going back to descriptions by Marty for meristematic root cells of *Euphorbia characias* (Marty, 1978) and has been further supported just recently by 3D electron tomography analyses of *Arabidopsis* root as well as stomatal lineage cells (Cui et al., 2019; Cao et al., 2022). The alternative model already came up in 1968. Investigations of vacuoles and ER-derived vesicles from *Zea mays* root tip cells led to the theory that the ER might be the donor compartment for the tonoplast by delivering membrane material via ER-derived vesicles or provacuoles (Matile and Moor, 1968). Analyses for vacuolar trafficking in *Arabidopsis* highly support the theory of ER to vacuole transit without involvement of Golgi and MVBs (Viotti et al., 2013). Furthermore, recent microscopic studies using fluorescent recovery after photobleaching (FRAP) assays demonstrate the vacuole to already be a tubular network even in the earliest developed root cells, thereby reasoning that it cannot solely originate from homotypic fusion of MVBs (Scheuring et al., 2024).

1.2.1 Trafficking to the vacuole

Even if there might be one major membrane donor for the LV, it seems plausible that all existing trafficking routes to the vacuole have at least some contribution to vacuolar enlargement. The different routes described so far are depicted in Fig. 3. Among these, the first route originates at the ER, passes Golgi, TGN as well as MVB, and involves the conversion of MVB-resident RAB5/RABF to RAB7/RABG proteins before reaching the vacuole. Following the same steps through the biosynthetic route of the endomembrane system, the second pathway also requires RAB5/RABF, but is independent of RAB7/RABG. The third pathway requires no

involvement of RAB5/RABF or RAB7/RABG but is dependent on the adaptor protein complex 3 (AP-3). Furthermore, there are two more pathways not passing Golgi or TGN. One direct route from ER to vacuole including the formation of provacuoles, as well as the fusion of *de novo* generated autophagosomes with the vacuole. In addition to these, also homotypic vacuole fusion takes place (Minamino and Ueda, 2019; Cui et al., 2020).

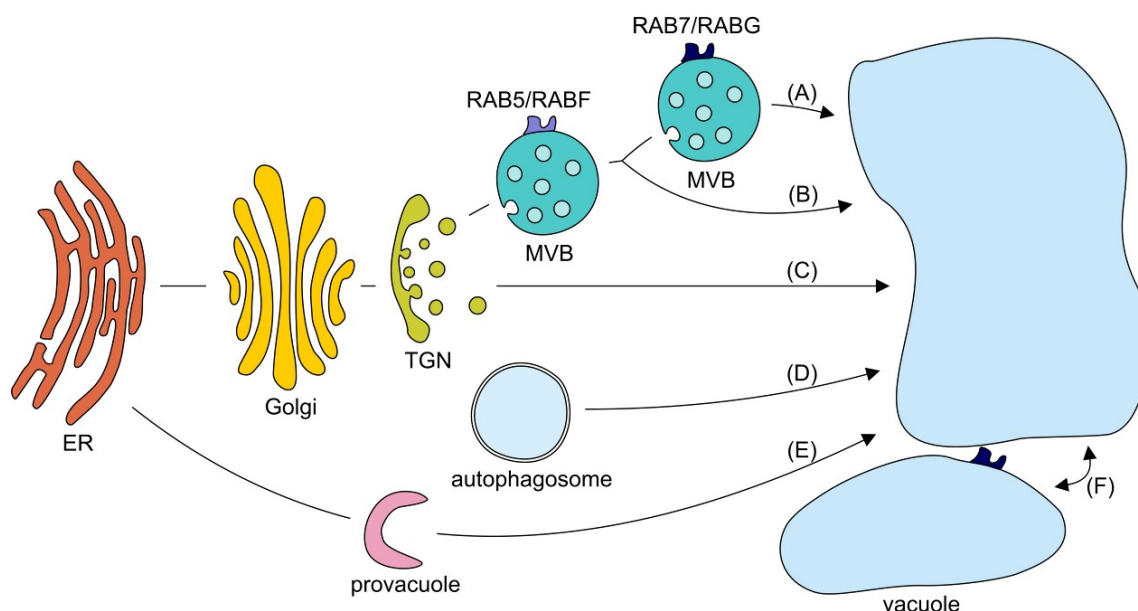


Figure 3: The many ways to the vacuole. (A) The RAB5/RABF- and RAB7/RABG-dependent pathway. This pathway starts at the endoplasmic reticulum (ER) along the biosynthetic transport route of the endomembrane system to the vacuole, passing Golgi, *trans*-Golgi network (TGN) and multivesicular body (MVB). It requires sequential action of RAB5/RABF and RAB7/RABG proteins, involving maturation of MVBs prior to vacuole fusion. (B) The RAB5/RABF-dependent pathway. Cargo within this pathway passes the same compartments as (A), but MVB to vacuole fusion is independent of RAB7/RABG proteins. (C) The AP-3-dependent pathway. This pathway relies on the adaptor protein complex 3 (AP-3). Cargo delivery to the vacuole requires neither RAB5/RABF nor RAB7/RABG. (D) The autophagosomal pathway. Autophagosomes are built *de novo* and fuse with the vacuole. (E) The ER to vacuole pathway. Material comes directly from the ER without passing the Golgi, TGN or MVB. (F) Homotypic fusion of vacuoles. RAB7/RABG proteins are relevant in this process. Based on Minamino and Ueda, 2019 and Cui et al., 2020.

Fusion of each specific donor with the target membrane is coordinated by several interacting proteins that function together as a fusion machinery. Such a machinery usually involves small guanosine triphosphatases (GTPases), tethers and soluble N-ethylmaleimide-sensitive factor attachment protein receptors (SNAREs) (Jurgens, 2004). GTPases are working like molecular switches. They can change between an inactive GDP- and an active GTP-bound form. Activation is facilitated by a cognate guanine exchange factor (GEF) and eventually followed by inactivation via a respective GTPase activating protein (GAP). In active state, they are able to recruit different effectors, like GEFs of other GTPases or specific tethers (Uemura and Ueda, 2014; Nielsen, 2020). The latter initiate the first contact between the two membranes to be fused by interacting with the respective GTPases, thereby bringing the membranes closer together. In this context, tethers often not only function as effectors of already activated

GTPases, but can act as regulators (e.g. GEFs) as well (Vukašinović and Žárský, 2016). Additional interaction of the respective tether with membrane-integral SNAREs on each opposing membrane can then trigger SNARE-mediated membrane fusion. This typically involves a so-called R-SNARE at the donor and a combination of either three or two variants of Q-SNAREs (Qa, Qb, Qc or Qa, Qb/Qc) at the target membrane, which are forming a hetero-tetrameric *trans*-SNARE complex. This process is further promoted by an N-ethylmaleimide-sensitive factor (NSF) and a soluble NSF attachment protein (SNAP) (Jurgens, 2004; Uemura and Ueda, 2014). The identification of all involved proteins and their sequentially interaction to facilitate one specific vacuolar fusion process is a still ongoing topic of plant research.

In case of homotypic vacuole fusion, RAB GTPases belonging to the RAB7/RABG protein subfamily are part of the specific fusion machinery (Minamino and Ueda, 2019). RAB proteins in general are conserved among eukaryotes and have regulatory roles at several fusion events within the endomembrane system. In *Arabidopsis*, there are 57 RAB proteins in total, categorized into eight subfamilies (RABA to RABG). The RABG subfamily includes the eight GTPases RABG1, RABG2 and RABG3a-f, which are related to the RAB7 subclass in mammals and therefore sometimes also referred to as RAB7 proteins (Rutherford and Moore, 2002). An important effector of RABG is the homotypic fusion and protein sorting (HOPS) complex (Fig. 4).

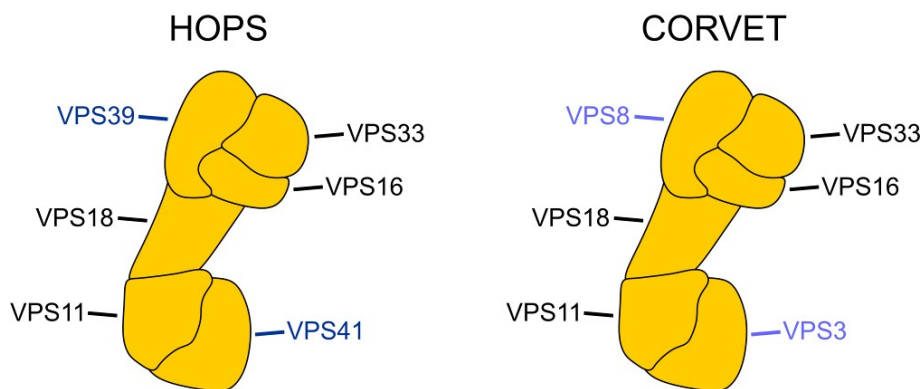


Figure 4: The HOPS and CORVET tethering complexes. Shown are the four core subunits (VPS11, VPS16, VPS18, VPS33) and the specific subunits VPS39 and VPS41 (marine blue) as well as VPS8 and VPS3 (steel blue) of HOPS (left) and CORVET (right), respectively. Based on Rodríguez-Furlan et al., 2019.

This tethering complex consists of six subunits: the four core subunits VPS11, VPS16, VPS18 and VPS33, as well as the specific subunits VPS39 and VPS41. Interaction with RABG proteins is proposed for the two specific ones (Takemoto et al., 2018; Rodríguez-Furlan et al., 2019). Furthermore, a SNARE complex consisting of the R-SNARE VAMP713 and the Q-SNAREs SYP22 (Qa), VTI11 (Qb) and SYP5 (Qc) seems to enable homotypic vacuole fusion eventually (Fig. 5). Here, an interaction of the HOPS core subunit VPS33 with Qa-SNARE SYP22 as well as HOPS interaction with the R-SNARE VAMP713 has been demonstrated

(Brillada et al., 2018; Takemoto et al., 2018). Interestingly, a recently published cryo-electron microscopy based structure of the conserved heterohexameric HOPS complex in yeast sheds new light on HOPS mechanics, pointing to a catalytic function for SNARE-mediated fusion in addition to membrane tethering (Shvarev et al., 2022).

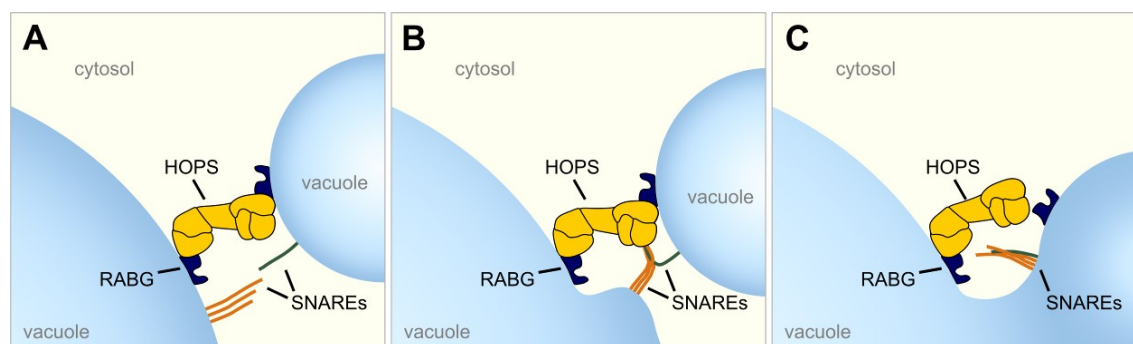


Figure 5: The process of homotypic vacuole fusion. (A) Subunit VPS39 and potentially VPS41 of the HOPS complex bind to RABG proteins localized at opposing vacuole membranes to initiate membrane tethering. (B) Additional interaction of HOPS subunit VPS33 with the R-SNARE VAMP713 (dark green) and one of the three Q-SNAREs (orange), SYP22, brings all SNAREs together, forming a fusion complex. (C) The action of this fusion complex eventually results in membrane fusion.

Fusion of MVBs with the vacuolar compartment, on the other hand, involves action of RABF proteins, homolog to the mammalian RAB5 subclass of GTPases. For the RAB5/RABF- and RAB7/RABG-dependent pathway, MVBs need to run through a maturation process prior to vacuole fusion (Fig. 3). This includes activation of RABF by its GEF VPS9a, followed by recruitment of its effector complex MON1/SAND1-CCZ1, which in turn causes exchange of RABF by RABG. Consecutive RABG activation then again leads to interaction with the HOPS complex and subsequent fusion steps eventually. According to its name, no RABG proteins are active in the RAB5/RABF-dependent and RAB7/RABG-independent pathway. Instead, the class C core vacuole/endosome tethering (CORVET) complex is recruited upon RABF activation. This tethering complex is composed of the same core subunits as HOPS, but two different specific subunits, namely VPS8 and VPS3 (Fig. 4). Furthermore, CORVET interacts with the MVB membrane-anchored R-SNARE VAMP727 before a SNARE complex of VAMP727 and the three vacuolar Q-SNAREs SYP22, VTI11 and SYP5 is formed to facilitate membrane fusion (Minamino and Ueda, 2019).

The absence of one or more vacuole fusion relevant proteins can be fatal. For example, Arabidopsis mutants lacking single subunits of the HOPS or CORVET complex, like VPS16 or VPS11 in *vacuoleless1 (vcl1)/vps16* or *vps11*, respectively, are reported to be defective in vacuole formation and die during embryogenesis (Rojo et al., 2001; Tan et al., 2017). Interestingly, conditional knockdown mutants for HOPS subunits VPS41 and VPS39, but not CORVET subunits VPS3 and VPS8, are described to have severely fragmented vacuoles in epidermal root cells of Arabidopsis seedlings. This indicates a HOPS-specific relevance for

central vacuole biogenesis during seedling development (Brillada et al., 2018; Takemoto et al., 2018). Single mutants for SNARE proteins are usually viable, but can cause several defects. For instance, absence of SYP22 leads to pleiotropic phenotypes including semi-dwarfism. In contrast, no obvious phenotypes have been shown for single mutants deficient of the other Qa SNAREs SYP21 or SYP23. Nonetheless, growth defects of *syp22* have been demonstrated to be gradually enhanced by additional deficiency of SYP23, SYP21 or both, eventually leading to plant death without bolting or flowering in *syp22 syp21* and *syp22 syp23 syp21* (Uemura et al., 2010; Shirakawa et al., 2010). As another example, *zig* mutants, lacking VTI11, have a defective response in shoot gravitropism, accompanied by abnormal vacuole shape of endodermis cells, as well as defective vascular patterning and transport of the plant hormone auxin. Additional absence of a second Qb SNARE (VTI12), which is proposed to act in a separate trafficking route, has been shown to be embryo lethal (Kato et al., 2002; Morita et al., 2002; Surpin et al., 2003; Sanmartín et al., 2007). This underlines their relevance and indicates a partial functional overlap for SNAREs classified into the same group, even though preferentially acting at different fusion sites of the endomembrane system. For *rabg* single mutants, no obvious phenotypes are reported, which can be explained by high functional redundancy within the RABG subfamily. Even higher order mutants are still viable. However, different *rabg3* quintuple and sextuple mutants have been shown to exhibit a changed vacuolar morphology for PSVs of embryos and LVs of epidermal leaf cells, in addition to an inhibited leaf growth (Ebine et al., 2014). Here, it can be speculated that residual amounts of RABG3f within the published sextuple mutant, as well as the presence of the remaining RABG1 and RABG2 proteins might still compensate for the loss of the other RABG proteins to prevent even stronger phenotypes and plant death. Taken together, these examples illustrate the general importance of correct vacuole formation and that the action and functional interplay of fusion relevant proteins is crucial for plant development and growth.

1.3 Auxin – a growth regulating plant hormone

The basic regulation of plant processes needs to be continuously adapted to changing environmental conditions. Such adaptations can be realized by a class of compounds called plant hormones (or phytohormones). Hormones are naturally synthesized by plants and do not have any nutritional value. They function at low concentrations as small moving signaling molecules either directly at the site of their production within a cell or after being transported to other areas in close proximity or far away distances (Leyser, 1998; Zhang et al., 2023). Due to their chemical structure and physiological function, different plant hormones can be distinguished. The major classes are auxins, gibberellins, ethylene, cytokinins and abscisic acid, which were initially identified and considered as “classical” plant hormones, but also

brassinosteroids, jasmonic acid, salicylic acid and strigolactones that were included later (Kende and Zeevaart, 1997; Santner et al., 2009). They control all kind of events, including plant growth, development, reproduction, stress responses and cell death. One hormone can thereby be involved in several different processes. Simultaneously, a single process is often governed by different hormones, which influence each other's impact (Dilworth et al., 2017).

Among all plant hormones discovered so far, auxin is a remarkably versatile one. It is a crucial growth regulator and orchestrates a variety of plant processes, such as phototropic and gravitropic responses, embryogenesis, apical dominance, vascular patterning as well as leaf, flower and root development. The first identified and most abundant naturally occurring auxin is indole-3-acetic-acid (IAA). On cellular level, auxin-mediated processes are basically carried out via correct modulation of cell division, elongation and differentiation and are dependent on local auxin level gradients. The formation of such gradients is conducted by local biosynthesis, intercellular directional transport via different influx and efflux carriers or inactivation of IAA molecules (Casanova-Sáez et al., 2021). Thus, internal or external stimuli, altering these mechanisms, can influence auxin-controlled processes by manipulating auxin distribution.

To facilitate an action in response to certain stimuli, plant hormones commonly bind to specific receptors, hence triggering a cellular signal transduction pathway that often results in big transcriptional changes but might also involve non-genomic responses. In case of auxin, one well-characterized receptor is the TRANSPORT INHIBITOR RESPONSE1 (TIR1) F-box protein (Tan et al., 2007). TIR1 as well as some other members of the F-box protein family, called AUXIN SIGNALING F-BOX (AFB), are collectively involved in most auxin responses (Dharmasiri et al., 2005). Binding of auxin to TIR1/AFB family members promotes interaction with members of the transcriptional repressor family AUXIN/INDOLE ACETIC ACID (Aux/IAA) and results in Aux/IAA protein degradation. Aux/IAA proteins usually interact with members of the transcription factor family AUXIN RESPONSE FACTOR (ARF), which in turn are associated to Auxin Response Elements (AREs) at auxin-inducible gene promoters. Aux/IAA-ARF interaction is stabilized by recruitment of further proteins and prevents expression of auxin-inducible genes under auxin-free conditions. Consequently, auxin-mediated Aux/IAA degradation releases ARFs and induces related gene expression (Quint and Gray, 2006; Leyser, 2018). Since each individual part of this de-repression signaling system can be facilitated by several family-related proteins, leading to differential interaction of possible family members, this system alone can offer various reactions to different stimuli. Nonetheless, some auxin responses cannot be derived to this system, which led to the identification and ongoing research of additional signaling mechanisms (Leyser, 2018).

Interestingly, in addition to varying responses to different concentrations, auxin affects plant cell growth also in a tissue-dependent manner. In roots, physiological auxin concentrations

lead to growth inhibition, while in shoots and leaves, cellular growth is increased (Evans et al.; Sauer et al., 2013; Dünser and Kleine-Vehn, 2015). How auxin mediates these cell-type specific changes on the molecular level appears to be very complex, involving different transcriptional and non-transcriptional signaling pathways, and is still not fully understood (Gallei et al., 2020). However, Löffke et al. demonstrated for *Arabidopsis* epidermal root cells that auxin not only impacts on cellular growth but also on the morphology of the vacuole, while having correlating effects (Löffke et al., 2015). Exogenous treatment with the synthetic auxin 1-naphthaleneacetic acid (NAA) as well as increased endogenous IAA concentrations led to both, a size reduction of vacuoles and cells in the still plastic late meristem zone, while IAA depletion resulted in an increase in size, accordingly (Löffke et al., 2015; Scheuring et al., 2016). The authors further found that NAA positively affects the abundance of vacuolar SNARE proteins in a posttranslational manner. Especially the SNARE VT111 seems to be of great importance, since *vti11* mutants were largely insensitive to auxin effects on vacuole and cell size. Notably, all these effects have been shown to display a dependency on TIR1/AFB auxin receptors as well as the activity of specific PI kinases (Löffke et al., 2015). Moreover, it was demonstrated that auxin directly influences the organization of actin filaments, but not microtubules, as a prerequisite for changing vacuolar morphology (Scheuring et al., 2016). Due to this finding, it is worth asking, how vacuolar morphology and actin cytoskeletal organization can be related.

1.4 The actin cytoskeleton

The cytoskeleton is a fundamental part of cells and can fulfill numerous important functions. In plant cells, it can be mainly divided into two separate networks that consist of either actin filaments or microtubules (Kost and Chua, 2002). While the cytoskeleton of animals is additionally composed of intermediate filaments, the existence of these structures in plants has been under debate for a long time. Only recently, a potential candidate for a plant intermediate filament protein has been reported (Utsunomiya et al., 2020). The structural organization of the cytoskeleton is unique in plants. Since plant cells are surrounded by cell walls and typically contain big vacuoles taking up most cellular space, the localization of the plant cytoskeletal networks is limited to few cytoplasmic regions. These include thin areas around the nucleus and near the PM, which are connected by transvacuolar cytoplasmic strands, reaching through the vacuole. In addition, actin cytoskeletal structures are also positioned near plasmodesmata, which represent specific cell wall channels for contact of neighboring cells (Kost and Chua, 2002). Actin filaments of higher plants play a major role during trafficking and organelle translocation. Here, these filaments constitute the tracks, on which vesicle and organelle transport can be executed. Transport further requires energy-

driven movement of myosins, a specific group of actin binding proteins (ABPs) that function as molecular motors (Mathur et al., 2002; Peremyslov et al., 2008; Ueda et al., 2010; Peremyslov et al., 2012). Interestingly, although actin filaments are conserved components, in animals, cytoplasmic transport is mainly executed by microtubules. Actin filaments, on the other hand, are main actors for cell motility and the control of cellular shape (Kost and Chua, 2002; Pollard and Cooper, 2009). In addition to its intra- or also intercellular transport function, the actin cytoskeleton of plants is also of great importance during several other plant physiological processes including cell division, cell elongation or response to environmental stresses (Volkmann and Baluška, 1999; Baluška et al., 2001; Barrero et al., 2002; Henty-Ridilla et al., 2013). Its highly dynamic formation is thereby of utmost significance. Filamentous actin (F-actin) is generally built by polymerization of monomeric globular actin proteins (G-actin) and arranged to a double-helical polymer. Generated polymers can be constantly modulated via assembly or disassembly of actin subunits and various arrays can be formed by bundling or cross-linking of F-actin. These actin dynamics and the organization to higher order structures are carried out and regulated by numerous ABPs (dos Remedios et al., 2003; Blanchoin et al., 2010; Li et al., 2015). Collectively, all ABPs and their impact on the actin cytoskeleton permit its broad involvement in a high number of various cellular processes (Staiger and Blanchoin, 2006; Thomas et al., 2009). Moreover, most organisms produce not only one, but several actin isoforms with partly distinct or overlapping functions. In *Arabidopsis*, there are eight known actin genes that are expressed in either vegetative (*ACT2*, *ACT7*, *ACT8*) or reproductive tissue (*ACT1*, *ACT3*, *ACT4*, *ACT11*, *ACT12*) and can be grouped accordingly into two main classes (Meagher et al., 1999; Kandasamy et al., 2007). The vegetative actins *ACT2* and *ACT8* are the most closely related isoforms, varying by only one amino acid. They show similar expression patterns in young and old vegetative tissues but differ in expression strength, with strong expression for *ACT2* and lowermost expression for *ACT8*. On the other hand, *ACT7* is predominantly expressed in young, still expanding tissues including the root meristem (McDowell et al., 1996a; McDowell et al., 1996b; Meagher et al., 1999). Analyses of various single and double mutants lacking actins of the vegetative class revealed an involvement in several important vegetative processes. In line with their close homology, *ACT2* and *ACT8* mainly function at the same cellular events. Both have been shown to be major players in root hair tip growth and the selection of bulge sites during root hair initiation (Ringli et al., 2002; Gilliland et al., 2002; Nishimura et al., 2003; Kandasamy et al., 2007). In contrast, *ACT7* has been demonstrated to be of great importance for a plethora of processes, including germination, specification of epidermal cells, cell division, cell elongation, root architecture and overall root organ growth (Gilliland et al., 2003; Kandasamy et al., 2007; Numata et al., 2022). Besides, higher order mutants for certain myosin proteins, more specifically some members of the myosin XI class that consists of 13 isoforms in *Arabidopsis*, have been described to show

pleiotropic defects, including a reduction of root length and root hair length (Prokhnevsky et al., 2008; Peremyslov et al., 2010). These myosins have additionally been shown to not only function as actin-based moving motor proteins for cytoplasmic transport but to actively take part in actin cytoskeletal remodeling (Cai et al., 2014; Duan and Tominaga, 2018). How such remodeling specifically impacts on certain actin-myosin-dependent processes and which other molecular components are involved is still under investigation for many physiological events.

More than 20 years ago, it has already been indicated that actin filaments play a role in mediating structural vacuolar changes (Uemura et al., 2002; Mathur et al., 2003). However, the underlying mechanism has been mainly elusive. Based on co-localization of actin filaments and tubular tonoplast structures during cell division, a direct physical connection has been suggested (Kutsuna et al., 2003). An intact actin cytoskeleton has been further demonstrated to be a requirement for vacuole changes in guard cells. Here, interfering with actin filament dynamics and reorganization resulted in impaired vacuole fusion and retarded stomatal opening (Li et al., 2013; Cao et al., 2022; Hawkins et al., 2023). Besides, as mentioned in the previous section, studies in relation to auxin-controlled root growth and cell expansion were able to link the remodeling of actin filaments with cell size limiting vacuolar constrictions (Scheuring et al., 2016). However, so far, it has not been shown in which way actin filaments are able to interact with the tonoplast to facilitate changes of vacuolar morphology. Either a direct binding of F-actin with specific tonoplast components or an indirect binding via one or more adaptor proteins might be feasible.

1.5 Connecting organelles with the cytoskeleton: Networked proteins

Several years back, a new superfamily of ABPs, termed Networked (NET) proteins, was identified in Arabidopsis (Deeks et al., 2012). All members of this superfamily are cytosolic proteins and share an N-terminal plant-specific NET actin binding (NAB) domain, which enables their interaction with F-actin. The sequence of this domain has no homology to any other identified actin-binding domain so far, and thus has been categorized as a novel actin-binding motif (Deeks et al., 2012). Noteworthy, bioinformatic analyses revealed that NAB containing proteins are only present in tracheophytes (vascular plants) and seem to have evolved in diversity and numbers in correlation to significant land plant developmental events (Hawkins et al., 2014). The NET superfamily of Arabidopsis is composed of 13 members that were originally grouped based on protein length, expression profiles, sequence and structural similarities into four families: NET1, NET2, NET3 and NET4. These phylogenetically distinct families are conserved among Angiosperms, while more simple and extant vascular plants contain only one family with closest homology to NET4 members (Deeks et al., 2012; Hawkins et al., 2014). In addition to their general actin-binding capacity, Arabidopsis NETs can be

recruited to different membranes (Deeks et al., 2012). For both the NET1 and NET2 families, which each consist of four members, tissue-specific recruitment to the PM has been reported. While NET1A has been shown to be enriched at plasmodesmata of root cells, NET2A and NET2B have been found to decorate specific puncta at the PM of growing pollen tubes (Deeks et al., 2012; Duckney et al., 2017). In contrast, the three members of the NET3 family all show localization at the ER. NET3A localizes preferentially to dot-like structures at the nuclear envelope, while NET3B and NET3C can each be found at foci of the ER network. In case of NET3C, these foci have been shown to represent specific ER-PM contact sites (Deeks et al., 2012; Wang et al., 2014; Wang and Hussey, 2017; Zang et al., 2021; Duckney et al., 2022). Lastly, an association with the vacuolar compartment has been reported for the NET4 family, which is comprised of the two members NET4A and NET4B. Here, GFP-labeled NET4A was observed at the tonoplast of epidermal root cells (Deeks et al., 2012).

NET recruitment to the respective membranes seems to be facilitated in different ways. Some NET proteins were shown to achieve membrane connections via binding to membrane integral proteins. For instance, NET2A is able to interact with certain transmembrane pollen receptor-like kinases (PRK4/5), whereas NET3C can interact with ER membrane integral VAMP-associated protein 27 (VAP27) proteins (Wang et al., 2014; Duckney et al., 2017). In addition, NET3C has been indicated to directly bind PM phospholipids via a specific C-terminal part (Wang et al., 2014). How NET4 proteins are recruited to the tonoplast has not been known for a long time, but interaction of NET4 and tonoplast-resident RABG proteins was only reported recently (Hawkins et al., 2023) in overlap with the execution of experiments for article 3 of this cumulative thesis (see section 2.3).

Functional characterization of specific NET members revealed their relevance in actin and organelle dynamics. For instance, enhanced expression of NET3B has been demonstrated to boost F-actin and ER association in a NET3B amount-dependent manner, showing more co-localization sites under increased NET3B expression levels. Moreover, NET3B overexpression also resulted in a morphological change of ER structures, exhibiting less membrane cisternae, as well as a reduced ER membrane diffusion (Wang and Hussey, 2017). These studies suggest that members of the NET superfamily can generally link actin filaments with different membrane systems and affect their morphology. Therefore, the NET4 proteins represent prime candidates for adaptor proteins that potentially connect actin filaments with the tonoplast in order to facilitate actin-dependent drastic changes in vacuole morphology.

1.6 Aims and structure of this thesis

The major goal of this project has been to decipher molecular links between the actin cytoskeleton and the vacuole as well as their impact on plant cell growth and development.

Auxin-induced changes of vacuolar morphology have been shown to rely on the actin cytoskeleton and an impact on root cell elongation was demonstrated (Scheuring et al., 2016). Due to their actin-binding capacity and association to the vacuole (Deeks et al., 2012), members of the Arabidopsis NET4 family can be hypothesized to integrate processes at the vacuole-cytoskeleton interface. However, their actual function and relevance for cell elongation and eventually plant growth has not been fully understood. For functional characterization of NET4, biochemical, genetic and cell biological approaches should be combined. This includes interaction studies, generation of Arabidopsis knockout and overexpression lines, phenotypical analysis based on confocal laser-scanning microscopy and 3D modeling as well as macroscopic studies of gene expression impact on organ growth.

For the present cumulative thesis, two peer-reviewed original research articles, one peer-reviewed review article and one preprint are combined.

In the first research article, the general impact of NET4 abundance, especially on vacuolar morphology, cell size and root growth is investigated (Kaiser et al., 2019). In the second research article, a general role of NET4 in cell elongation is explored (Kaiser et al., 2021). In the third article, NET4 function in relation to the actin cytoskeleton is mechanistically investigated (Kaiser et al., 2023).

To facilitate discussion, the aforementioned review article is attached and has been integrated for parts of the discussion (section 3.1) of this thesis (Kaiser and Scheuring, 2020).

2 Overview of included articles

2.1 Article 1:

“NET4 Modulates the Compactness of Vacuoles in *Arabidopsis thaliana*”

Published in the International Journal of Molecular Sciences 20(19):4752, in October 2019 (<https://doi.org/10.3390/ijms20194752>).

Authors: Sabrina Kaiser,^{1,†} Ahmed Eisa,^{2,†} Jürgen Kleine-Vehn,² and David Scheuring^{1,2}

Authors' information:

¹Plant Pathology, University of Kaiserslautern, 67663 Kaiserslautern, Germany

²Department of Applied Genetics and Cell Biology, University of Natural Resources and Applied Life Sciences (BOKU), 1190 Vienna, Austria

[†]These authors contributed equally to this work.

Article summary:

Within this article, a functional characterization of NET4A with emphasis on vacuolar morphology and its impact on cell elongation and plant growth has been carried out for the model plant *Arabidopsis thaliana*.

Seedlings expressing NET4A-GFP under the endogenous promoter (NET4A::NET4A-GFP; Deeks et al., 2012) were used to analyze subcellular localization by confocal laser-scanning microscopy (CLSM). To assess specific co-localization with the tonoplast, the endocytic dye FM4-64 (Scheuring et al., 2015) was used as tonoplast stain. In addition, *NET4* gene expression levels and protein abundance was evaluated upon morphological changes of the vacuole caused by treatments with different compounds.

The results of these studies revealed that NET4A is preferentially expressed in the late meristem of the root, an area contributing to root growth by cell division and early elongation events. NET4A expression in the root starts in the transition zone, the onset of cell elongation, and is not expressed in aerial tissues at all. A co-localization of NET4A and the tonoplast could be confirmed. On the subcellular level, we could demonstrate that NET4A decorates the tonoplast in a bead-on-a-string pattern and the signal was strongest in areas of high membrane curvature. In accordance, treatment with the synthetic auxin NAA, which leads to more vacuolar constrictions, resulted in a dosage-dependent higher abundance of NET4A protein. Treatment with the auxin biosynthesis inhibitor kynurenine (kyn), reducing vacuolar constrictions, led to lower NET4A abundance. In addition, no upregulation of *NET4A* or *NET4B*

gene expression could be detected upon NAA treatment. Based on this, we concluded that NET4A is generally recruited to constricted tonoplast areas and NET4 abundance might be stabilized on protein level, but is not regulated on transcriptional level.

To study the effects of altered NET4 expression, *net4* single mutants, a *net4a net4b* double mutant as well as an overexpression line were established. In the overexpression line, NET4A-GFP expression is constitutively driven by the strong 35S cauliflower mosaic virus promoter (35S::NET4A-GFP or NET4A-GFP^{OE}). The introduced lines were inspected for differences in vacuolar morphology, cell size and root growth. To assess vacuolar morphology on single layer images, the dyes MDY-64 in combination with propidium iodide was used, which stain the tonoplast and cell wall, respectively (Scheuring et al., 2015). BCECF-AM, which stains the vacuolar lumen (Scheuring et al., 2015), was used if performing z-stack recordings as basis to render 3D models of complete cells and vacuoles was desired.

On 2D level, these experiments demonstrated that lack of NET4 as well as NET4A overexpression both lead to more roundish vacuoles with less tubular membrane structures. Treatment with auxin on the other hand still led to typical constrictions, indicating that NET4 proteins might not be essential for auxin-mediated effects. Notably, vacuoles of the NET4A overexpressing line were more condensed around the nucleus, leaving more space between the PM and the vacuole than usual. This effect of NET4A overexpression was even increased upon NAA treatment. On 3D level, it was further shown that vacuoles of a *net4a net4b* double mutant were larger compared to wild type and occupied more of the given cellular space, while vacuoles of NET4A-GFP^{OE} were not only positioned near the nucleus but were also smaller, occupying significantly less space.

In line with this, NET4A-GFP^{OE} also exhibited smaller cells and a reduced root length. On the other hand, the double mutant showed no obvious effect on cell or root size. Interestingly, upon treatment with NAA, already shorter cells and roots of NET4A-GFP^{OE} were partially resistant to auxin-induced limitations on cell and root growth. Taken together, these results led us to conclude that NET4 has a function in modulating the compactness of vacuoles. Due to its identified expression, this function might be relevant especially prior to root cell transit from the meristem into the elongation zone, but seems not to directly affect previously described auxin-related morphological changes of the vacuole that depend on the actin cytoskeleton. Nonetheless, increased vacuolar compactness by enhanced NET4A expression was correlated with restricted cell and overall root organ growth, similar to auxin-induced vacuole constrictions. This correlation could be explained by a previously suggested space-filling function of the vacuole during cell elongation, which can enable fast growth due to a minimal energy investment for the production of cytosol (Scheuring et al., 2016; Dünser et al., 2019). Thus, NET4-dependent vacuolar modulations might influence growth by limiting this function.

In the context of this cumulative thesis, this publication laid the foundation for the subsequent experimental work by establishing overexpression and knockout lines. Moreover, a role for NET4 in modifying vacuolar morphology and size along with an impact in cell elongation and organ growth has been demonstrated. This allowed to follow the original research aims further.

2.2 Article 2:

“Vacuolar occupancy is crucial for cell elongation and growth regardless of the underlying mechanism”

Published in Plant Signaling & Behavior 16(8):1922796, in May 2021 (<https://doi.org/10.1080/15592324.2021.1922796>).

Authors: Sabrina Kaiser¹, Sophie Eisele¹, David Scheuring¹

Authors' information:

¹Plant Pathology, University of Kaiserslautern, Kaiserslautern, Germany

Article summary:

Within this publication, NET4 function on vacuolar morphology in dependence of the plant hormone auxin was investigated. Furthermore, transcriptional regulation of other NET superfamily members was monitored.

Previously, it has been shown that NET4 proteins have a function in modulating the compactness of vacuoles in Arabidopsis. More compact vacuoles were accompanied with restricted cell size and root growth (Kaiser et al., 2019). On the other hand, auxin also impacts on vacuolar morphology, thereby regulating the size of cells and roots in an actin-dependent manner (Löffke et al., 2015; Scheuring et al., 2016). Since NET4 proteins possess actin-binding capacity (Deeks et al., 2012), it would have been plausible to assume that they have an involvement in auxin-controlled processes. However, although both, auxin treatment as well as overexpression of NET4A, was demonstrated to restrict vacuole size, NET4-dependent smaller vacuoles were more roundish and thus different from the reported morphology of auxin-induced more constricted vacuoles (Scheuring et al., 2016; Kaiser et al., 2019).

To evaluate this in more detail, 3D models of vacuoles and cells from the late meristematic zone of the root epidermis were generated from Arabidopsis wild type and the previously established *net4a net4b* and NET4A-GFP^{OE} lines (Kaiser et al., 2019) upon treatment with auxin. These models revealed that all lines are susceptible to auxin-induced vacuolar constrictions. In relation to vacuolar volume, however, the already more compact vacuoles of NET4A-GFP^{OE} were partial resistant to a further auxin-induced decrease in size. On the other hand, vacuoles of *net4a net4b* reacted like wild type.

To further investigate, if unchanged auxin-responsiveness of the *net4a net4b* mutant might be based on a compensatory upregulation of other NET superfamily members with potentially similar functions, transcript levels of all remaining NET members were analyzed. For this, real-

time quantitative PCR was carried out for wild type and *net4a net4b* seedlings. As a result, no upregulation of *NET* expression levels was identified for *net4a net4b* in comparison to wild type background. The expression of *NET2A-C* and *NET3B* was even below detection level in both backgrounds. Therefore, we excluded a compensatory effect of other NETs within the *net4a net4b* double mutant by transcriptional upregulation.

Taken together, these results in combination with previous findings led us to conclude that NET4 is not essential for auxin-mediated vacuolar constrictions. Hence, apart from NET4 proteins, additional players must be involved in the general regulation of actin-dependent vacuole changes. NET4-mediated modulation of vacuolar compactness could represent an additional mechanism for regulating vacuole volume and growth. Thus, NET4 might be part of an amendatory fine-tuning mechanism to regulate vacuole-dependent cellular expansion in plants. Since both mechanisms, NET4-mediated more compact vacuoles as well as auxin-mediated more constricted vacuoles, are able to limit cell size and growth, we further hypothesized that control of vacuole volume must be a universal system to control cell expansion. All pathways might thereby be able to contribute until a certain minimal size is reached, which would explain a partial auxin resistance for already smaller vacuoles of NET4A-GFP^{OE}.

In the context of this thesis, this work sheds new light on the role of NET4 as part of a novel mechanism for modulating vacuole size beside auxin-mediated regulations. Furthermore, it emphasizes a relevance of additional molecular players at the actin cytoskeleton – vacuole nexus.

2.3 Article 3:

“Networked proteins redundantly interact with VAP27 and RABG3 to regulate membrane tethering at the vacuole and beyond”

Published as a preprint on bioRxiv in September 2023; updated version 2 from February 2024 (<https://doi.org/10.1101/2023.09.29.560113>).

Authors: Sabrina Kaiser¹, Dietmar Mehlhorn², Paulina Ramirez Miranda¹, Fabian Ries³, Frederik Sommer⁴, Michael Schroda⁴, Karin Schumacher⁵, Felix Willmund³, Christopher Grefen² and David Scheuring¹

Authors' information:

¹ Plant Pathology, University of Kaiserslautern-Landau, Germany

² Molecular and Cellular Botany, Ruhr University Bochum, Germany

³ Molecular Plant Physiology, University of Marburg, Germany

⁴ Molecular Biotechnology & Systems Biology, University of Kaiserslautern-Landau, Germany

⁵ COS Heidelberg, University of Heidelberg, Germany

Article summary:

Within this work, a characterization of NET4 with emphasis on its impact on the actin cytoskeleton and its mechanistic functions was performed. Moreover, a relevance of potential additional molecular players was examined.

NET4A was previously shown to localize preferentially at constricted tonoplast structures and overexpression of NET4A resulted in smaller, more spherical and compact vacuoles, limiting cell elongation and root size (Kaiser et al., 2019). Using newly established Arabidopsis lines, expressing NET4B-GFP under the endogenous promoter and NET4B-mCherry under the strong constitutive 35S promoter (NET4B-mCherry^{OE}), similar results could be observed for NET4B. Furthermore, analysis of generated lines expressing the reporter β -Glucuronidase (GUS) as well as GFP under the NET4A or NET4B promoter (NET4A::GUS-GFP and NET4B::GUS-GFP) demonstrated a mainly complementary expression of the two proteins within the root. Together, this indicates that NET4A and NET4B have redundant functions on the molecular level and might be able to work independent of each other at different plant parts.

To monitor actin filament organization in relation to NET4 abundance, the actin marker line lifeact-RFP (Riedl et al., 2008) was crossed with the previously established NET4A-GFP overexpression line (NET4A-GFP^{OE}, Kaiser et al., 2019). CLSM of the lifeact-RFP and lifeact-RFP x NET4A-GFP^{OE} crossing line showed that overexpression of NET4A leads to a changed

actin filament organization. In epidermal cells from the root transition zone, a bundling of actin filaments from the cell borders towards the nucleus at the cell center could be observed and was accompanied by well co-localizing and seemingly brighter NET4A-GFP signals at this area. To further analyze effects of altered NET4 abundance when the actin cytoskeleton is impaired, NET4A-GFP^{OE} was crossed with different vegetative actin or myosin mutants. Examination of the crossed lines revealed a reduced effect of NET4A overexpression on vacuole modulation in the triple *myosin xi-k/1/2* mutant background, demonstrating the importance of the actin-myosin system for NET4-mediated vacuole modulation. On the other hand, severe growth related defects of the *act7-4* or *act2 act8* mutants were partially reverted by overexpression of NET4A. This indicated that lack of these actin isoforms might be compensated upon elevated NET4A abundance by an enhanced recruitment of actin filaments. In line with this, treatment with the actin polymerization inhibitor latrunculin B (LatB), causing vacuole fragmentation and restricted root growth in wild type (Scheuring et al., 2016), showed only a reduced effect in NET4A-GFP^{OE}. Moreover, an accumulation of NET4A-GFP signals could be observed at connection points of separating vacuole structures when seedlings were treated with LatB. Together, these results led us to conclude that NET4 stabilizes existing actin filaments, especially at potential vacuolar fusion sites, and might therefore play a role during (homotypic) vacuole fusion.

To shed light on a role of NET4 in vacuolar fusion events more directly, an artificial microRNA-based conditional mutant for VPS16 (*amiR-vps16*), a subunit of the known vacuolar fusion tethering complexes HOPS and CORVET, was used and crossed with NET4A-GFP^{OE}. In addition, an existing sextuple mutant for RABG3 GTPases (*rabg3a,b,c,d,e,f*; Ebine et al., 2014), which are important for initiating vacuole fusion, was used to generate *rabg3a,b,c,d,e,f net4a* septuple mutants via CRISPR/Cas9-based partial deletion of *NET4A*. While overexpression of NET4A diminished vacuole fragmentation caused by lack of VPS16, additional knockout of *NET4* in *rabg3a,b,c,d,e,f* seemingly increased the observed effect on the vacuole for lack of RABG3 proteins and resulted in fragmented vacuoles that occupied less cellular space compared to *rabg3a,b,c,d,e,f*. These results confirmed NET4 participation in vacuole fusion events.

To uncover the molecular connection of NET4 proteins to the tonoplast, different interaction studies were carried out. These included protein-lipid overlay assays to test for direct binding of NET4 to compartment-specific membrane lipids as well as co-immunoprecipitation (Co-IP) experiments for seedlings expressing NET4A-GFP as bait, followed by mass spectrometry (MS) analysis of the precipitate to identify previously unknown NET4 interacting proteins. The results of these experiments showed that NET4A does not only bind to tonoplast-residing lipids, but also to lipid species that are incorporated to other membranes within the

endomembrane system. Furthermore, NET4A interaction with two RABG3 proteins, a known TGN-localized protein (RABC1), as well as a protein of unknown localization and function (At4g01245) was identified and verified by ratiometric Bimolecular Fluorescence Complementation (rBiFC) in *N. benthamiana* and the mating-based Split-Ubiquitin System (mbSUS) in yeast. Worth noting, NET4 was shown just recently to only interact with the GTP-bound active form of RABG3 proteins. Binding was further found to be dependent on a specific C-terminal sequence part of NET4A and NET4B (termed IRQ domain), which also exists in NET3A and NET3C, as well as a short non-homolog part downstream of the IRQ (Hawkins et al., 2023). Together, these findings indicated that NET4 recruitment to the tonoplast and its function in vacuole fusion can be facilitated by binding of the NET4 IRQ domain to active RABG3. Additionally, it could be speculated that this tonoplast recruitment might not be exclusive for NET4 proteins but potentially also happening for NET3 family members, while NET4 might additionally be able to build connections to other compartments.

Subsequent inspection of NET4 membrane recruitment, expressing different newly created truncated NET4A- as well as full length NET4A- and NET4B-fluophor fusions in *N. benthamiana* leaf cells, confirmed a tonoplast recruitment of the NET4A C-terminus (amino acids (aa) 504-558), which includes the IRQ domain (aa 504-542) plus remaining downstream sequence (aa 543-558). Moreover, a secondary membrane recruitment of NET4A and NET4B to the nuclear envelope was discovered and verified by co-localization with known ER-markers upon transient co-expression in tobacco as well as for crossed Arabidopsis lines, stably expressing NET4-fluophor fusion and ER-marker constructs. Further mbSUS yeast growth assays additionally demonstrated interaction of NET3A and NET3C with RABG3 proteins, as well as interaction of both NET4 members with the ER membrane intrinsic protein VAP27-1. The latter is known to facilitate NET3C recruitment to the ER (Wang et al., 2014) and together with NET3C participate in complex formation to establish a membrane contact site between the PM and the ER. Based on this, we hypothesized that NET4 might have another function in generating a, yet not described, contact site between the ER and the vacuole. We speculated that to this end, VAP27-1, RABG3, NET3 and NET4 must participate and suspected redundant functions for members of the NET3 and NET4 family. Since no transcriptional upregulation was previously found for NET3 proteins in the *net4a net4b* mutant background, it seemed plausible that lack of NET4A and NET4B is compensated by NET3 on protein level, explaining the observed mild phenotypes for *net4a net4b* (Kaiser et al., 2019; Kaiser et al., 2021). The establishment of different higher order *net3 net4* mutants showed that a *net3a net4a net4b* full CRISPR knockout mutant exhibits smaller, sometimes partially fragmented vacuoles in root cells, and is restricted in root growth. In contrast, these phenotypes could not be observed for a single *net3c* (CRISPR) mutant, the previously analyzed *net4a net4b* (T-DNA) double mutant

(Kaiser et al., 2019) or *net3a* (CRISPR) *net4a net4b* (T-DNA) triple mutants, demonstrating at least partially overlapping functions and the importance of NET4 and NET3 family members during plant growth.

In the context of this cumulative thesis, this article demonstrates how NET4 recruitment of actin filaments contributes to vacuolar fusion events. Furthermore, novel molecular player have been discovered, linking new functions (establishment of membrane contact sites) to NET4. A membrane contact site between the ER and the vacuole has not been reported yet and hence might represent a novel and exciting process to study in the future.

2.4 Article 4:

“To Lead or to Follow: Contribution of the Plant Vacuole to Cell Growth”

Published in Frontiers in Plant Science 11:553, in May 2020
(<https://doi.org/10.3389/fpls.2020.00553>).

Authors: Sabrina Kaiser¹, David Scheuring¹

Authors' information:

¹ Plant Pathology, University of Kaiserslautern, Kaiserslautern, Germany

Article summary:

This article is a review about the events during plant cell elongation. While focusing on the role of the vacuole, it gives an overview about the general knowledge in this field. The well established “acid growth theory” is discussed with emphasis on cell wall loosening and changes of the vacuole. In this context, the question whether vacuolar enlargement or cell wall loosening is the driving force for cell elongation is directly addressed.

Related to this cumulative thesis, in which the connection between the vacuole and the actin cytoskeleton is investigated along with a relevance in plant cell elongation, this review article provides a broader context for a better understanding of the original research results.

3 Closing discussion and future prospects

The research of this thesis primarily explored the relationship between the vacuole and the actin cytoskeleton, as well as its impact on cell elongation and eventually plant growth. Characterization of actin-binding and tonoplast-localized NET4 proteins, along with identification and functional analysis of associated molecular players, helped to deepen our understanding of the general intracellular processes of root growth. In particular, it shed light on the underlying modulation of actin-dependent vacuole alterations. Therefore, the following chapters discuss the stages of cell elongation in a broader context and integrate new findings of this thesis with the current knowledge in this field. Besides, additional roles of NET4 or connected proteins within further processes are considered.

3.1 The different events of cell elongation and the importance of the vacuole

Cellular elongation is a fundamental part of plant growth. Since vacuoles occupy most of the space in mature cells, it has been assumed that they provide the driving force for this process by building up the necessary turgor pressure (Marty, 1999). For suspension cultures of plant cotyledon cells, a general correlation between cell and vacuole size was found (Owens and Poole, 1979). Moreover, cell elongation has been shown to be accompanied by the expression of specific water channels (γ -TIPs), indicating a relevance of vacuolar inflation for cell growth (Ludevid et al., 1992). However, for roots of *Arabidopsis*, TIP expression seemed to be eminent for elongating but not meristematic cells (Gattolin et al., 2009; Gattolin et al., 2010). This implies that cell elongation is initiated prior to vacuolar inflation, raising doubts on the assumption of the vacuole being the driving force. In accordance, an inhibitory effect on cell elongation and root growth has been demonstrated when the volume of the vacuole was restrained by treatment with the plant hormone auxin. On the other hand, an increase in vacuole size, as described for some mutants (e.g. *vti11*), did not necessarily entail better growth (Löffke et al., 2015; Scheuring et al., 2016). Similar observations were made for NET4-dependent vacuole modulation. Here, overexpression of NET4, which led to smaller vacuoles, also resulted in reduced cell size and restricted root length. Evidently larger vacuoles in a *net4a net4b* double mutant, however, were not accompanied with an effect on cell or root size (Kaiser et al., 2019, Fig. 4; Kaiser et al., 2023, Supplementary Fig. 1).

A limitation of cell expansion despite the presence of a large vacuole could be seen in the rigidity of the cell wall. Consequently, it seems to be impossible for plant cells to elongate via turgor pressure without softening the wall in advance. An explanation how loosening of the cell wall can be accomplished first came up over five decades ago during research on the plant hormone auxin and has been postulated as the “acid growth theory” (Rayle and Cleland, 1970; Cleland, 1971; Hager et al., 1971). This hypothesis describes that cell wall loosening is

dependent on an auxin-mediated acidification of the extracellular matrix, which eventually (indirectly) alters the wall's properties. Over the years, more and more participating players were found, elucidating key steps to substantiate the general theory. First, PM-residing H⁺-ATPases are activated by auxin, which leads to the acidifying proton export. Then, cell wall modifying proteins, especially expansins (EXPs), are activated by the drop in pH, and subsequently can remodel the cell wall into a more loosened state. This, in addition to an enhanced uptake of solutes and water, enables cells to expand eventually (Rayle and Cleland, 1992; McQueen-Mason et al., 1992; Hager, 2003). Auxin-regulated increase in H⁺-ATPase activity was shown to be facilitated via different pathways. On the one hand, TIR1/AFB receptor-based signaling results in the expression of so-called SAUR proteins. These prevent dephosphorylation of H⁺-ATPases by inhibiting PP2C-D, a subfamily of type 2C protein phosphatases, at the PM, hence holding the proton pumps in its activated phosphorylated state (Spartz et al., 2014; Fendrych et al., 2016; Wong et al., 2019). On the other hand, auxin also promotes their initial phosphorylation (Takahashi et al., 2012). Recent findings clarified that this process happens via a cell surface signaling mechanism, in which transmembrane kinases (TMKs) directly bind and phosphorylate H⁺-ATPases at the PM (Lin et al., 2021). In contrast to aerial tissue, auxin is known to have an inhibitory effect on underground tissue at physiological concentrations. Yet, an auxin-based acidification of the extracellular matrix was demonstrated to have a positive effect on root cell elongation as well (Barbez et al., 2017). However, it has been shown for roots that in addition to the TMK-based activation of H⁺-ATPases, here, auxin induces a further antagonistically acting non-genomic TIR1/AFB-dependent rapid pathway. This mechanism causes a proton influx, resulting in an alkalinization of the apoplast. Thus, precise and fast root growth regulations in response to different environmental challenges were suggested to be enabled via the combined pH adaptation from both antagonistic pathways (Fendrych et al., 2018; Li et al., 2021).

After the cell wall properties have been changed, the resulting cell wall status must be transmitted to the vacuole in order to follow the changes. It has been shown that the cell wall status can be sensed mechanistically via the interplay of extracellular leucine-rich repeat extensins (LRX) and a PM-localized receptor-like kinase, FERONIA (FER), which in turn seems to have an impact on the coordination of intracellular vacuolar enlargement during cell elongation (Dünser et al., 2019). So far, it remains unclear how the LRX-FER-mediated sensing process transmits signals to the vacuole. Since auxin-induced vacuolar constrictions were shown to depend on the actin cytoskeleton (Scheuring et al., 2016), this could be a putative handle to link cell wall status and vacuolar morphology. In line with this, FER has been shown to regulate the activity of certain RHO-like GTPases (RAC/ROPs) via phosphorylation of the Rho of plants guanine nucleotide exchange factor 1 (ROP GEF1), which can activate

RAC/ROPs (Duan et al., 2010). Some effectors of RAC/ROP further play a role in actin dynamics and organization. Thus, a connection via this signaling pathway was suggested (Dünser et al., 2019). Together, these findings illustrate the order of different auxin-mediated signaling pathways and show that not vacuolar inflation, but pH-dependent cell wall loosening is presumably the leading step for cell elongation (Fig. 6).

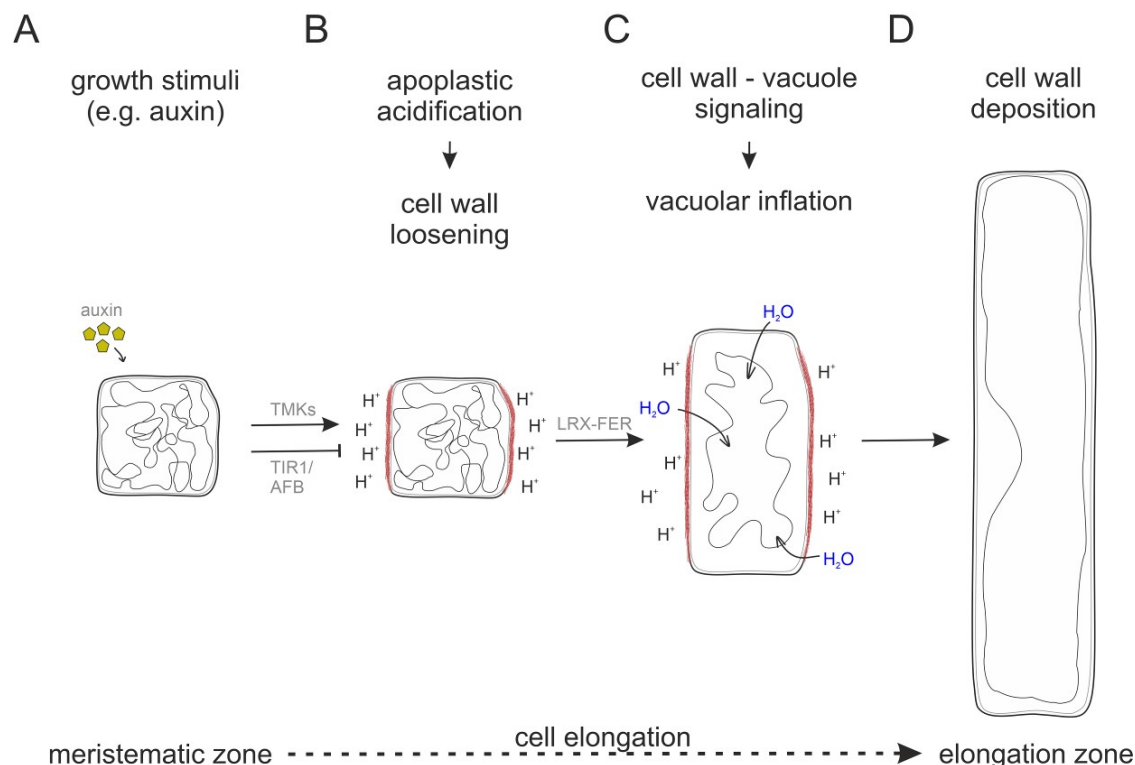


Figure 6: The process of root cell elongation. (A) In response to auxin, transmembrane kinases (TMKs) activate H⁺-ATPases at the plasma membrane (PM) leading to a proton efflux. On the other hand, a TIR1/AFB-dependent pathway is induced and results in a proton influx. Thus, dependent on the specific auxin concentration and other factors, the extracellular pH can be adapted. (B) In case a drop of the extracellular pH (apoplastic acidification) is achieved, expansins and other cell wall modifying proteins loosen the cell wall. (C) A module composed of leucine-rich repeat extensins (LRXs) and the receptor-like kinase FERONIA (FER) can sense the extracellular cell wall status and transmit it inside the cell to align vacuolar and cellular enlargement. The actin cytoskeleton is important for morphological alterations of the vacuole and the uptake of water via tonoplast-residing water channels enables vacuolar inflation. (D) Besides the delivery of tonoplast and PM material, cell wall deposition is necessary to enable cell elongation. Limiting the execution of any cell growth-promoting step inhibits cell elongation. Figure adapted from Kaiser and Scheuring, 2020.

Even without fully expanded vacuoles, cell expansion is not necessarily stopped completely. However, in roots, an inhibition of cell elongation in response to elevated auxin levels was shown to be based on highly constricted vacuoles that occupied less cellular space (Scheuring et al., 2016). Thus, the vacuole was suggested to fulfill a space-filling function (Scheuring et al., 2016; Krüger and Schumacher, 2018). According to this theory, vacuole inflation enables a more rapid cell elongation, since less energy must be invested for the production of cytoplasm. This explains how restrictions of vacuolar size can decelerate cellular expansion

and eventually growth. Vacuole volume measurements, which demonstrate an increase in vacuolar occupancy for epidermal root cells from the early meristem to the late elongation zone, while the cytosolic volume is kept relatively constant, further support this assumption (Dünser et al., 2019) (Fig. 7).

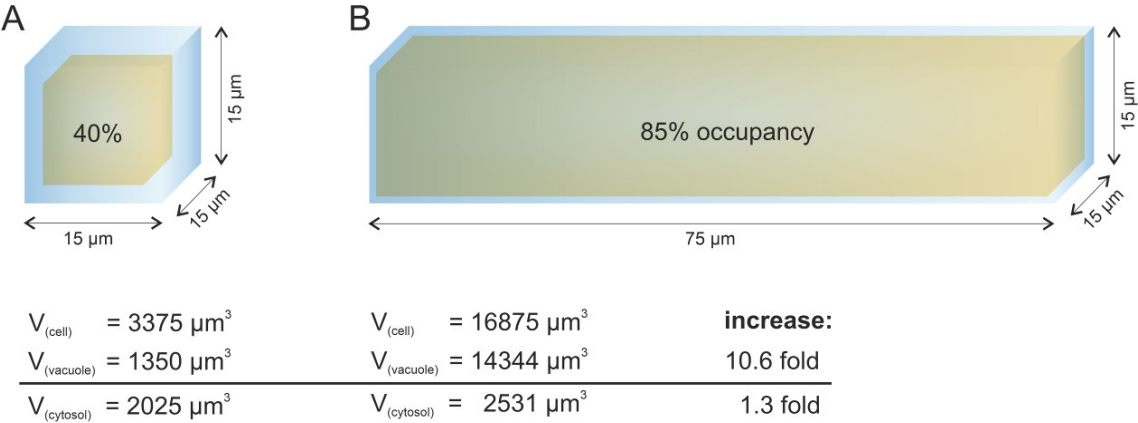


Figure 7: A calculation model for the cytosolic volume during cell elongation. For the shown calculation, values were based on published measurements for the cellular space that is taken in by the vacuole (vacuolar occupancy) for epidermal root cells from different developmental zones (Dünser et al., 2019). (A) Depiction of a meristematic root epidermal Arabidopsis cell. Edge length = 15 µm. (B) Depiction of a 5-fold elongated epidermis cell. As a simplification measure, cuboid shapes were used for the vacuolar (yellow) and cellular volume (blue). Cytosolic volume was calculated by subtracting the vacuole volume from the cell volume. The calculation demonstrates that in the course of cell elongation, the vacuolar occupancy raises dramatically. Here, the increase is more than 10-fold from (A) to (B). In contrast, the volume of the cytosol can be kept at a rather constant level. Figure taken from Kaiser and Scheuring, 2020.

Since members of the NET4 protein family are not only able to bind actin filaments but are also recruited to the vacuolar membrane (Deeks et al., 2012; Kaiser et al., 2019, Fig. 1; Hawkins et al., 2023; Kaiser et al., 2023, Supplemental Fig. 1), they represented suitable candidates for connecting the actin cytoskeleton with the tonoplast. Due to their expression patterns within the root, (Kaiser et al., 2019, Fig. 1; Kaiser et al., 2023, Supplementary Fig. S1, S10 and S11), it seemed plausible that NET4 proteins could be the mediators for actin-dependent changes of vacuolar morphology. Noteworthy, NET4 could be observed especially at constricted tonoplast sites (Kaiser et al., 2019, Fig. 1), whose appearance is enhanced by auxin within root epidermal meristem cells (Löfke et al., 2015), and elevated auxin concentrations led to an increase of NET4 abundance on the protein level (Kaiser et al., 2019, Fig. 2). However, although overexpression of NET4, similar to auxin treatment, led to smaller vacuoles that occupied less cellular space, their morphology did not resemble the highly tubular vacuole network that can be seen upon auxin treatment. Instead, vacuoles of NET4 overexpressing lines exhibited even fewer tubular structures, were more spherical and condensed around the nucleus (Kaiser et al., 2019, Fig. 3; Kaiser et al., 2023, Supplementary Fig. 1). In line with this, a reorientation of cortical actin filaments towards the cell center was observed when analyzing the actin cytoskeleton upon NET4A overexpression (Kaiser et al., 2023, Fig. 1, Supplementary

Fig. S2). This suggests that NET4 proteins can modulate actin organization and are indeed able to regulate vacuole morphology in this way. Upon auxin treatment, however, not only the NET4A overexpressing line (NET4A-GFP^{OE}), but also a *net4a net4b* double mutant still displayed more constricted vacuoles, which are typical for an auxin treatment. Interestingly, the overexpressor, having already smaller vacuoles, was partly resistant against a further auxin-induced decrease in vacuole size (Kaiser et al., 2021, Fig. 1). Hence, we concluded that NET4s are not the direct facilitators for auxin-mediated vacuole modulation, but seem to integrate vacuole alterations from another signaling pathway, which might be influenced by auxin via cross-talk but results in a different vacuole morphology. In this context, the observation that more compact vacuoles upon overexpression of NET4 were also correlated with restricted cell and root size (Kaiser et al., 2019, Fig. 4; Kaiser et al., 2023, Supplementary Fig. 1), emphasizes that limiting the vacuolar volume might be a general mechanism to restrict cell elongation, irrespective of the specific way, in which the limitation is realized (Kaiser et al., 2021). This corroborates the assumption that the vacuole in general has a space-filling function and, as such, can enable or impede fast cell elongation and determine the cell size in response to different signals, not only auxin.

3.2 Vacuole dynamics: fission and fusion

The vacuole is a very dynamic compartment where fission and fusion events constantly occur, often even simultaneously. To ensure vacuole integrity, these processes need to be coordinated. Interestingly, it has been shown in yeast that the vacuolar H⁺-ATPase (v-ATPase), an ATP-driven proton pump, does not only play a role for vacuole fission but also seems to have a stimulating function in vacuole fusion, and was thus suggested to be a regulator for vacuolar membrane dynamics (Baars et al., 2007; Strasser et al., 2011). However, besides v-ATPases, especially the action of major fission or fusion relevant proteins must be important to keep the balance. Dynamins and dynamin-related proteins, a group of large GTPases, play an important role for many membrane fission processes in eukaryotic cells (Praefcke and McMahon, 2004; Antonny et al., 2016). The dynamin-related proteins Vps1 and Dnm1 were shown to act in concert to enable vacuole fission in the fission yeast *Schizosaccharomyces pombe* (Röthlisberger et al., 2009). Notably, Vps1 is also able to control membrane fusion via direct action on SNARE proteins (Alpadi et al., 2013). The latter are commonly known for their function in membrane fusion and lack of specific vacuolar SNAREs has been reported to result in altered vacuole shape in *Arabidopsis* (Morita et al., 2002; Surpin et al., 2003; Takemoto et al., 2018; Jahn et al., 2024). In general, if the process of vacuole fission or fusion is impaired, more fused and larger or smaller individual vacuoles might occur, respectively. Thus,

regulation of vacuolar fission or fusion processes represents a general possibility to alter vacuolar size and morphology.

As mentioned in section 1.3, auxin has been shown to affect the abundance of SNARE proteins. Moreover, especially lack of the SNARE VTI11 was demonstrated to result in a strong insensitivity to auxin-mediated vacuole changes and root growth inhibition (Löffke et al., 2015). Since VTI11 is a known part of vacuole fusion machineries, the modulation of homotypic vacuole fusion via manipulating SNARE complex stability or activity was suggested as a method how auxin could induce vacuole changes. Apart from SNARE proteins, several other proteins, including GTPases of the RAB7/RABG subclass and the different subunits of the HOPS tethering complex, were shown to be important for governing homotypic vacuole fusion in plants (see section 1.3). Thus, they all represent further points of attack for modulation.

In yeast, vacuole-bound actin as well as regulatory membrane lipids were demonstrated in addition to be mandatory for vacuolar fusion events (Eitzen et al., 2002; Starr and Fratti, 2019). Here, an enrichment of PI(3)P marks the future site of homotypic vacuole fusion and enables the recruitment of RAB7-like GTPases, which further leads to the recruitment of HOPS and the pairing of respective SNARE proteins from the donor and acceptor membrane. Noteworthy, fusion specificity is provided by HOPS, which has a proof-reading function for monitoring the accurate assembly of SNAREs (Wickner, 2010; Balderhaar and Ungermann, 2013). To facilitate membrane fusion during HOPS-mediated tethering and docking of the two opposed membranes, their contact area becomes flattened and forms the so-called “boundary membrane”, which is surrounded by the “vertex ring”. The latter structure can be seen as a microdomain at the edge of the boundary membrane to which exclusively fusion relevant components are accumulated when needed. Apart from RAB7-like GTPases, which first enclose an emerging vertex ring, this includes subsequent accumulation of HOPS and SNAREs, but involves also coordinated enrichment of specific key regulatory lipids as well as actin filaments. (Wang et al., 2002; Eitzen et al., 2002; Wang et al., 2003; Fratti et al., 2004). Lipids play an important role throughout most fusion stages and certain regulatory lipids have either an inhibiting effect or promote fusion, e.g. by recruiting fusion driving proteins as mentioned for PI(3)P (Starr and Fratti, 2019). Actin remodeling, on the other hand, seems to be a necessity at two distinct points in the course of fusion. Prior to tethering, actin filaments at the site where the two membranes should come into contact are required to depolymerize, allowing membrane docking and vertex ring formation. Later, during the assembly of SNAREs, polymerization of enriched actin monomers (G-actin) into F-actin is necessary to support the last part of fusion. Actin is thereby hypothesized either to build fences for collecting enough fusion-driving SNARE proteins at the vertex ring or to produce energy in the form of membrane tension for the deformation of the membrane. Actin dynamics were further shown to be guided

by proteins of the fusion machinery and certain regulatory lipids, including ergosterol, PI(3)P and PI(4,5)P₂ (Eitzen et al., 2002; Karunakaran et al., 2012).

The amount of regulatory lipids within membranes, in particular PIP level dynamics, impacts fusion processes in plants as well. For instance, inhibition of the PI(3)P synthesizing phosphatidylinositol 3-kinase (PI3K) was reported to result in changes of MVB or vacuole fusion, albeit the effects were not consistent for different reports (Wang et al., 2009; Takáč et al., 2013; Zheng et al., 2014). Only a couple of years back, interaction of the two HOPS subunits VPS41 and VPS33 with several PIPs was demonstrated in protein-lipid binding assays using flat lipid stripes, whereas binding to curved liposomes was shown to be possible but inhibited by PI(3)P or PI(3,5)P₂. Due to these results, the specific PIP composition and curvature of membranes was speculated to regulate vacuole fusion by differential HOPS recruitment (Brillada et al., 2018). Noteworthy, auxin-induced vacuole changes were not only shown to rely on an intact actin cytoskeleton but interference with the activity of PI3 and PI4 kinases diminished the auxin effect on vacuolar morphology as well (Löffke et al., 2015; Scheuring et al., 2016).

In the scope of this thesis, it was possible to show that NET4 can alter vacuolar morphology by influencing the process of homotypic vacuole fusion. In addition, it was revealed that these changes in vacuole fusion can be linked to NET4-mediated alterations of the actin cytoskeleton. The effects of treatment with the actin polymerization preventing toxin LatB, as well as conditional knockdown of the HOPS core subunit VPS16, which both led to smaller and fragmented vacuoles, were partly inhibited by overexpression of NET4A (Kaiser et al., 2023, Fig. 3, Fig. 4). In line with this, additional knockout of NET4A within the *rabg3a,b,c,d,e,f* sextuple mutant further increased its already visible defects in vacuole fusion (Kaiser et al., 2023, Fig. 4). These results demonstrated that NET4 proteins can promote vacuolar fusion events. Furthermore, NET4A overexpression seemed to reduce the disassembly of actin filaments caused by LatB (Kaiser et al., 2023, Supplementary Fig. S4) and the localization of NET4A-GFP signals was especially prominent at connection points of separating vacuoles, potential vortex rings (Kaiser et al., 2023, Fig. 3). Therefore, we hypothesized that NET4 proteins attach actin filaments to defined fusion sites at the tonoplast (similar to yeast vertex rings) and thus, stabilize F-actin at these sites. This would also explain the reduced sensitivity for actin depolymerization and vacuole fission when NET4A is overexpressed.

The finding that NET4A and NET4B can interact with proteins belonging to the vacuole fusion-relevant group of Arabidopsis RABG3 GTPases (Kaiser et al., 2024, Fig. 5, Fig 6, Supplementary Fig. S6) further provides specific binding partners for NET4s at tonoplast sites that are prone for fusion. Besides, NET4A interaction with several lipid species, including PI(3)P and PI(3,5)P₂, could be demonstrated on lipid spotted stripes (Kaiser et al., 2023,

Supplementary Fig. S7). Since PI(3)P and PI(3,5)P₂ can be found in the membrane of vacuoles (Noack and Jallais, 2017), a tonoplast recruitment of NET4 proteins via direct lipid binding might be possible as well. However, NET4A also bound to other lipid species that are typically incorporated at different membranes of the endomembrane system. Thus, albeit interacting regulatory lipids might influence NET4 localization, specificity at the tonoplast is more likely facilitated by RABG3 protein interaction. Supportingly, Hawkins et al. only lately reported that NET4 proteins exclusively interact with RABG3s when these proteins are in their GTP-bound active states, indicating that NET4s are recruited as effectors of RABG3s. Furthermore, it was demonstrated for NET4B that this interaction requires a certain C-terminal region, from which a specific part, termed IRQ domain, is present in NET4A as well, but also exists in NET3A and NET3C (Hawkins et al., 2023). Taking this finding into account, an interaction of RABG3 proteins with NET3A and NET3C was tested and verified (Kaiser et al., 2024, Fig. 6).

Moreover, simultaneous loss of NET3C, NET4A and NET4B resulted in smaller vacuoles with some apparently disconnected substructures, indicating potential fusion defects. This was accompanied with inhibited root growth of the *net3c net4a net4b* #2 triple mutant (Kaiser et al., 2023, Fig. 7). The absence of these phenotypes in the *net3c* single or *net4a net4b* double mutant (Kaiser et al., 2024, Fig. 7; Kaiser et al., 2019, Fig. 4) strongly suggests an at least partial functional overlap. Remaining NET proteins most likely compensate the loss of their functional redundant variants on protein level, since no transcriptional upregulation of any NET superfamily member was found in the *net4a net4b* double mutant (Kaiser et al., 2021, Fig. 2). Notably, no obvious vacuole or root growth phenotypes were found for *net3a net4a net4b* triple mutants as well (Kaiser et al., 2024, Supplementary Fig. S12). Due to its RABG3 binding capacity, an additional relevance of NET3A for vacuole fusion events appears to be likely, but its potentially weaker impact might only be observable within a *net3a net3c net4a net4b* quadruple mutant. Thus, the investigation of such a mutant would be an interesting future task.

Taken together, the results so far led us to conclude that probably all IRQ domain containing NET proteins (but at least NET3C, NET4A and NET4B) can redundantly be recruited by tonoplast-localized RABG3s for connecting actin filaments with the fusion sites of opposing vacuole membranes to potentially stabilize or even enable the following steps of homotypic vacuole fusion (Fig. 8).

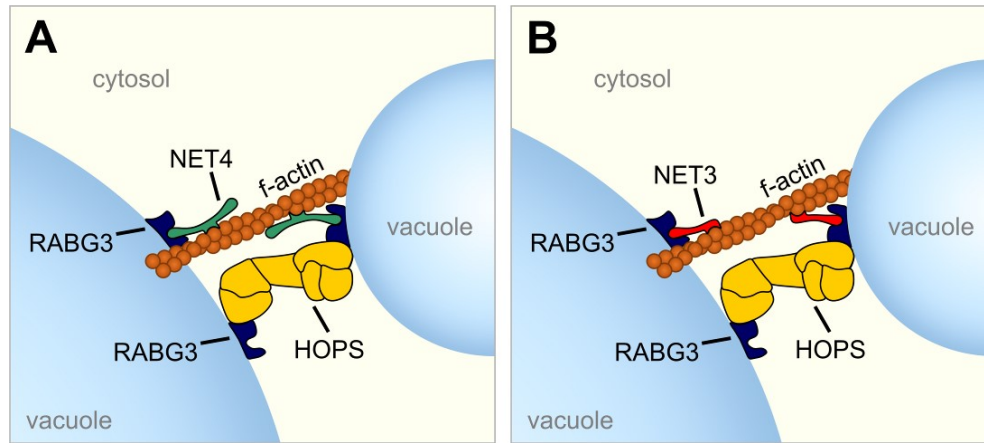


Figure 8: Working model for NET-mediated homotypic vacuole fusion. (A) The NAB domain of NET4 proteins binds to actin filaments. Recruitment of NET4s to the vacuole is facilitated via interaction of their IRQ domains and downstream C-terminal parts with tonoplast-resident active RABG3 GTPases. Additional interaction between RABG3s and the HOPS tethering complex closes the distance of the opposing membranes and allows SNARE proteins to facilitate membrane fusion. (B) Due to functional redundancy, NET3C and potentially also NET3A can replace the two NET4 proteins, enabling the same processes. Figure modified from Kaiser et al., 2023.

RABG GTPases in general are not exclusively found at the tonoplast, but are additionally located at MVBs to aid their fusion with the vacuole as well (Minamino and Ueda, 2019). Therefore, NET3 and NET4 proteins could fulfill similar functions during these heterotypic fusion processes, which also contribute to vacuolar enlargement.

The observation that vacuole size limitations of a *net3c net4a net4b* triple knockout mutant were accompanied with restricted root growth (Kaiser et al., 2024, Fig. 7) is further in accordance with the concept of the vacuole carrying out a space-filling function during cell elongation. This establishes a connection between NET3/NET4-influenced vacuole fusion processes and root cell expansion in plants. Interestingly, CRISPR/Cas9-derived knockout mutants for another NET4A interaction partner, a yet unnamed protein with the Arabidopsis gene bank accession code At4g01245 (Kaiser et al., 2024, Fig. 5, Supplementary Fig. S6), showed also smaller vacuole structures and slightly restricted root growth when compared to wild type Arabidopsis seedlings (data not shown). This could indicate participation of At4g01245 in the same process. However, since nothing certain is known about its localization so far, it remains to be tested at which location NET4A - At4g01245 interaction actually takes place and how At4g01245 specifically can affect growth on the molecular level.

3.3 Membrane contact sites and their potential function

In contrast to the newly identified connection with the vacuole, NET3 proteins are rather known for their localization and function at the ER (see section 1.5). While NET3A was found preferably at puncta of the nuclear envelope (Deeks et al., 2012), NET3C primarily localizes at contact sites between cortical ER and the PM and has been reported to participate in their

formation (Wang et al., 2014). For this purpose, NET3C interacts not only with ER-residing VAP27 proteins, such as VAP27-1, but also with kinesin-light-chain-related (KLCR) proteins that provide a bridge to microtubules via binding to IQ67-domain 2 (IQD2) and potentially further microtubule-localized members of the plant-specific IQD family. Together, these complexes connect the actin as well as microtubule network with the respective membranes and are crucial for the morphology of the ER at the ER-PM contact sites (Wang et al., 2014; Wang et al., 2016; Zang et al., 2021).

Membrane contact sites (MCSs), especially between the ER and several other organelles, have been shown for many eukaryotic organisms. In general, they are described as dynamically regulated areas of close proximity between two opposing membranes that are enabled by the interaction and complex formation of several tether proteins but unable to fuse. Their functions seem to be diverse and involve not only the exchange of ions, lipids and other molecules, but also lipid metabolism, intracellular signaling, organelle trafficking and morphology, autophagy and more (Scorrano et al., 2019; Tamura et al., 2019; Prinz et al., 2020). VAPs, especially VAP27 proteins as well as their better studied homologues in yeast (Scs2) or animals (VAPA/VAPB) were shown to play a role in numerous MCSs while interacting with a high amount of different partners (Scorrano et al., 2019; Wang et al., 2023).

In the frame of this dissertation, it could be shown that besides NET3 proteins also NET4A and NET4B can interact with the ER-integral protein VAP27-1 (Kaiser et al., 2023, Fig. 6). Moreover, a partial ER localization at the nuclear envelope was observed for both NET4 proteins in *N. benthamina* leaf as well as Arabidopsis root cells (Kaiser et al., 2023, Fig. 6, Supplementary Fig. S9). This strongly suggests that NET4s have an additional function in forming MCSs at the ER, which might especially be overlapping to NET3A at the nuclear envelope, and thereby reveals a direct link between the vacuole and ER. Together with the finding that NET3A and NET3C can bind tonoplast-localized RABG3 proteins, it can be hypothesized that NET3 and NET4 proteins act redundantly to generate bridging complexes with RABG3s and VAP27-1 for connecting the actin cytoskeleton, tonoplast and ER membrane (Fig. 9). This way, vacuole-ER contact sites (VECSs) can be introduced. Apart from the already indicated proteins in Fig. 9, this process could involve additional help of further proteins. Since NET3C and NET3A were both demonstrated to interact with microtubule associated KLCRs (Zang et al., 2021), it would be interesting to see, if these proteins can also bind to NET4s and have an additional relevance for the formation of VECSs, or might even enable NET4s to act at ER-PM contact sites (EPCSs) as well.

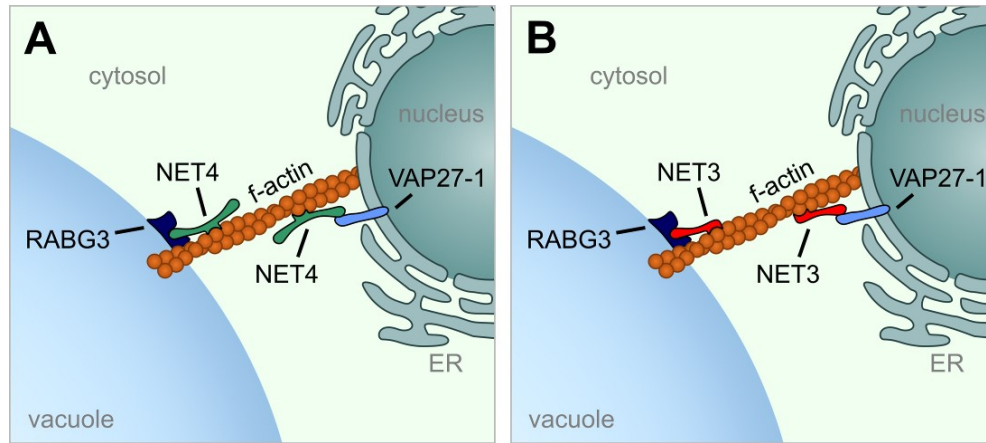


Figure 9: Working model for NET-mediated establishment of vacuole-ER contact sites. (A) Similar to vacuole fusion, NET4 proteins bind to actin filaments and are recruited to active RABG3s at the vacuole. Simultaneously, NET4s are able to also interact with the ER membrane-integral protein VAP27-1, bringing the vacuole and ER membrane into close proximity. Due to the absence of compatible fusion proteins at the opposing membranes, no fusion can be facilitated between the vacuole and ER. Instead, a membrane contact site (MCS) can be introduced. Further proteins might be participating during this process. (B) Since NET3A and NET3C have the same binding capacities as NET4A and NET4B, a redundant function is expected for the establishment of a MCS between the vacuole and ER. Figure modified from Kaiser et al., 2023.

Although several MCSs were discovered in plants during the last couple of years (Wang et al., 2023), the existence of a VECS has not been demonstrated before. However, in yeast, MCSs between vacuole and ER, especially the perinuclear ER, were already explored and are known as nucleus-vacuole junctions (NVJs) (Pan et al., 2000; Jeong et al., 2017). Like many MCSs, these function in the transport of ions and lipids, and were further shown to have several special roles. This includes, for instance, an involvement in the so-called piecemeal microautophagy of the nucleus (PMN), a variant of selective microautophagy during which small nonessential parts of the nucleus are released into the vacuole (Roberts et al., 2003). In animal cells, the existence of lysosome-ER contact sites was addressed only lately. Here, it could be shown that contact sites are established between damaged lysosomes and the ER to enable a rapid repair of these lysosomes via lipid transfer from the ER (Tan and Finkel, 2022).

Since the conserved actin-binding domain of NET proteins (NAB) is only present in higher plants (Hawkins et al., 2014), NET-mediated MCSs might execute plant-specific functions. However, lipid transport appears to be a common capacity of MCSs among eukaryotes and can often be facilitated via interaction of VAP proteins with different lipid transfer proteins. Albeit unrelated to the vacuole, some plant lipid transfer proteins have already been found at the ER membrane (Wang et al., 2023). Noteworthy, oxysterol-binding protein-related protein 2A (ORP2A) has been shown to interact with VAP27-1 and further proteins to mediate ER-autophagosomal MCSs and regulates autophagy by affecting PI(3)P redistribution (Ye et al., 2022). Moreover, ORP2A further acts at MCSs between chloroplast and ER, where it seems

to have an involvement in chloroplast lipid homeostasis (Renna et al., 2024). Thus, it seems likely that lipid transfer in general can also be executed at VECs in plants. Especially for vacuole biogenesis, direct ER to vacuole transport pathways are already a concept (Viotti et al., 2013; Scheuring et al., 2024). While VECs in plants might contribute to this process, they could further implement a potential lipid transfer ability to aid the process of vacuole inflation, necessary for cell elongation. Here, VECs might act as a direct and, hence, fast delivery route for lipids and potentially other membrane components from the ER to the vacuole to cope with the massive need of new tonoplast material during rapid vacuolar enlargement.

Interestingly, it was recently postulated that also endocytic vesicle trafficking from the PM to the vacuole contributes to vacuole growth during cell elongation, since this process was demonstrated to be enhanced in fast growing root cells. While the promoting effect on vacuolar size in this case simultaneously limits enlargement of the PM, it was concluded to be a mechanism for ensuring tightly coordinated cell and vacuole expansion during cell growth (Dünser et al., 2022). Strikingly, endocytosis is a process that has been shown to be influenced by EPCSs (Wang et al., 2023). Due to the finding that VAP27 proteins are connected to endosomes, and lack of VAP27 proteins led to impaired endocytosis and inhibited root growth in *Arabidopsis* (Stefano et al., 2018), it seems plausible to assume that the discovered enhanced endocytic trafficking during cell elongation might be (to some extent) mediated by EPCSs. A potentially accompanied direct lipid transfer via these contact sites from the ER to the PM could thereby provide the needed membrane material to enable faster endocytosis rates.

Taken together, in addition to their more direct relevance in vacuole fusion, it can be hypothesized that NET3 and NET4 proteins act in complexes with other proteins to coordinate at least one, but possibly even two MCSs that might both affect cell elongation via various eventually vacuole size determining processes. Further investigations need to be done to evaluate these theories. For instance, the discovery of VEC-associated lipid transfer proteins could strengthen the idea of a direct lipid delivery from the ER to the vacuole. Moreover, deletion mutants of suspected candidates might give some indications about the precise relevance of such a process for plant cell elongation and growth. On the other hand, observation of endocytosis for mutants lacking other EPCS-related proteins beside VAP27 (e.g. NET3s, KLCRs), could shed further light on a general involvement of EPCSs for endocytic processes.

3.4 Other putative NET4 and NET3 functions

In addition to VAP27-1, RABG3s and At4g01245, one more protein was found as NET4A interaction partner (Kaiser et al., 2023, Fig. 5, Supplementary Fig. S6). This protein, RABC1, belongs to the RABC class of RAB GTPases (Rutherford and Moore, 2002). Although a function within roots has not been shown yet, it is known to be localized at the TGN and has been established as a marker for this compartment (Geldner et al., 2009). This links NET4 proteins to at least one additional compartment, where they might play another role in fusion events or the establishment of MCSs. Whether this might represent a novel link to the vacuole remains elusive and needs to be elucidated in the future. Surprisingly, despite its common usage as a TGN marker, RABC1 was only lately found to be also associated with the ER in guard cells (Ge et al., 2022). Here, it was shown to interact with SEIPIN proteins, which act as RABC1 effectors and are relevant for the formation of lipid droplets (LDs). In general, LDs are specialized organelles that store energy-rich lipids and play a role in several biological processes, including membrane remodeling and stress response (Ischebeck et al., 2020). In stomata, their dynamics seem to be affected by RABC1, which in turn impacts on stomata morphogenesis and function. Malfunction of RABC1 was further demonstrated to also affect the size of the vacuole (Ge et al., 2022). In yeast, the biogenesis of LDs was shown to be one of the functions that is coordinated by NVJs (Hariri et al., 2018; Henne and Hariri, 2018). Furthermore, SEIPIN proteins were additionally shown to interact with Arabidopsis VAP27-1 and appear to be relevant for LD biogenesis in seeds (Greer et al., 2020). Thus, it seems plausible that RABC1 and SEIPIN proteins might actually act together with VAP27-1 within VECSs in guard cells to regulate the formation of LDs. RABC1 does not only interact with NET4A (Kaiser et al., 2023, Fig. 5, Supplementary Fig. S6), but also NET4B (data not shown). Since NET4B is expressed in stomata (Kaiser et al., 2023, Supplementary Fig. S10 and S11), participation in LD formation seems feasible. Thus, NET4B and RABC1 together with the actin cytoskeleton and tonoplast-localized RABG3 GTPases might enable the establishment of VECSs in guard cells. Intriguingly, NET4s as well as one member of the RABG3 family, RABG3b, were reported to be important for the long-term closure of stomata in response to microbial patterns. Again, this seems to be related to NET4-dependent actin remodeling in guard cells (Hawkins et al., 2023). Together with the discovered function for RABC1 and VAP27-1 in LD formation, and the NET4 capacity to bind not only actin filaments and RABG3b but also RABC1 and VAP27-1, it could be speculated that NET4- and RABG3b-dependent functions in microbial pattern-induced stomatal closure are linked with LD formation at potential VECSs. Resolving whether this is true, requires future studies.

Having another look at the root epidermis, NET4A overexpression resulted in meristem cells with smaller sized vacuoles that were further away from the PM (Kaiser et al., 2019, Fig. 3). In general, leaving more space between PM and vacuole for the cytosol, while altering the actin

cytoskeletal organization, could also affect the natural movement of cellular fluids, which occurs due to directional actin-myosin XI based organelle trafficking. Interestingly, the velocity of this cytoplasmic streaming was shown to impact on cell and plant size. While accelerated cytoplasmic streaming, achieved via expression of high-speed myosins, led to bigger cells and plants, a reduced velocity, caused by low-speed myosin expression, inhibited cell and plant growth of *Arabidopsis* (Tominaga et al., 2013). On the other hand, the partial localization of NET4 proteins at the nuclear envelope (Kaiser et al., 2024, Fig. 6) might also indicate a role in controlling the position and shape of the nucleus. Moving nuclei have been described for a plethora of examples and are usually occurring during specific developmental processes, such as cell division, root hair tip or pollen tube growth, as well as in response to biotic or abiotic stimuli or stresses. Here, nuclear migration seems to rely mainly on the actin-myosin system (Griffis et al., 2014), making NET4 as well as NET3 proteins reasonable candidates for mediating movement during these processes. Albeit no obvious changes in nuclear positioning could be observed in root cells of NET4A-GFP^{OE} or *net4a net4b* (data not shown), an involvement of NET4s cannot be excluded and might be important for specific cell types or events. Besides, a compensation by remaining NET3 proteins upon lack of NET4s cannot be excluded, hence phenotypes might be only visible for higher order mutants.

Among the previously listed developmental processes, in which a movement of the nucleus takes place, especially cell division might be of note. Here, not only nuclear migration but also restricting vacuole size might be important. Prior to mitosis, microtubules as well as actin filaments usually form a so-called preprophase band at the cortical cell area, which marks the future plane of division. After its disassembly and the end of mitosis, a structure, termed phragmoplast, which mainly consists of microtubules but also actin, emerges between the two generated daughter nuclei and guides the delivery of cell wall material to the forming cell plate. This way, the new cell wall is generated throughout cytokinesis, until it reaches the former location of the preprophase band at the cell cortex (Smith, 2001). The vacuolar volume was shown to be drastically decreased during this process and it has been postulated that this is a requirement to increase the cytosolic content and provide enough space for the phragmoplast and cell plate structures to be formed (Seguí-Simarro and Staehelin, 2006). In accordance, unequal cell division could be observed for early embryos of the mutant *gravitropism defective 2* (*grv2*), which exhibited abnormally large vacuoles, and was hence considered the consequence of phragmoplast misalignment (Silady et al., 2008). Moreover, planned asymmetric division of *Arabidopsis* zygotes, which usually results in a small apical and large basal cell, was shown to strongly depend on a dynamic modulation and directional migration of vacuoles towards the basal end of the cell (Matsumoto et al., 2021). Changes of vacuole shape and distribution further rely on the organization of actin filaments, and the mutant *shoot*

gravitropism 2 (sgr2), which is impaired in performing vacuole changes and possesses large apical vacuoles, was reported to be disturbed in nuclear migration, leading to an unnatural more symmetric zygote division (Kimata et al., 2019). For root meristem development in *Arabidopsis*, ACT7 seems to be the most important actin of the three vegetative actin isoforms. Among other phenotypes, mutants lacking ACT7 are strongly retarded in root growth and show not only inhibited cell elongation but severe defects in cell division (Gilliland et al., 2003; Kandasamy et al., 2009; Numata et al., 2022). While the other two vegetative actin isoforms, ACT2 and ACT8, are mostly known for their impact in root hair development, several *act2* mutants were further reported to show enhanced root waving (Lanza et al., 2012; Vaškebová et al., 2018). Interestingly, this wavy root phenotype was linked to a deregulation of cell division plane orientation, caused by alterations of the actin cytoskeletal organization (Vaškebová et al., 2018). Overexpression of NET4A partly compensated the root growth and cell division defects of an analyzed mutant lacking ACT7 (*act7-4*) as well as the wavy root phenotype observed for an investigated *act2 act8* double mutant (Kaiser et al., 2023, Fig. 2). Thus, it is tempting to assume that NET4A, but potentially also NET4B and the NET3s, have a function in cell division. This function is likely related to an actin-based impact on the vacuole, but might also affect nuclear migration. Moreover, a direct effect for the recruitment of actin filaments to the cell division plane could be speculated, e.g. during the formation of the phragmoplast. Due to NET4 expression patterns (Kaiser et al., 2023, Supplemental Fig. S10 and S11), such a NET4 involvement during cell division might not only be relevant in the root meristem, but particularly interesting for lateral root formation. However, further investigations will be necessary to elucidate the precise mode of action for NET4 and NET3 proteins in cell division and to evaluate their specific relevance in root meristem or lateral root development.

3.5 Final remarks

Plant cell elongation is a complex and tightly regulated process during rapid growth. Here, vacuole modulation is an important factor, which is dependent on actin filament remodeling and can be regulated by the plant hormone auxin. In the range of this dissertation, it was possible to elucidate that NET4 and NET3 proteins can contribute to this process by recruiting actin filaments to the vacuole fusion machinery while not being directly regulated by auxin. In this way, they promote vacuole fusion and most likely further help to establish plant-specific contact sites between the vacuole and the ER via interacting with additional proteins, including the ER-resident and known contact site protein VAP27-1, to form bridging complexes. Moreover, NET4s, and to some extent NET3s, probably also fulfill other functions that are somehow connected to the vacuole and the actin cytoskeleton. These involve processes, such as cell division, which directly affect plant growth as well, but also stomata closing. The latter

could have a more indirect effect on growth due to changes in CO₂ uptake while being rather relevant for plant defense. Taken together, it might be concluded that NET4 (and NET3) proteins are universal connectors between actin and the vacuole to mediate not only cell elongation but potentially several other processes that depend on dynamic vacuole and cytoskeletal changes, and might either directly or indirectly influence plant growth.

4 Summary

Cellular elongation contributes to fast and efficient plant growth. In root cells of *Arabidopsis thaliana*, elongation is inhibited by the plant hormone auxin. Auxin-induced restrictions in cell size are accompanied by morphological alterations of the plants largest organelle, the vacuole. Changes of vacuolar morphology and decrease of vacuolar size upon auxin application have been shown to be dependent on the actin cytoskeleton. However, the connection between actin filaments and the vacuole remained elusive.

In this thesis, putative candidates for actin-tonoplast linkage, the NET4 family members NET4A and NET4B from the plant-specific actin-binding and membrane-associated Networked (NET) superfamily, were functionally characterized by combining genetic, biochemical and cell biological approaches. Examination of knockout and overexpression lines by confocal laser-scanning microscopy revealed that NET4 proteins are able to alter vacuolar morphology as well as actin organization. Using 3D surface rendering of cells and vacuoles, elevated NET4 levels were demonstrated to result in more compact and smaller vacuoles. Similar to auxin-induced smaller vacuoles, this reduction of vacuole size was accompanied by restricted cellular and organ growth. However, NET4-mediated morphological changes of the vacuole were found not to be directly facilitated by auxin, suggesting that NET4 proteins act in another mechanism for regulating vacuole morphology. Thus, limiting vacuole size was further hypothesized to be a general method to restrict cell expansion.

Experiments to investigate the impact of NET4 upon impairments of the actin cytoskeleton or the vacuole fusion machinery indicated that NET4 participates in homotypic vacuole fusion. This was further substantiated by interaction and gene deletion studies. Surprisingly, both NET4 proteins but also NET3A and NET3C were found to interact with tonoplast-residing RAB GTPases (RABG3s), thereby recruiting actin filaments to vacuolar fusion sites. Moreover, an additional interaction was demonstrated for NET4 and the ER-resident contact site protein VAP27-1, which is known to interact with NET3C for establishing ER-PM contact sites. When analyzing CRISPR-based *net3c net4a net4b* triple mutants, misshaped and sometimes partially fragmented and smaller vacuoles could be observed, which was correlated with restricted root growth. This supports a role of NET3/NET4 in homotypic vacuole fusion and demonstrates the importance of vacuole integrity for plant growth. Based on these results, it could be concluded that NET4 and NET3 proteins redundantly function to recruit actin filaments to tonoplast-localized RABG3s, altering vacuolar morphology and size by enabling homotypic vacuole fusion. In addition, NET3s and NET4s were hypothesized to redundantly interact with VAP27-1, RABG3 and actin filaments to establish a yet unknown plant membrane contact sites between the vacuole and the ER.

5 Zusammenfassung

Die zelluläre Streckung ist wichtig für ein schnelles und effizientes Pflanzenwachstum. In Wurzelzellen von *Arabidopsis thaliana* wird dieser Streckungsprozess durch das Phytohormon Auxin inhibiert. Auxin-induzierte Limitierungen der Zellgröße werden von morphologischen Veränderungen des größten Pflanzenorganells, der Vakuole, begleitet. Es ist gezeigt worden, dass diese Änderungen der Vakuolenmorphologie sowie die damit einhergehende Vakuolenverkleinerung vom Aktin-Zytoskelett abhängen. Die Verbindung zwischen Aktinfilamenten und der Vakuole verblieb bislang jedoch weitgehend unklar.

In dieser Arbeit wurden mittels genetischer, biochemischer und zellbiologischer Methoden die NET4 Familienmitglieder NET4A und NET4B von der pflanzenspezifischen Aktin-bindenden und Membran-assoziierten „Networked“ (NET)-Überfamilie als vermeintliche Kandidaten für eine Aktin-Tonoplast Verbindung funktionell charakterisiert. Mittels konfokaler Laser-Scanning-Mikroskopie untersuchte Knockout- und Überexpressions-Linien zeigten, dass NET4-Proteine in der Lage sind die Vakuolenmorphologie sowie die Organisation von Aktinfilamenten zu verändern. Durch 3D-Oberflächenmodellierung von Zellen und Vakuolen konnte nachgewiesen werden, dass erhöhte Mengen an NET4 zu kompakteren und kleineren Vakuolen führen. Diese Verringerung der Vakuolengröße war, ebenso wie bei der Auxin-induzierten Vakuolenverkleinerung, von einem reduzierten Zell- und Organwachstum begleitet. Eine direkte Vermittlung der NET4-bedingten Veränderungen der Vakuolenmorphologie über Auxin konnte jedoch ausgeschlossen werden, was darauf hindeutet, dass NET4-Proteine die Vakuolenmorphologie über einen anderen Mechanismus beeinflussen. Es wurde daher die Hypothese aufgestellt, dass die Limitierung der Vakuolengröße eine generelle Methode zur Inhibierung der Zellexpansion darstellt.

Untersuchungen zum NET4-Einfluss bei Beschädigung des Aktin-Zytoskeletts oder der vakuolären Fusionsmaschinerie legten nahe, dass NET4 an der homotypischen Vakuolenfusion beteiligt ist. Dies konnte durch zusätzliche Interaktions- und Gendelektionsstudien untermauert werden. Für beide NET4-Proteine, aber auch für NET3A und NET3C, konnten überraschenderweise Interaktionen mit Tonoplast-ansässigen RAB GTPases (RABG3s) nachgewiesen werden, wodurch sie Aktinfilamente an vakuoläre Fusionsstellen rekrutieren können. Weiterhin wurden zusätzliche Interaktionen zwischen NET4 und dem im ER ansässigen Membrankontaktstellenprotein VAP27-1 gezeigt, welches für eine Interaktion mit NET3C zum Aufbau von ER-PM Kontaktstellen bekannt ist. Bei der Analyse von CRISPR-generierten *net3c net4a net4b* Dreifachmutanten konnten deformierte und manchmal teilweise fragmentierte sowie kleinere Vakuolen beobachtet werden, was mit einem eingeschränkten Wurzelwachstum korrelierte. Dies untermauert eine Rolle von NET3/NET4 bei der homotypischen Vakuolenfusion und demonstriert die Relevanz der vakuolären Integrität für

das Pflanzenwachstum. Aus diesen Ergebnissen konnte geschlossen werden, dass NET4 und NET3 Proteine in redundanter Weise Aktin-Filamente an Tonoplast-lokalisierte RABG3s rekrutieren und damit die Morphologie sowie Größe der Vakuole durch Regulierung der homotypischen Vakuolenfusion verändern. Zudem wurde die Hypothese aufgestellt, dass NET3s und NET4s gleichermaßen mit VAP27-1, RABG3 sowie Aktin-Filamenten interagieren, um bislang unbekannte Membrankontaktstellen zwischen der Vakuole und dem ER zu etablieren.

6 Abbreviations

aa	amino acid
ABP	actin-binding protein
ACT	actin (protein)
AFB	AUXIN SIGNALING F-BOX (protein)
amiR	artificial microRNA
AP-3	adaptor protein complex 3
ARE	Auxin Response Element
ARF	AUXIN RESPONSE FACTOR (protein)
ATP	adenosine triphosphate
ATPase	adenosine triphosphatase (protein)
Aux/IAA	AUXIN/INDOLE ACETIC ACID (protein)
BCECF-AM	2',7'-Bis-(2-Carboxyethyl)-5-(and-6)-Carboxyfluorescein - Acetoxymethyl Ester
Cas	CRISPR-associated (protein)
CCZ1	CALCIUM CAFFEINE ZINC SENSITIVITY1 (protein)
CLSM	confocal laser-scanning microscopy
Co-IP	Co-immunoprecipitation
CORVET	class C core vacuole/endosome tethering (protein complex)
CRISPR	Clustered Regularly Interspaced Short Palindromic Repeats
DZ	differentiation zone
EE	early endosome
EPCS	ER-PM contact site
ER	endoplasmic reticulum
EXP	expansin (protein)
EZ	elongation zone
F-actin	filamentous actin
FER	FERONIA (protein)
FM4-64	N-(3-Triethylammoniumpropyl)-4-(6-(4-(Diethylamino) Phenyl) Hexatrienyl) Pyridiniumdibromid
FRAP	fluorescent recovery after photobleaching
G-actin	globular actin
GAP	GTPase activating protein
GDP	guanosine diphosphate
GEF	guanine exchange factor
grv2	gravitropism defective 2 (mutant)
GTP	guanosine triphosphate
GTPase	guanosine triphosphatase (protein)
GUS	β -Glucuronidase
HOPS	homotypic fusion and protein sorting (protein complex)
IAA	indole-3-acetic-acid
IQD	IQ67-domain (protein)
KEG	KEEP ON GOING (protein)
KLCR	kinesin-light-chain-related (protein)
kyn	kynurenine
LatB	latrunculin B
LD	lipid droplet
LE	late endosome
LRX	leucine-rich repeat extensin (protein)
LV	lytic vacuole
mbSUS	mating-based Split-Ubiquitin System
MCS	membrane contact site
MDY-64	membrane dye for yeast vacuoles
MON1	MONENSIN SENSITIVITY1 (protein)

MS	mass spectrometry
MVB	multivesicular body
MZ	meristematic zone
NAA	1-naphthaleneacetic acid
NAB	NET actin-binding
NE	nuclear envelope
NET	Networked (protein)
NSF	N-ethylmaleimide-sensitive factor (protein)
ORP	oxysterol-binding protein-related protein
PI	phosphatidylinositol
PI	propidium iodide
PIP	phosphatidylinositol phosphate
PM	plasma membrane
PMN	piecemeal microautophagy of the nucleus
PP	protein phosphatase
PRK	pollen receptor-like kinase (protein)
PSV	protein storage vacuole
RAB	Ras-related in brain (protein)
RAC	Ras-related C3 botulinum toxin substrate (protein)
rBiFC	rationometric Bimolecular Fluorescence Complementation
RHO	Ras homologous (protein)
ROP	Rho of plants (protein)
SA	salicylic acid
SAC	suppressor of actin (protein)
SAUR	SMALL AUXIN UP RNA (protein)
Scs2	Suppressor of Choline Sensitivity (protein)
sgr2	shoot gravitropism 2 (mutant)
SNAP	soluble NSF attachment protein
SNARE	soluble N-ethylmaleimide-sensitive factor attachment protein receptor
SYP	syntaxins of plants (protein)
TGN	trans-Golgi network
TIP	tonoplast intrinsic protein
TIR1	TRANSPORT INHIBITOR RESPONSE1 (protein)
TMK	transmembrane kinase (protein)
v-ATPase	vacuolar H ⁺ -ATPase (protein)
VAMP	vesicle-associated membrane protein
VAP	VAMP-associated protein
vcl1	vacuoleless 1 (mutant)
VECS	vacuole-ER contact site
VPS	vacuolar protein sorting (protein)
VTI	vesicle transport through interaction with t-SNAREs (protein)

7 References

- Alpadi, K., Kulkarni, A., Namjoshi, S., Srinivasan, S., Sippel, K.H., Ayscough, K., Zieger, M., Schmidt, A., Mayer, A., Evangelista, M., Quiococho, F.A., and Peters, C.** (2013). Dynamin-SNARE interactions control trans-SNARE formation in intracellular membrane fusion. *Nature Communications* **4**: 1704.
- Andrés, Z., Pérez-Hormaeche, J., Leidi, E.O., Schlücking, K., Steinhorst, L., McLachlan, D.H., Schumacher, K., Hetherington, A.M., Kudla, J., Cubero, B., and Pardo, J.M.** (2014). Control of vacuolar dynamics and regulation of stomatal aperture by tonoplast potassium uptake. *Proceedings of the National Academy of Sciences of the United States of America* **111** (17): E1806-14.
- Aniento, F., Sánchez de Medina Hernández, V., Dagdas, Y., Rojas-Pierce, M., and Russinova, E.** (2022). Molecular mechanisms of endomembrane trafficking in plants. *The Plant Cell* **34** (1): 146–173.
- Antonny, B., Burd, C., Camilli, P. de, Chen, E., Daumke, O., Faelber, K., Ford, M., Frolov, V.A., Frost, A., Hinshaw, J.E., Kirchhausen, T., Kozlov, M.M., Lenz, M., Low, H.H., McMahon, H., Merrifield, C., Pollard, T.D., Robinson, P.J., Roux, A., and Schmid, S.** (2016). Membrane fission by dynamin: what we know and what we need to know. *The EMBO journal* **35** (21): 2270–2284.
- Baars, T.L., Petri, S., Peters, C., and Mayer, A.** (2007). Role of the V-ATPase in regulation of the vacuolar fission-fusion equilibrium. *Molecular Biology of the Cell* **18** (10): 3873–3882.
- Balderhaar, H.J.k., and Ungermann, C.** (2013). CORVET and HOPS tethering complexes - coordinators of endosome and lysosome fusion. *Journal of cell science* **126** (Pt 6): 1307–1316.
- Baluška, F., Jasik, J., Edelmann, H.G., Salajová, T., and Volkmann, D.** (2001). Latrunculin B-induced plant dwarfism: Plant cell elongation is F-actin-dependent. *Developmental Biology* **231** (1): 113–124.
- Barbez, E., Dünser, K., Gaidora, A., Lendl, T., and Busch, W.** (2017). Auxin steers root cell expansion via apoplastic pH regulation in *Arabidopsis thaliana*. *Proceedings of the National Academy of Sciences of the United States of America* **114** (24): E4884-E4893.
- Barrero, R.A., Umeda, M., Yamamura, S., and Uchimiya, H.** (2002). *Arabidopsis* CAP Regulates the Actin Cytoskeleton Necessary for Plant Cell Elongation and Division. *The Plant Cell* **14** (1): 149–163.
- Blanchoin, L., Boujemaa-Paterski, R., Henty, J.L., Khurana, P., and Staiger, C.J.** (2010). Actin dynamics in plant cells: a team effort from multiple proteins orchestrates this very fast-paced game. *Current opinion in plant biology* **13** (6): 714–723.
- Brillada, C., Zheng, J., Krüger, F., Rovira-Diaz, E., Askani, J.C., Schumacher, K., and Rojas-Pierce, M.** (2018). Phosphoinositides control the localization of HOPS subunit VPS41, which together with VPS33 mediates vacuole fusion in plants. *Proceedings of the National Academy of Sciences of the United States of America* **115** (35): E8305-E8314.
- Cai, C., Henty-Ridilla, J.L., Szymanski, D.B., and Staiger, C.J.** (2014). *Arabidopsis* myosin XI: a motor rules the tracks. *Plant Physiology* **166** (3): 1359–1370.
- Cao, W., Li, Z., Huang, S., Shi, Y., Zhu, Y., Lai, M.N., Lok, P.L., Wang, X., Cui, Y., and Jiang, L.** (2022). Correlation of vacuole morphology with stomatal lineage development by whole-cell electron tomography. *Plant Physiology* **188** (4): 2085–2100.
- Casanova-Sáez, R., Mateo-Bonmatí, E., and Ljung, K.** (2021). Auxin Metabolism in Plants. *Cold Spring Harb Perspect Biol* **13** (3): a039867.
- Cleland, R.** (1971). Cell Wall Extension. *Annu. Rev. Plant. Physiol.* **22** (1): 197–222.
- Cui, Y., Cao, W., He, Y., Zhao, Q., Wakazaki, M., Zhuang, X., Gao, J., Zeng, Y., Gao, C., Ding, Y., Wong, H.Y., Wong, W.S., Lam, H.K., Wang, P., Ueda, T., Rojas-Pierce, M.,**

- Toyooka, K., Kang, B.-H., and Jiang, L.** (2019). A whole-cell electron tomography model of vacuole biogenesis in Arabidopsis root cells. *Nature plants* **5** (1): 95–105.
- Cui, Y., Zhao, Q., Hu, S., and Jiang, L.** (2020). Vacuole Biogenesis in Plants: How Many Vacuoles, How Many Models? *Trends in plant science* **25** (6): 538–548.
- Deeks, M.J., Calcutt, J.R., Ingle, E.K.S., Hawkins, T.J., Chapman, S., Richardson, A.C., Mentlak, D.A., Dixon, M.R., Cartwright, F., Smertenko, A.P., Oparka, K., and Hussey, P.J.** (2012). A superfamily of actin-binding proteins at the actin-membrane nexus of higher plants. *Current Biology* **22** (17): 1595–1600.
- Dharmasiri, N., Dharmasiri, S., Weijers, D., Lechner, E., Yamada, M., Hobbie, L., Ehrismann, J.S., Jürgens, G., and Estelle, M.** (2005). Plant development is regulated by a family of auxin receptor F box proteins. *Developmental cell* **9** (1): 109–119.
- Dilworth, L.L., Riley, C.K., and Stennett, D.K.** (2017). Plant Constituents. In *Pharmacognosy* (Elsevier), pp. 61–80.
- dos Remedios, C.G., Chhabra, D., Kekic, M., Dedova, I.V., Tsubakihara, M., Berry, D.A., and Nosworthy, N.J.** (2003). Actin binding proteins: regulation of cytoskeletal microfilaments. *Physiological reviews* **83** (2): 433–473.
- Duan, Q., Kita, D., Li, C., Cheung, A.Y., and Wu, H.-M.** (2010). FERONIA receptor-like kinase regulates RHO GTPase signaling of root hair development. *Proceedings of the National Academy of Sciences of the United States of America* **107** (41): 17821–17826.
- Duan, Z., and Tominaga, M.** (2018). Actin-myosin XI: an intracellular control network in plants. *Biochemical and Biophysical Research Communications* **506** (2): 403–408.
- Duckney, P., Deeks, M.J., Dixon, M.R., Kroon, J., Hawkins, T.J., and Hussey, P.J.** (2017). Actin-membrane interactions mediated by NETWORKED2 in Arabidopsis pollen tubes through associations with Pollen Receptor-Like Kinase 4 and 5. *New Phytol* **216** (4): 1170–1180.
- Duckney, P.J., Wang, P., and Hussey, P.J.** (2022). Membrane contact sites and cytoskeleton-membrane interactions in autophagy. *FEBS letters* **596** (17): 2093–2103.
- Dujardin, F.** (1841). *Histoire Naturelle Des Zoophytes: Infusoires, Comprenant La Physiologie Et La Classification De Ces Animaux, Et La Manière De Les Étudier A L'Aide Du Microscope* (Paris: Roret; Fain et Thunot).
- Dünser, K., Gupta, S., Herger, A., Feraru, M.I., Ringli, C., and Kleine-Vehn, J.** (2019). Extracellular matrix sensing by FERONIA and Leucine-Rich Repeat Extensins controls vacuolar expansion during cellular elongation in Arabidopsis thaliana. *The EMBO journal* **38** (7): e100353.
- Dünser, K., and Kleine-Vehn, J.** (2015). Differential growth regulation in plants—the acid growth balloon theory. *Current opinion in plant biology* **28**: 55–59.
- Dünser, K., Schöller, M., Rößling, A.-K., Löffke, C., Xiao, N., Pařízková, B., Melnik, S., Rodriguez-Franco, M., Stöger, E., Novák, O., and Kleine-Vehn, J.** (2022). Endocytic trafficking promotes vacuolar enlargements for fast cell expansion rates in plants. *eLife* **11**: e75945.
- Ebine, K., Inoue, T., Ito, J., Ito, E., Uemura, T., Goh, T., Abe, H., Sato, K., Nakano, A., and Ueda, T.** (2014). Plant vacuolar trafficking occurs through distinctly regulated pathways. *Current Biology* **24** (12): 1375–1382.
- Eitzen, G., Wang, L., Thorngren, N., and Wickner, W.** (2002). Remodeling of organelle-bound actin is required for yeast vacuole fusion. *The Journal of cell biology* **158** (4): 669–679.
- Evans, M.L., Ishikawa, H., and Estelle, M.A.** Responses of Arabidopsis roots to auxin studied with high temporal resolution: Comparison of wild type and auxin-response mutants. *Planta* **194** (2): 215–222.

- Feeney, M., Kittelmann, M., Menassa, R., Hawes, C., and Frigerio, L.** (2018). Protein Storage Vacuoles Originate from Remodeled Preexisting Vacuoles in *Arabidopsis thaliana*. *Plant Physiology* **177** (1): 241–254.
- Fendrych, M., Akhmanova, M., Merrin, J., Glanc, M., Hagihara, S., Takahashi, K., Uchida, N., Torii, K.U., and Friml, J.** (2018). Rapid and reversible root growth inhibition by TIR1 auxin signalling. *Nature plants* **4** (7): 453–459.
- Fendrych, M., Leung, J., and Friml, J.** (2016). TIR1/AFB-Aux/IAA auxin perception mediates rapid cell wall acidification and growth of *Arabidopsis* hypocotyls. *eLife* **5**: e19048.
- Fratti, R.A., Jun, Y., Merz, A.J., Margolis, N., and Wickner, W.** (2004). Interdependent assembly of specific regulatory lipids and membrane fusion proteins into the vertex ring domain of docked vacuoles. *The Journal of cell biology* **167** (6): 1087–1098.
- Frigerio, L., Hinz, G., and Robinson, D.G.** (2008). Multiple vacuoles in plant cells: rule or exception? *Traffic (Copenhagen, Denmark)* **9** (10): 1564–1570.
- Fujimoto, M., and Ueda, T.** (2012). Conserved and Plant-Unique Mechanisms Regulating Plant Post-Golgi Traffic. *Frontiers in Plant Science* **3**: 197.
- Gallei, M., Luschig, C., and Friml, J.** (2020). Auxin signalling in growth: Schrödinger's cat out of the bag. *Current opinion in plant biology* **53**: 43–49.
- Gattolin, S., Sorieul, M., and Frigerio, L.** (2010). Tonoplast intrinsic proteins and vacuolar identity. *Biochemical Society transactions* **38** (3): 769–773.
- Gattolin, S., Sorieul, M., Hunter, P.R., Khonsari, R.H., and Frigerio, L.** (2009). In vivo imaging of the tonoplast intrinsic protein family in *Arabidopsis* roots. *BMC plant biology* **9**: 133.
- Ge, S., Zhang, R.-X., Wang, Y.-F., Sun, P., Chu, J., Li, J., Sun, P., Wang, J., Hetherington, A.M., and Liang, Y.-K.** (2022). The *Arabidopsis* Rab protein RABC1 affects stomatal development by regulating lipid droplet dynamics. *The Plant Cell* **34** (11): 4274–4292.
- Geldner, N., Dénervaud-Tendon, V., Hyman, D.L., Mayer, U., Stierhof, Y.-D., and Chory, J.** (2009). Rapid, combinatorial analysis of membrane compartments in intact plants with a multicolor marker set. *The Plant journal for cell and molecular biology* **59** (1): 169–178.
- Gilliland, L.U., Kandasamy, M.K., Pawloski, L.C., and Meagher, R.B.** (2002). Both Vegetative and Reproductive Actin Isovariants Complement the Stunted Root Hair Phenotype of the *Arabidopsis* act2-1 Mutation1. *Plant Physiology* **130** (4): 2199–2209.
- Gilliland, L.U., Pawloski, L.C., Kandasamy, M.K., and Meagher, R.B.** (2003). *Arabidopsis* actin gene ACT7 plays an essential role in germination and root growth. *The Plant journal for cell and molecular biology* **33** (2): 319–328.
- Greer, M.S., Cai, Y., Gidda, S.K., Esnay, N., Kretzschmar, F.K., Seay, D., McClinchie, E., Ischebeck, T., Mullen, R.T., Dyer, J.M., and Chapman, K.D.** (2020). SEIPIN Isoforms Interact with the Membrane-Tethering Protein VAP27-1 for Lipid Droplet Formation. *The Plant Cell* **32** (9): 2932–2950.
- Griffis, A.H.N., Groves, N.R., Zhou, X., and Meier, I.** (2014). Nuclei in motion: movement and positioning of plant nuclei in development, signaling, symbiosis, and disease. *Frontiers in Plant Science* **5**: 129.
- Gu, Y., and Innes, R.W.** (2012). The KEEP ON GOING protein of *Arabidopsis* regulates intracellular protein trafficking and is degraded during fungal infection. *The Plant Cell* **24** (11): 4717–4730.
- Hager, A.** (2003). Role of the plasma membrane H⁺-ATPase in auxin-induced elongation growth: historical and new aspects. *Journal of plant research* **116** (6): 483–505.
- Hager, A., Menzel, H., and Krauss, A.** (1971). Versuche und Hypothese zur Primärwirkung des Auxins beim Streckungswachstum. *Planta* **100** (1): 47–75.
- Hariri, H., Rogers, S., Ugrankar, R., Liu, Y.L., Feathers, J.R., and Henne, W.M.** (2018). Lipid droplet biogenesis is spatially coordinated at ER-vacuole contacts under nutritional stress. *EMBO reports* **19** (1): 57–72.

- Hawkins, T.J., Deeks, M.J., Wang, P., and Hussey, P.J.** (2014). The evolution of the actin binding NET superfamily. *Frontiers in Plant Science* **5**: 254.
- Hawkins, T.J., Kopischke, M., Duckney, P.J., Rybak, K., Mentlak, D.A., Kroon, J.T.M., Bui, M.T., Richardson, A.C., Casey, M., Alexander, A., Jaeger, G. de, Kalde, M., Moore, I., Dagdas, Y., Hussey, P.J., and Robatzek, S.** (2023). NET4 and RabG3 link actin to the tonoplast and facilitate cytoskeletal remodelling during stomatal immunity. *Nature Communications* **14** (1): 5848.
- Henne, W.M., and Hariri, H.** (2018). Endoplasmic Reticulum-Vacuole Contact Sites “Bloom” With Stress-Induced Lipid Droplets. *Contact* (Thousand Oaks (Ventura County, Calif.)) **1**: 2515256418756112.
- Henty-Ridilla, J.L., Li, J., Blanchoin, L., and Staiger, C.J.** (2013). Actin dynamics in the cortical array of plant cells. *Current opinion in plant biology* **16** (6): 678–687.
- Hirano, T., Stecker, K., Munnik, T., Xu, H., and Sato, M.H.** (2017). Visualization of Phosphatidylinositol 3,5-Bisphosphate Dynamics by a Tandem ML1N-Based Fluorescent Protein Probe in Arabidopsis. *Plant & cell physiology* **58** (7): 1185–1195.
- Ischebeck, T., Krawczyk, H.E., Mullen, R.T., Dyer, J.M., and Chapman, K.D.** (2020). Lipid droplets in plants and algae: Distribution, formation, turnover and function. *Seminars in cell & developmental biology* **108**: 82–93.
- Jahn, R., Cafiso, D.C., and Tamm, L.K.** (2024). Mechanisms of SNARE proteins in membrane fusion. *Nature reviews. Molecular cell biology* **25** (2): 101–118.
- Jauh, G.Y., Phillips, T.E., and Rogers, J.C.** (1999). Tonoplast intrinsic protein isoforms as markers for vacuolar functions. *The Plant Cell* **11** (10): 1867–1882.
- Jeong, H., Park, J., Kim, H.-I., Lee, M., Ko, Y.-J., Lee, S., Jun, Y., and Lee, C.** (2017). Mechanistic insight into the nucleus-vacuole junction based on the Vac8p-Nvj1p crystal structure. *Proceedings of the National Academy of Sciences of the United States of America* **114** (23): E4539-E4548.
- Jurgens, G.** (2004). Membrane trafficking in plants. *Annual review of cell and developmental biology* **20**: 481–504.
- Kaiser, S., Eisa, A., Kleine-Vehn, J., and Scheuring, D.** (2019). NET4 Modulates the Compactness of Vacuoles in Arabidopsis thaliana. *International journal of molecular sciences* **20** (19): 4752.
- Kaiser, S., Eisele, S., and Scheuring, D.** (2021). Vacuolar occupancy is crucial for cell elongation and growth regardless of the underlying mechanism. *Plant Signaling & Behavior* **16** (8): 1922796.
- Kaiser, S., Mehlhorn, D., Ramirez Miranda, P., Ries, F., Sommer, F., Schroda, M., Schumacher, K., Willmund, F., Grefen, C., and Scheuring, D.** (2023). Networked proteins redundantly interact with VAP27 and RABG3 to regulate membrane tethering at the vacuole and beyond. *bioRxiv*.
- Kaiser, S., and Scheuring, D.** (2020). To Lead or to Follow: Contribution of the Plant Vacuole to Cell Growth. *Frontiers in Plant Science* **11**: 553.
- Kandasamy, M.K., Burgos-Rivera, B., McKinney, E.C., Ruzicka, D.R., and Meagher, R.B.** (2007). Class-specific interaction of profilin and ADF isoforms with actin in the regulation of plant development. *The Plant Cell* **19** (10): 3111–3126.
- Kandasamy, M.K., McKinney, E.C., and Meagher, R.B.** (2009). A single vegetative actin isoform overexpressed under the control of multiple regulatory sequences is sufficient for normal Arabidopsis development. *The Plant Cell* **21** (3): 701–718.
- Karunakaran, S., Sasser, T., Rajalekshmi, S., and Fratti, R.A.** (2012). SNAREs, HOPS and regulatory lipids control the dynamics of vacuolar actin during homotypic fusion in *S. cerevisiae*. *Journal of cell science* **125** (Pt 7): 1683–1692.

- Kato, T., Morita, M.T., Fukaki, H., Yamauchi, Y., Uehara, M., Niihama, M., and Tasaka, M.** (2002). SGR2, a phospholipase-like protein, and ZIG/SGR4, a SNARE, are involved in the shoot gravitropism of *Arabidopsis*. *The Plant Cell* **14** (1): 33–46.
- Kende, H., and Zeevaert, J.** (1997). The Five “Classical” Plant Hormones. *The Plant Cell* **9** (7): 1197–1210.
- Kimata, Y., Kato, T., Higaki, T., Kurihara, D., Yamada, T., Segami, S., Morita, M.T., Maeshima, M., Hasezawa, S., Higashiyama, T., Tasaka, M., and Ueda, M.** (2019). Polar vacuolar distribution is essential for accurate asymmetric division of *Arabidopsis* zygotes. *Proceedings of the National Academy of Sciences of the United States of America* **116** (6): 2338–2343.
- Kost, B., and Chua, N.-H.** (2002). The plant cytoskeleton: vacuoles and cell walls make the difference. *Cell* **108** (1): 9–12.
- Krüger, F., and Schumacher, K.** (2018). Pumping up the volume - vacuole biogenesis in *Arabidopsis thaliana*. *Seminars in cell & developmental biology* **80**: 106–112.
- Kutsuna, N., Kumagai, F., Sato, M.H., and Hasezawa, S.** (2003). Three-dimensional reconstruction of tubular structure of vacuolar membrane throughout mitosis in living tobacco cells. *Plant & cell physiology* **44** (10): 1045–1054.
- Lanza, M., Garcia-Ponce, B., Castrillo, G., Catarcha, P., Sauer, M., Rodriguez-Serrano, M., Páez-García, A., Sánchez-Bermejo, E., T C, M., Leo del Puerto, Y., Sandalio, L.M., Paz-Ares, J., and Leyva, A.** (2012). Role of actin cytoskeleton in brassinosteroid signaling and in its integration with the auxin response in plants. *Developmental cell* **22** (6): 1275–1285.
- Leyser, H.M.** (1998). Plant hormones. *Current Biology* **8** (1): R5–7.
- Leyser, O.** (2018). Auxin Signaling. *Plant Physiology* **176** (1): 465–479.
- Li, J., Blanchoin, L., and Staiger, C.J.** (2015). Signaling to actin stochastic dynamics. *Annual review of plant biology* **66**: 415–440.
- Li, L., Verstraeten, I., Roosjen, M., Takahashi, K., Rodriguez, L., Merrin, J., Chen, J., Shabala, L., Smet, W., Ren, H., Vanneste, S., Shabala, S., Rybel, B. de, Weijers, D., Kinoshita, T., Gray, W.M., and Friml, J.** (2021). Cell surface and intracellular auxin signalling for H⁺ fluxes in root growth. *Nature* **599** (7884): 273–277.
- Li, L.-J., Ren, F., Gao, X.-Q., Wei, P.-C., and Wang, X.-C.** (2013). The reorganization of actin filaments is required for vacuolar fusion of guard cells during stomatal opening in *Arabidopsis*. *Plant, cell & environment* **36** (2): 484–497.
- Lin, W., Zhou, X., Tang, W., Takahashi, K., Pan, X., Dai, J., Ren, H., Zhu, X., Pan, S., Zheng, H., Gray, W.M., Xu, T., Kinoshita, T., and Yang, Z.** (2021). TMK-based cell-surface auxin signalling activates cell-wall acidification. *Nature* **599** (7884): 278–282.
- Löfke, C., Dünser, K., Scheuring, D., and Kleine-Vehn, J.** (2015). Auxin regulates SNARE-dependent vacuolar morphology restricting cell size. *eLife* **4**: e05868.
- Ludevid, D., Höfte, H., Himelblau, E., and Chrispeels, M.J.** (1992). The Expression Pattern of the Tonoplast Intrinsic Protein γ -TIP in *Arabidopsis thaliana* Is Correlated with Cell Enlargement 1. *Plant Physiology* **100** (4): 1633–1639.
- Marty, F.** (1978). Cytochemical studies on GERL, provacuoles, and vacuoles in root meristematic cells of *Euphorbia*. *Proceedings of the National Academy of Sciences of the United States of America* **75** (2): 852–856.
- Marty, F.** (1999). Plant vacuoles. *The Plant Cell* **11** (4): 587–600.
- Mathur, J., Mathur, N., and Hülskamp, M.** (2002). Simultaneous visualization of peroxisomes and cytoskeletal elements reveals actin and not microtubule-based peroxisome motility in plants. *Plant Physiology* **128** (3): 1031–1045.
- Mathur, J., Mathur, N., Kernebeck, B., and Hülskamp, M.** (2003). Mutations in actin-related proteins 2 and 3 affect cell shape development in *Arabidopsis*. *The Plant Cell* **15** (7): 1632–1645.

- Matile, P., and Moor, H.** (1968). Vacuolation: Origin and Development of the Lysosomal Apparatus in Root-Tip Cells. *Planta* **80**: 159–175.
- Matsumoto, H., Kimata, Y., Higaki, T., Higashiyama, T., and Ueda, M.** (2021). Dynamic Rearrangement and Directional Migration of Tubular Vacuoles are Required for the Asymmetric Division of the Arabidopsis Zygote. *Plant & cell physiology* **62** (8): 1280–1289.
- McDowell, J.M., An, Y.Q., Huang, S., McKinney, E.C., and Meagher, R.B.** (1996a). The Arabidopsis ACT7 actin gene is expressed in rapidly developing tissues and responds to several external stimuli. *Plant Physiology* **111** (3): 699–711.
- McDowell, J.M., Huang, S., McKinney, E.C., An, Y.Q., and Meagher, R.B.** (1996b). Structure and Evolution of the Actin Gene Family in Arabidopsis thaliana. *Genetics* **142** (2): 587–602.
- McQueen-Mason, S., Durachko, D.M., and Cosgrove, D.J.** (1992). Two endogenous proteins that induce cell wall extension in plants. *The Plant Cell* **4** (11): 1425–1433.
- Meagher, R.B., McKinney, E.C., and Vitale, A.V.** (1999). The evolution of new structures: clues from plant cytoskeletal genes. *Trends in Genetics* **15** (7): 278–284.
- Melotto, M., Underwood, W., Koczan, J., Nomura, K., and He, S.Y.** (2006). Plant stomata function in innate immunity against bacterial invasion. *Cell* **126** (5): 969–980.
- Minamino, N., and Ueda, T.** (2019). RAB GTPases and their effectors in plant endosomal transport. *Current opinion in plant biology* **52**: 61–68.
- Morita, M.T., Kato, T., Nagafusa, K., Saito, C., Ueda, T., Nakano, A., and Tasaka, M.** (2002). Involvement of the Vacuoles of the Endodermis in the Early Process of Shoot Gravitropism in Arabidopsis. *The Plant Cell* **14** (1): 47–56.
- Morita, M.T., and Shimada, T.** (2014). The plant endomembrane system—a complex network supporting plant development and physiology. *Plant & cell physiology* **55** (4): 667–671.
- Morré, D.J., and Mollenhauer, H.H.** (1974). The endomembrane concept: A functional integration of endoplasmic reticulum and Golgi apparatus. In *Dynamic Aspects of Plant Ultrastructure*, A.W. Robards, ed (London: McGraw-Hill), pp. 84–137.
- Nielsen, E.** (2020). The Small GTPase Superfamily in Plants: A Conserved Regulatory Module with Novel Functions. *Annual review of plant biology* **71**: 247–272.
- Nishimura, T., Yokota, E., Wada, T., Shimmen, T., and Okada, K.** (2003). An Arabidopsis ACT2 dominant-negative mutation, which disturbs F-actin polymerization, reveals its distinctive function in root development. *Plant & cell physiology* **44** (11): 1131–1140.
- Noack, L.C., and Jaillais, Y.** (2017). Precision targeting by phosphoinositides: how PIs direct endomembrane trafficking in plants. *Current opinion in plant biology* **40**: 22–33.
- Nováková, P., Hirsch, S., Feraru, E., Tejos, R., van Wijk, R., Viaene, T., Heilmann, M., Lerche, J., Rycke, R. de, Feraru, M.I., Grones, P., van Montagu, M., Heilmann, I., Munnik, T., and Friml, J.** (2014). SAC phosphoinositide phosphatases at the tonoplast mediate vacuolar function in Arabidopsis. *Proceedings of the National Academy of Sciences of the United States of America* **111** (7): 2818–2823.
- Numata, T., Sugita, K., Ahamed Rahman, A., and Rahman, A.** (2022). Actin isovariant ACT7 controls root meristem development in Arabidopsis through modulating auxin and ethylene responses. *Journal of experimental botany* **73** (18): 6255–6271.
- Owens, T., and Poole, R.J.** (1979). Regulation of cytoplasmic and vacuolar volumes by plant cells in suspension culture. *Plant Physiology* **64** (5): 900–904.
- Pan, X., Roberts, P., Chen, Y., Kvam, E., Shulga, N., Huang, K., Lemmon, S., and Goldfarb, D.S.** (2000). Nucleus–Vacuole Junctions in *Saccharomyces cerevisiae* Are Formed Through the Direct Interaction of Vac8p with Nvj1p. *Molecular Biology of the Cell* **11** (7): 2445–2457.
- Peremyslov, V.V., Klocko, A.L., Fowler, J.E., and Dolja, V.V.** (2012). Arabidopsis Myosin XI-K Localizes to the Motile Endomembrane Vesicles Associated with F-actin. *Frontiers in Plant Science* **3**: 184.

- Peremyslov, V.V., Prokhnevsky, A.I., Avisar, D., and Dolja, V.V.** (2008). Two Class XI Myosins Function in Organelle Trafficking and Root Hair Development in Arabidopsis. *Plant Physiology* **146** (3): 1109–1116.
- Peremyslov, V.V., Prokhnevsky, A.I., and Dolja, V.V.** (2010). Class XI myosins are required for development, cell expansion, and F-Actin organization in Arabidopsis. *The Plant Cell* **22** (6): 1883–1897.
- Pizarro, L., and Norambuena, L.** (2014). Regulation of protein trafficking: posttranslational mechanisms and the unexplored transcriptional control. *Plant science an international journal of experimental plant biology* **225**: 24–33.
- Pollard, T.D., and Cooper, J.A.** (2009). Actin, a Central Player in Cell Shape and Movement. *Science (New York, N.Y.)* **326** (5957): 1208–1212.
- Praefcke, G.J.K., and McMahon, H.T.** (2004). The dynamin superfamily: universal membrane tubulation and fission molecules? *Nature reviews. Molecular cell biology* **5** (2): 133–147.
- Prinz, W.A., Toulmay, A., and Balla, T.** (2020). The functional universe of membrane contact sites. *Nature reviews. Molecular cell biology* **21** (1): 7–24.
- Prokhnevsky, A.I., Peremyslov, V.V., and Dolja, V.V.** (2008). Overlapping functions of the four class XI myosins in Arabidopsis growth, root hair elongation, and organelle motility. *Proceedings of the National Academy of Sciences of the United States of America* **105** (50): 19744–19749.
- Quint, M., and Gray, W.M.** (2006). Auxin signaling. *Current opinion in plant biology* **9** (5): 448–453.
- Rayle, D.L., and Cleland, R.** (1970). Enhancement of Wall Loosening and Elongation by Acid Solutions 1. *Plant Physiology* **46** (2): 250–253.
- Rayle, D.L., and Cleland, R.E.** (1992). The Acid Growth Theory of auxin-induced cell elongation is alive and well. *Plant Physiology* **99** (4): 1271–1274.
- Renna, L., Stefano, G., Puggioni, M.P., Kim, S.-J., Lavell, A., Froehlich, J.E., Burkart, G., Mancuso, S., Benning, C., and Brandizzi, F.** (2024). ER-associated VAP27-1 and VAP27-3 proteins functionally link the lipid-binding ORP2A at the ER-chloroplast contact sites. *Nature Communications* **15** (1): 6008.
- Riedl, J., Crevenna, A.H., Kessenbrock, K., Yu, J.H., Neukirchen, D., Bista, M., Bradke, F., Jenne, D., Holak, T.A., Werb, Z., Sixt, M., and Wedlich-Soldner, R.** (2008). Lifeact: a versatile marker to visualize F-actin. *Nature Methods* **5** (7): 605–607.
- Ringli, C., Baumberger, N., Diet, A., Frey, B., and Keller, B.** (2002). ACTIN2 Is Essential for Bulge Site Selection and Tip Growth during Root Hair Development of Arabidopsis. *Plant Physiology* **129** (4): 1464–1472.
- Roberts, P., Moshitch-Moshkovitz, S., Kvam, E., O'Toole, E., Winey, M., and Goldfarb, D.S.** (2003). Piecemeal Microautophagy of Nucleus in *Saccharomyces cerevisiae*. *Molecular Biology of the Cell* **14** (1): 129–141.
- Rodriguez-Furlan, C., Minina, E.A., and Hicks, G.R.** (2019). Remove, Recycle, Degrade: Regulating Plasma Membrane Protein Accumulation. *The Plant Cell* **31** (12): 2833–2854.
- Rojo, E., Gillmor, C.S., Kovaleva, V., Somerville, C.R., and Raikhel, N.V.** (2001). VACUOLELESS1 is an essential gene required for vacuole formation and morphogenesis in Arabidopsis. *Developmental cell* **1** (2): 303–310.
- Röthlisberger, S., Jourdain, I., Johnson, C., Takegawa, K., and Hyams, J.S.** (2009). The dynamin-related protein Vps1 regulates vacuole fission, fusion and tubulation in the fission yeast, *Schizosaccharomyces pombe*. *Fungal genetics and biology FG & B* **46** (12): 927–935.
- Rothman, J.E.** (2002). The machinery and principles of vesicle transport in the cell. *Nature medicine* **8** (10): 1059–1062.
- Rutherford, S., and Moore, I.** (2002). The Arabidopsis Rab GTPase family: another enigma variation. *Current opinion in plant biology* **5** (6): 518–528.

- Sanmartín, M., Ordóñez, A., Sohn, E.J., Robert, S., Sánchez-Serrano, J.J., Surpin, M.A., Raikhel, N.V., and Rojo, E.** (2007). Divergent functions of VTI12 and VTI11 in trafficking to storage and lytic vacuoles in Arabidopsis. *Proceedings of the National Academy of Sciences of the United States of America* **104** (9): 3645–3650.
- Santner, A., Calderon-Villalobos, L.I.A., and Estelle, M.** (2009). Plant hormones are versatile chemical regulators of plant growth. *Nature chemical biology* **5** (5): 301–307.
- Sauer, M., Robert, S., and Kleine-Vehn, J.** (2013). Auxin: simply complicated. *Journal of experimental botany* **64** (9): 2565–2577.
- Scheuring, D., Löffke, C., Krüger, F., Kittelmann, M., Eisa, A., Hughes, L., Smith, R.S., Hawes, C., Schumacher, K., and Kleine-Vehn, J.** (2016). Actin-dependent vacuolar occupancy of the cell determines auxin-induced growth repression. *Proceedings of the National Academy of Sciences of the United States of America* **113** (2): 452–457.
- Scheuring, D., Minina, E.A., Krueger, F., Lupanga, U., Krebs, M., and Schumacher, K.** (2024). Light at the end of the tunnel: FRAP assays combined with super resolution microscopy confirm the presence of a tubular vacuole network in meristematic plant cells. *The Plant Cell*: koae243.
- Scheuring, D., Schöller, M., Kleine-Vehn, J., and Löffke, C.** (2015). Vacuolar staining methods in plant cells. *Methods in molecular biology (Clifton, N.J.)* **1242**: 83–92.
- Schleiden, M.J.** (1842). *Grundzüge der Wissenschaftlichen Botanik: Nebst einer Methodologischen Einleitung als Anleitung zum Studium der Pflanze* (Leipzig: W. Engelmann).
- Scorrano, L., Matteis, M.A. de, Emr, S., Giordano, F., Hajnóczky, G., Kornmann, B., Lackner, L.L., Levine, T.P., Pellegrini, L., Reinisch, K., Rizzuto, R., Simmen, T., Stenmark, H., Ungermann, C., and Schuldiner, M.** (2019). Coming together to define membrane contact sites. *Nature Communications* **10** (1): 1287.
- Seguí-Simarro, J.M., and Staehelin, L.A.** (2006). Cell cycle-dependent changes in Golgi stacks, vacuoles, clathrin-coated vesicles and multivesicular bodies in meristematic cells of Arabidopsis thaliana: a quantitative and spatial analysis. *Planta* **223** (2): 223–236.
- Shirakawa, M., Ueda, H., Shimada, T., Koumoto, Y., Shimada, T.L., Kondo, M., Takahashi, T., Okuyama, Y., Nishimura, M., and Hara-Nishimura, I.** (2010). Arabidopsis Qa-SNARE SYP2 proteins localized to different subcellular regions function redundantly in vacuolar protein sorting and plant development. *The Plant journal for cell and molecular biology* **64** (6): 924–935.
- Shvarev, D., Schoppe, J., König, C., Perz, A., Füllbrunn, N., Kiontke, S., Langemeyer, L., Janulienė, D., Schnelle, K., Kümmel, D., Fröhlich, F., Moeller, A., and Ungermann, C.** (2022). Structure of the HOPS tethering complex, a lysosomal membrane fusion machinery. *eLife* **11**: e80901.
- Silady, R.A., Ehrhardt, D.W., Jackson, K., Faulkner, C., Oparka, K., and Somerville, C.R.** (2008). The GRV2/RME-8 protein of Arabidopsis functions in the late endocytic pathway and is required for vacuolar membrane flow. *The Plant journal for cell and molecular biology* **53** (1): 29–41.
- Simon, M.L.A., Platre, M.P., Assil, S., van Wijk, R., Chen, W.Y., Chory, J., Dreux, M., Munnik, T., and Jaillais, Y.** (2014). A multi-colour/multi-affinity marker set to visualize phosphoinositide dynamics in Arabidopsis. *The Plant journal for cell and molecular biology* **77** (2): 322–337.
- Smith, L.G.** (2001). Plant cell division: building walls in the right places. *Nature reviews. Molecular cell biology* **2** (1): 33–39.
- Spartz, A.K., Ren, H., Park, M.Y., Grandt, K.N., Lee, S.H., Murphy, A.S., Sussman, M.R., Overvoorde, P.J., and Gray, W.M.** (2014). SAUR Inhibition of PP2C-D Phosphatases Activates Plasma Membrane H⁺-ATPases to Promote Cell Expansion in ArabidopsisCW. *The Plant Cell* **26** (5): 2129–2142.

- Staiger, C.J., and Blanchoin, L.** (2006). Actin dynamics: old friends with new stories. *Current opinion in plant biology* **9** (6): 554–562.
- Starr, M.L., and Fratti, R.A.** (2019). The Participation of Regulatory Lipids in Vacuole Homotypic Fusion. *Trends in biochemical sciences* **44** (6): 546–554.
- Stefano, G., Renna, L., Wormsbaeher, C., Gamble, J., Zienkiewicz, K., and Brandizzi, F.** (2018). Plant Endocytosis Requires the ER Membrane-Anchored Proteins VAP27-1 and VAP27-3. *Cell reports* **23** (8): 2299–2307.
- Strasser, B., Iwaszkiewicz, J., Michielin, O., and Mayer, A.** (2011). The V-ATPase proteolipid cylinder promotes the lipid-mixing stage of SNARE-dependent fusion of yeast vacuoles. *The EMBO journal* **30** (20): 4126–4141.
- Surpin, M., Zheng, H., Morita, M.T., Saito, C., Avila, E., Blakeslee, J.J., Bandyopadhyay, A., Kovaleva, V., Carter, D., Murphy, A., Tasaka, M., and Raikhel, N.** (2003). The VTI Family of SNARE Proteins Is Necessary for Plant Viability and Mediates Different Protein Transport Pathways. *The Plant Cell* **15** (12): 2885–2899.
- Takáč, T., Pechan, T., Šamajová, O., and Šamaj, J.** (2013). Vesicular trafficking and stress response coupled to PI3K inhibition by LY294002 as revealed by proteomic and cell biological analysis. *Journal of proteome research* **12** (10): 4435–4448.
- Takahashi, K., Hayashi, K.-i., and Kinoshita, T.** (2012). Auxin activates the plasma membrane H⁺-ATPase by phosphorylation during hypocotyl elongation in Arabidopsis. *Plant Physiology* **159** (2): 632–641.
- Takemoto, K., Ebine, K., Askani, J.C., Krüger, F., Gonzalez, Z.A., Ito, E., Goh, T., Schumacher, K., Nakano, A., and Ueda, T.** (2018). Distinct sets of tethering complexes, SNARE complexes, and Rab GTPases mediate membrane fusion at the vacuole in Arabidopsis. *Proceedings of the National Academy of Sciences of the United States of America* **115** (10): E2457–E2466.
- Tamura, Y., Kawano, S., and Endo, T.** (2019). Organelle contact zones as sites for lipid transfer. *Journal of biochemistry* **165** (2): 115–123.
- Tan, J.X., and Finkel, T.** (2022). A phosphoinositide signalling pathway mediates rapid lysosomal repair. *Nature* **609** (7928): 815–821.
- Tan, X., Calderon-Villalobos, L.I.A., Sharon, M., Zheng, C., Robinson, C.V., Estelle, M., and Zheng, N.** (2007). Mechanism of auxin perception by the TIR1 ubiquitin ligase. *Nature* **446** (7136): 640–645.
- Tan, X., Wei, J., Li, B., Wang, M., and Bao, Y.** (2017). AtVps11 is essential for vacuole biogenesis in embryo and participates in pollen tube growth in Arabidopsis. *Biochemical and Biophysical Research Communications* **491** (3): 794–799.
- The Arabidopsis Genome Initiative** (2000). Analysis of the genome sequence of the flowering plant *Arabidopsis thaliana*. *Nature* **408** (6814): 796–815.
- Thomas, C., Tholl, S., Moes, D., Dieterle, M., Papuga, J., Moreau, F., and Steinmetz, A.** (2009). Actin bundling in plants. *Cell motility and the cytoskeleton* **66** (11): 940–957.
- Tominaga, M., Kimura, A., Yokota, E., Haraguchi, T., Shimmen, T., Yamamoto, K., Nakano, A., and Ito, K.** (2013). Cytoplasmic streaming velocity as a plant size determinant. *Developmental cell* **27** (3): 345–352.
- Ueda, H., Yokota, E., Kutsuna, N., Shimada, T., Tamura, K., Shimmen, T., Hasezawa, S., Dolja, V.V., and Hara-Nishimura, I.** (2010). Myosin-dependent endoplasmic reticulum motility and F-actin organization in plant cells. *Proceedings of the National Academy of Sciences of the United States of America* **107** (15): 6894–6899.
- Uemura, T., Morita, M.T., Ebine, K., Okatani, Y., Yano, D., Saito, C., Ueda, T., and Nakano, A.** (2010). Vacuolar/pre-vacuolar compartment Qa-SNAREs VAM3/SYP22 and PEP12/SYP21 have interchangeable functions in Arabidopsis. *The Plant journal for cell and molecular biology* **64** (5): 864–873.

- Uemura, T., and Ueda, T.** (2014). Plant vacuolar trafficking driven by RAB and SNARE proteins. *Current opinion in plant biology* **22**: 116–121.
- Uemura, T., Yoshimura, S.H., Takeyasu, K., and Sato, M.H.** (2002). Vacuolar membrane dynamics revealed by GFP-AtVam3 fusion protein. *Genes to cells devoted to molecular & cellular mechanisms* **7** (7): 743–753.
- Utsunomiya, H., Fujita, M., Naito, F., and Kaneta, T.** (2020). Cell cycle-dependent dynamics of a plant intermediate filament motif protein with intracellular localization related to microtubules. *Protoplasma* **257** (5): 1387–1400.
- Vaškebová, L., Šamaj, J., and Ovecka, M.** (2018). Single-point ACT2 gene mutation in the Arabidopsis root hair mutant der1-3 affects overall actin organization, root growth and plant development. *Annals of botany* **122** (5): 889–901.
- Veytsman, B.A., and Cosgrove, D.J.** (1998). A model of cell wall expansion based on thermodynamics of polymer networks. *Biophysical Journal* **75** (5): 2240–2250.
- Viotti, C., Krüger, F., Krebs, M., Neubert, C., Fink, F., Lupanga, U., Scheuring, D., Boutté, Y., Frescatada-Rosa, M., Wolfenstetter, S., Sauer, N., Hillmer, S., Grebe, M., and Schumacher, K.** (2013). The endoplasmic reticulum is the main membrane source for biogenesis of the lytic vacuole in Arabidopsis. *The Plant Cell* **25** (9): 3434–3449.
- Volkman, D., and Baluška, F.** (1999). Actin cytoskeleton in plants: from transport networks to signaling networks. *Microscopy research and technique* **47** (2): 135–154.
- Vukašinović, N., and Žárský, V.** (2016). Tethering Complexes in the Arabidopsis Endomembrane System. *Frontiers in cell and developmental biology* **4**: 46.
- Wang, J., Cai, Y., Miao, Y., Lam, S.K., and Jiang, L.** (2009). Wortmannin induces homotypic fusion of plant prevacuolar compartments*. *Journal of experimental botany* **60** (11): 3075–3083.
- Wang, L., Merz, A.J., Collins, K.M., and Wickner, W.** (2003). Hierarchy of protein assembly at the vertex ring domain for yeast vacuole docking and fusion. *The Journal of cell biology* **160** (3): 365–374.
- Wang, L., Seeley, E.S., Wickner, W., and Merz, A.J.** (2002). Vacuole fusion at a ring of vertex docking sites leaves membrane fragments within the organelle. *Cell* **108** (3): 357–369.
- Wang, P., Duckney, P., Gao, E., Hussey, P.J., Kriechbaumer, V., Li, C., Zang, J., and Zhang, T.** (2023). Keep in contact: multiple roles of endoplasmic reticulum-membrane contact sites and the organelle interaction network in plants. *New Phytol* **238** (2): 482–499.
- Wang, P., Hawkins, T.J., Richardson, C., Cummins, I., Deeks, M.J., Sparkes, I., Hawes, C., and Hussey, P.J.** (2014). The plant cytoskeleton, NET3C, and VAP27 mediate the link between the plasma membrane and endoplasmic reticulum. *Current Biology* **24** (12): 1397–1405.
- Wang, P., and Hussey, P.J.** (2017). NETWORKED 3B: a novel protein in the actin cytoskeleton-endoplasmic reticulum interaction. *Journal of experimental botany* **68** (7): 1441–1450.
- Wang, P., Richardson, C., Hawkins, T.J., Sparkes, I., Hawes, C., and Hussey, P.J.** (2016). Plant VAP27 proteins: domain characterization, intracellular localization and role in plant development. *New Phytol* **210** (4): 1311–1326.
- Wickner, W.** (2010). Membrane fusion: five lipids, four SNAREs, three chaperones, two nucleotides, and a Rab, all dancing in a ring on yeast vacuoles. *Annual review of cell and developmental biology* **26**: 115–136.
- Wink, M.** (1993). The plant vacuole: a multifunctional compartment. *Journal of experimental botany* **44**: 231–246.
- Wong, J.H., Spartz, A.K., Park, M.Y., Du, M., and Gray, W.M.** (2019). Mutation of a Conserved Motif of PP2C.D Phosphatases Confers SAUR Immunity and Constitutive Activity. *Plant Physiology* **181** (1): 353–366.

- Ye, H., Gao, J., Liang, Z., Lin, Y., Yu, Q., Huang, S., and Jiang, L.** (2022). Arabidopsis ORP2A mediates ER-autophagosomal membrane contact sites and regulates PI3P in plant autophagy. *Proceedings of the National Academy of Sciences of the United States of America* **119** (43): e2205314119.
- Zang, J., Klemm, S., Pain, C., Duckney, P., Bao, Z., Stamm, G., Kriechbaumer, V., Bürstenbinder, K., Hussey, P.J., and Wang, P.** (2021). A novel plant actin-microtubule bridging complex regulates cytoskeletal and ER structure at ER-PM contact sites. *Current biology CB* **31** (6): 1251-1260.e4.
- Zhang, Y., Berman, A., and Shani, E.** (2023). Plant Hormone Transport and Localization: Signaling Molecules on the Move. *Annual review of plant biology* **74**: 453–479.
- Zheng, H., and Staehelin, L.A.** (2011). Protein storage vacuoles are transformed into lytic vacuoles in root meristematic cells of germinating seedlings by multiple, cell type-specific mechanisms. *Plant Physiology* **155** (4): 2023–2035.
- Zheng, J., Han, S.W., Rodriguez-Welsh, M.F., and Rojas-Pierce, M.** (2014). Homotypic vacuole fusion requires VTI11 and is regulated by phosphoinositides. *Molecular plant* **7** (6): 1026–1040.

8 Curriculum Vitae

Personal Details

Name: Sabrina Kaiser
 Date of birth: personal information
 Place of birth: personal information
 Address: personal information

Education

Since 2018	PhD candidate RPTU Kaiserslautern-Landau/TU Kaiserslautern in plant cell biology Thesis: „The characterization of the vacuole – actin cytoskeleton connection in <i>Arabidopsis thaliana</i> “ Prize: best poster award (“Botanik-Tagung”, Bonn, 2022)
2013 – 2016	Master of Science TU Kaiserslautern in Microbial and Plant Biotechnology Thesis: „Die Regulation durch nicht-codierende csRNAs in <i>Streptococcus pneumoniae</i> : Eine Deletionsanalyse“
2010 – 2013	Bachelor of Science TU Kaiserslautern in Biowissenschaften Thesis: „Phänotypische und genetische Analysen von <i>Botrytis fabae</i> und <i>Botrytis cinerea</i> im Vergleich“ Prize: best graduate of the year (“Akademische Jahresfeier”, 2014)
2001 – 2010	Abitur Leibniz Gymnasium Neustadt/Wstr.

Employment history

Since 02/2024	Research associate (plant cell biology) in the group of PD Dr. David Scheuring, department of plant pathology, RPTU Kaiserslautern-Landau
07/2018 – 06/2023	Research associate (plant cell biology) in the group of PD Dr. David Scheuring, department of plant pathology, RPTU Kaiserslautern-Landau /TU Kaiserslautern
05/2017 – 06/2018	Research associate (molecular biology) in the group of PD Dr. Reinhold Brückner, department of microbiology, TU Kaiserslautern
12/2016 – 03/2017	Research assistant (geomicrobiology) in the group of Dr. Michelle Gehringer, department of plant ecology, TU Kaiserslautern
09/2014, 11/2015 – 02/2016, 10/2016 – 01/2017	Research assistant/course supervisor in the department of microbiology, TU Kaiserslautern
09 – 10/2013	Laboratory intern (grapevine biotechnology) in the group of Prof. Dr. Günther Buchholz, department of grapevine biotechnology, AIPlanta, Institute for Plant Research RLP AgroScience GmbH, Neustadt/Wstr.

List of publications

- 2024 Mueller, J., Koenig, Y., Kaiser, S., Loeffke, C., Krebs, M., & Scheuring, D. (2024). Salicylic Acid restricts cell elongation and induces changes of vacuolar morphology and pH. *bioRxiv*, 2024-09.
- 2023 Kaiser, S., Mehlhorn, D., Miranda, P. R., Ries, F., Sommer, F., Schroda, M., Schumacher, K., Willmund, F., Grefen, C. & Scheuring, D. (2023). Networked proteins redundantly interact with VAP27 and RABG3 to regulate membrane tethering at the vacuole and beyond. *bioRxiv*, 2023-09.
- Jeblick, T., Leisen, T., Steidele, C. E., Albert, I., Müller, J., Kaiser, S., Mahler, F., Sommer, F., Keller, S., Hueckelhoven, R., Hahn, M., & Scheuring, D. (2023). *Botrytis* hypersensitive response inducing protein 1 triggers noncanonical PTI to induce plant cell death. *Plant Physiology*, 191(1), 125-141.
- 2021 Kaiser, S., Eisele, S., & Scheuring, D. (2021). Vacuolar occupancy is crucial for cell elongation and growth regardless of the underlying mechanism. *Plant Signaling & Behavior*, 16(8), 1922796.
- 2020 Kaiser, S., & Scheuring, D. (2020). To lead or to follow: contribution of the plant vacuole to cell growth. *Frontiers in Plant Science*, 11, 553.
- Kaiser, S., Hoppstädter, L. M., Bilici, K., Heieck, K., & Brückner, R. (2020). Control of acetyl phosphate-dependent phosphorylation of the response regulator CiaR by acetate kinase in *Streptococcus pneumoniae*. *Microbiology*, 166(4), 411-421.
- 2019 Kaiser, S., Eisa, A., Kleine-Vehn, J., & Scheuring, D. (2019). NET4 modulates the compactness of vacuoles in *Arabidopsis thaliana*. *International Journal of Molecular Sciences*, 20(19), 4752.

Talk and Poster Contributions

- 2024 Talk at European Network of Plant Endomembrane Research (ENPER) meeting, Porto (Portugal)
- 2022 Poster at International Conference of the German Society for Plant Sciences (Botanik-Tagung), Bonn (Germany)
- Talk at Fachbereichsseminar Biologie, Thallichtenberg (Germany)
- 2021 Poster (video & livestream presentation) at Plant Cell Dynamics (PCD) meeting, online meeting (USA)
- 2019 Talk at European Network of Plant Endomembrane Research (ENPER) meeting, Valencia (Spain)
- Talk at Fachbereichsseminar Biologie, Thallichtenberg (Germany)
- 2018 Poster at European Network of Plant Endomembrane Research (ENPER) meeting, Vienna (Austria)

9 Acknowledgements

First of all, I would like to thank PD Dr. David Scheuring for entrusting me with this fascinating project and being a great doctoral supervisor. While he gave me guidance throughout this thesis, he also gave me plenty of freedom to follow my ideas and the opportunity to try out a number of different techniques that were not yet established in our lab. At the same time, he always lent me an ear and made time to discuss results and upcoming challenges. This open and motivational working atmosphere surely helped me developing as a scientist.

I also would like to express my gratitude to Prof. Dr. Matthias Hahn for not only welcoming me in the department of plant pathology and literally providing our small plant cell biology group the room to work in, but always being interested in my work and making helpful suggestions.

Prof. Dr. Stefanie Müller-Schüssele as well as Prof. Dr. Ekkehard Neuhaus, I thank for embracing the roles as my second examiner and head of the examination board, respectively.

Further thanks go to Prof. Dr. Michael Schroda, Prof. Dr. Karin Schumacher and Dr. Melanie Krebs for their time to discuss my research progress and giving me valuable advice. I also am thankful to all the people that provided guidance for different experiments: Prof. Dr. Felix Willmund and Dr. Fabian Ries, who helped me planning Co-IP experiments and showed me how to use Perseus software to evaluate MS data; Dr. Rachel Röhrich, who answered several questions about CRISPRing. Another thank you goes to Prof. Dr. Christopher Grefen for the possibility to visit his lab in Bochum and Dr. Dietmar Mehlhorn, who showed me the experimental procedure of mbSUS in yeast and also the cool places at the Campus during my stay.

I also want to say thank you to all my co-workers in the lab for the constant mutual support and our great time together. I enjoyed all the little or sometimes also longer chats with you and am very grateful for every reassuring word, when days were sometimes exhausting or things did not work out as planned. It wouldn't have been as fun without you all!

In this regard, I further want to thank all my friends and former fellow students that accompanied me along the way. Especially Achim Herrmann, who attended nearly all lectures and practical with me since the first semester and whom I probably spent most time with at university. With great joy, I will always look back on the lunch breaks we spent together in the university canteen. Moreover, I want to show my appreciation to Roman Kowalew for the constant supply of silly animal pictures. These often made my day in the most random situations.

I am also grateful to my family, who approved my road of life since I was little and tried their best to support my academic ambitions, even when times were hard due to the illnesses of my parents.

Finally, a special thank you goes to my boyfriend Markus Fögen for making every day, good or bad, a better day. You always encouraged me when things were getting stressful and helped me living through the most difficult times when my father was on his deathbed. I am grateful for every cup of tea and piece of cake you gave me while I was writing this thesis. You were a great support throughout this whole journey!

10 Declaration of Originality

I hereby declare that this cumulative thesis has been written only by me. I confirm that no other than the indicated sources and materials have been used for this work. I have not submitted this thesis or parts of it for graduation elsewhere.

My personal contribution to the presented articles in this thesis is clarified in the following section.

Kaiser, Sabrina

Place, Date

11 Declaration of personal contribution

Sabrina Kaiser

Characterization of the vacuole-cytoskeleton relationship in *Arabidopsis thaliana*

Article 1:

“NET4 Modulates the Compactness of Vacuoles in *Arabidopsis thaliana*”

Published in the International Journal of Molecular Sciences 20(19):4752, in October 2019 (<https://doi.org/10.3390/ijms20194752>).

Authors: Sabrina Kaiser, Ahmed Eisa, Jürgen Kleine-Vehn, and David Scheuring

Personal contribution to this article:

The *net4a net4b* double mutant was established personally by crossing *net4a-1* and *net4b*. Experiments for figure 3 and 4 as well as for supplementary figure S2A and C were carried out personally. Data analysis and interpretation as well as figure assembly was carried out together with PD Dr. David Scheuring. Writing of the manuscript was carried out mainly by PD Dr. David Scheuring and Prof. Dr. Jürgen Kleine-Vehn with contributions by me.

Experiments for figure 1, 2A-D and supplementary figure S1 and S3 were performed by PD Dr. David Scheuring. He also generated the 35S::NET4A-GFP (NET4A-GFP^{OE}) line. Experiments for figure 2E-G and most experiments for supplementary figure S2 were performed by Dr. Ahmed Eisa.

Article 2:

“Vacuolar occupancy is crucial for cell elongation and growth regardless of the underlying mechanism”

Published in Plant Signaling & Behavior 16(8):1922796, in May 2021 (<https://doi.org/10.1080/15592324.2021.1922796>).

Authors: Sabrina Kaiser, Sophie Eisele, David Scheuring

Personal contribution to this article:

Preparation of all figures, data analysis and experiments for figure 1 were carried out personally. Experiments for figure 2 were performed by Sophie Eisele under my supervision. Interpretation of results and writing of the manuscript was conducted together with PD Dr. David Scheuring, in which I had the leading part in preparing the manuscript.

Article 3:

“Networked proteins redundantly interact with VAP27 and RABG3 to regulate membrane tethering at the vacuole and beyond”

Published as a preprint on bioRxiv in September 2023; updated version 2 from February 2024 (<https://doi.org/10.1101/2023.09.29.560113>).

Authors: Sabrina Kaiser, Dietmar Mehlhorn, Paulina Ramirez Miranda, Fabian Ries, Frederik Sommer, Michael Schroda, Karin Schumacher, Felix Willmund, Christopher Grefen and David Scheuring

Personal contribution to this article:

Most experiments were carried out personally. Almost all plant vector constructs were cloned and nearly all stably transformed Arabidopsis lines established personally. All CRISPR/Cas9 based mutants and crossed lines were established personally as well. Furthermore, the material for recombinant protein expression in *E. coli* and part of the vector constructs for rBiFC and mbSUS experiments were generated personally. Data analysis and interpretation, as well as figure assembly was carried out with contribution of PD Dr. David Scheuring. Writing of the manuscript was conducted together with PD Dr. David Scheuring.

The following experiments were performed and the following constructs were generated by students under my supervision: The truncated NET4A-GFP fusion constructs were cloned by Anne Lau. For figure 6B, Benjamin Ziehmer performed localization studies using the truncated NET4A-GFP fusions in *N. benthamiana* for his bachelor thesis. Additionally, he performed the experiments shown in supplementary figure S7A and B. Sophie Eisele performed the root growth experiment shown in supplementary figure S1D. RT-qPCR experiments shown in supplementary figure S1E were performed by Johanna Abel during her bachelor thesis. Genotyping of the CRISPR/Cas9 based mutants *net3c* and *net3c net4a net4b* #1 was partly carried out by Paulina Ramirez Miranda during her master thesis. In addition, Paulina Ramirez Miranda performed part of the experiments for figure 7A and all experiments shown in figure 7B. Lastly, she contributed all data for supplementary figure S12.

For figure 4, the DEX-inducible *amiR-vps16* line was provided by Prof. Dr. Karin Schumacher (Heidelberg). For figure 5, Dr. Fabian Ries (lab of Prof. Dr. Felix Willmund, Kaiserslautern) helped planning the experimental outline of the Co-IPs and provided technical help for using Perseus software. Dr. Frederik Sommer (lab of Prof. Dr. Michael Schroda, Kaiserslautern) conducted MS-MS analysis and provided processed MS data. Dr. Dietmar Mehlhorn (lab of Prof. Dr. Christopher Grefen, Bochum) cloned part of the constructs for mbSUS and rBiFC experiments, performed rBiFC experiments as well as part of the mbSUS experiments, and

provided the analyzed results and pictures for figure 5C and supplementary figure S6. Dr. Dietmar Mehlhorn further provided guidance and technical help during the mbSUS experiments shown in figure 6D, E, G and supplementary figure S8 that were conducted by me.

Article 4:

“To Lead or to Follow: Contribution of the Plant Vacuole to Cell Growth”

Published in Frontiers in Plant Science 11:553, in May 2020
(<https://doi.org/10.3389/fpls.2020.00553>).

Authors: Sabrina Kaiser, David Scheuring

Personal contribution to this article:

Figure preparation and writing of the manuscript was carried out together with PD Dr. David Scheuring.

The presented evaluation for the contribution of third parties was mutually agreed with the aforementioned persons.

Date, Sabrina Kaiser

Date, PD Dr. David Scheuring

12 Declaration of used tools and assistance

Sabrina Kaiser

Characterization of the vacuole-cytoskeleton relationship in *Arabidopsis thaliana*

Devices and software used for execution of experiments and processing of data, shown in the presented articles, are indicated in the respective articles. Furthermore, the following software were used for this work:

ZEN 2.3 (blue edition) and ZEN 2.3 (black edition) were used for processing of microscopy images. CorelDRAW 2021 and GIMP2.10 were used for drawing schematics and assembling figures. Microsoft Excel 2016 and Microsoft Word 2016 were used for preparing tables and writing this thesis, respectively. Citavi 6 was used for managing references.

Date, Sabrina Kaiser

13 Full articles for this cumulative thesis

13.1 Article 1

“NET4 Modulates the Compactness of Vacuoles in *Arabidopsis thaliana*”



Article

NET4 Modulates the Compactness of Vacuoles in *Arabidopsis thaliana*

Sabrina Kaiser ^{1,†}, Ahmed Eisa ^{2,3,†}, Jürgen Kleine-Vehn ²  and David Scheuring ^{1,2,*}

¹ Plant Pathology, University of Kaiserslautern, 67663 Kaiserslautern, Germany; kaisers@rhrk.uni-kl.de

² Department of Applied Genetics and Cell Biology, University of Natural Resources and Applied Life Sciences (BOKU), 1190 Vienna, Austria; Ahmed.Eisa@lmu.de (A.E.); juergen.kleine-vehn@boku.ac.at (J.K.-V.)

³ Current address: Plant Biochemistry and Physiology, Ludwig-Maximilians-University Munich, 80539 Munich, Germany

* Correspondence: scheurin@rhrk.uni-kl.de; Tel.: +49-631-2052219

† These authors contributed equally to this work.

Received: 22 August 2019; Accepted: 23 September 2019; Published: 25 September 2019



Abstract: The dimension of the plants largest organelle—the vacuole—plays a major role in defining cellular elongation rates. The morphology of the vacuole is controlled by the actin cytoskeleton, but molecular players remain largely unknown. Recently, the Networked (NET) family of membrane-associated, actin-binding proteins has been identified. Here, we show that NET4A localizes to highly constricted regions of the vacuolar membrane and contributes to vacuolar morphology. Using genetic interference, we found that deregulation of NET4 abundance increases vacuolar occupancy, and that overexpression of NET4 abundance decreases vacuolar occupancy. Our data reveal that NET4A induces more compact vacuoles, correlating with reduced cellular and organ growth in *Arabidopsis thaliana*.

Keywords: *Arabidopsis*; cell biology; cell size; plant growth; vacuole; actin cytoskeleton; vacuolar occupancy; compactness

1. Introduction

Vacuolar size correlates and contributes to cell size determination, thereby defining cellular elongation rates [1–3]. In animals, the cytoskeleton plays an important role for maintaining cellular shape and especially actin has been shown to regulate cell shape and thereby cell size [4,5]. Since plants are surrounded by shape-giving cell walls, the actin cytoskeleton cannot directly impact on cell shape. Nevertheless, it was demonstrated that actin filaments play a direct role in regulating structural changes of the vacuole [6,7]. The phytohormone auxin impacts on actin filament organization [8–10] as well as on vacuolar morphology. Here, auxin induces tonoplast constrictions [1] which in turn leads to a reduction of cellular space occupied by the vacuole [2]. Notably, genetic or pharmacological impairment of the actin–myosin system abolished auxin-induced changes of the vacuole and restored meristematic cell-size control and root organ growth in *Arabidopsis* [2].

Due to the close proximity of the vacuolar membrane (tonoplast) and actin filaments it has been suggested that there might be a direct physical connection [11]. However, little is known about involved molecular players and the employed mechanism for this connection. In a screen for GFP-fusion proteins labelling actin filaments, the plant-specific Networked (NET) family was identified [12]. NET proteins possess an actin-binding region and are membrane-associated, thus they specifically link actin filaments to cell organelles. From the 13 identified family members, NET4A and NET4B could potentially impact on the actin–vacuole interface, since NET4A has been shown to bind actin and overlaps with the tonoplast [12].

2. Results

2.1. NET4A Shows a Bead-on-a-String Pattern at the Tonoplast

To investigate the potential role of NET4 proteins in vacuolar morphology, we initially inspected NET4A::NET4A-GFP localization in root epidermal cells of *Arabidopsis thaliana* seedlings. While NET4A-GFP under its endogenous promoter (hereafter referred to as NET4A-GFP) is weakly detectable in meristematic cells [1], we noted that it is preferentially expressed in the late meristematic zone, correlating with the onset of cellular elongation (Figure 1a). The root epidermis is regularly spaced between longer atrichoblast and shorter trichoblast cells, which later differentiate into non-hair and root-hair cells [13]. NET4A expression seems to precede in trichoblast cells and is more tightly associated with the onset of elongation in the atrichoblast cells (Figure 1a and Figure S1a,b). To confirm vacuolar localization of the NET4A-GFP signal, tonoplast staining using FM4-64 [14] was employed. NET4A-GFP did not only show a typical tonoplast signal and colocalization with the endocytic dye FM4-64, but also displayed a more filamentous signal distribution in the cell cortex, suggesting a dual localization (Figure 1b,c). This cortical NET4A-GFP signal (Figure 1c) strongly resembles actin filaments, which is in agreement with its in vitro actin binding capacity [12].

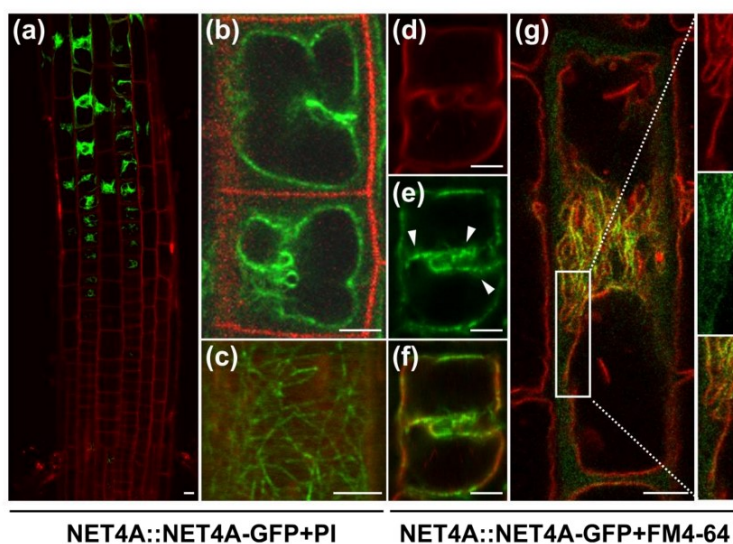


Figure 1. NET4A shows a bead-on-a-string pattern at the tonoplast. (a) NET4A-GFP expression under the endogenous promoter in *Arabidopsis* roots. Expression starts in the late meristem, initially only in trichoblast cells. (b) NET4A-GFP signal distribution in atrichoblast cells of the root epidermis. (c) Filamentous NET4A-GFP signals at the root cell cortex. (d–f) Vacuole staining by FM4-64 (3 h) shows NET4A localization preferentially at curved tonoplast areas. (g) NET4A-GFP signal accumulation at constrictions in elongating root cells. Detail: areas with folded tonoplast membranes show stronger NET4A-GFP accumulation in comparison to expanding areas. White arrowheads highlight punctate signals. Propidium iodide was used to stain the cell exterior, FM4-64 to stain the tonoplast. Scale bars: 5 μ m.

2.2. NET4A Localizes to Highly Constricted Vacuolar Membranes

NET4A-GFP distribution at the tonoplast was not uniform but showed a stronger vacuolar label in the center of the cell, correlating with regions of higher vacuolar constrictions (Figure 1d–f). Vacuoles are highly constricted in meristematic cells and dramatically increase in volume during cellular elongation [3]. In agreement, in elongating cells the NET4A-GFP accumulation at the tonoplast correlated well with the remaining membrane constrictions (Figure 1g). In line with this, elongated

root cells, possessing fully expanded vacuoles with no or only little constrictions, displayed only a very faint NET4A-GFP signal (Figure S1c).

To assess if NET4A-GFP accumulation indeed correlates with vacuolar constrictions, we next induced alterations in vacuolar morphology. The phytohormone auxin reduces vacuolar size by inducing smaller luminal vacuoles [1,2]. We used the synthetic auxin naphthalene acetic acid (NAA) and the auxin biosynthesis inhibitor kynurenine (kyn) to increase and decrease vacuolar constrictions in the root cells, respectively. In late meristematic cells, auxin treatment (200 nM NAA) induced vacuolar constrictions and a more uniform colocalization of NET4A-GFP with FM4-64 at the tonoplast (Figure 2a,b). On the contrary, kyn-induced reduction of vacuolar constrictions correlated with faint NET4A-GFP localization at the tonoplast (Figure 2c), being reminiscent of fully elongated cells. Auxin does not markedly interfere with NET4A-GFP intensity of already highly constricted vacuoles in meristematic cells [1], but in late meristematic cells the overall signal intensity of NET4A was detectably increased and decreased in auxin treated and deprived cells, respectively (Figure 2d).

To confirm this finding, we determined NET4A levels in response to increasing auxin concentrations by immunoblotting. Using a GFP antibody, we analyzed NET4A-GFP signal intensity in whole root extracts (Figure 2e). In a dosage-dependent manner, NAA application increased the NET4A-GFP protein amounts (Figure 2f). On the other hand, auxin application did neither elevate endogenous *NET4A* nor *NET4B* expression (Figure 2g). This indicates that auxin treatment leads to a higher NET4A protein abundance which is independent of transcriptional regulation. This set of data suggests that NET4A is recruited to highly constricted regions of the tonoplast, which possibly indirectly modulates protein levels of NET4A.

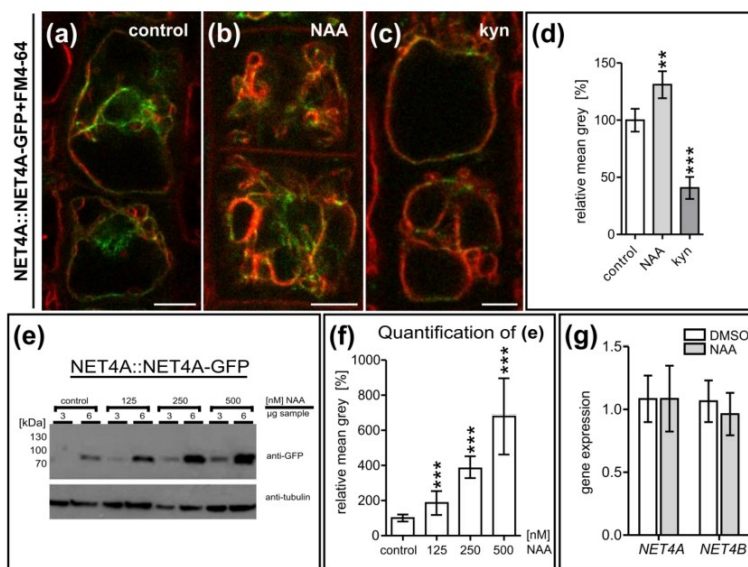


Figure 2. NET4A localizes to highly constricted vacuolar membranes. (a–c) Altered NET4A-GFP protein abundance upon exogenous auxin (NAA) application and depletion by the auxin biosynthesis inhibitor kynurenine (kyn). Seedlings were treated with DMSO as control ($n = 17$), 250 nM NAA ($n = 15$) and 3 μ M kyn ($n = 15$). Five cells per root were considered. (d) Quantification of signal intensity. (e) Western blot analysis of NET4A-GFP (endogenous promoter) abundance upon rising NAA concentration. *Arabidopsis* root tissue was probed using a GFP-antibody. To avoid signal saturation, two different sample concentrations were loaded (3 and 6 μ g). (f) Signal intensity of the individual NET4A-GFP bands were quantified in respect to the corresponding tubulin control bands. (g) To test for auxin-induced gene expression changes, qRT-PCR for both NET4 family members, *NET4A* and *NET4B*, was carried out. Error bars represent s.e.m. Student's *t*-test, *p*-values: ** $p < 0.01$; *** $p < 0.001$. Scale bars: 5 μ m.

2.3. NET4A Impacts on Vacuolar Morphology

To investigate NET4A function in maintaining vacuolar morphology, we isolated *net4a* and *net4b* knock-out lines (Figure S2a–d). We next investigated the NET4-dependent effect on vacuolar morphology in late meristematic cells, because they mark the onset of NET4A expression. We used the vacuolar morphology index (VMI) [1–3], which depicts the size of the biggest luminal vacuolar structure and is highly sensitive to reveal alterations in vacuolar morphology. Both *net4a-1* (SALK_017623) and *net4b* (SALK_056957) mutants displayed more spherical vacuoles accompanied with increased VMI (Figure S2e–h). To confirm that this phenotype is attributable to *NET4* gene function, we analyzed two additional alleles, *net4a-3* (SALK_010530C) and *net4a-4* (SALK_083604C). Both lines showed a significant increase of the VMI (Figure S2i,j). Thus, we concluded that the observed phenotype is linked to *NET4A* gene function. Together, this suggests that NET4 association at the constricted vacuolar membranes impact on vacuolar morphology.

Subsequently, we used *net4a-1* for crossing with *net4b*, creating a double mutant (hereafter referred to as *net4a net4b*). Although the *net4a net4b* double mutant also showed more spherical vacuoles, the VMI was largely not distinguishable from the single mutants (Figure 3b,d and Figure S2f–h). This proposes a higher redundancy in the actin–vacuole pathway.

Next we generated 35S::NET4A-GFP (hereafter referred to as NET4A-GFP^{OE}) overexpression lines to assess ectopic NET4A expression. NET4A-GFP^{OE} lines showed expression throughout the root, including the meristematic region. The subcellular characteristics of NET4A-GFP^{OE} remained, showing the filamentous signal at the cell cortex and the enhanced labelling of constricted tonoplast membranes (Figure S3a–f). Interestingly, trichoblast cells, possessing more compact and constricted vacuoles, showed a higher signal intensity when compared to atrichoblast cells (Figure S3g–i). To assess the effect of NET4A overexpression on vacuolar morphology, the VMI for NET4A-GFP^{OE} was determined. Markedly, NET4A overexpression lines showed more roundish vacuoles (Figure 3c), and increased VMI in comparison to the control (Figure 3d). Accordingly, we conclude that NET4A overexpression as well as *net4a* loss-of-function induces more roundish vacuoles. This finding is reminiscent to the stabilization and depolymerization of the actin cytoskeleton, which also both induce more roundish vacuoles and increase the VMI [2].

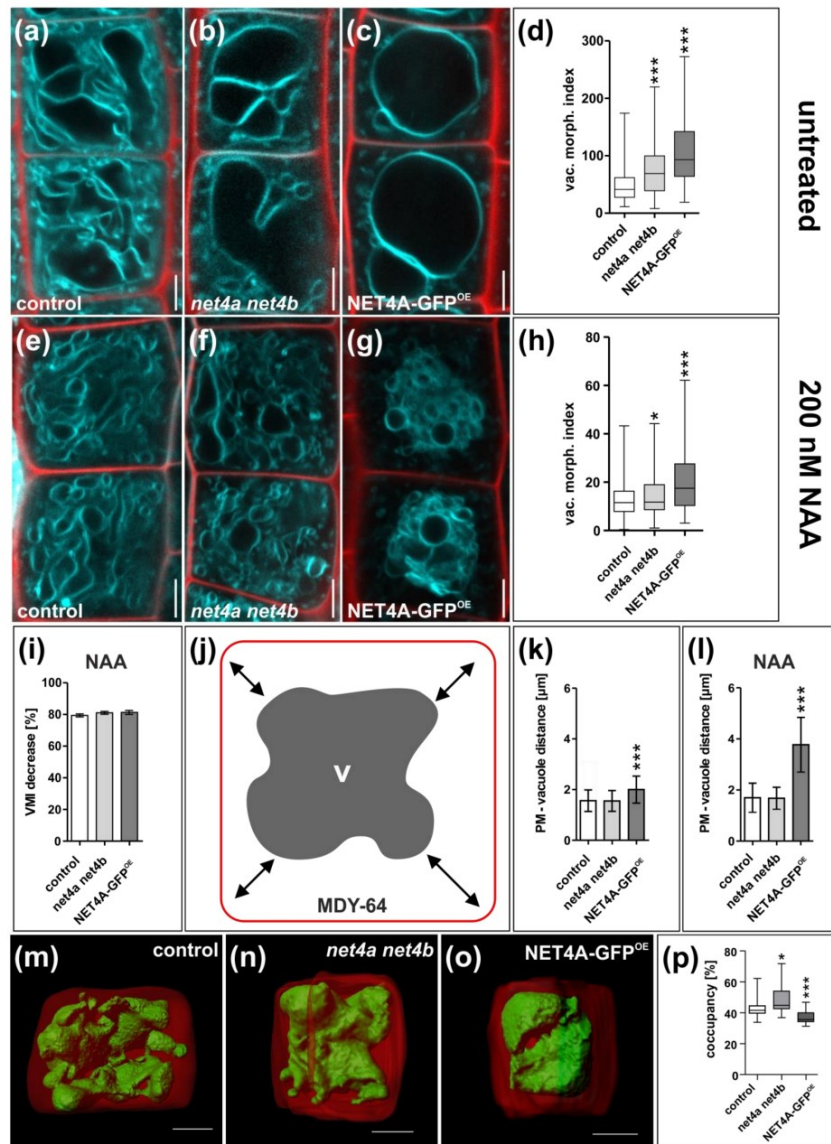


Figure 3. NET4 abundance impacts on vacuolar morphology, modulating compactness. (a–d) Vacuolar morphology in the late root meristem of the *net4a net4b* double knockout line ($n = 145$) and of the NET4A-GFP line driven by the 35S promoter (NET4A-GFP^{OE}; $n = 99$) in comparison to the Col-0 control ($n = 334$). (e–h) Vacuolar morphology upon auxin treatment (200 nM NAA) in the control ($n = 147$), *net4a net4b* ($n = 153$) and NET4A-GFP^{OE} ($n = 88$) line. (i) Relative VMI decrease. (j) Vacuolar compactness was assessed by measuring plasma membrane to vacuole distance based on MDY-64 staining. The distance was measured in every cell corner and the mean calculated. (k) Quantification of plasma membrane to vacuole distance in *net4a net4b* ($n = 72$) and NET4A-GFP^{OE} ($n = 22$) in comparison to the Col-0 control ($n = 75$). (l) Quantification of auxin-induced changes (200 mM, 20h) of plasma-membrane–vacuole distance in the control ($n = 59$), *net4a net4b* ($n = 42$) and NET4A-GFP^{OE} ($n = 20$). (m–o) Three-dimensional reconstructions of PI-stained cell wall (red) and BCECF-stained vacuole (green) of late meristematic cells from control ($n = 20$), *net4a net4b* ($n = 19$) and NET4A-GFP^{OE} ($n = 22$) lines. (p) Quantification of vacuolar occupancy of the cell. Columns of bar charts represent mean values, error bars represent s.e.m. Box limits of boxplots represent 25th percentile and 75th percentile, horizontal line represents median. Whiskers display minimum to maximum values. Student's *t*-test, *p*-values: * $p < 0.05$; *** $p < 0.001$. Scale bars: 5 μ m.

2.4. NET4 and Auxin Spatially Define Vacuolar Occupation within the Cell

To further assess the contribution of NET4 controlling vacuolar morphology, we used auxin to induce vacuolar constrictions. Following the exogenous application of auxin (200 nM, 20 h), vacuoles of *net4a net4b* double mutants and the NET4A-GFP^{OE} line were slightly less constricted when compared to wild type seedlings (Figure 3e–h). However, considering that untreated *net4a net4b* double mutants and the NET4A-GFP^{OE} lines showed already more roundish vacuoles and higher VMIs, the relative responses were not distinguishable from wild type seedlings (Figure 3i).

Based on our data, we conclude that NET4 activity affects vacuolar morphology, but does not have a major impact on the auxin effect on vacuolar shape.

However, when inspecting vacuoles of NET4A-GFP^{OE} we noted that vacuoles seemed more condensed around the nucleus, showing a larger distance to the plasma membrane (Figure 3j). Accordingly, we quantified vacuolar distance to the plasma membrane (PM) in the respective genotypes and revealed that NET4A-GFP^{OE} indeed affected this cellular trait (Figure 3k). Auxin treatments did not alter the PM to vacuole distance in wild type, but considerably increased PM to vacuole distance in NET4A-GFP^{OE} (Figure 3l).

Next, we assessed the relative vacuolar volume of *net4a net4b* double mutants and the NET4A-GFP^{OE} line in late meristematic root cells. For that, we recorded z-stacks from cells stained with a combination of the fluorescent dye BCECF (2',7'-Bis-(2-carboxyethyl)-5(6)-carboxyfluorescein), accumulating in the vacuolar lumen, with propidium iodide, staining the exterior of cells [14]. Three-dimensional rendering of cellular and vacuolar volume allowed us to calculate the space the vacuole occupies in a given cell (vacuolar occupancy of the cell) [2]. In comparison to the control (Figure 3m), the occupancy of double mutant (Figure 3n) was increased and that of the overexpressor (Figure 3o) significantly decreased, respectively (Figure 3p). Furthermore, while control vacuoles showed tubular connections between clearly distinguishable substructures NET4 deregulation seems to render the vacuole less constricted and more spherical in general (Supplemental Movies S1–S3). Based on this set of data, we conclude that NET4 deregulation leads to vacuoles that are more spherical and in addition, that NET4A overexpression induces highly compact vacuoles.

2.5. NET4A-Dependent Compacting of the Vacuole Correlates with Reduced Cell Size and Root Organ Growth

Changes in vacuolar morphology correlate with stomata movement [15] and overall cellular elongation rates [1,3,16,17]. Therefore, we initially investigated whether NET4 proteins impact on cell size in the meristematic region (Figure 4a) [18]. This region displays not only the onset of NET4A expression, but also marks the transition of cells entering the elongation zone. While cell size in the *net4a net4b* double mutant remained unchanged in comparison to the control, NET4A-GFP^{OE} showed a significant reduction in cell length (Figure 4b). In agreement, the altered cell size determination correlated with reduced root organ growth (Figure 4c–e).

Considering that auxin treatment was additive to the NET4A effect on the compactness of vacuoles, we next assessed cell length and root length changes upon NAA treatment in the *net4a net4b* double mutant and in the NET4A-GFP^{OE} lines. Based on the untreated lines, we calculated the relative cell and root length. For this, cell length and root growth were set to 100% in untreated lines and used to normalize auxin-treated cells and roots. The atrichoblast cell length of *net4a net4b* as well as NET4A-GFP^{OE} were partially resistant to auxin (200 nM NAA) when compared to wild type (Figure 4f). NET4A overexpression also caused a reduced root growth sensitivity to exogenous auxin (125 nM NAA) (Figure 4g–i).

Taken together, we show that NET4A localizes to highly constricted regions in the vacuolar membrane and contributes to the compactness of the vacuole. We moreover show that the NET4A-induced changes in vacuolar shape also impacts on cellular and organ growth.

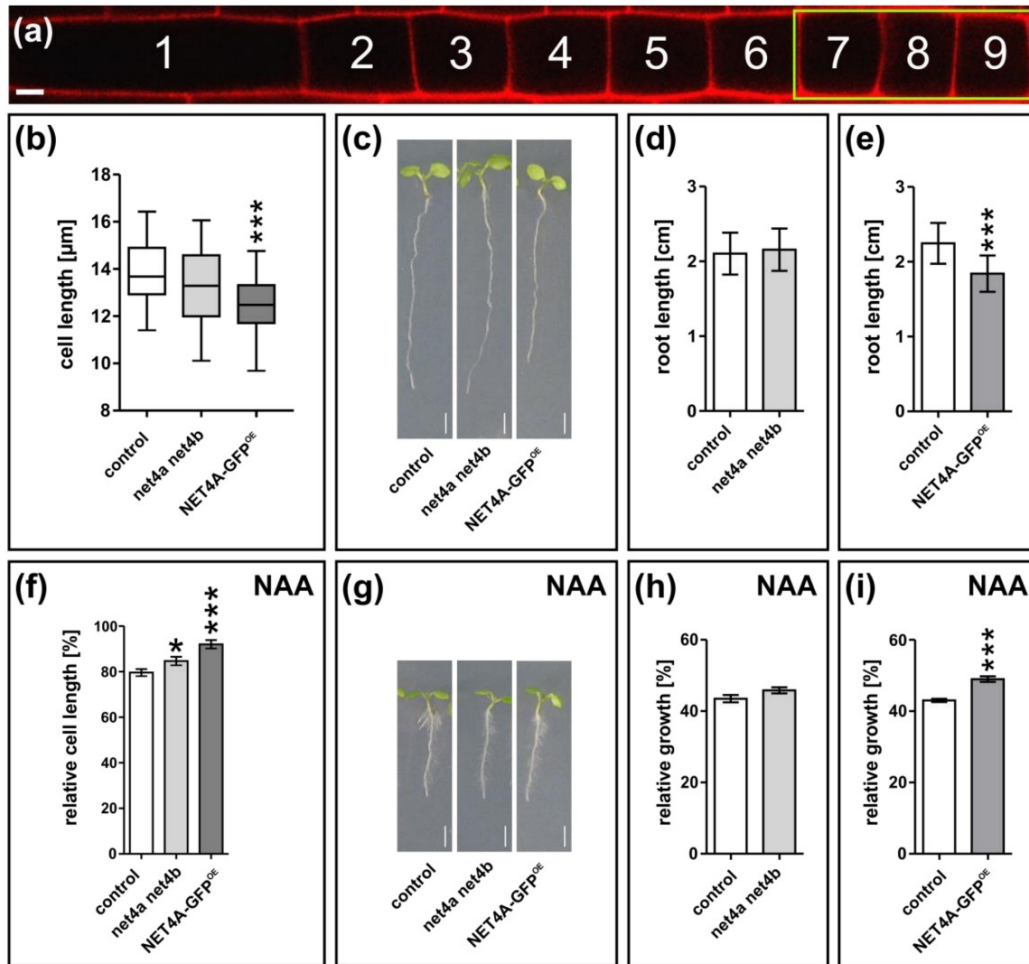


Figure 4. NET4A-dependent compacting of the vacuole correlates with reduced cell size and root organ growth. (a) Representative atrichoblast cell file for cell length quantification. The green box marks the three quantified cells per file (7 to 9). (b) Cell length of the *net4a net4b* ($n = 81$) double knockout line and of the NET4A-GFP line driven by the 35S promoter (NET4A-GFP^{OE}; $n = 72$) in respect to the control ($n = 147$). (c–e) Root length of the *net4a net4b* ($n = 27$) double knockout and the NET4A-GFP^{OE} ($n = 24$) lines in respect to the corresponding control ($n = 29$ and $n = 52$). One representative experiment is shown. (f) Auxin-dependent (200 nM NAA, 20 h) relative cell length of the double knockout ($n = 81$) and NET4A-GFP^{OE} ($n = 81$) in comparison to the control ($n = 147$). (g–i) Relative root length of the control ($n = 27$ and $n = 50$), *net4a net4b* ($n = 29$) and NET4A-GFP^{OE} ($n = 26$) upon auxin treatment (125 nM NAA, 6 d). One representative experiment is shown. Columns of bar charts represent mean values, error bars display s.e.m. Box limits of boxplots represent 25th percentile and 75th percentile, horizontal line represents median. Whiskers display minimum to maximum values. Student's *t*-test, *p*-values: * $p < 0.05$; *** $p < 0.001$. Scale bar: 5 μm.

3. Discussion

The plant vacuole is essential for development and growth [19,20]. In growing cells, vacuole size and cell size are correlated [13,21,22]. Thus, a role of the vacuole in cell size determination has been proposed [1], which was recently supported by the finding that increased vacuolar volume allows for rapid cellular elongation [2,3,23]. However, the underlying forces regulating vacuolar morphology are not yet well understood.

Previously, it was shown that the structural organization and dynamics of the vacuole rely on the interaction between cytoskeleton and the tonoplast [2,24]. It has been suggested that the actin cytoskeleton plays a major role during vacuole inflation in the late meristematic region (or transition zone) shortly prior to the onset of cellular elongation. Here, it could provide the force to bring vacuolar structures into close proximity to allow for homotypic fusion events. In yeast, it has been reported that actin is enriched at the vacuole at sites where fusion occurs [25]. This involves tethering, docking and fusion processes which in turn are dependent on Rab-family GTPases, vacuolar SNAREs and homotypic fusion and vacuole protein sorting (HOPS) complex [26]. In plants, pharmacological actin interference using profilin led to the disappearance of transvacuolar strands and ceased cytoplasmatic streaming, thereby affecting vacuolar shape as well [27]. Furthermore, actin interference has been shown to inhibit vacuole fusion during stomatal opening [28].

The role of NET4 within the regulation of vacuolar morphology was characterized due to its actin binding capacity [5] and localization at the tonoplast (Figure 1). We have shown that NET4 abundance is crucial to maintaining vacuolar morphology and that overexpression leads to restriction in and loss-of-function to an increase of vacuolar occupancy, respectively (Figure 3). As shown recently, increase in vacuolar volume allows for rapid cellular elongation with relatively little *de novo* production of cytosolic content [3]. Thus, decreased vacuolar occupancy induced by NET4A overexpression might explain the observed cell size and root length limitations.

However, compared to the importance of the actin–myosin system [2], loss of NET4A and NET4B has only mild impacts on vacuolar morphology and cell size. Accordingly, we conclude that higher molecular complexity provides a high level of redundancy for tethering the actin cytoskeleton to the vacuolar membranes. It has been shown that NET3C interacts with VAP27, a contact site protein, which is required to form complexes with the cytoskeleton [29]. Notably, NET3C turnover seems to be modulated by actin [29]. It is hence tempting to assume that the auxin effect on the actin cytoskeleton [2] may indirectly affect NET protein turnover in a similar manner. In metazoans, a variety of adaptor proteins (e.g., spectrin and filamin) are known to provide specific contact sites for the actin cytoskeleton and various membranes [29]. However, most of these protein families are not present in plants and it needs to be seen how these molecular functions are achieved in plants.

4. Materials and Methods

4.1. NET4 Gene Accession Codes

Sequence data from this article can be found in The Arabidopsis Information Resource (TAIR; <http://www.arabidopsis.org/>) or GenBank/EMBL databases under the following accession numbers: NET4A (At5g58320) and NET4B (At2g30500).

4.2. Plant Material, Growth Conditions and DNA Constructs

Arabidopsis thaliana, Columbia 0 (Col-0) ecotype was used as control. The transgenic line NET4A::NET4A-GFP (NET4A-GFP) has been described previously [12]. The line 35S::NET4A-GFP (NET4A-GFP^{OE}) was generated using Gateway cloning. The NET4A coding sequence was amplified via PCR using root cDNA from 8-days-old *Arabidopsis* seedlings. The primers are listed in Table S1. The cDNA fragment was cloned into the pDONR221 (Invitrogen, Thermo Fisher Scientific, Carlsbad, CA, USA) using BP-clonase according to the manufacturer's instructions. Then, the coding sequence was transferred from the entry vector into the destination vector pH7WG2 [30] using the LR clonase from Invitrogen. Transformation into *Arabidopsis thaliana* Col-0, using the floral-dip method was carried out as described before [31].

The insertion lines *net4a-1* (SALK_017623), *net4a-3* (SALK_010530C), *net4a-4* (SALK_083604C) and *net4b* (SALK_056957) were obtained from the Nottingham Arabidopsis Stock Centre (NASC) (Nottingham University, Nottingham, UK). The double mutant *net4a net4b* was generated by crossing *net4a-1* and *net4b*. For identification of homozygous lines, genotyping of all insertion lines was

performed using the NASC-recommended primers (Table S1). Insertion sites for *net4a-1* and *net4b* were located by sequencing within the third exon (*net4a-1*) and the promoter (*net4b*), respectively. Gene knockout of the respective NET4 transcript was shown by qRT-PCR.

Seeds were surface sterilized with ethanol, plated on solid one-half Murashige and Skoog (MS) medium, pH 5.7–5.8 (Duchefa, Haarlem, Netherlands), containing 1% (*w/v*) sucrose (Roth, Karlsruhe, Germany), 2.56 mM MES (Biomol, Hamburg, Germany) and 1% (*w/v*) Phytoagar (Duchefa), and stratified at 4 °C for 1–2 days in the dark. Seedlings were grown in vertical orientation at 20–22 °C under long day conditions (16 h light/8 h dark).

4.3. Chemicals and Treatments

α -Naphthaleneacetic acid (NAA) was purchased from Duchefa; L-kynurenine (kyn) from Sigma (St. Louis, MO, USA); and BCECF-AM, FM4-64, MDY-64 and propidium iodide (PI) from Life Technologies (Carlsbad, CA, USA). All chemicals except PI were dissolved in dimethyl sulfoxide (DMSO). NAA and Kyn were applied in solid one-half MS medium, the dyes BCECF-AM, FM4-64 and MDY-64 in liquid one-half MS medium, and PI in distilled water.

4.4. RNA Extraction and Quantitative Real Time PCR

Total RNA of seedlings was extracted using the innuPREP Plant RNA kit (analytic-jena, Jena, Germany). RNA samples were reverse transcribed using the iScript cDNA synthesis kit (Bio-Rad, Hercules, CA, USA). All steps were performed according to the manufacturer's recommendations. qPCR was performed with the iQ SYBR Green Supermix (Bio-Rad) in a C1000 Touch Thermal Cycler equipped with a CFX96 Touch Real-Time PCR Detection System (Bio-Rad). The reaction procedure was set to a 95 °C heating step for 3 min, followed by 40 cycles of denaturing at 95 °C for 10 s, annealing at 55 °C for 30 s and elongation at 72 °C for 30 s. Target-specific and control primers used for quantification are given in Table S1. Expression levels were normalized to the expression levels of Ubiquitin 5 (UBQ5). Relative expression ratios were calculated according to the so-called " $2^{-\Delta\Delta Ct}$ " method [32] and statistical analyses were performed using Excel software.

4.5. Phenotype Analysis

The quantification of vacuolar morphology, compactness and occupancy as well as cell length was carried out using 6–7-days-old seedlings. To evaluate changes upon kynurenine or auxin treatment, seedlings were transferred to solid one-half MS medium supplemented with 2 μ M Kyn or 200 nM NAA 18–22 h prior to image acquisition. For the analysis of the vacuolar morphology index, confocal sections above the nucleus of the root epidermis were acquired [1]. Calculations of the vacuolar morphology index were carried out in four late (distal) meristematic cells of atrichoblast files, as described previously [3]. For the quantification of plasma-membrane–vacuole distance, the same cells of the late meristematic region were analyzed. Therefore, the distance from the plasma membrane (PM) corner to the first tonoplast structure in diagonal reach was measured for all four corners of a cell, then, mean was calculated and considered as single value for the PM–vacuole distance per cell.

For quantifying the vacuolar occupancy, only one to two cells of the same defined meristematic region before the elongation zone were used per atrichoblast cell file. Cell length was measured in three early (proximal) meristematic cells of atrichoblast cell files (Figure 4a) as described before [18]. For measurements of signal intensity (mean gray value), a defined detector gain was used and individual cells in the late meristematic zone of the root were quantified. All confocal images taken to assess the vacuolar morphology index, PM–vacuole distance and cell length were analyzed using Fiji software (<https://imagej.net/Fiji>). Z-stack confocal images to assess the vacuolar occupancy of the cell were further processed using Imaris 8.4 (Bitplane) software (<https://imaris.oxinst.com/>).

For root growth determination, 6–7-days-old seedlings grown vertically on one-half MS medium plates were used, and root length quantified using Fiji software. To analyze auxin-dependent changes in root growth, solid one-half MS medium supplemented with 125 nM NAA was used. Statistical

evaluation for all data were performed using Graphpad Prism 5 software (<https://www.graphpad.com/scientific-software/prism/>).

4.6. 3D Surface Rendering

Surface rendering for the reconstruction of cells and vacuoles was performed with Imaris 8.4 (Bitplane) as described previously [3]. Generated 3D models were used for the quantification of the vacuolar occupancy of the cell.

4.7. Western Blotting

Roots of 7-days-old seedlings expressing NET4A::NET4A-GFP were homogenized in liquid nitrogen and solubilized in extraction buffer (200 mM Tris pH 6.8, 400 mM DTT, 8% SDS, 40% glycerol, 0.05% bromophenol blue). After incubation at 95 °C for 5–10 min, samples were centrifuged and the proteins contained in the supernatant separated using SDS-PAGE (10% gel). For blotting a polyvinylidene difluoride (PVDF) membrane (Immobilon-P, pore size 0.45 µm, Millipore, Burlington, MA, USA) was used and after blocking with 5% skim milk powder in TBST (150 mM NaCl, 10 mM Tris/HCl pH 8.0, 0.1% Tween 20), the membrane was probed with a 1:20,000 dilution of mouse anti-GFP antibody (JL-8, Roche, Roche Holding AG, Basel, Switzerland) or mouse anti-alpha-tubulin antibody (B-511, Sigma). As secondary antibody, a 1:20,000 dilution of horseradish-peroxidase-conjugated goat anti-mouse antibody (pAB, Dianova, Hamburg, Germany) was used. Signals were detected using the SuperSignal West Pico chemiluminescent substrate detection reagent (Thermo Scientific) and quantified using Fiji software. Signal intensities of GFP were normalized to alpha-tubulin and statistical evaluation was performed using Graphpad Prism 5 software.

4.8. Confocal Microscopy

For live cell imaging, except when FM4-64 staining was performed, roots were mounted in PI solution (0.01 mg/mL) to counterstain cell walls. FM4-64 and MDY-64 staining of the tonoplast was performed as described before [14]. For 3D imaging, vacuoles were stained with BCECF-AM (10 µM solution in one-half MS liquid medium) for at least 1 h in the dark. For staining of auxin treated samples, the staining solution was supplemented with NAA in the respective concentration. Confocal images were acquired using either a Leica SP5 (DM6000 CS), TCS acousto-optical beam splitter confocal laser-scanning microscope, equipped with a Leica HC PL APO CS 20 × 0.70 IMM UV objective and Leica HCX PL APO CS 63 × 1.20 water-immersion objective or a Zeiss LSM880, AxioObserver SP7 confocal laser-scanning microscope, equipped with a Zeiss C-Apochromat 40×/1.2 W AutoCorr M27 water-immersion objective. Fluorescence signals of MDY-64 (Leica-System, excitation/emission 458 nm/465–550 nm; Zeiss-System, excitation/emission 458 nm/473–527 nm), GFP and BCECF (Leica, excitation/emission 488 nm/500–550 nm; Zeiss, excitation/emission 488 nm/500–571 nm), FM4-64 and PI (Leica-System, excitation/emission 561 nm/599–680 nm (FM4-64), 644–753 nm (PI); Zeiss-System, excitation/emission 543 nm/580–718 nm (PI)) were processed using Leica software LAS AF 3.1, Zeiss software ZEN 2.3 or Fiji software. For double labeling, images were acquired using sequential scan mode to avoid channel crosstalk. Z-stacks were recorded with a step size of 540 nm, resulting in approximately 25–35 single images.

Supplementary Materials: Supplementary Materials can be found at <http://www.mdpi.com/1422-0067/20/19/4752/s1>.

Author Contributions: S.K. and A.E. performed experiments, analyzed data and interpreted the results. D.S. conceived and designed the study, performed experiments, analyzed data and interpreted the results. J.K.-V. and D.S. wrote and all co-authors commented on the manuscript.

Funding: This work was supported by grants from the German Research Foundation (DFG; SCHE 1836/4-1) to D.S., the Vienna Science and Technology Fund (WWTF) to J.K.-V. and the European Research Council (AuxinER-ERC starting grant 639478) to J.K.-V.

Acknowledgments: We would like to thank Patrick Hussey for sharing published material, Kai Dünser and Christian Löffke for technical help, Matthias Hahn for critical reading of the manuscript and the BOKU-VIBT Imaging Centre for access and expertise.

Conflicts of Interest: The authors declare no conflict of interest.

References

1. Löffke, C.; Dünser, K.; Scheuring, D.; Kleine-Vehn, J. Auxin regulates SNARE-dependent vacuolar morphology restricting cell size. *Elife* **2015**, *4*, e05868.
2. Scheuring, D.; Löffke, C.; Krüger, F.; Kittelmann, M.; Eisa, A.; Hughes, L.; Smith, R.S.; Hawes, C.; Schumacher, K.; Kleine-Vehn, J. Actin-dependent vacuolar occupancy of the cell determines auxin-induced growth repression. *Proc. Natl. Acad. Sci. USA* **2016**, *113*, 452–457. [\[PubMed\]](#)
3. Dünser, K.; Gupta, S.; Herger, A.; Feraru, M.I.; Ringli, C.; Kleine-Vehn, J. Extracellular matrix sensing by FERONIA and Leucine-Rich Repeat Extensins controls vacuolar expansion during cellular elongation in *Arabidopsis thaliana*. *EMBO J.* **2019**, *38*, e100353. [\[PubMed\]](#)
4. Faix, J.; Steinmetz, M.; Boves, H.; Kammerer, R.A.; Lottspeich, F.; Mintert, U.; Murphy, J.; Stock, A.; Aebi, U.; Gerisch, G. Cortexillins, major determinants of cell shape and size, are actin-bundling proteins with a parallel coiled-coil tail. *Cell* **1996**, *86*, 631–642. [\[PubMed\]](#)
5. Fletcher, D.A.; Mullins, R.D. Cell mechanics and the cytoskeleton. *Nature* **2010**, *463*, 485–492.
6. Uemura, T.; Yoshimura, S.H.; Takeyasu, K.; Sato, M.H. Vacuolar membrane dynamics revealed by GFP-AtVam3 fusion protein. *Genes Cells* **2002**, *7*, 743–753.
7. Mathur, J.; Mathur, N.; Kernebeck, B.; Hülskamp, M. Mutations in Actin-Related Proteins 2 and 3 Affect Cell Shape Development in *Arabidopsis*. *Plant. Cell* **2003**, *15*, 1632–1645.
8. Rahman, A.; Bannigan, A.; Sulaman, W.; Pechter, P.; Blancaflor, E.B.; Baskin, T.I. Auxin, actin and growth of the *Arabidopsis thaliana* primary root. *Plant. J.* **2007**, *50*, 514–528.
9. Li, G.; Liang, W.; Zhang, X.; Ren, H.; Hu, J.; Bennett, M.J.; Zhang, D. Rice actin-binding protein RMD is a key link in the auxin-actin regulatory loop that controls cell growth. *Proc. Natl. Acad. Sci. USA* **2014**, *111*, 10377–10382.
10. Lanza, M.; Garcia-Ponce, B.; Castrillo, G.; Catarecha, P.; Sauer, M.; Rodriguez-Serrano, M.; Pérez-García, A.; Sánchez-Bermejo, E.; Mohan, T.C.; del Puerto, Y.L.; et al. Role of actin cytoskeleton in brassinosteroid signaling and in its integration with the auxin response in plants. *Dev. Cell* **2012**, *22*, 1275–1285.
11. Kutsuna, N.; Kumagai, F.; Sato, M.H.; Hasezawa, S. Three-dimensional reconstruction of tubular structure of vacuolar membrane throughout mitosis in living tobacco cells. *Plant. Cell Physiol.* **2003**, *44*, 1045–1054. [\[PubMed\]](#)
12. Deeks, M.J.; Calcutt, J.R.; Ingle, E.K.S.; Hawkins, T.J.; Chapman, S.; Richardson, A.C.; Mentlak, D.A.; Dixon, M.R.; Cartwright, F.; Smertenko, A.P.; et al. A superfamily of actin-binding proteins at the actin-membrane nexus of higher plants. *Curr. Biol.* **2012**, *22*, 1595–1600. [\[PubMed\]](#)
13. Löffke, C.; Dünser, K.; Kleine-Vehn, J. Epidermal patterning genes impose non-cell autonomous cell size determination and have additional roles in root meristem size control. *J. Integr. Plant. Biol.* **2013**, *55*, 864–875. [\[PubMed\]](#)
14. Scheuring, D.; Schöller, M.; Kleine-Vehn, J.; Löffke, C. Vacuolar staining methods in plant cells. *Methods Mol. Biol.* **2015**, *1242*, 83–92. [\[PubMed\]](#)
15. Andrés, Z.; Pérez-Hormaeche, J.; Leidi, E.O.; Schlücking, K.; Steinhorst, L.; McLachlan, D.H.; Schumacher, K.; Hetherington, A.M.; Kudla, J.; Cubero, B.; et al. Control of vacuolar dynamics and regulation of stomatal aperture by tonoplast potassium uptake. *Proc. Natl. Acad. Sci. USA* **2014**, *111*, E1806–E1814. [\[PubMed\]](#)
16. Hawes, C.; Saint-Jore, C.M.; Brandizzi, F.; Zheng, H.; Andreeva, A.V.; Boevink, P. Cytoplasmic illuminations: In planta targeting of fluorescent proteins to cellular organelles. *Protoplasma* **2001**, *215*, 77–88. [\[PubMed\]](#)
17. Singh, M.K.; Krüger, F.; Beckmann, H.; Brumm, S.; Vermeer, J.E.M.; Munnik, T.; Mayer, U.; Stierhof, Y.-D.; Grefen, C.; Schumacher, K.; et al. Protein delivery to vacuole requires SAND protein-dependent Rab GTPase conversion for MVB-vacuole fusion. *Curr. Biol.* **2014**, *24*, 1383–1389. [\[PubMed\]](#)
18. Barbez, E.; Dünser, K.; Gaidora, A.; Lendl, T.; Busch, W. Auxin steers root cell expansion via apoplastic pH regulation in *Arabidopsis thaliana*. *Proc. Natl. Acad. Sci. USA* **2017**, *114*, E4884–E4893. [\[PubMed\]](#)

19. Rojo, E.; Gillmor, C.S.; Kovaleva, V.; Somerville, C.R.; Raikhel, N.V. VACUOLELESS1 is an essential gene required for vacuole formation and morphogenesis in Arabidopsis. *Dev. Cell* **2001**, *1*, 303–310.
20. Schumacher, K.; Vafeados, D.; McCarthy, M.; Sze, H.; Wilkins, T.; Chory, J. The Arabidopsis det3 mutant reveals a central role for the vacuolar H⁺-ATPase in plant growth and development. *Genes Dev.* **1999**, *13*, 3259–3270.
21. Owens, T.; Poole, R.J. Regulation of cytoplasmic and vacuolar volumes by plant cells in suspension culture. *Plant. Physiol.* **1979**, *64*, 900–904. [[PubMed](#)]
22. Berger, F.; Hung, C.Y.; Dolan, L.; Schiefelbein, J. Control of cell division in the root epidermis of Arabidopsis thaliana. *Dev. Biol.* **1998**, *194*, 235–245. [[PubMed](#)]
23. Krüger, F.; Schumacher, K. Pumping up the volume-vacuole biogenesis in Arabidopsis thaliana. *Semin. Cell Dev. Biol.* **2018**, *80*, 106–112. [[PubMed](#)]
24. Higaki, T.; Kutsuna, N.; Okubo, E.; Sano, T.; Hasezawa, S. Actin microfilaments regulate vacuolar structures and dynamics: Dual observation of actin microfilaments and vacuolar membrane in living tobacco BY-2 Cells. *Plant. Cell Physiol.* **2006**, *47*, 839–852. [[PubMed](#)]
25. Eitzen, G.; Wang, L.; Thorngren, N.; Wickner, W. Remodeling of organelle-bound actin is required for yeast vacuole fusion. *J. Cell Biol.* **2002**, *158*, 669–679. [[PubMed](#)]
26. Zhang, C.; Hicks, G.R.; Raikhel, N.V. Plant vacuole morphology and vacuolar trafficking. *Front. Plant Sci.* **2014**, *5*, 476. [[PubMed](#)]
27. Staiger, C.J.; Yuan, M.; Valenta, R.; Shaw, P.J.; Warn, R.M.; Lloyd, C.W. Microinjected profilin affects cytoplasmic streaming in plant cells by rapidly depolymerizing actin microfilaments. *Curr. Biol.* **1994**, *4*, 215–219.
28. Li, L.-J.; Ren, F.; Gao, X.-Q.; Wei, P.-C.; Wang, X.-C. The reorganization of actin filaments is required for vacuolar fusion of guard cells during stomatal opening in Arabidopsis. *Plant. Cell Environ.* **2013**, *36*, 484–497.
29. Wang, P.; Hawkins, T.J.; Richardson, C.; Cummins, I.; Deeks, M.J.; Sparkes, I.; Hawes, C.; Hussey, P.J. The plant cytoskeleton, NET3C, and VAP27 mediate the link between the plasma membrane and endoplasmic reticulum. *Curr. Biol.* **2014**, *24*, 1397–1405.
30. Karimi, M.; De Meyer, B.; Hilson, P. Modular cloning in plant cells. *Trends Plant Sci.* **2005**, *10*, 103–105.
31. Barbez, E.; Kubeš, M.; Rolčík, J.; Béziat, C.; Pěnčík, A.; Wang, B.; Rosquete, M.R.; Zhu, J.; Dobrev, P.I.; Lee, Y.; et al. A novel putative auxin carrier family regulates intracellular auxin homeostasis in plants. *Nature* **2012**, *485*, 119–122. [[PubMed](#)]
32. Livak, K.J.; Schmittgen, T.D. Analysis of relative gene expression data using real-time quantitative PCR and the 2⁻(Delta Delta C(T)) Method. *Methods* **2001**, *25*, 402–408. [[PubMed](#)]



© 2019 by the authors. Licensee MDPI, Basel, Switzerland. This article is an open access article distributed under the terms and conditions of the Creative Commons Attribution (CC BY) license (<http://creativecommons.org/licenses/by/4.0/>).

Supplementary materials:

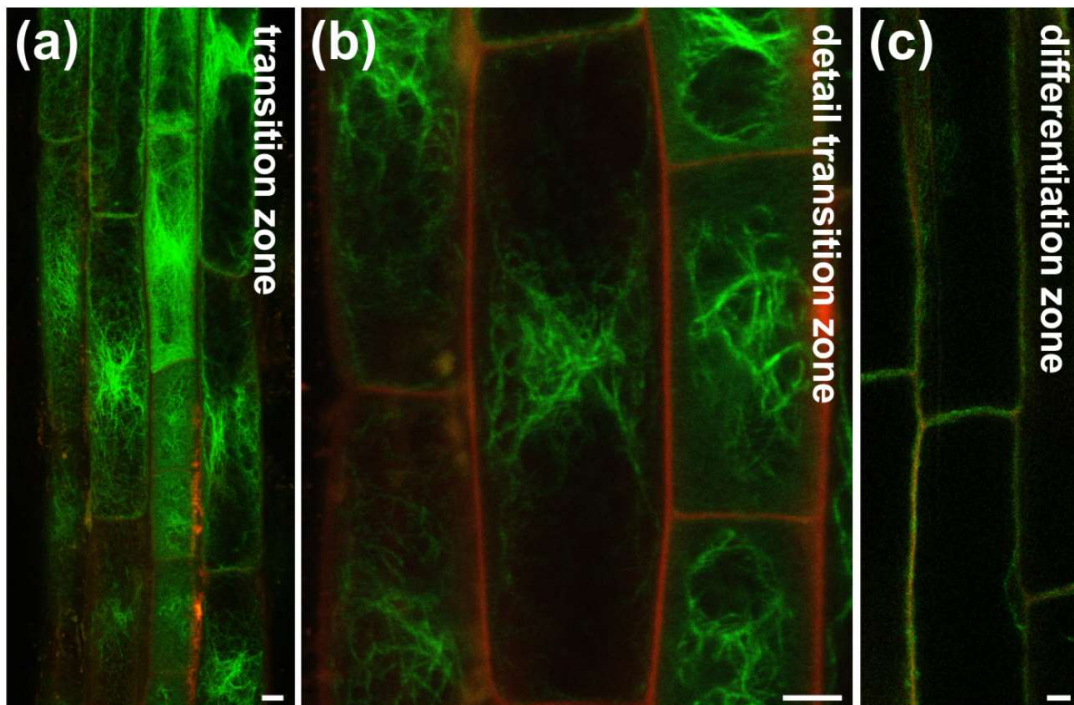


Figure S1. Spatial localization of NET4A. NET4A-GFP expression under its endogenous promoter in *Arabidopsis* roots. Expression starts in the late meristem, initially only in trichoblast cells (Figure 1a). (a and b) In (larger) atrichoblast cells, expression starts in the transition zone and continuous until the elongation zone. (c) NET4A-GFP is only weakly expressed in the differentiation zone. Propidium iodide (red) was used to stain cell walls. Scale bars: 5 μ m.

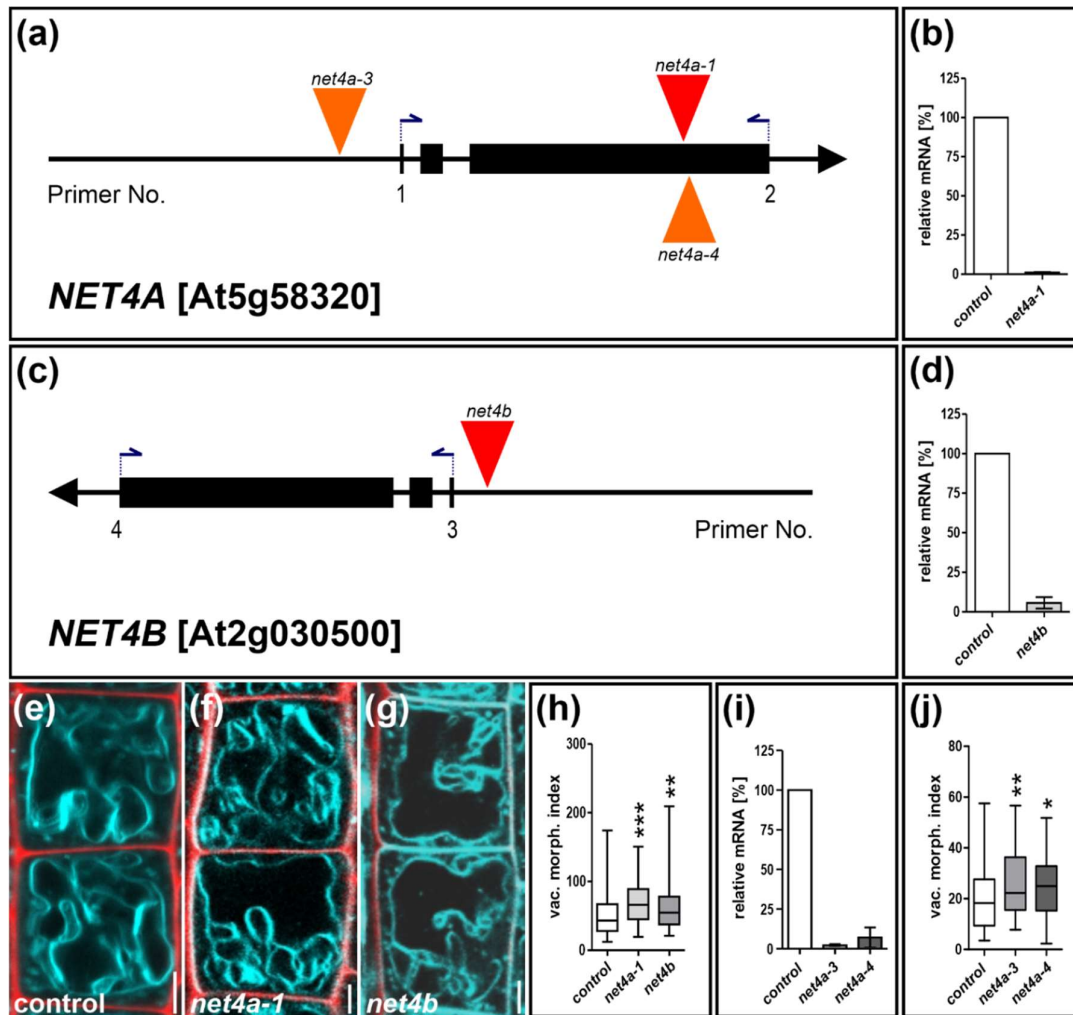
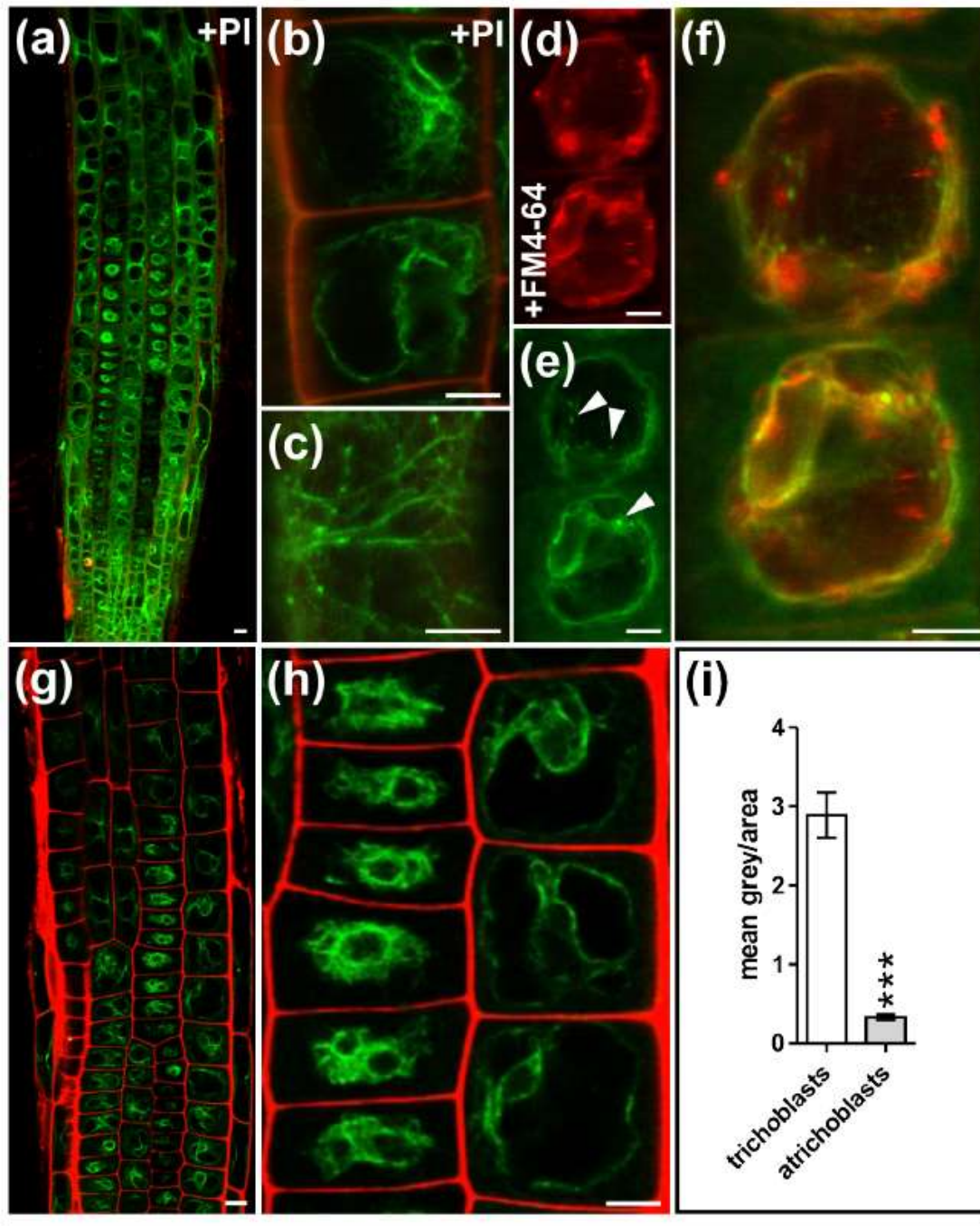


Figure S2. Loss-of-function mutants of *NET4A* and *NET4B*. **(a-d)** T-DNA insertion sites of *net4a-1* (SALK_017623), *net4a-3* (SALK_010530C), *net4a-4* (SALK_083604C) **(a)** and *net4b* (SALK_056957) **(c)** together with the according qRT-PCR to test for gene expression levels of *net4a-1* **(b)** and *net4b* **(d)**. Red arrowheads show verified, orange arrowheads predicted sites of insertion. Arrows indicate position of primers. Primers used are listed in supplemental table S1. **(e-h)** Vacuolar morphology of Col-0 control ($n = 126$), the *net4a-1* ($n = 54$) and the *net4b* single mutant ($n = 99$). MDY-64 (cyan) was used to stain vacuoles, propidium iodide (red) to stain cell walls. **(i)** qRT-PCR to test for gene expression levels of *net4a-3* and *net4a-4*. **(j)** Quantification of vacuolar morphology for Col-0 control ($n = 64$), the *net4a-3* ($n = 63$) and the *net4a-4* single mutant ($n = 67$). Columns of bar charts represent mean values, error bars represent s.e.m. Box limits of boxblots represent 25th percentile and 75th percentile, horizontal line represents median. Whiskers display minimum to maximum values. Student's t-test, p -values: * $p < 0.05$; ** $p < 0.01$; *** $p < 0.001$. Scale bars: 5 μm .



NET4A-GFP^{OE}

Figure S3. Localization of NET4A driven by the CMV 35S promoter (NET4A-GFP^{OE}). (a) Uniform signal distribution within the Arabidopsis root meristem. (b) Vacuolar signal in atrichoblast cells and (c) filamentous signal at the cell cortex. (d-f) Vacuole staining by FM4-64 (3 h) shows NET4A colocalization at the tonoplast. White arrowheads highlight punctate signals. (g-i) More constricted vacuoles in trichoblast cells ($n = 34$) show a higher signal accumulation per area in comparison to less folded vacuoles in atrichoblast cells ($n = 35$). Propidium iodide was used to stain cell walls, FM4-64 to stain the tonoplast. Error bars represent s.e.m. Student's t-test, p -values: *** $p < 0.001$. Scale bars: 5 μ m.

Table S1: Used primers.

Gateway Cloning Primers		Sequence
NET4A_FW	GGGGACAAGTTTGTACAAAAAAGCAGGCTTTATGGATTATGATCTGCTTCGTTTC	
NET4A_REV	GGGGACAAGTTTGTACAAAAAAGCAGGCTTAAGAAGCAAGAATGGATGATG	
Genotyping Primers		Sequence
SALK_LBb1.3	ATTTTGCCGATTTCGGAAC	
SALK_017623(S1)_FW	AATGGATGATGGTCTTGTGTTGG	
SALK_017623(S1)_REV	GAACACTGAGAGCTTGTGTC	
SALK_056957_net4b_FW	AATCACGATAGAGCCACATGC	
SALK_056957_net4b_REV	TACATGCGGTAGAATTCCTCG	
SALK_010530C(S3)_FW	TAGTCGCTTACACATTGGCAG	
SALK_010530C(S3)_REV	TGAGAATTCGGTTGTTTTGG	
SALK_083604C(S4)_FW	TCCGGGTGTTAGCTGTACAG	
SALK_083604C(S4)_REV	CATCTGGGTTGGATGATGAAC	
qRT-PCR Primers		Sequence
UBQ-5_fw	GACGCTTCATCTCGTCC	
UBQ-5_rev	GTAAACGTAGGTGAGTCCA	
NET4A_FW (1)	GGGGACAAGTTTGTACAAAAAAGCAGGCTTTATGGATTATGATCTGCTTCGTTTC	
NET4A_REV (2)	GGGGACAAGTTTGTACAAAAAAGCAGGCTTAAGAAGCAAGAATGGATGATG	
NET4B_FW (3)	GGGGACAAGTTTGTACAAAAAAGCAGGCTTTATGGCTTCGTCTACGGCTCAG	
NET4B_REV (4)	GGGGACAAGTTTGTACAAAAAAGCAGGCTTCAAGTTGATAAGACCACTACTCTCTT	

13.2 Article 2

“Vacuolar occupancy is crucial for cell elongation and growth regardless of the underlying mechanism”

SHORT COMMUNICATION



Vacuolar occupancy is crucial for cell elongation and growth regardless of the underlying mechanism

Sabrina Kaiser , Sophie Eisele, and David Scheuring 

Plant Pathology, University of Kaiserslautern, Kaiserslautern, Germany

ABSTRACT

In the physiological range, the phytohormone auxin inhibits the growth of underground tissues. In the roots of *Arabidopsis thaliana*, cell size inhibition has been shown to be accompanied by auxin-mediated reduction of vacuole size. A tonoplast-localized protein family (Networked 4) with actin-binding capacity was demonstrated to modulate the compactness of the vacuole. Overexpression of NET4A led to smaller, more spherical and compact vacuoles, which occupied less cellular space compared to wild type. This reduction of vacuolar occupancy is similar to the observed auxin-induced decrease in occupancy, albeit there are enormous morphological differences. Here, we show that a *net4a net4b* double mutant and a NET4A overexpressor line are still sensitive to auxin-induced vacuolar constrictions. However, the overexpressor showed a partial auxin resistance accompanied by more compact vacuoles, thereby indicating an additional regulatory mechanism. Furthermore, we show that other NET superfamily members do not compensate for the loss of NET4A and NET4B expression on the transcriptional level. This leads us to hypothesize that regulation of vacuole size is a general mechanism to regulate cell expansion and that other players besides NET4 must participate in regulating the vacuole–cytoskeleton interface.

ARTICLE HISTORY

Received 29 March 2021
Revised 23 April 2021
Accepted 23 April 2021

KEYWORDS



Arabidopsis; vacuole; actin cytoskeleton; auxin; NET4; cell elongation; vacuolar occupancy

The phytohormone auxin is a vital growth regulator with diametrical effects on roots and shoots. Increased abundance of root tissue leads to inhibition of cellular elongation.¹ For root epidermal cells of *Arabidopsis thaliana*, it has been shown that growth inhibition by auxin is a result of changed vacuolar morphology.² Auxin induced more constricted, tubular vacuoles, which occupied less cellular space than usual.³ This led to the conclusion that vacuoles have a space-filling function during growth. Therefore, it was hypothesized that this mechanism allows rapid cell elongation with relatively little energy investment.^{3–7}

The observed auxin-induced vacuolar constrictions and the resulting space constraints were shown to be dependent on the actin cytoskeleton.³ To shed light on the cytoskeleton–vacuole connection, members of the actin-binding Networked (NET) 4 protein family,⁸ which are localized at the tonoplast, were investigated.⁵ While a *net4a net4b* double mutant showed only a weak phenotype, overexpression of NET4A in a 35S::NET4A-GFP line (NET4A-GFP^{OE}) led to more spherical and compact vacuoles, which consequently also occupied less cellular space.⁵ Despite morphological differences of vacuoles in NET4A-GFP^{OE} and auxin-treated vacuoles in Col-0 wild type, reduced occupancy in both cases was accompanied by reduced cell size and root length.^{2,5} Therefore, it seems plausible that reducing the vacuolar occupancy of the cell, regardless of the underlying mechanism, inhibits cellular elongation and eventually root growth in general.

To analyze this further, we examined the vacuolar occupancy of NET4A-GFP^{OE} and *net4a net4b* compared to Col-0

wild type upon treatment with the synthetic auxin naphthalene acetic acid (NAA). To this end, the vacuolar lumen of *Arabidopsis* root epidermal cells within the late meristematic zone was stained with BCECF (2',7'-Bis-(2-carboxyethyl)-5(6)-carboxyfluorescein) and the corresponding cell walls with propidium iodide (PI) as described previously in Scheuring et al.⁹ Based on 3D modeling of vacuoles and cells,⁴ vacuolar occupancy was quantified. While vacuoles of all tested lines showed tubular constrictions, vacuoles of NET4A-GFP^{OE} remained spherical and more compact (Figure 1a–c). This is in accordance with previous findings, showing no differences in the auxin-induced decrease in the vacuolar morphology index, as a measure for the extent of vacuolar constrictions.⁵ On the other hand, it led to an additional increase in compactness of the already more compact vacuoles in NET4A-GFP^{OE}.⁵ It has been shown that in general, auxin-induced constrictions lead to a reduced vacuolar occupancy in root meristematic cells.³ This finding in combination with the observed higher compactness of NET4A-GFP^{OE} vacuoles tempted us to expect a stronger reduction of vacuolar occupancy when the overexpressor is treated with NAA. However, despite the described effects on vacuolar morphology and compactness, the occupancy of NET4A-GFP^{OE} was higher than that of the control (Figure 1d). Consequently, quantification of occupancy upon auxin treatment relative to control conditions revealed a significantly lower decrease for NET4A-GFP^{OE} than for the control (Figure 1e), indicating a partial resistance. In contrast, quantification of the occupancy as well as the relative change of occupancy upon NAA treatment for the *net4a net4b* double

CONTACT David Scheuring  scheuring@rhrk.uni-kl.de  Plant Pathology, University of Kaiserslautern, Paul-Ehrlich-Straße 2267663, Kaiserslautern, Germany

© 2021 The Author(s). Published with license by Taylor & Francis Group, LLC.

This is an Open Access article distributed under the terms of the Creative Commons Attribution-NonCommercial-NoDerivatives License (<http://creativecommons.org/licenses/by-nc-nd/4.0/>), which permits non-commercial re-use, distribution, and reproduction in any medium, provided the original work is properly cited, and is not altered, transformed, or built upon in any way.

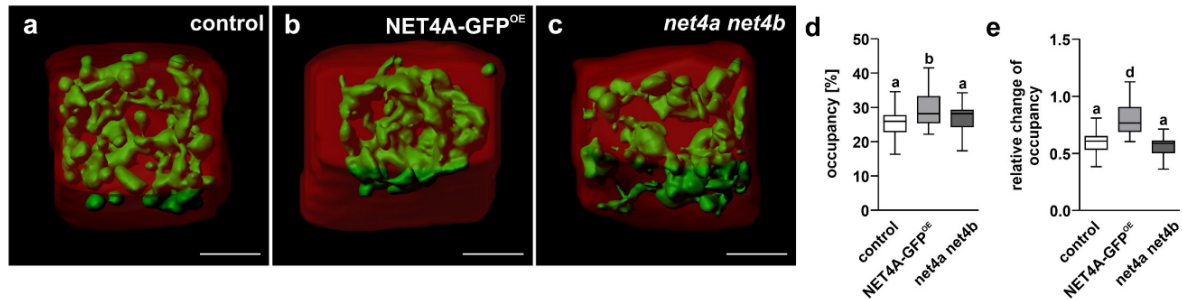


Figure 1. Only vacuoles of NET4A-GFP^{OE} show partial resistance to auxin treatment. (a–c) Three-dimensional modeling (using Imaris software) of PI-stained cell walls (red) and BCECF-stained vacuoles (green) of late meristematic root cells from Columbia-0 control ($n = 27$), NET4A-GFP^{OE} ($n = 16$) and *net4a net4b* ($n = 14$) upon auxin treatment (200 nM NAA, 20 h). (d) Quantification of the vacuolar occupancy of the cell (occupancy) upon auxin treatment. (e) Change in vacuolar occupancy upon auxin treatment relative to untreated conditions. Box limits of boxplots display 25th percentile and 75th percentile, horizontal line depicts median. Whiskers represent minimum to maximum values. Statistical analysis was performed using one-way ANOVA followed by Tukey post hoc test, p -value b: $p < .05$, d: $p < .001$ compared to a. Scale bars: 5 μ m.

mutant showed no significant difference in comparison to the wild-type control (Figure 1d,e). These findings indicate that neither NET4A nor NET4B are essential for auxin-mediated vacuolar constrictions. Instead, it might be assumed that NET4A-mediated increase in vacuolar compactness relies on an additional pathway, which is only indirectly affected by auxin. Hence, the observed partial auxin resistance of NET4A-GFP^{OE} might be explained by already smaller and more compact vacuoles, which only allow constrictions to a certain extent.

Since all members of the NET superfamily possess actin-binding domains and are associated with different membranes, it is also conceivable that a lacking phenotype of *net4a net4b* is due to functional redundancy by other NETs. To test for possible transcriptional upregulation of other NETs in the *net4a net4b* mutant background, we performed real-time quantitative PCR¹⁰ for all family members of NET1, NET2 and NET3. Transcript levels of 7-d-old Arabidopsis seedlings in the double mutant background were compared to control (Col-0) levels (Figure 2). While for NET2A-C and NET3B expression was not detectable, all other NETs were not up-regulated, giving no indication of a compensatory effect in the *net4a net4b* double mutant.

In general, the molecular function of NET4 is far from being understood. Actin-binding capacity and localization at the tonoplast suggest a regulatory function of the cytoskeleton at the vacuole. In this scenario, the more spherical and compact vacuoles of NET4A-GFP^{OE} would be followed by changes of the actin cytoskeleton. Recently, it has been shown that NET3C not only binds to actin and the plasma membrane (PM) but also forms complexes with other proteins – vesicle-associated protein 27 (VAP27), kinesin light chain-related protein 1 (KLCR1), IQ67 domain 2 (IQD2) – at contact sites of the PM and the endoplasmic reticulum (ER). Notably, these complexes bridge the actin and microtubule network and seem to directly affect the morphology of the ER.^{11,12} It is conceivable that similar complexes including NET4 might be formed at specific tonoplast sites.

Functional reasons to have more compact vacuoles might be manifold. Besides slowing down growth, for instance, as reaction to certain stresses, preventing the tonoplast from coming in direct contact with the PM could also have an influence on cytoplasmic streaming. Interestingly, it has been demonstrated that accelerating or decelerating cytoplasmic streaming velocity correlated with increased or reduced cell size and overall plant growth, respectively.¹³ Hence, one could even assume

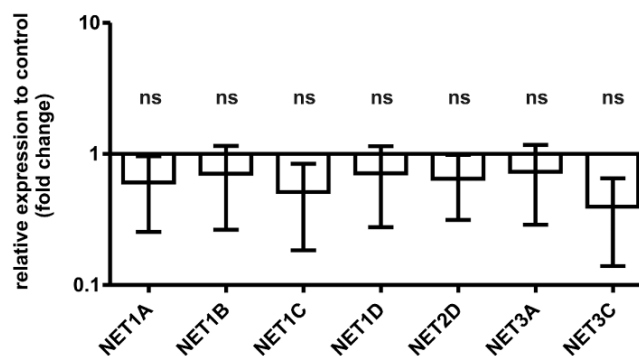


Figure 2. No compensatory upregulation on transcript level is detectable in the *net4a net4b* double mutant. Expression levels of NET1-3 in *net4a net4b* are presented as the mean fold change to the expression levels in Columbia-0 wild-type control on a logarithmic scale. Experiment was performed thrice with at least two technical replicates. Error bars represent standard error of the mean. Student's t -test was used for statistical analysis, ns: not significant.

some kind of feedback regulation. Apart from that, the proximity between the tonoplast and the nucleus (especially in NET4A-GFP^{OE}) could also indicate some connection to nucleus positioning. It has been reported that positioning of the nucleus in root hairs is regulated by modulation of the filamentous actin organization.^{14,15}

However, the lack of a strong phenotype in the *net4a net4b* double mutant implies that a higher molecular complexity provides redundancy for tethering the actin cytoskeleton to the tonoplast. The finding that NET4 seems not to be essential for mediating auxin-dependent changes in the vacuolar morphology⁵ makes it tempting to assume that there must be additional molecular players. It will be an exciting future task to identify these yet unknown players and to decipher molecular processes at the vacuole–cytoskeleton interface.

Acknowledgments

We would like to thank Kai Dünser and Achim Herrmann for critical reading of the manuscript.

Disclosure of potential conflicts of interest

No potential conflicts of interest were disclosed.

Funding

Support for this work was granted to DS by the German Research Foundation [DFG; SCHE 1836/4-1] and the BioComp Research Initiative from the state Rhineland-Palatinate (Germany).

ORCID

Sabrina Kaiser  <http://orcid.org/0000-0001-8104-140X>
David Scheuring  <http://orcid.org/0000-0001-9048-3330>

References

1. Sauer M, Robert S, Kleine-Vehn J. Auxin: simply complicated. *J Exp Bot*. 2013;64(9):2565–2577. doi:10.1093/jxb/ert139.
2. Löffke C, Dünser K, Scheuring D, Kleine-Vehn J. Auxin regulates SNARE-dependent vacuolar morphology restricting cell size. *eLife*. 2015;4:e05868. doi:10.7554/eLife.05868.
3. Scheuring D, Löffke C, Krüger F, Kittelmann M, Eisa A, Hughes L, Smith RS, Hawes C, Schumacher K, Kleine-Vehn J. Actin-dependent vacuolar occupancy of the cell determines auxin-induced growth repression. *Proc Natl Acad Sci USA*. 2016;113(2):452–457. doi:10.1073/pnas.1517445113.
4. Dünser K, Gupta S, Herger A, Feraru MI, Ringli C, Kleine-Vehn J. Extracellular matrix sensing by FERONIA and Leucine-Rich Repeat Extensins controls vacuolar expansion during cellular elongation in *Arabidopsis thaliana*. *EMBO J*. 2019;38(7):e100353. doi:10.15252/embj.2018100353.
5. Kaiser S, Eisa A, Kleine-Vehn J, Scheuring D. NET4 modulates the compactness of vacuoles in *Arabidopsis thaliana*. *Int J Mol Sci*. 2019;20(19):4752. doi:10.3390/ijms20194752.
6. Kaiser S, Scheuring D. To lead or to follow: contribution of the plant vacuole to cell growth. *Front Plant Sci*. 2020;11:553. doi:10.3389/fpls.2020.00553.
7. Krüger F, Schumacher K. Pumping up the volume - vacuole biogenesis in *Arabidopsis thaliana*. *Semin Cell Dev Biol*. 2018;80:106–112. doi:10.1016/j.semcdb.2017.07.008.
8. Deeks MJ, Calcutt JR, Ingle EKS, Hawkins TJ, Chapman S, Richardson AC, Mentlak DA, Dixon MR, Cartwright F, Smertenko AP, et al. A superfamily of actin-binding proteins at the actin-membrane nexus of higher plants. *Curr Biol*. 2012;22(17):1595–1600. doi:10.1016/j.cub.2012.06.041.
9. Scheuring D, Schöller M, Kleine-Vehn J, Löffke C. Vacuolar staining methods in plant cells. *Methods Mol Biol (Clifton, NJ)*. 2015;1242:83–92.
10. Jeblick T, Leisen T, Steidele CE, Müller J, Mahler F, Sommer F, Keller S, Hückelhoven R, Hahn M, Scheuring D. The secreted hypersensitive response inducing protein 1 from *Botrytis cinerea* displays non-canonical PAMP-activity. *bioRxiv*. 2020. doi:10.1101/2020.12.16.423131.
11. Wang P, Hawkins TJ, Richardson C, Cummins I, Deeks MJ, Sparkes I, Hawes C, Hussey PJ. The plant cytoskeleton, NET3C, and VAP27 mediate the link between the plasma membrane and endoplasmic reticulum. *Curr Biol*. 2014;24(12):1397–1405. doi:10.1016/j.cub.2014.05.003.
12. Zang J, Klemm S, Pain C, Duckney P, Bao Z, Stamm G, Kriechbaumer V, Bürstenbinder K, Hussey PJ, Wang P. A novel plant actin-microtubule bridging complex regulates cytoskeletal and ER structure at ER-PM contact sites. *Curr Biol*. 2021;31(6):1251–1260. doi:10.1016/j.cub.2020.12.009.
13. Tominaga M, Kimura A, Yokota E, Haraguchi T, Shimmen T, Yamamoto K, Nakano A, Ito K. Cytoplasmic streaming velocity as a plant size determinant. *Dev Cell*. 2013;27(3):345–352. doi:10.1016/j.devcel.2013.10.005.
14. Chytilova E, Macas J, Sliwinski E, Rafelski SM, Lambert GM, Galbraith DW. Nuclear dynamics in *Arabidopsis thaliana*. *Mol Biol Cell*. 2000;11(8):2733–2741. doi:10.1091/mbc.11.8.2733.
15. Ketelaar T, Faivre-Moskalenko C, Esseling JJ, de Ruijter NCA, Grierson CS, Dogterom M, Emons AMC. Positioning of nuclei in *Arabidopsis* root hairs: an actin-regulated process of tip growth. *Plant Cell*. 2002;14(11):2941–2955. doi:10.1105/tpc.005892.

13.3 Article 3

“Networked proteins redundantly interact with VAP27 and RABG3 to regulate membrane tethering at the vacuole and beyond”

Networked proteins redundantly interact with VAP27 and RABG3 to regulate membrane tethering at the vacuole and beyond

Sabrina Kaiser¹, Dietmar Mehlhorn², Paulina Ramirez Miranda¹, Fabian Ries³, Frederik Sommer⁴, Michael Schroda⁴, Karin Schumacher⁵, Felix Willmund³, Christopher Grefen² and David Scheuring^{1,*}

¹ Plant Pathology, University of Kaiserslautern-Landau, Germany

² Molecular and Cellular Botany, Ruhr University Bochum, Germany

³ Molecular Plant Physiology, University of Marburg, Germany

⁴ Molecular Biotechnology & Systems Biology, University of Kaiserslautern-Landau, Germany

⁵ COS Heidelberg, University of Heidelberg, Germany

*Correspondence: scheuring@bio.uni-kl.de

Abstract

Biological processes in eukaryotes depend on the spatio-temporal compartmentalization of their cells. Integrity and positioning of organelles on the other hand rely on the organization of the actin cytoskeleton. Previously, it has been shown that changes of the plants largest organelle, the vacuole, depend on a functional actin organization. The connection between actin filaments and the vacuole is established by the family of Networked (NET) 4 proteins and, consequently, altering NET4 abundance impacts vacuolar morphology. However, the precise regulatory mechanism is unknown and gene deletions of *NET4* did not result in a global growth phenotype. Here, we show that NET4 functions redundantly with NET3, interacting with RABG3-GTPases at the vacuole to allow for homotypic fusion or, alternatively, the generation of endoplasmic reticulum (ER) - vacuole contact sites. We found that ER-resident NET3 is able to interact with RABG3 residing at the tonoplast and that NET4 interacts with the contact site protein VAP27-1 at the ER. Generation of *net3 net4* triple mutants by CRSIPR-guided mutagenesis helped us to overcome functional redundancy, resulting in impaired plant growth and development. Our results demonstrate how diversification of *NET* genes led to functional redundancy between different family members to create cellular plasticity of vascular plants. We hypothesize that establishment of a direct ER-vacuole connection enables direct lipid and protein transfer which is especially important in young and fast-growing cells. Availability of lipids would facilitate rapidly expanding vacuoles, which are the basis for high cell elongation rates and eventually fast plant growth.

Introduction

Compartmentalization of cells is a hallmark of all eukaryotes. Despite their chemical, physical and structural integrity, organelles need to communicate and exchange material. To this end, all compartments of the endomembrane system are connected via vesicle transport and in addition form membrane contact sites between compartments. Protein transport requires sorting into vesicles via coat proteins, interaction with GTPases, tethering and eventual SNARE (soluble N-ethylmaleimide-sensitive factor attachment receptor)-mediated fusion with the target membrane. In order to target proteins to the lytic vacuole, different trafficking routes can be used (Cui et al., 2020). The best studied transport pathway towards the vacuole includes the sequential recruitment of Rab5-like and Rab7-like GTPases which act as molecular switches, having an inactive GDP-bound and an active GTP-bound state (Ebine et al., 2014). Notably, Rab7-like proteins, called RABGs in plants; have been shown to interact with the HOPS (HOMOTYPIC FUSION AND VACUOLE PROTEIN SORTING) tethering complex at the vacuole (Takemoto et al., 2018). Impairment of any of the HOPS subunits has severe consequences ranging from male sterility (Brillada et al., 2018) to embryo lethality (Rojo et al., 2001), and induced genetic interference results in dramatic fragmentation of the vacuole (Takemoto et al., 2018; Brillada et al., 2018). Together with the CORVET (CLASS C CORE VACUOLE/ENDOSOME TETHERING) complex, the HOPS tethering complex mediates the initial contact between two membranes, thereby regulating vacuolar trafficking (Aniento et al., 2022). Both complexes share a core, consisting of VPS16, VPS18, VPS11, and VPS33 with HOPS having additionally the two specific subunits VPS39 and VPS41. Based on cryo-electron microscopy, the high-resolution structure of the HOPS complex was recently revealed in yeast (Shvarev et al., 2022). Here, SNARE attachment to the core of the hexameric complex is shown and Rab-GTPase binding occurs at the extremities. This represents ideal positioning of molecules to tether two membranes and catalyse their simultaneous fusion (Shvarev et al., 2022).

The formation of membrane contact sites on the other hand involves generally the cytoskeleton, functional and regulatory proteins as well as tethering complexes (Scorrano et al., 2019). The inability of closely associated membranes to fuse, defines membrane contact sites and might be explained by the lack of fusion-competent SNARE complexes. In yeast and animals, numerous contact sites between different organelles have been characterized, most often involving the endoplasmic reticulum (Scorrano et al., 2019). Notably, the formation of contact sites between the ER and lysosomes in animal cells has been reported recently (Tan and Finkel, 2022). Investigations on membrane contact sites in plants came only recently into focus, but in most of the reported cases the ER plays a central role like in animals (Wang et al., 2023). The best studied membrane contact sites in plants are ER-

plasma membrane contact sites (EPCS), whose formation involves a complex interplay of actin filaments, actin-recruiting proteins, microtubules and integral ER proteins (Wang et al., 2014; Zang et al., 2021). The formation of membrane contact sites including plant specific compartments, however, has not been proven unequivocally.

In plants, members of the Networked (NET) family possess actin-binding capacity, localize to different compartments and have been shown to participate in membrane contact site formation (Duckney et al., 2022). Actin filaments and microtubules represent the molecular tracks for moving organelles and molecules within a cell (Vale, 2003). While in animals microtubules are responsible for vesicle trafficking and organelle organization, in plants predominantly actin filaments maintain these functions (Kost and Chua, 2002). The connection between the actin cytoskeleton and the vacuole is mediated by NET4A (Deeks et al., 2012; Kaiser et al., 2019) and misexpression of NET4 impacts size and structure of the vacuole. Whereas a *net4a net4b* double mutant showed more spherical and slightly larger vacuoles, overexpression of *NET4A* (NET4A-GFP^{OE}) rendered vacuoles more spherical but smaller and more condensed around the nucleus (Kaiser et al., 2019). Intriguingly, the appearance of small vacuoles was accompanied by restricted cell elongation and root length similar to what has been previously shown for auxin-induced smaller vacuoles (Scheuring et al., 2016). It seems plausible that limiting vacuole size, regardless of the underlying molecular mechanism, generally inhibits cellular elongation and eventually root growth (Kaiser et al., 2021). It is, however, unclear how NET4 abundance impacts on the organization of the cytoskeleton and which other molecular players are involved in changing vacuolar morphology. Additionally, gene deletions of *NET4* did not result in a general growth phenotype and we hence expect functional redundancy provided by other proteins.

Here, we show that recruitment of actin filaments by NET4 regulates vacuole fusion, thus providing the driving force to change vacuolar morphology and size. Moreover, NET3 and NET4 proteins redundantly form complexes with RABG3-GTPases, VAP27-1 and actin filaments to establish ER-vacuole membrane contact sites, providing a high level of cellular plasticity. Higher-order *net3 net4* knockout mutants display abnormally shaped and sometimes partially fragmented vacuoles occupying less cellular space. This is accompanied by restricted growth and development, demonstrating that the NET3-NET4 tandem is essential for the development of higher plants.

Results

NET4A abundance changes actin architecture in root cells

The precise regulatory mechanism of changing vacuolar morphology is not yet fully understood and gene deletions of NET4A and NET4B did not result in a general growth phenotype. Previously, we have shown that overexpression of NET4A led to smaller and more compact vacuoles (Kaiser et al., 2019). We could observe the same effect when overexpressing NET4B (Supplementary Fig S1A-E). Since both proteins not only localize to the tonoplast (Kaiser et al., 2019; Supplementary Fig S1F) but also possess a plant specific actin-binding domain (NAB), we expected a reorganization of the cytoskeleton in case of overexpression. To test how NET4 abundance impacts actin architecture, we crossed NET4A-GFP^{OE} with the actin marker lifeact-RFP (Riedl et al., 2008) and quantified changes of filament organization in epidermis cells of the Arabidopsis root tip. Using z-stack recordings, we found a NET4-dependent reorientation of actin filaments towards the cell center, i.e. the nucleus (Fig 1A and 1B). For quantification, we measured parallelness of actin filaments using the LPixel Inc. plugins for ImageJ (<https://lpixel.net/en/products/lpixel-imagej-plugins/>) according to Higaki (Higaki, 2017), and detected significant differences in actin organization (Fig 1C). This was especially prominent in cells of the transition zone, where central optical sections reveal focusing of actin bundles from the cell periphery towards the nucleus. Accordingly, an impact on vacuole shape could be observed in that area (Supplementary Fig S2). Notably, NET4 signals seem to be pronounced here and colocalize well with the actin marker lifeact-RFP (Fig 1D).

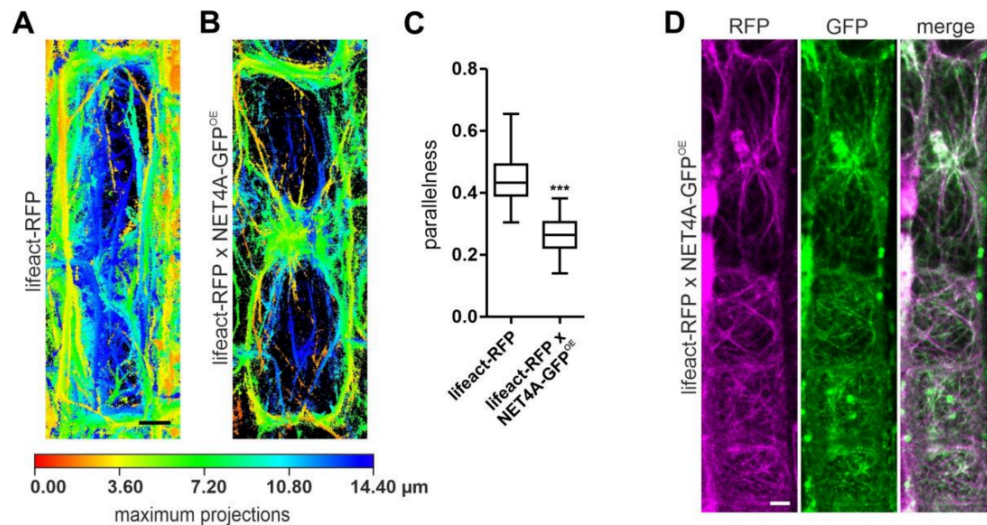


Figure 1 NET4 overexpression changes organization of the actin cytoskeleton. A and B, Maximum projections (depth coded) of actin filaments highlighted by lifeact-RFP for a representative epidermal cell from the transition zone of the Arabidopsis root. A, Control conditions; B, Effect of NET4A overexpression on actin filament organization. C, Quantification of parallelness for the actin cytoskeleton in lifeact-RFP (n=18) and lifeact-RFP x NET4A-GFP^{OE} (n=24). Box limits in the graph represent 25th-75th percentile, the horizontal line the median and whiskers minimum to maximum

values. Significant differences were analyzed by Student's t-test; *** $P < 0.001$. D, Colocalization of NET4A-GFP (green) and lifeact-RFP (magenta). Scale bars in all pictures = 5 μm .

Phenotypes of actin mutants are reverted by *NET4A* overexpression

We hypothesized that overexpression of NET4A led to increased recruitment of actin filaments. To test this, we investigated the effect of NET4A overexpression in different actin-myosin mutant backgrounds. On the subcellular level, we observed that the previously reported more compact vacuoles of the overexpressor line (Kaiser et al., 2019) were more wild type (wt) -like in the *xi-k/1/2* myosin triple mutant (Fig 2A). This effect was more pronounced when the phytohormone auxin (NAA), inducing vacuolar constrictions and further retraction of the tonoplast away from the plasma membrane (Kaiser et al., 2019; Scheuring et al., 2016) was exogenously applied (Fig 2B). To confirm that these changes were indeed caused by NET4A, we crossed the previously described *net4a net4b* double mutant (Kaiser et al., 2019) with NET4A-GFP^{OE}. In the complementation line, both, vacuolar morphology and distance to the plasma membrane (PM), reverted to wt-like appearance (Supplementary Fig S3). When NET4A was overexpressed in the *act7-4* background, the normally irregular cellular organization of the mutant in the root meristem was recovered and cell wall defects were fewer (Fig 2C). Recovery of the *act7-4* mutant phenotype by NET4A could also be observed on the organ level, indicated by longer roots of *act7-4* x NET4A-GFP^{OE} compared to *act7-4* (Fig 2D). Interestingly, while root length for the *act2 act8* mutant was inconspicuous, the observed wavy root phenotype could be largely reversed by NET4A overexpression (Fig 2E).

This suggests that higher NET4 abundance leads to increased recruitment of actin filaments, which compensate for the loss of certain vegetative actin isoforms such as *ACTIN 2*, *ACTIN7* and *ACTIN 8*.

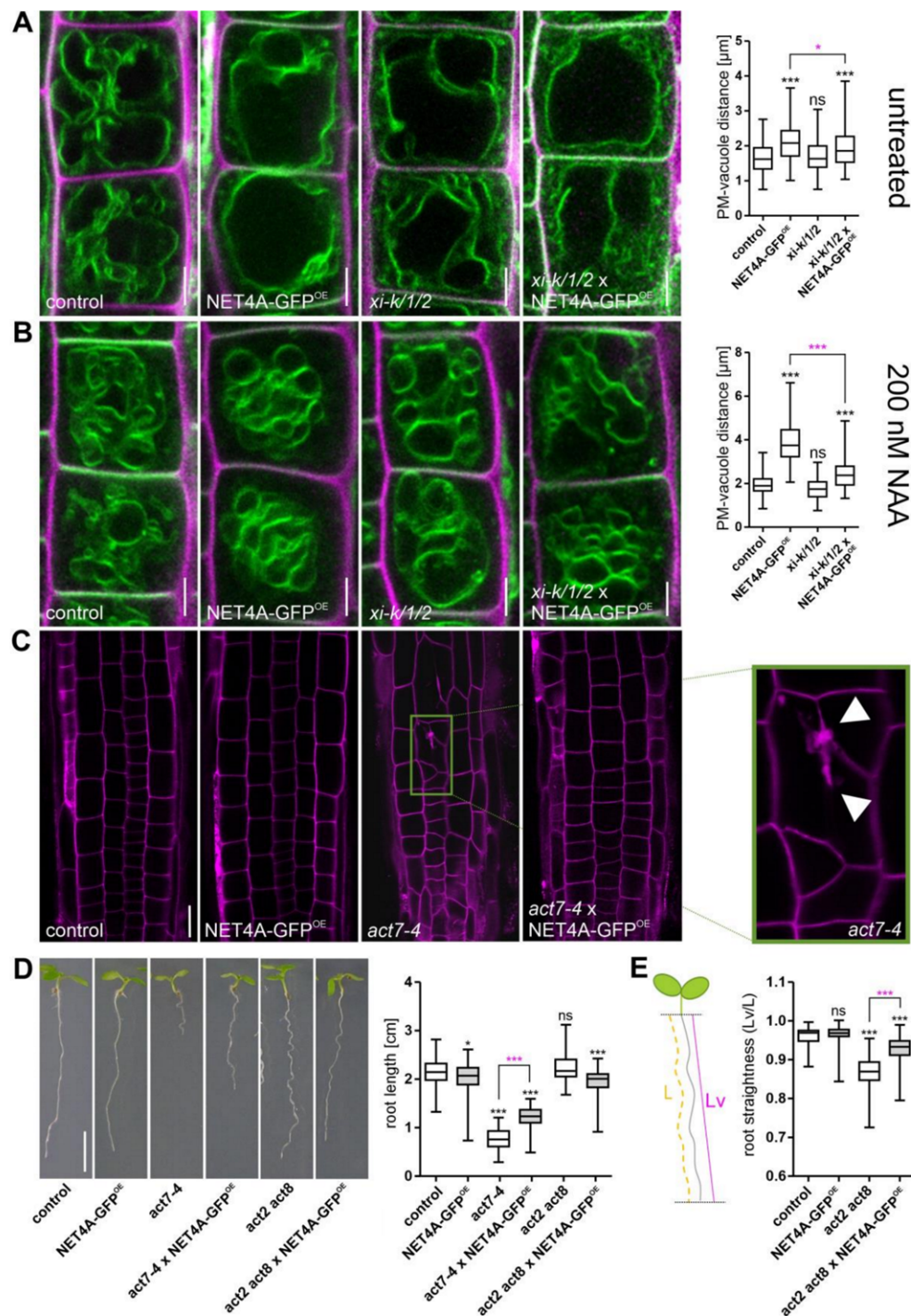


Figure 2 Recovery of actin related phenotypes by NET4 overexpression. A, PM to tonoplast distance in dependence of NET4A overexpression and myosin triple knockout mutant (*xi-k/1/2*). n=124 cells from 31 seedlings for control, n=132 cells from 33 seedlings for NET4A-GFP^{OE}, n=124 cells from 31 seedlings for *xi-k/1/2*, n=136 cells from 34 seedlings for *xi-k/1/2* x NET4A-GFP^{OE}. B, Effect of exogenous auxin (NAA) on PM to tonoplast distance. n=92 cells from 22 seedlings for control, n=92

cells from 22 seedlings for NET4A-GFP^{OE}, n=96 cells from 24 seedlings for *xi-k/1/2*, n=76 cells from 19 seedlings for *xi-k/1/2* x NET4A-GFP^{OE}. The tonoplast is stained with MDY-64, cell walls are stained with propidium iodide (PI). Scale bars = 5 μ m (A and B). C, Cellular organization of the epidermis in the Arabidopsis root meristem in dependence of NET4A-GFP^{OE} and the actin mutant *act7-4*. Cell walls are highlighted by PI and arrowheads depict disorganization of cell walls in the mutant. Scale bar = 20 μ m. D, Effect of NET4A overexpression on root length of actin mutants. n=153 for control, n=154 for NET4A-GFP^{OE}, n=48 for *act7-4*, n=59 for *act7-4* x NET4A-GFP^{OE}, n=57 for *act2 act8* and n=57 for *act2 act8* x NET4A-GFP^{OE}. Scale bar = 5 mm. E, Quantification of *act2 act8* root straightness in dependence of NET4A overexpression. n=60 for control, n=60 for NET4A-GFP^{OE}, n=57 for *act2 act8* and n=57 for *act2 act8* x NET4A-GFP^{OE}. Box limits in all graphs represent 25th-75th percentile, the horizontal line the median and whiskers minimum to maximum values. Significant differences compared with the wild type (control) are shown (one-way ANOVA and Tukey post hoc test; **P* < 0.05; ****P* < 0.001). Selected differences between lines are highlighted in magenta (based on one-way ANOVA and Tukey post hoc test).

NET4A localizes to vacuole-vacuole connection sites, regulating homotypic fusion

To investigate NET4 localization at the tonoplast under actin-depleting conditions, we pharmacologically interfered with filament formation by using the marine toxin latrunculin B (LatB). It has been previously shown that LatB treatment leads to vacuole fragmentation, inducing numerous small isolated vacuolar structures (Scheuring et al., 2016). While NET4 localized in a bead-on-a-string pattern at the tonoplast (Fig 3A), LatB treatment led to an accumulation of NET4 signals at specific foci, at which vacuolar substructures seem to be physically connected (Fig 3B). This might indicate a NET4 recruitment to distinct tonoplast areas, presumably where (homotypic) vacuole fusion occurs. Consequently, overexpression of NET4 should allow for more efficient fusion. To test for this, we induced vacuole fragmentation by LatB treatment and investigated changes of vacuolar morphology. To highlight the vacuolar lumen, we used the dye BCECF (Scheuring et al., 2015) and monitored morphology in the *net4a net4b* double mutant and in the NET4A overexpression line compared to Col-0 wt as control. As expected, LatB induced fragmentation of vacuoles in the control. However, NET4A-GFP^{OE} was largely resistant against LatB, displaying vacuoles of almost unchanged size and shape (Fig 3C and 3D). The approximated vacuole size in control and *net4a net4b* significantly decreased and the number of vacuolar structures increased in parallel; the latter, however, to a lower extent in the double mutant (which already showed more structures under untreated conditions). NET4A-GFP^{OE} vacuoles on the other hand remained larger and the already fewer numbers under normal conditions hardly increased (Fig. 3E and 3F). This LatB resistance could be confirmed on the level of root growth, where LatB-dependent growth inhibition of the overexpressor but also that of the double mutant was significantly reduced (Fig. 3G). When monitoring lifeact-RFP during LatB treatment, we observed a seemingly slower actin filament depolymerization in the NET4A-GFP^{OE} background (Supplementary Fig S4).

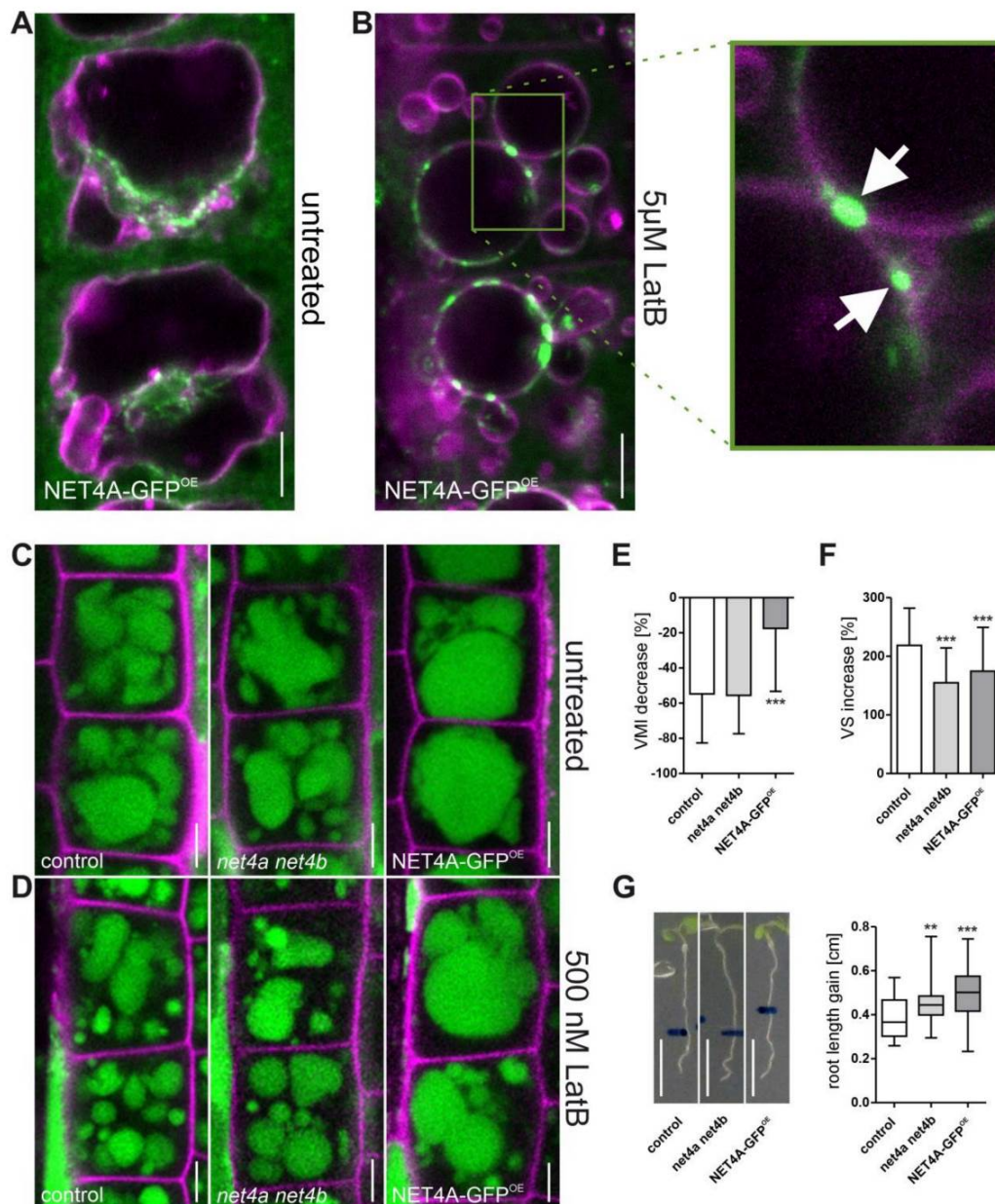


Figure 3 NET4 localizes to vacuole connections and impacts actin stability. A, Tonoplast staining by FM4-64 in the NET4A-GFP^{OE} background. B, 5 μM LatB treatment (5h) to depolymerize actin. C, Vacuoles stained by BCECF in cells (stained by PI) of Col-0 (control), the *net4a net4b* double mutant and the NET4A-GFP^{OE} line. D, LatB impact (5h) on vacuolar morphology. E, Quantification of vacuolar morphology index (VMI) changes. F, Quantification of the relative number of vacuolar structures (VS). n=97 cells from 20 seedlings for control, n=86 cells from 20 seedlings for *net4a net4b* and n=112 cells from 18 seedlings for NET4A-GFP^{OE}. G, Root growth (48h) upon seedling transfer of 4-days-old plants on 50 nM LatB containing half-strength MS medium plates. n=54 for control, n=52 for *net4a net4b* and n=47 for NET4A-GFP^{OE}. Scale bars = 5 μm (A-D) and 5 mm (G). Bar chart columns display mean values and error bars the standard deviation. Box limits in all graphs represent 25th-75th percentile, the horizontal line the median and whiskers minimum to maximum values.

Significant differences compared with the wild type (control) are shown (one-way ANOVA and Dunnett's post hoc test; * $P < 0.05$; ** $P < 0.01$; *** $P < 0.001$).

More compact vacuoles, recovery of mutants with impaired cytoskeleton organization and partial resistance to vacuole changes by actin depolymerization led us to hypothesize that NET4 participates in membrane fusion events at the tonoplast. To test for this, we used *amiR-vps16*, a conditional, on artificial microRNA (amiR) based, mutant of the VPS16 subunit from the HOPS tethering complex and crossed it with NET4A-GFP^{OE}. Vacuolar morphology was assessed upon knock down by Dexamethasone (DEX)-induced expression of the specific amiR. This resulted in fragmented vacuoles for *amiR-vps16* as reported for *amiR-vps39* (Takemoto et al., 2018). In contrast, vacuole fragmentation was significantly reduced in the crossed line (compare Fig 4A and 4B), confirming a role for NET4 in fusion processes at the vacuole. Trafficking towards and fusion with the vacuole requires the recruitment of fusiogenic proteins which is initiated by activated GTPases RAB5 and RAB7 (RABF and RABG in plants) (Aniento et al., 2022). Since RABG3 proteins directly interact with the VPS39 subunit of the HOPS complex (Takemoto et al., 2018), we took advantage of the already existing *rabg3a,b,c,d,e,f* sextuple mutant (Ebine et al., 2014) and investigated vacuolar morphology (Fig 4C and 4D). Additionally, we knocked out *NET4A* in the mutant background creating two septuple mutants. The sextuple as well as the two septuple mutants showed large vacuolar bodies in the cell centre with numerous smaller, possibly disconnected vesicles in the periphery. Sometimes, and more often for the septuple mutants, the large vacuole body appeared to be replaced by two or more smaller vacuole parts (Fig 4C, Supplementary Fig S5A). Notably, root length of sextuple and septuple mutants was severely reduced (Supplementary Fig S5B). To address the cytological basis for these structural changes, we used 3D reconstructions of epidermal cell vacuoles. While control cells showed largely interconnected vacuolar cisternae as reported previously (Scheuring et al., 2016), the sextuple and even more pronounced the analyzed septuple mutant displayed non-fused, disconnected vacuolar substructures/vesicles which in the latter case occupied less cellular space (Fig 4E).

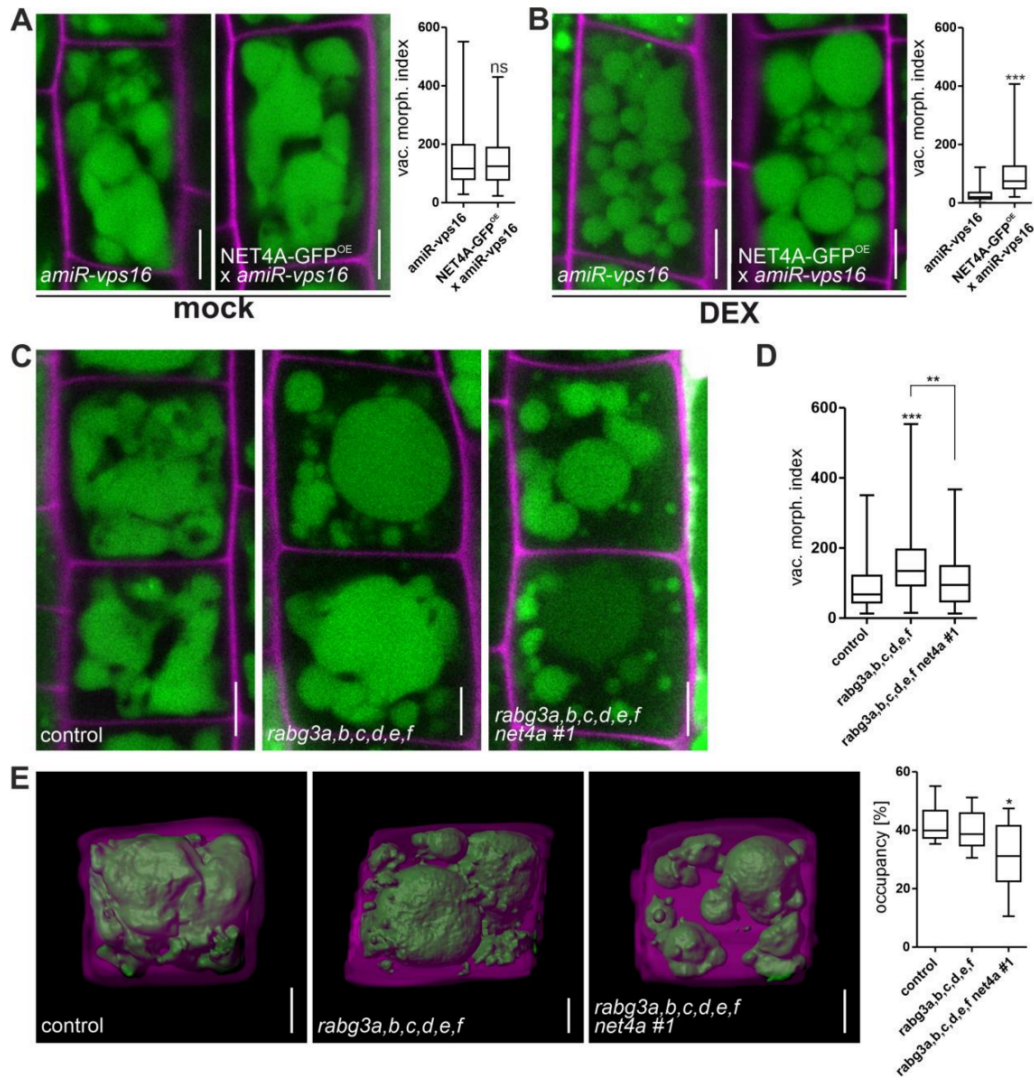


Figure 4 NET4 participates in vacuole fusion events. Conditional knockdown of HOPS and CORVET subunits induces vacuole (stained by BCECF) fragmentation. A, Vacuolar morphology upon knock down of *VPS16* by DEX induction of amiRNA in comparison to the same line crossed with NET4A-GFP^{OE}. B, Quantification of vacuolar morphology index (VMI) for *amiR-vps16* and NET4A-GFP^{OE} x *amiR-vps16* under mock (n=109 and 107) or DEX treatment (n=100 and 97). C, Vacuolar morphology of the *rabg3a,b,c,d,e,f* sextuple and the *rabg3a,b,c,d,e,f net4a #1* septuple mutant compared to Col-0 wild type (control). D, Quantification of (C) using the VMI (n=96 for control, 100 for *rabg3a,b,c,d,e,f* and 92 for *rabg3a,b,c,d,e,f net4a #1*). E, 3D reconstruction of cells and vacuoles as well as quantification of the vacuolar occupancy of cells for control (n=8), *rabg3a,b,c,d,e,f* (n=9) and *rabg3a,b,c,d,e,f net4a #1* (n=9). Box limits represent 25th-75th percentile, the horizontal line the median and whiskers minimum to maximum values. Significant differences are shown and were analyzed by Student's t-test (A, B) or one-way ANOVA and Tukey post hoc test (D, E); **P* < 0.05; ***P* < 0.01; ****P* < 0.001. Scale bars = 5 μ m.

NET4 interacts with RAB-GTPases and unknown proteins

To unravel how NET4 connects to the HOPS complex and RABG3 GTPases, we searched for NET4A interaction partners. To this end, we carried out co-immunoprecipitation

followed by MS-MS analysis. Using NET4A-GFP (endogenous promoter) and NET4A-GFP^{OE} lines (35S promoter), several proteins co-precipitated with the NET4A-GFP fusion protein and were significantly enriched compared to the wt control (Fig 5A and 5B). Among them were two proteins with unknown function (At2g15042 and At4g01245), RABC1 and two RABG3-GTPases. Interestingly, while RABG3-GTPases are localized at multivesicular bodies and the vacuole, RABC1 is considered a *bona fide* marker for the *trans*-Golgi network (Geldner et al., 2009), suggesting a NET4 function in addition to its function at the vacuole. To confirm the interactions, ratiometric Bimolecular Fluorescence Complementation (rBiFC) measurements in transiently transformed *N. benthamiana* were carried out. Except for At2g15042, all tested interactions could be confirmed albeit signal strength was differing (Fig 5C). In addition, testing the same combinations, this finding was confirmed using the mating-based Split-Ubiquitin System (mbSUS) (Grefen et al., 2009) in yeast (Supplementary Fig S6).

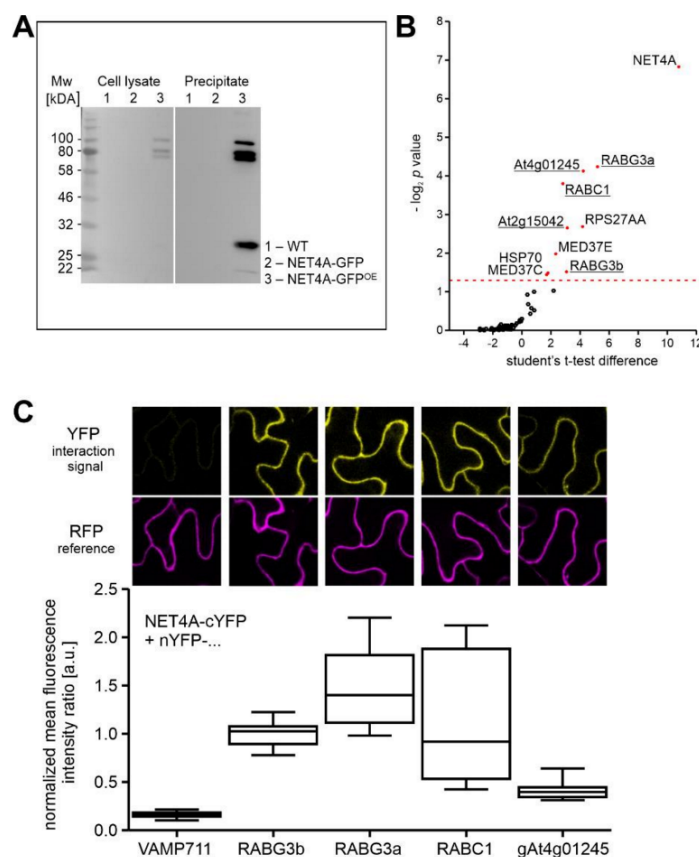


Figure 5 Identification and confirmation of NET4A interaction partners. **A**, Detection of NET4A-GFP fusion protein for the indicated lines using a GFP specific antibody after co-immunoprecipitation of NET4A-GFP interaction partners with GFP-trap magnetic agarose beads. **B**, LC-MS/MS-based identification of proteins that were co-immunoprecipitated with NET4A-GFP. The dashed line marks the threshold for significant increase in protein abundance compared to the wild type (control). Proteins used for confirmation are underlined. **C**, Representative images and quantification of ratiometric bimolecular fluorescence complementation (rBiFC) measurements in *N. benthamiana* leaf epidermis cells. For quantification, YFP signals were normalized to the respective RFP signals to allow comparison of interaction strength. VAMP711, a SNARE localized to the tonoplast was used as negative control.

In order to interact, NET4 and partners must at least partially colocalize. All NET proteins are cytosolic proteins, which are recruited to their target membranes post-translationally. To investigate the possibility of NET4 membrane binding, we conducted

protein-lipid overlay assays. For detection, a NET4 antibody was generated against the full length NET4A protein. To test for specificity, we could show that the antigen is recognized as well as the native protein and GFP-fusion proteins in plant cell extracts when using the anti NET4 antibody (Supplementary Fig S7A). Immunoblotting with an anti GFP antibody showed signals corresponding to the right size only in extracts from GFP-fusion lines (Supplementary Fig S7B). When incubated with a lipid array, NET4 interacted with all negatively charged phospholipids, namely phosphoinositides (PIPs) and phosphatidic acid (PA) (Supplementary Fig S7C). This was confirmed by using an anti HIS antibody for detection of HIS-tagged NET4A (Supplementary Fig S7D). Since individual PIPs are differentially distributed in the endomembrane system and thereby contribute to organelle identity (Noack and Jaillais, 2017), binding of NET4A to all PIPs was casting doubts on its exclusive function in connection with the vacuole.

NET3 and NET4 redundantly interact with tonoplast-residing RABG3s and ER membrane integral VAP27-1

Recently, it has been shown that NET4 interacts with active RABG3 members, indicating that vacuole membrane recruitment of NET4 occurs via this binding (Hawkins et al., 2023). The authors could show that RABG3-binding requires a so-called IRQ-domain, which is present not only in NET4A and NET4B but also in NET3A and NET3C. To investigate membrane recruitment of NET4, we generated truncated GFP-tagged versions of NET4A covering its entire length (Fig 6A). While the Networked-specific actin binding (NAB) domain highlighted filaments as expected, aa 106-503, the middle part of NET4A, showed cytosolic localization and signals at the nuclear envelope (Fig 6B), which colocalized with the ER marker RFP-HDEL during coexpression in *N. benthamiana* leaf epidermal cells (Fig 6C). Intriguingly, the IRQ domain expressed alone (aa 504-542) also highlighted the nuclear envelope (Fig 6B and 6C) and addition of the C-terminus (aa 504-558) was sufficient to result in a clear tonoplast signal (Fig 6B). This is in agreement with published data showing that the IRQ domain plus the C-terminus together are required for RABG3 binding (Hawkins et al., 2023). Performing mbSUS growth assays in yeast, we could also confirm NET4-binding to different RABG3s (Supplementary Fig S6, Fig 6D). Intriguingly, we also found NET3A and NET3C to interact with RABG3A and RABG3B (Fig 6E, Supplementary Fig S8). This finding, together with localization of NET4 truncations at the nuclear envelope, led us to hypothesize that both NET families might be able to carry out exchangeable functions. Therefore, we tested whether NET4 is found at the ER in addition to its association to the tonoplast (Kaiser et al., 2019). To this end, we transiently coexpressed full length NET4A-mTurquoise and NET4B-GFP individually with the ER marker RFP-HDEL. In both cases, a

partial colocalization specifically at the nuclear envelope could be observed (Supplementary Fig S9). In addition, we could confirm NET4 at the nuclear envelope by crossing NET4A-GFP expressing Arabidopsis lines with ER marker lines expressing RFP-HDEL or SR β -mTurquoise, a subunit of the signal recognition particle at the ER membrane (Fig 6F).

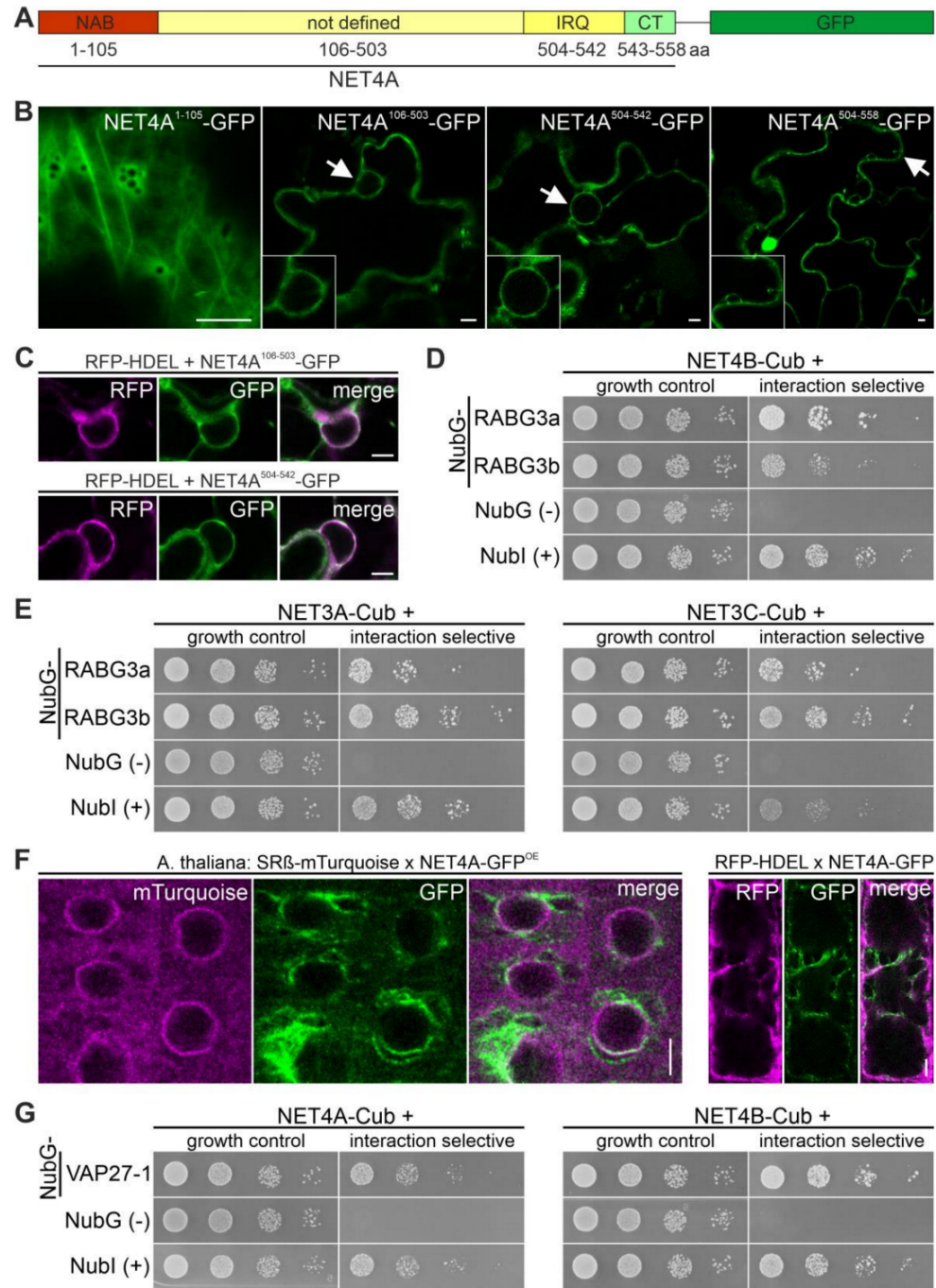


Figure 6 NET3 and NET4 display interchangeable functions. A, Schematic representation of the NET4 domain structure. B, Localization of shortened NET4A upon transient gene expression in *N. benthamiana*. C, Colocalization of either NET4A¹⁰⁵⁻⁵⁰³-GFP or NET4A⁵⁰⁴⁻⁵⁴²-GFP with the ER marker RFP-HDEL upon transient coexpression in *N. benthamiana*. D and E, mating-based Split-Ubiquitin System (mbSUS) growth assays in yeast using NET4B-, NET3A- and NET3C-Cub to test for interaction with NubG-RABG3A and -RABG3B. F, NET4A-GFP^{OE} (35S-promoter) and NET4A-GFP (endogenous promoter) were crossed with the ER marker SRβ-mTurquoise and RFP-HDEL, respectively, and colocalization was determined. G, mbSUS growth assays testing NET4A- and NET4B-Cub for NubG-VAP27-1 interaction. For mbSUS growth assays (D, E and G) THY.AP4 (MATα) yeast strains transformed with Cub-fusions were mated with THY.AP5 (MATα) strains transformed with NubG-fusions. Growth was assayed in dilution series of OD₆₀₀ from 1 to 0.001 at 28°C on growth control media for 36 h to confirm presence of vector fusion constructs and interaction selective media for 72 h to test for specific interaction dependent activation of the reporter genes. NubG was used as negative, Nubl as positive control. **Note:** Nub controls for NET4B in D and G are identical since they are from the same plate. Scale bars: 5 μm.

Since it has been shown that NET3C recruitment to the ER is mediated by its interaction with the ER-resident VAP27-1 (Wang et al., 2014), we tested whether NET4 can also interact with VAP27-1. Yeast mbSUS growth assays confirmed the interaction of both, NET4A and NET4B, with VAP27-1, supporting their presence at the nuclear envelope (Fig 6G).

Higher order NET3-NET4 mutants display impaired vacuolar morphology and reduced growth

Following the hypothesis that NET3 and NET4 families might carry out overlapping functions, higher order NET3/NET4 mutants were generated using either T-DNA insertion mutants or newly generated mutants. To this end, we established a modified CRISPR/Cas9 protocol harbouring fluorescent seed coat markers for efficient detection of transformants. Gene deletions of *NET3A* and *NET3C* in wild type and *net4a net4b* (T-DNA) background as well as full-CRISPR *net3c net4a net4b* deletion lines were established.

Notably, gene expression of *NET4A* and *NET4B* seemed to be remarkably different on the organismal level. While *NET4A* expression started in the transition zone of the root and hardly showed expression in aerial tissue, *NET4B* was expressed strongly in the root meristem and in guard cells of cotyledons (Supplementary Fig S10 and S11). Since *NET4A* and *NET4B* expression in most parts of young seedlings seemed to be mutually exclusive, we monitored general growth defects in the established mutants. Phenotypic analysis revealed that the full-CRISPR *net3c net4a net4b* mutant but neither *net3c* alone nor *net3a* (CRISPR) *net4a net4b* (T-DNA) mutants (Supplementary Fig 12), displayed decreased VMI and vacuolar occupancy (Fig 7A and Fig 7B) together with inhibited root growth (Fig 7C).

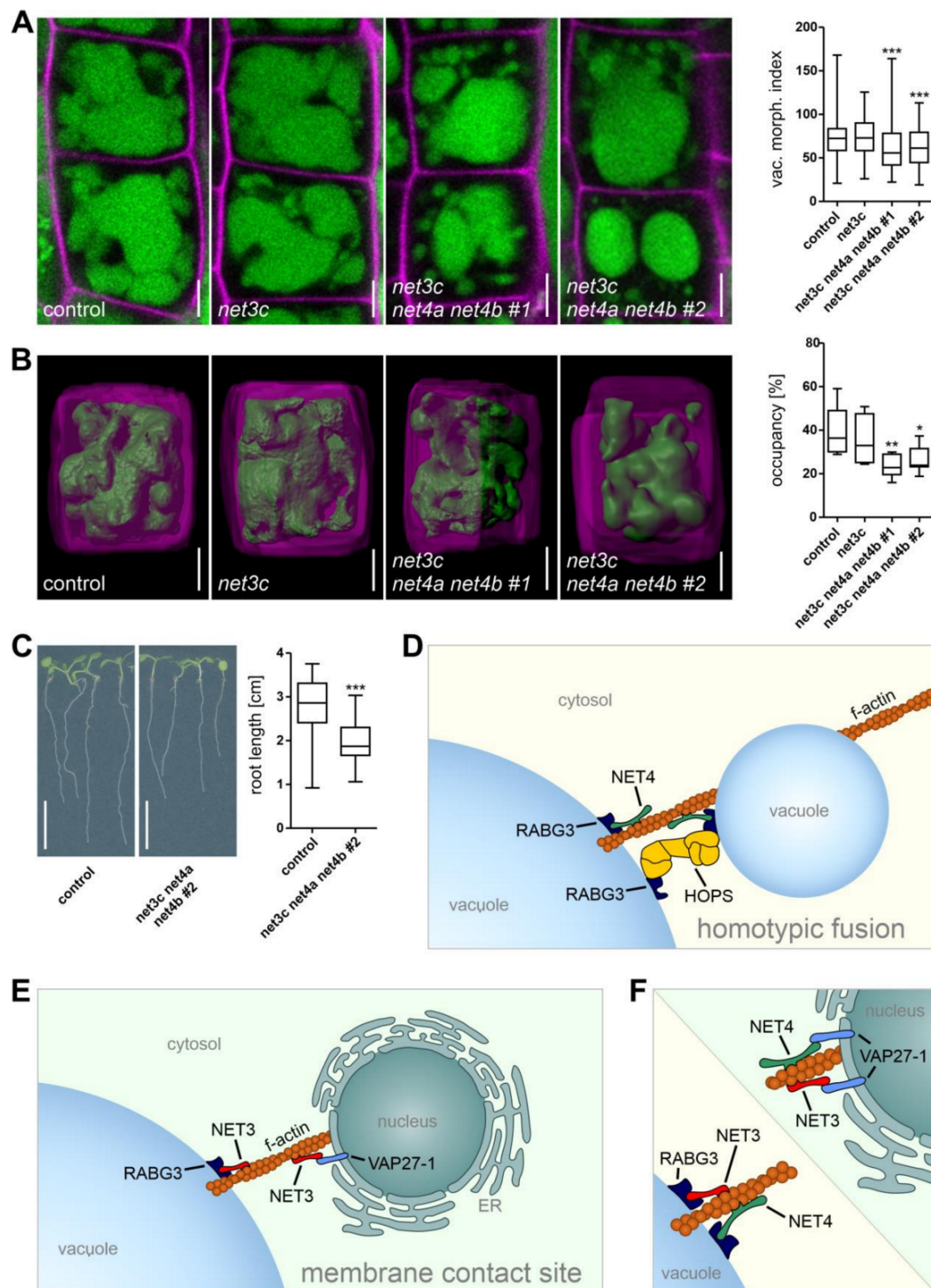


Figure 7 Phenotypic analysis of NET3-NET4 multiple mutants and working model of NET4 function. A, Investigation of vacuolar morphology for lines with CRISPR/Cas9 derived deletion of *NET3C* in Col-0 wild type (*net3c*, n=84), *net4a net4b* t-DNA mutant (*net3c net4a net4b* #1, n=88) and also CRISPR/Cas9 derived deletions of *NET4A* and *NET4B* (*net3c net4a net4b* #2, n=124) compared to Col-0 control (n=212). B, 3D vacuole and cell reconstructions and quantification of vacuolar

occupancy for Col-0 control (n=6), *net3c* (n=6), *net3c net4a net4b #1* (n=8) and *net3c net4a net4b #2* (n=7). Box limits represent 25th-75th percentile, the horizontal line the median and whiskers minimum to maximum values. Significant differences are shown and were analyzed by one-way ANOVA and Dunnett's post hoc test; * $P < 0.05$; ** $P < 0.01$; *** $P < 0.001$. Scale bars = 5 μm for (A) and (B). C, Root growth of 6 days old Arabidopsis seedlings for Col-0 control (n=55) and *net3c net4a net4b #2* (n=49). Scale bar = 1 cm. D, Working model indicating homotypic vacuole fusion: NET4 binds actin filaments and is recruited via its IRQ domain to vacuole-bound RABG3. Binding of RABG3 to the HOPS tethering complex will allow membranes to come into close proximity and SNARE-interaction will mediate membrane fusion. E, The ability of ER-localized NET3A or NET3C to bind RABG3 at the vacuole connects these organelles, but since neither HOPS tether complex nor the correct set of SNAREs are present at the ER, no fusion will occur. This could potentially represent an unknown and plant specific membrane contact site between the ER and the lytic vacuole. F, Since NET4 is able to bind the membrane contact site protein VAP27-1 at the ER, functional redundancy of NET3 and NET4 occurs at both locations, tonoplast and ER.

Discussion

NET4A reorganizes actin filaments towards the nuclear envelope compensating defects in actin mutants

Our previous findings indicate that the vacuole-cytoskeleton interface is crucial to regulate vacuolar morphology and relative vacuole size (Scheuring et al., 2016). The present data indicate that remodeling of actin filaments contributes to shape the vacuole. More compact vacuoles of NET4 are accompanied by actin filaments focused towards the nucleus (Fig 1). Thus, in addition to the original description that NET4 accumulates at sites of vacuolar constrictions (Kaiser et al., 2019), NET4 seems to be especially abundant next to the nucleus. Enhanced recruitment of actin filaments towards the cells' centre can compensate for the loss of vegetative actin isoforms such as *ACTIN 7* (Fig 2). *ACT7* has been shown to be specifically involved in root growth and root architecture as well as being highly responsive towards treatment with the plant hormone auxin (McDowell et al., 1996; Kandasamy et al., 2009). Actin filaments recruited towards the nuclear envelope by NET4A-GFP^{OE} are in close proximity of the nucleus, which could indicate a function in nucleus positioning. In animal cells, maintaining nuclear shape and position requires lamins, a type of intermediate filaments which do not exist in plants (Gundersen and Worman, 2013). In plants, nucleus positioning in root hairs has been reported to depend on filamentous actin organization (Ketelaar et al., 2002; Chytilova et al., 2000). Thus, we tested nucleus positioning in NET4A-GFP^{OE} and *net4a net4b* but could not detect any changes in epidermal root cells of the meristem (data not shown). However, limited vacuole fragmentation (Fig 3) and slower actin depolymerisation (Supplementary Fig S4) upon LatB treatment strongly suggests a stabilizing function of NET4A at the tonoplast.

NET localizes to fusion sites at the vacuole

It has been shown that organelle-bound actin is required for vacuole fusion events in yeast (Eitzen et al., 2002). Prior to fusion, vacuoles come close, thereby forming the so-

called boundary membrane, which resembles a flattened disc. The edge of this boundary is termed the vertex ring, where lipids and fusogenic proteins (responsible for fusion) accumulate (Starr and Fratti, 2019). Intriguingly, upon vacuole disassembly by LatB, NET4 signals at contact sites of still docked vacuoles strongly resemble these vertex rings (Fig 3). In yeast, vertex rings accumulate lipids such as phosphoinositides and ergosterol but also actin becomes enriched (Eitzen et al., 2002). After phosphoinositide enrichment (phosphatidylinositol 3-phosphate, PI3P), a Rab7-GTPase is recruited to the vacuolar membrane (Wickner, 2010). The HOPS-specific subunits Vps39p and Vps41p subsequently bind to Rab7 and allow for assembly of the SNARE proteins and eventually membrane fusion (Balderhaar and Ungermann, 2013). The interaction with RABG3a and RABG3b directly links NET4 to specific fusion sites at the vacuole (Fig 5, Supplementary Fig S6). Since NET4A overexpression partially rescued HOPS knockdown and *NET4A* deletion enhanced the fusion-defective RABG3 sextuple mutant, it is possible that NET4 defines actin anchor points at vertex rings. Interestingly, upon HOPS knockdown, connections between vacuolar substructures were lost and several, fragmented and entirely spherical vacuoles occurred.

Identification of interaction partners

The identification of four interaction partners, which are localized to different organelles, suggests additional functions for NET4 apart from connecting actin to the tonoplast. We hypothesize that depending on the interaction partner, adaptor complexes of different composition can be formed to connect different organelles via actin filaments (Fig 7D-F). Prior to the formation of PM-ER contact sites, several proteins (including NET3C, VAP27, KLCR1 and IQD2) have been shown to interact, forming adaptor complexes to bridge the cytoskeleton with the respective organelles (Zang et al., 2021). NET3 proteins have been demonstrated to reside close to the nucleus, at the ER and the nuclear envelope, where they form membrane contact sites, connecting the PM with the ER via the cytoskeleton (Wang et al., 2014; Zang et al., 2021). Notably, a so-called IRQ domain has been identified in NET3A and NET3C which is also present in the tonoplast-residing NET4A and NET4B (Hawkins et al., 2023). While it has been shown already that NET4A and NET4B interact with active RABG3s via this domain (Hawkins et al., 2023), we could extend this finding demonstrating that the ER-resident NET3A and NET3C interact with tonoplast residing RABG3 GTPases as well. Together with the partial ER-localization of NET4 and its ability to interact with the ER-PM contact site protein VAP27 (Wang et al., 2014), this establishes a direct connection between the ER and the vacuole. This could represent an efficient way to provide ER-derived lipids to the expanding vacuole or to deliver distinct sets of proteins to developing (pro-) vacuoles (Viotti et al., 2013; Minina et al., 2021). NET3- and

NET4-mediated bridging of the ER and the vacuole to establish a membrane contact site would be novel in plants. A lysosome-ER contact site has just been demonstrated for animal cells (Tan and Finkel, 2022). Interestingly, although RABC1 has been used as marker for the *trans*-Golgi network (Geldner et al., 2009), it has been localized to the ER as well lately (Ge et al., 2022).

NET3 and NET4 function redundantly and seem to be involved in the generation of an ER-vacuole membrane contact site.

The (at least partial) functional redundancy between NET3 and NET4 might also explain the lack of an obvious and global *net4a net4b* phenotype (Kaiser et al., 2019; Hawkins et al., 2023). While none of the other NET superfamily members were transcriptionally upregulated in the *net4a net4b* background (Kaiser et al., 2021), compensation could be achieved by NET3s on the protein level. Only the generation of multifold *net3 net4* mutants resulted in a clear phenotype on different levels (Fig 7). The presence of numerous small vacuolar structures and the smaller relative size (occupancy) of the *net4a net4b net3c* triple mutant lines suggests disturbance of homotypic fusion processes. In addition, restricting vacuolar occupancy of the cell seems likely to be the cause for impaired root growth, since it interferes with the space-filling-function of the vacuole as reported previously (Kaiser and Scheuring, 2020).

Taken together, NET4 seems to participate in homotypic vacuole fusion events by interacting with the HOPS complex via RABG3 binding (Fig 7D). In addition, NET3 and NET4 proteins redundantly form complexes with RABG3-GTPases, VAP27-1 and actin filaments, potentially to establish a, yet unknown and plant-specific, membrane contact site between the ER and the vacuole (Fig 7E and F). This direct connection would allow direct lipid and protein transfer, which is especially important in young and expanding cells. Here, the availability of lipids would facilitate a rapid expansion of vacuoles, which are the basis for high cell elongation rates and fast plant growth.

Material and Methods

Plant Material and Growth Conditions

Arabidopsis thaliana ecotype Columbia-0 (Col-0) was used as wild type control. The following lines were described previously: lifeact-RFP (Rosero et al., 2016), 35S::NET4A-GFP (NET4A-GFP^{OE}) (Kaiser et al., 2019), NET4A::NET4A-GFP (NET4A-GFP) (Deeks et al., 2012), RFP-HDEL, *xi-k/1/2* (Peremyslov et al., 2010), *act7-4* (Gilliland et al., 2003), *act2 act8* (Kandasamy et al., 2009), *net4a net4b* (Kaiser et al., 2019) and *rabg3a,b,c,d,e,f* (Ebine et al., 2014). Seeds were surface sterilized with ethanol and plates were stratified at 4 °C for 1–2 days in the dark and grown vertically at 22 °C under a 16 h light/8 h dark-cycle. For seedling growth, half-strength Murashige and Skoog (MS) medium (Duchefa,

Netherlands), including 1% (w/v) sucrose (Roth, Germany), 2.56 mM MES (Duchefa) and 1% (w/v) Phytoagar (Duchefa) was used at pH 5.7.

Chemicals and Treatments

The dyes MDY-64, propidium iodide (PI), FM4-64 and BCECF-AM were acquired from Life Technologies (CA, USA). The synthetic auxin α -Naphthaleneacetic acid (NAA) and dexamethasone (DEX) were obtained from Duchefa and latrunculin B (LatB) from Sigma-Aldrich (MO, USA). Except PI, all chemicals were obtained in powder form and dissolved in dimethyl sulfoxide (DMSO).

RNA Extraction and Quantitative Real Time PCR

RNA extraction and transcription into cDNA was carried out as described previously (Jeblick et al., 2023). For qRT-PCR, the PerfeCTa SYBR Green SuperMix for iQ (Quanta BioSciences, USA) was used and reactions were carried out in a CFX Connect Real-Time PCR Detection System (Bio-Rad, USA). Reaction procedures were set to an initial heating step of 95 °C for 3 min as well as 40 cycles of denaturing at 95 °C for 10 s followed by combined annealing-extension at 60 °C for 40 s. Primers used for target and housekeeping genes (*PP2A*) are shown in Supplemental Table S1. To calculate relative expression ratios, the efficiency corrected calculation model was used (Pfaffl, 2001).

Cloning

All expression constructs were generated using the GreenGate system (Lampropoulos et al., 2013) and are listed in Supplemental Table S2. Primers used to amplify sequences for the creation of new GreenGate entry vectors are given in Supplemental Table S3. GFP, mTurquoise and mCherry modules (pGGD011, pGGD-GSL-mTurquoise, pGGD010 and pGGF Alli-mCherry) were published before (Lupanga et al., 2020; Stührwohldt et al., 2020; Waadt et al., 2017; Stephani et al., 2020). Internal *Bsa*I sites were mutated. To this end, additional internal primers were used to introduce suitable silent point mutations during the amplification of separate sequence parts, and the resulting PCR products were fused. In case *Bsa*I sites were present in promoter sequences, no entry vector was generated. Instead, the sequence was amplified using suitable primers to produce matching overhangs by using alternative restriction enzymes. Subsequently, the final construct was generated preassembling all modules without the promoter module. Later, the promoter sequence with matching overhangs was added by ligation in a separate reaction. A list of all entry modules generated is provided as Supplemental Table S4. The DEX-inducible amiRNA based knockdown constructs for *VPS16* (*amiR-vps16*) was cloned as described for other *VPS* (Takemoto et al., 2018). Primers used to amplify intermediate and final amiR sequences against *VPS16* are listed in Supplementary Table S5. Deletion mutants were obtained using the egg cell-specific promoter-controlled CRISPR/Cas9 cloning system based on the vector pHEE401E (Wang et al., 2015). To improve the screening for transformed plants, the hygromycin resistance cassette of the original vector was replaced by a mCherry seed coat marker cassette from the GreenGate vector pGGF Alli-mCherry (Stephani et al., 2020), resulting in the generation of pHEE-mCherry. To this end, available *Eco*RI and *Sac*II restriction sites of pHEE401E were used to cut out the hygromycin resistance cassette. Vector backbone sequences that were thereby deleted in addition to the cassette were amplified by PCR and cloned back together with the PCR-amplified seed coat marker cassette. Used Primers are given in Supplemental Table S6. The web tools CHOPCHOP

(<https://chopchop.cbu.uib.no/>; (Labun et al., 2016)) and CCTop (<https://cctop.cos.uni-heidelberg.de/>; (Stemmer et al., 2015)) were used to select suitable guide RNAs (gRNAs). All constructs were generated by inserting a PCR fragment with two gRNAs for the same gene in the used vector as described in Xing et al. (Xing et al., 2014), aiming to delete the region between the two target sites (Supplementary Fig S13). Amplification of the respective insertion fragments was performed using the primers listed in Supplemental Table S7 and vector pHEE2E-TRI as a template. All generated CRISPR/Cas9 constructs are listed in Supplemental Table S8 and details about the used base vector and gRNAs are given. The obtained mutant lines are shown in Supplemental Table S9.

DNA constructs for rBiFC and mbSUS assays were generated via the 2in1 cloning system (Mehlhorn et al., 2018) or Gateway™ technology (Invitrogen, Thermo Fisher Scientific, Carlsbad, CA, USA). Coding sequences were PCR amplified from Col-0 seedling's cDNA or suitable vectors harbouring the sequence. In case of At4g01245, the non-spliced gene was amplified from genomic DNA of Col-0 leaves. All primers are given in Supplemental Table S10. PCR products were recombined into pDONR221-P1P4 or pDONR221-P3P2 for rBiFC and pDONR207 for mbSUS via BP reaction according to the manufacturer's instructions (Invitrogen). Eventually, LR recombination was performed to clone sequences from the generated entry vectors into the appropriate destination vectors pBiFCt-2in1-NC for rBiFC and pNX35-DEST-1 or pMetOYC-Dest for mbSUS. The resulting final constructs are listed in Supplemental Table S11. For recombinant protein expression, the coding sequence of NET4A was amplified from Col-0 cDNA and cloned into pET28a(+) (Sigma-Aldrich) using the restriction sites for *BtgZI* and *XhoI*. Used primers are given in Supplemental Table S12. All generated constructs were confirmed by sequencing.

Crossing of Arabidopsis and generation of new lines

For generation of stable Arabidopsis plants, *A. tumefaciens* was transformed as described previously (Jeblick et al., 2023), and floral inoculation performed as described by Nurusaka et al. (Nurusaka et al., 2010). The lines lifeact-RFP x NET4A-GFP^{OE}, *xi-k/1/2* x NET4A-GFP^{OE}, *act7-4* x NET4A-GFP^{OE}, *act2 act8* x NET4A-GFP^{OE}, NET4A-GFP^{OE} x *amiR-vps16*, SRβ-mTurquoise x NET4A-GFP^{OE}, RFP-HDEL x NET4A-GFP were generated by crossing the respective parental lines as shown in Supplemental Table S13. Homozygous lines were identified by genotyping using the corresponding genotyping primers in Supplemental Table S14. In case of fluorophor-fusion lines, the offspring of a potential homozygous plant was checked for fluorescence signals to verify homozygosity. CRISPR/Cas9 deletion mutants were additionally selected according to the loss of the CRISPR/Cas9 construct in the following generation. All newly established Arabidopsis lines are homozygous, except two of the crossing lines as stated in Supplemental Table S13.

Confocal Microscopy

Live cell imaging, except for rBiFC assays, was performed with a Zeiss LSM880, AxioObserver SP7 confocal laser-scanning microscope, equipped with either a Zeiss C-Apochromat 40x/1.2 W AutoCorr M27 water-immersion objective or a Plan-Apochromat 20x/0.8 M27 objective (INST 248/254-1). Vacuole stainings were carried out as described previously (Scheuring et al., 2015). Cell walls were stained by mounting roots in 0.01 mg/ml PI solution. Fluorescence signals were acquired for mTurquoise (excitation/emission 405 nm/464-482 nm), MDY-64 (excitation/emission 458 nm/473-527 nm), GFP and BCECF (excitation/emission 488 nm/500-571 nm), RFP/mCherry (excitation/emission 594 nm/598-

687 nm), FM4-64 (excitation/emission 543 nm/583–758 nm) and PI (excitation/emission 543 nm/580–718 nm), and processed using Zeiss software ZEN 2.3 or Fiji software (<https://imagej.net/Fiji>). Z-stacks were recorded with a step size of either 400 nm (for quantitative analysis of actin filament organization) or 540 nm (for 3D reconstruction of cells and vacuoles and assessment of vacuolar occupancy). For rBiFC experiments, samples were imaged using the Leica TCS SP8 WLL SMD-FLIM-FCS with an HC PL APO CS2 63x/1.20 (water) objective. Fluorophores were excited using a white laser (514 nm for YFP, 570 nm for RFP) and the emission was detected using hybrid detectors (HyD SMD; 520–560 nm for YFP, 580–630 nm for RFP).

Phenotype Analysis

Root length, calculation of vacuolar morphology index (vac. morph. index, VMI), plasma membrane-tonoplast distance and vacuolar occupancy of the cell (occupancy) were carried out as described previously (Kaiser et al., 2019). For the quantification of vacuolar structures (VS), epidermis cells from the late meristem were used to count seemingly disconnected structures based on single subcortical confocal images. VMI measurements of *amiR-vps16* and NET4A-GFP^{OE} x *amiR-vps16* were conducted in the early elongation zone, taken into account cells that were twice as long as wide. To assess differences in root waviness, root straightness was analyzed as an indirect representation. Therefore, the standard root length (L), in which the extra length due to root waves is included, was measured as usual. In addition, the vertical root length (Lv) was measured as a straight line from root tip to collet start (Fig 2E) and root straightness indicated as the Lv/L ratio.

Quantification of actin filament organization

To investigate the actin filament organization, z-stacks of root epidermal cells were acquired for the late meristematic/early elongated zone. For quantitative analysis, z-stack recordings were processed to half z-stacks, covering early elongated cells of atrichoblast files from the outer cortical confocal section to the cell center (at the position of the nucleus), and used to create maximum intensity projections. Parallelness of actin filaments was then quantified for a defined rectangular area (24.39x11.62 μ m) within a single early elongated atrichoblast cell (excluding cell borders) on each maximum intensity projection using the LPX plugin for ImageJ (URL: <https://lpx.net/services/research/lpx-imagej-plugins/>) according to Higaki (Higaki, 2017). Briefly, a box outlining the defined area of a cell used for quantification was created using the “rectangle” tool of the toolbar menu and added as ROI to the ROI manager. Actin filaments were skeletonized using the “Lpx Filter2d” plugin with “lineFilters” set as filter and “lineExtract” set as linemode. The parameters for “lineExtract” were set to giwsiter = 5, mdnmsLen = 15, pickup = otsu, shaveLen = 5 and delLen = 5. To exclude skeletonized actin filaments outside the desired area of the image, they were masked by inverting the previously created ROI (“Edit→Selection→Make Inverse”) and painting it black using “Edit→Fill” while the intensity value of the “Color picker” tool from the toolbar menu is set to zero. The “Lpx Filter2d” plugin was then used on this masked image with “lineFilters” set as filter and “lineFeature” set as linemode to eventually calculate parallelness (given as “a_normAvgRad” value).

3D Surface Rendering

3D reconstruction of cells and vacuoles was performed using Imaris 8.4 (Bitplane) software (<https://imaris.oxinst.com/>). For the creation of cell models, the manual drawing function (distance) of the surface creation tool was used. Cell borders were marked according to the signals for PI channel on at least every third slice of a z-stack. Subsequently, a surface representing the whole cell was created based on these markings. The surface was then used to produce a masked version of the BCECF-AM channel by using the mask selection function in the edit menu and setting the voxels outside the surface to 0. For the creation of the vacuole models, this masked channel was used to automatically create a second surface corresponding to the BCECF signals. Before completing the surface rendering, the displayed model was visually compared to the underlying BCECF signals and adjustments were made using the absolute intensity threshold option. Eventually, the volumes of the generated 3D models, each given in the statistic menu of the respective surface, were used to calculate the vacuolar occupancy of the cell.

Protein extraction

Arabidopsis proteins, except for Co-immunoprecipitation, were extracted from 8 days old seedlings' roots. Frozen material was grinded in liquid nitrogen and the powder resuspended in four times of its amount of extraction buffer (100 mM KCl, 20 mM 4-(2-hydroxyethyl)-1-piperazineethanesulfonic acid (HEPES), 2 mM Dithiothreitol (DTT), 1 mM phenylmethylsulfonyl fluoride (PMSF), 0.1 mM ethylenediaminetetraacetic acid (EDTA) and 1x cOmplete™, EDTA-free Protease Inhibitor Cocktail (Roche, Switzerland); pH 7.5). The supernatant after centrifugation was used to determine protein concentration via Pierce assay and equal amounts of samples were further processed for immunological detections. For *N. benthamina* leaf samples from rBIFC experiments, protein extraction was performed using Lyse and Load (LL-) buffer (50 mM Tris/HCl; pH 6.8, including 2 % sodium dodecylsulfate (SDS), 7 M urea, 30 % glycerol, 0.1 M DTT and 0.04 % bromophenol blue. Proteins of cell culture samples from mbSUS assays were extracted using the same LL-buffer according to Asseck and Grefen (Asseck and Grefen, 2018).

Immunological detection

For immunological detection, samples were separated via sodium dodecylsulfate polyacrylamide gel electrophoresis (SDS-PAGE). If necessary, samples were mixed with loading dye, incubated at 95 °C for 5 min and shortly centrifuged prior to loading. Blotting was performed using either a nitrocellulose (GE Healthcare, USA) or a polyvinylidene difluoride (PVDF) membrane (Sigma-Aldrich). Membranes were blocked with 5 % skim milk powder in TBS-T (150 mM NaCl, 10 mM Tris/HCl pH 8.0, 0.1% Tween 20), washed with TBS-T and then incubated with the first antibody solution. After washing the membrane again, it was probed with the second antibody for 1 h. Subsequently, the membrane was washed another three times at least, submerged with ECL solution (ECL Prime Kit; Amersham, UK) and chemiluminescence signals were detected using the ChemiDoc system from BioRad. The following antibodies were used: monoclonal anti GFP antibody (1:500; Roche), monoclonal anti HA antibody (1:1000, Roche), polyclonal anti VP16 antibody (Genetex; 1:1000), polyclonal anti NET4 (1:10000) and monoclonal anti HIS antibody (1:3000; Thermo-Fisher).

Co-Immunoprecipitation and mass spectrometry

For the co-immunoprecipitation, 7-day-old seedlings (Col-0, NET4A-GFP, NET4A-GFP^{OE}) were grown on plates. From every plate, 500 mg plant material was harvested, frozen and grinded in liquid nitrogen. Four individual replicates were carried out. 1.5 ml extraction buffer (50 mM NaCl, 50 mM HEPES pH 8, 5 mM MgCl₂, 1 mM PMSF, 2 mM DSP (crosslinker) and 1x cOmplete™, EDTA-free Protease Inhibitor) was added and the samples incubated for 30 min at 4°C. After quenching, lysates were clarified by centrifugation twice at 16,000 g at 4°C. Supernatant was applied onto GFP-nanobodies coupled to magnetic agarose beads (GFP-trap, ChromoTek, Germany) equilibrated in lysis buffer. Beads were incubated with the lysate on an end over end shaker for 1 h at 4°C. To wash the beads, tubes were magnetized for 1 min, the supernatant discarded and 750 µl wash-buffer (50 mM NaCl, 50 mM Tris-HCL pH 8.0, 0.05% Tween-20; 5 mM MgCl₂) was added and tubes were agitated on an end over end shaker for 1 min at 4°C. Two wash cycles were done, followed by three in wash-buffer lacking Tween-20. The final bead pellet was resuspended in 100 µl 2xSDS sample buffer (120 mM Tris-HCL pH 6.8, 20% glycerol, 4% SDS, 0.04 bromphenol blue, 100 mM DTT) and boiled for 1 min at 98°C. After magnetizing again, the eluate was transferred into a new tube and 20 µl were loaded on a 10% SDS-PAGE. Samples were run for approximately 1.5 cm into the separating gel, gels were stained with colloidal Coomassie for 3 h. Visible protein bands were cut out and destained for 30 s using destaining solution (10 % acetic acid, 25 % methanol). Before and after cutting, pictures were taken for documentation purposes. After destaining, the cut bands were diced into 1 x 1 mm cubes and transferred into a reaction tube filled with 0.5 ml of 25 % methanol. The prepared samples were then further processed and analyzed by mass spectrometry as described previously (Müller et al., 2018). After analysis, the raw data were processed with MaxQuant (1.6.3.3) using the latest Uniprot Arabidopsis proteome fasta file. Statistical data analysis was performed using Perseus (Tyanova et al., 2016). First, protein LFQ-values were Log₂-transformed and accessions were removed that were identified in less than two replicates in one of the two categories (Col-0, NET4A-GFP^{OE}). For statistics, missing values were imputed, based on all measured log₂ LFQ intensities, with random numbers. Enrichment between NET4A-GFP^{OE} and Col-0 was determined by one-sided *t*-test and permutation-based FDR of 0.05 and $S_0 = 1$ (when both compared sample sets contained at least three valid values).

Recombinant protein expression and antibody generation

Recombinant protein expression of NET4A in *E. coli* strain was carried out as previously described (Jeblick et al., 2023). The antibody against NET4A was raised by immunizing rabbits with the full-length protein.

Protein-Lipid overlay assay

Lipid overlay assays, using P-6001 PIP stripes (Echelon Biosciences) were performed according to the manufacturer's instructions.

Ratiometric Bimolecular Fluorescence Complementation (rBiFC)

Agrobacterium-mediated transient transformation of approximately 4-week old *N. benthamiana* leaves with 2in1 rBiFC constructs was performed as described previously (Mehlhorn et al., 2018). Fluorescence intensities were recorded 2 days' post infiltration for approximately 20-30 images per construct. Ratios between complemented YFP fluorescence and RFP were calculated and plotted using Fiji and Graphpad Prism5 software.

Immunoblotting verified protein expression utilizing anti NET4A antibody and anti HA peroxidase conjugated antibody, respectively.

Mating-based split ubiquitin system (mbSUS)

Bait/Cub fusions and prey/Nub fusions were generated by cloning the desired genes of interest into the Gateway-compatible vectors pMetOYC-Dest and pNX35-Dest, respectively. These were transformed into haploid yeast strains THY.AP4 (Cub fusion) and THY.AP5 (Nub fusions) as described previously (Asseck and Grefen, 2018). After mating, diploid yeasts were dropped in 10 times OD dilutions on growth control (CSM-Leu-, Trp-, Ura-) and interaction-selective media (CSM-Leu-, Trp-, Ura-, Ade-, His-) supplemented with 50 or 500 μ M methionine. The non-mutated N-terminal ubiquitin moiety (NubI) was used as positive control, and NubI13G (NubG) as negative control. Protein expression was verified in haploid yeast using antibodies against the VP16 domain for the Cub fusion or the HA epitope tag for the Nub fusions.

Transient gene expression

Transient expression was performed as previously described (Jeblick et al., 2023). Infiltrated areas were marked for easier identification and plants were incubated under reduced light conditions for 48-72 h prior microscopic analysis.

GUS-staining

GUS staining of NET4A::GUS-GFP and NET4B::GUS-GFP seedlings was performed as described elsewhere (Béziat et al., 2017). Samples were recorded using a Leica MZ125 stereomicroscope or a Zeiss Observer A.1 microscope with a Leica DMC 4500 camera attached.

Gene Accession Codes

Sequence data of gene and protein sequences used in this article can be found at the Arabidopsis Information Resource (TAIR; <http://www.arabidopsis.org/>), GenBank/EMBL, Aramemnon (<http://aramemnon.uni-koeln.de/>), or UniProt (<https://www.uniprot.org/proteomes/UP000006548databases>) under the following accession numbers: NET4A (At5g58320), NET4B (At2g30500), NET3A (At1g03470), NET3C (At2g47920), RABG3A (At4g09720), RABG3B (At1g22740), VPS16 (At2g38020), VAMP711 (At4g32150), RABC1 (At1g43890) and VAP27-1 (At3g60600).

Statistical analysis

All quantitative data was analyzed using the GraphPad Prism 5 or 9 software (<https://www.graphpad.com/scientific-software/prism/>). The precise statistical method used is given in the respective figure legends. Box-plot borders in the graphs represent 25th to 75th percentile, the horizontal line the median and whiskers minimum to maximum values.

Supplemental data

Supplementary Figure S1. NET4B functions similar to NET4A.

Supplementary Figure S2. NET4A overexpression leads to actin bundling from the cell periphery to the nucleus.

Supplementary Figure S3. Crossing of *net4a net4b* and NET4A-GFP^{OE} complements vacuolar phenotypes.

Supplementary Figure S4. NET4A overexpression stabilizes actin filaments.
 Supplementary Figure S5. *rabg3a,b,c,d,e,f* sextuple and *rabg3a,b,c,d,e,f net4a* septuple mutants show more round vacuoles and inhibited root growth.
 Supplementary Figure S6. Confirmation of NET4A interaction.
 Supplementary Figure S7. Lipid overlay assays (PIP-strips) using NET4 protein.
 Supplementary Figure S8. Expression control for mbSUS experiments in Fig 6.
 Supplementary Figure S9. NET4A and NET4B both show localization at the nuclear envelope.
 Supplementary Figure S10. *NET4A* and *NET4B* gene expression in Arabidopsis using promoter-GUS fusions.
 Supplementary Figure S11. *NET4A* and *NET4B* expression using promoter-GFP fusions.
 Supplementary Figure S12. Phenotypic characterization of *net3a* and *net4a net4b net3a* mutants.
 Supplementary Figure S13. Schematic overview of CRISPR/Cas9 derived deletions for *NET4A*, *NET4B*, *NET3A* and *NET3C*.
 Supplemental Table S1: Primers used for qRT-PCR.
 Supplemental Table S2: List of used expression constructs generated by GreenGate cloning.
 Supplemental Table S3: Primers used for GreenGate cloning.
 Supplemental Table S4: List of entry vectors used for GreenGate cloning.
 Supplemental Table S5: Primers for amplification of *amiR-vps16* sequence.
 Supplemental Table S6: Primers used to generate pHEE-mCherry.
 Supplemental Table S7: Primers used for the generation of CRISPR/Cas9 constructs.
 Supplemental Table S8: List of used CRISPR/Cas9 constructs for generating deletion mutants.
 Supplemental Table S9: List of CRISPR/Cas9 derived deletion mutants.
 Supplemental Table S10: Primers used for the generation of rBiFC and mbSUS constructs.
 Supplemental Table S11: List of generated Gateway expression constructs used for rBiFC and mbSUS experiments.
 Supplemental Table S12: Primers used to clone constructs for recombinant protein expression.
 Supplemental Table S13: List of Arabidopsis lines obtained by crossing.
 Supplemental Table S14: Primers used for genotyping.

Acknowledgements

We would like to thank Takashi Ueda for providing the *rabg3a,b,c,d,e,f* sextuple mutant and Joe McKenna for the RFP-HDEL Arabidopsis line and plasmid. We thank Matthias Hahn for critical reading of the manuscript and constructive advice throughout the project. Technical help from Patrick Pattar, Anne Lau, Sophie Eisele and Benjamin Ziehmer is highly appreciated. For the kind willingness to share facilities and equipment, we thank Ekkehard Neuhaus. This work was supported by grants from the *BioComp* research initiative (Rhineland-Palatinate, Germany) and the German research foundation (DFG; SCHE 1836/4-1 and SCHE 1836/4-2) to D.S.

Literature

- Aniento, F., Sánchez de Medina Hernández, V., Dagdas, Y., Rojas-Pierce, M., and Russinova, E.** (2022). Molecular mechanisms of endomembrane trafficking in plants. *The Plant Cell* **34** (1): 146–173.
- Asseck, L.Y., and Grefen, C.** (2018). Detecting Interactions of Membrane Proteins: The Split-Ubiquitin System. *Methods in molecular biology* (Clifton, N.J.) **1794**: 49–60.
- Balderhaar, H.J.k., and Ungermann, C.** (2013). CORVET and HOPS tethering complexes - coordinators of endosome and lysosome fusion. *Journal of cell science* **126** (Pt 6): 1307–1316.
- Brillada, C., Zheng, J., Krüger, F., Rovira-Diaz, E., Askani, J.C., Schumacher, K., and Rojas-Pierce, M.** (2018). Phosphoinositides control the localization of HOPS subunit VPS41, which together with VPS33 mediates vacuole fusion in plants. *Proceedings of the National Academy of Sciences of the United States of America* **115** (35): E8305–E8314.
- Chytilova, E., Macas, J., Sliwinska, E., Rafelski, S.M., Lambert, G.M., and Galbraith, D.W.** (2000). Nuclear dynamics in *Arabidopsis thaliana*. *Molecular Biology of the Cell* **11** (8): 2733–2741.
- Cui, Y., Zhao, Q., Hu, S., and Jiang, L.** (2020). Vacuole Biogenesis in Plants: How Many Vacuoles, How Many Models? *Trends in plant science* **25** (6): 538–548.
- Deeks, M.J., Calcutt, J.R., Ingle, E.K.S., Hawkins, T.J., Chapman, S., Richardson, A.C., Mentlak, D.A., Dixon, M.R., Cartwright, F., Smertenko, A.P., Oparka, K., and Hussey, P.J.** (2012). A superfamily of actin-binding proteins at the actin-membrane nexus of higher plants. *Current biology CB* **22** (17): 1595–1600.
- Duckney, P.J., Wang, P., and Hussey, P.J.** (2022). Membrane contact sites and cytoskeleton-membrane interactions in autophagy. *FEBS letters* **596** (17): 2093–2103.
- Ebine, K., Inoue, T., Ito, J., Ito, E., Uemura, T., Goh, T., Abe, H., Sato, K., Nakano, A., and Ueda, T.** (2014). Plant vacuolar trafficking occurs through distinctly regulated pathways. *Current biology CB* **24** (12): 1375–1382.
- Eitzen, G., Wang, L., Thorngren, N., and Wickner, W.** (2002). Remodeling of organelle-bound actin is required for yeast vacuole fusion. *The Journal of cell biology* **158** (4): 669–679.
- Ge, S., Zhang, R.-X., Wang, Y.-F., Sun, P., Chu, J., Li, J., Sun, P., Wang, J., Hetherington, A.M., and Liang, Y.-K.** (2022). The *Arabidopsis* Rab protein RABC1 affects stomatal development by regulating lipid droplet dynamics. *The Plant Cell* **34** (11): 4274–4292.
- Geldner, N., Dénervaud-Tendon, V., Hyman, D.L., Mayer, U., Stierhof, Y.-D., and Chory, J.** (2009). Rapid, combinatorial analysis of membrane compartments in intact plants with a multicolor marker set. *The Plant journal for cell and molecular biology* **59** (1): 169–178.
- Gilliland, L.U., Pawloski, L.C., Kandasamy, M.K., and Meagher, R.B.** (2003). *Arabidopsis* actin gene ACT7 plays an essential role in germination and root growth. *The Plant journal for cell and molecular biology* **33** (2): 319–328.
- Grefen, C., Obrdlik, P., and Harter, K.** (2009). The determination of protein-protein interactions by the mating-based split-ubiquitin system (mbSUS). *Methods in molecular biology* (Clifton, N.J.) **479**: 217–233.
- Gundersen, G.G., and Worman, H.J.** (2013). Nuclear positioning. *Cell* **152** (6): 1376–1389.

- Hawkins, T.J., Kopischke, M., Duckney, P.J., Rybak, K., Mentlak, D.A., Kroon, J.T.M., Bui, M.T., Richardson, A.C., Casey, M., Alexander, A., Jaeger, G. de, Kalde, M., Moore, I., Dagdas, Y., Hussey, P.J., and Robatzek, S.** (2023). NET4 and RabG3 link actin to the tonoplast and facilitate cytoskeletal remodelling during stomatal immunity. *Nature Communications* **14** (1): 5848.
- Higaki, T.** (2017). Quantitative evaluation of cytoskeletal organizations by microscopic image analysis. *PLANT MORPHOL* **29** (1): 15–21.
- Jeblick, T., Leisen, T., Steidele, C.E., Albert, I., Müller, J., Kaiser, S., Mahler, F., Sommer, F., Keller, S., Hückelhoven, R., Hahn, M., and Scheuring, D.** (2023). Botrytis hypersensitive response inducing protein 1 triggers noncanonical PTI to induce plant cell death. *Plant Physiology* **191** (1): 125–141.
- Kaiser, S., Eisa, A., Kleine-Vehn, J., and Scheuring, D.** (2019). NET4 Modulates the Compactness of Vacuoles in *Arabidopsis thaliana*. *International journal of molecular sciences* **20** (19).
- Kaiser, S., Eisele, S., and Scheuring, D.** (2021). Vacuolar occupancy is crucial for cell elongation and growth regardless of the underlying mechanism. *Plant Signaling & Behavior* **16** (8): 1922796.
- Kaiser, S., and Scheuring, D.** (2020). To Lead or to Follow: Contribution of the Plant Vacuole to Cell Growth. *Frontiers in Plant Science* **11**: 553.
- Kandasamy, M.K., McKinney, E.C., and Meagher, R.B.** (2009). A single vegetative actin isovariant overexpressed under the control of multiple regulatory sequences is sufficient for normal *Arabidopsis* development. *The Plant Cell* **21** (3): 701–718.
- Ketelaar, T., Faivre-Moskalenko, C., Esseling, J.J., Ruijter, N.C.A. de, Grierson, C.S., Dogterom, M., and Emons, A.M.C.** (2002). Positioning of nuclei in *Arabidopsis* root hairs: an actin-regulated process of tip growth. *The Plant Cell* **14** (11): 2941–2955.
- Kost, B., and Chua, N.-H.** (2002). The plant cytoskeleton: vacuoles and cell walls make the difference. *Cell* **108** (1): 9–12.
- Labun, K., Montague, T.G., Gagnon, J.A., Thyme, S.B., and Valen, E.** (2016). CHOPCHOP v2: a web tool for the next generation of CRISPR genome engineering. *Nucleic Acids Research* **44** (W1): W272–6.
- Lampropoulos, A., Sutikovic, Z., Wenzl, C., Maegele, I., Lohmann, J.U., and Forner, J.** (2013). GreenGate - A Novel, Versatile, and Efficient Cloning System for Plant Transgenesis. *PLOS ONE* **8** (12).
- Lupanga, U., Röhrich, R., Askani, J., Hilmer, S., Kiefer, C., Krebs, M., Kanazawa, T., Ueda, T., and Schumacher, K.** (2020). The *Arabidopsis* V-ATPase is localized to the TGN/EE via a seed plant-specific motif. *eLife* **9**.
- McDowell, J.M., An, Y.Q., Huang, S., McKinney, E.C., and Meagher, R.B.** (1996). The *Arabidopsis* ACT7 actin gene is expressed in rapidly developing tissues and responds to several external stimuli. *Plant Physiology* **111** (3): 699–711.
- Mehlhorn, D.G., Wallmeroth, N., Berendzen, K.W., and Grefen, C.** (2018). 2in1 Vectors Improve In Planta BiFC and FRET Analyses. *Methods in molecular biology* (Clifton, N.J.) **1691**: 139–158.
- Minina, E.A., Scheuring, D., Askani, J., Krueger, F., and Schumacher, K.** (2021). Light at the end of the tunnel: FRAP assay reveals that plant vacuoles start as a tubular network. *bioRxiv* **10.1101/2021.05.13.444058**.

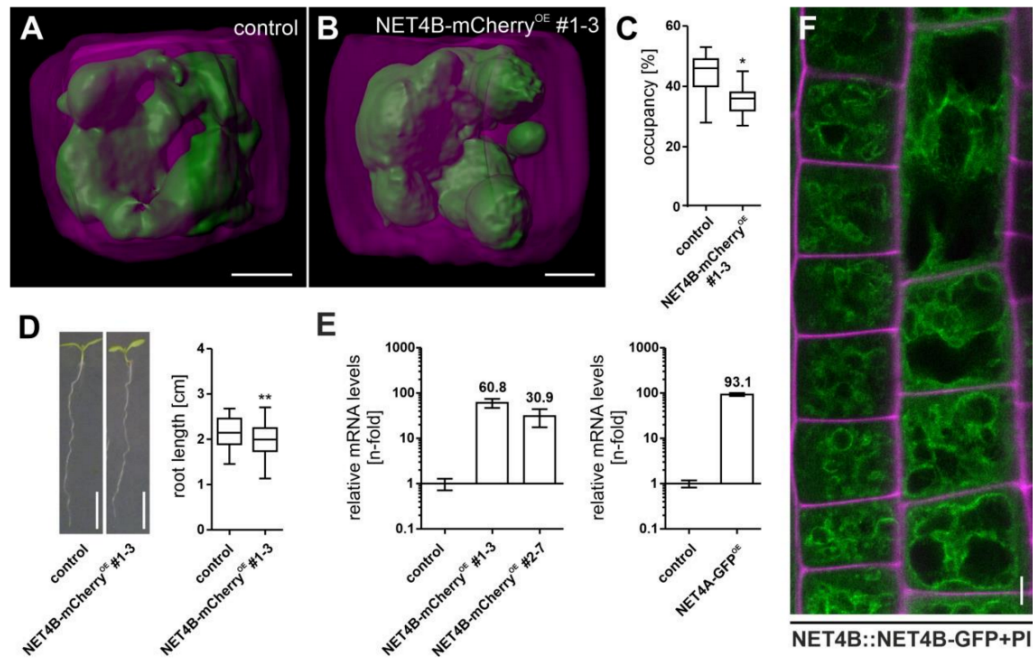
- Müller, N., Leroch, M., Schumacher, J., Zimmer, D., Könnel, A., Klug, K., Leisen, T., Scheuring, D., Sommer, F., Mühlhaus, T., Schroda, M., and Hahn, M.** (2018). Investigations on VELVET regulatory mutants confirm the role of host tissue acidification and secretion of proteins in the pathogenesis of *Botrytis cinerea*. *The New phytologist* **219** (3): 1062–1074.
- Narusaka, M., Shiraishi, T., Iwabuchi, M., and Narusaka, Y.** (2010). The floral inoculating protocol: a simplified *Arabidopsis thaliana* transformation method modified from floral dipping. *Plant Biotechnology* **27** (4): 349–351.
- Noack, L.C., and Jaillais, Y.** (2017). Precision targeting by phosphoinositides: how PIs direct endomembrane trafficking in plants. *Current opinion in plant biology* **40**: 22–33.
- Peremyslov, V.V., Prokhnevsky, A.I., and Dolja, V.V.** (2010). Class XI myosins are required for development, cell expansion, and F-Actin organization in *Arabidopsis*. *The Plant Cell* **22** (6): 1883–1897.
- Pfaffl, M.W.** (2001). A new mathematical model for relative quantification in real-time RT-PCR. *Nucleic Acids Research* **29** (9): e45.
- Riedl, J., Crevenna, A.H., Kessenbrock, K., Yu, J.H., Neukirchen, D., Bista, M., Bradke, F., Jenne, D., Holak, T.A., Werb, Z., Sixt, M., and Wedlich-Soldner, R.** (2008). Lifeact: a versatile marker to visualize F-actin. *Nature Methods* **5** (7): 605–607.
- Rajo, E., Gillmor, C.S., Kovaleva, V., Somerville, C.R., and Raikhel, N.V.** (2001). *VACUOLELESS1* is an essential gene required for vacuole formation and morphogenesis in *Arabidopsis*. *Developmental cell* **1** (2): 303–310.
- Rosero, A., Oulehlová, D., Stillerová, L., Schiebertová, P., Grunt, M., Žárský, V., and Cvrčková, F.** (2016). *Arabidopsis* FH1 Formin Affects Cotyledon Pavement Cell Shape by Modulating Cytoskeleton Dynamics. *Plant & cell physiology* **57** (3): 488–504.
- Scheuring, D., Löffke, C., Krüger, F., Kittelmann, M., Eisa, A., Hughes, L., Smith, R.S., Hawes, C., Schumacher, K., and Kleine-Vehn, J.** (2016). Actin-dependent vacuolar occupancy of the cell determines auxin-induced growth repression. *Proceedings of the National Academy of Sciences of the United States of America* **113** (2): 452–457.
- Scheuring, D., Schöller, M., Kleine-Vehn, J., and Löffke, C.** (2015). Vacuolar staining methods in plant cells. *Methods in molecular biology* (Clifton, N.J.) **1242**: 83–92.
- Scorrano, L., Matteis, M.A. de, Emr, S., Giordano, F., Hajnóczky, G., Kornmann, B., Lackner, L.L., Levine, T.P., Pellegrini, L., Reinisch, K., Rizzuto, R., Simmen, T., Stenmark, H., Ungermann, C., and Schuldiner, M.** (2019). Coming together to define membrane contact sites. *Nature Communications* **10**.
- Shvarev, D., Schoppe, J., König, C., Perz, A., Füllbrunn, N., Kiontke, S., Langemeyer, L., Janulienė, D., Schnelle, K., Kümmel, D., Fröhlich, F., Moeller, A., and Ungermann, C.** (2022). Structure of the HOPS tethering complex, a lysosomal membrane fusion machinery. *eLife* **11**.
- Starr, M.L., and Fratti, R.A.** (2019). The Participation of Regulatory Lipids in Vacuole Homotypic Fusion. *Trends in biochemical sciences* **44** (6): 546–554.
- Stemmer, M., Thumberger, T., Del Sol Keyer, M., Wittbrodt, J., and Mateo, J.L.** (2015). CCTop: An Intuitive, Flexible and Reliable CRISPR/Cas9 Target Prediction Tool. *PLOS ONE* **10** (4): e0124633.
- Stephani, M., Picchianti, L., Gajic, A., Beveridge, R., Skarwan, E., Sanchez de Medina Hernandez, V., Mohseni, A., Clavel, M., Zeng, Y., Naumann, C., Matuszkiewicz, M., Turco, E., Loeffke, C., Li, B., Dürnberger, G., Schutzbier, M., Chen, H.T.,**

- Abdrakhmanov, A., Savova, A., Chia, K.-S., Djamei, A., Schaffner, I., Abel, S., Jiang, L., Mechtler, K., Ikeda, F., Martens, S., Clausen, T., and Dagdas, Y.** (2020). A cross-kingdom conserved ER-phagy receptor maintains endoplasmic reticulum homeostasis during stress. *eLife* **9**.
- Stührwoldt, N., Scholl, S., Lang, L., Katzenberger, J., Schumacher, K., and Schaller, A.** (2020). The biogenesis of CLEL peptides involves several processing events in consecutive compartments of the secretory pathway. *eLife* **9**.
- Takemoto, K., Ebine, K., Askani, J.C., Krüger, F., Gonzalez, Z.A., Ito, E., Goh, T., Schumacher, K., Nakano, A., and Ueda, T.** (2018). Distinct sets of tethering complexes, SNARE complexes, and Rab GTPases mediate membrane fusion at the vacuole in Arabidopsis. *Proceedings of the National Academy of Sciences of the United States of America* **115** (10): E2457-E2466.
- Tan, J.X., and Finkel, T.** (2022). A phosphoinositide signalling pathway mediates rapid lysosomal repair. *Nature* **609** (7928): 815–821.
- Tyanova, S., Temu, T., and Cox, J.** (2016). The MaxQuant computational platform for mass spectrometry-based shotgun proteomics. *Nature protocols* **11** (12): 2301–2319.
- Vale, R.D.** (2003). The molecular motor toolbox for intracellular transport. *Cell* **112** (4): 467–480.
- Viotti, C., Krüger, F., Krebs, M., Neubert, C., Fink, F., Lupanga, U., Scheuring, D., Boutté, Y., Frescatada-Rosa, M., Wolfenstetter, S., Sauer, N., Hillmer, S., Grebe, M., and Schumacher, K.** (2013). The endoplasmic reticulum is the main membrane source for biogenesis of the lytic vacuole in Arabidopsis. *The Plant Cell* **25** (9): 3434–3449.
- Waadt, R., Krebs, M., Kudla, J., and Schumacher, K.** (2017). Multiparameter imaging of calcium and abscisic acid and high-resolution quantitative calcium measurements using R-GECO1-mTurquoise in Arabidopsis. *New Phytol* **216** (1): 303–320.
- Wang, P., Duckney, P., Gao, E., Hussey, P.J., Kriechbaumer, V., Li, C., Zang, J., and Zhang, T.** (2023). Keep in contact: multiple roles of endoplasmic reticulum-membrane contact sites and the organelle interaction network in plants. *New Phytol* **238** (2): 482–499.
- Wang, P., Hawkins, T.J., Richardson, C., Cummins, I., Deeks, M.J., Sparkes, I., Hawes, C., and Hussey, P.J.** (2014). The plant cytoskeleton, NET3C, and VAP27 mediate the link between the plasma membrane and endoplasmic reticulum. *Current biology CB* **24** (12): 1397–1405.
- Wang, Z.-P., Xing, H.-L., Dong, L., Zhang, H.-Y., Han, C.-Y., Wang, X.-C., and Chen, Q.-J.** (2015). Egg cell-specific promoter-controlled CRISPR/Cas9 efficiently generates homozygous mutants for multiple target genes in Arabidopsis in a single generation. *Genome biology* **16** (1): 144.
- Wickner, W.** (2010). Membrane fusion: five lipids, four SNAREs, three chaperones, two nucleotides, and a Rab, all dancing in a ring on yeast vacuoles. *Annual review of cell and developmental biology* **26**: 115–136.
- Xing, H.-L., Dong, L., Wang, Z.-P., Zhang, H.-Y., Han, C.-Y., Liu, B., Wang, X.-C., and Chen, Q.-J.** (2014). A CRISPR/Cas9 toolkit for multiplex genome editing in plants. *BMC plant biology* **14**: 327.
- Zang, J., Klemm, S., Pain, C., Duckney, P., Bao, Z., Stamm, G., Kriechbaumer, V., Bürstenbinder, K., Hussey, P.J., and Wang, P.** (2021). A novel plant actin-microtubule

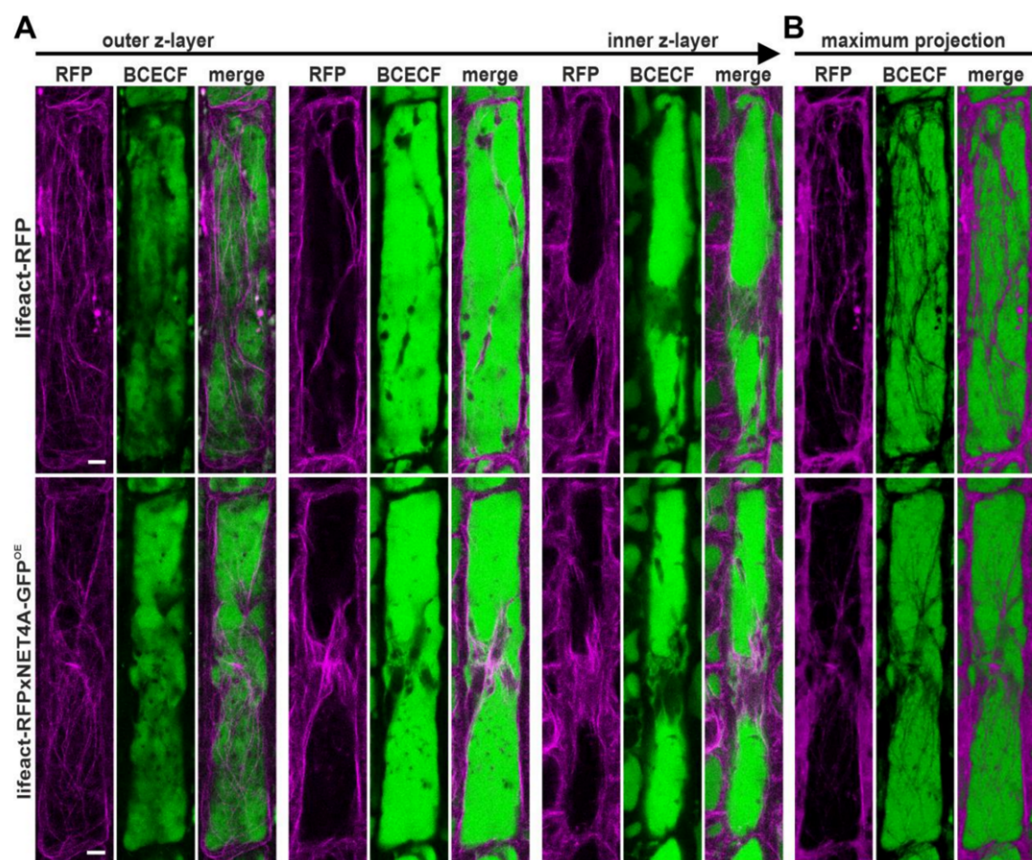
bridging complex regulates cytoskeletal and ER structure at ER-PM contact sites.
Current biology CB **31** (6): 1251-1260.e4.

Supplemental Data: Kaiser et al., 2023

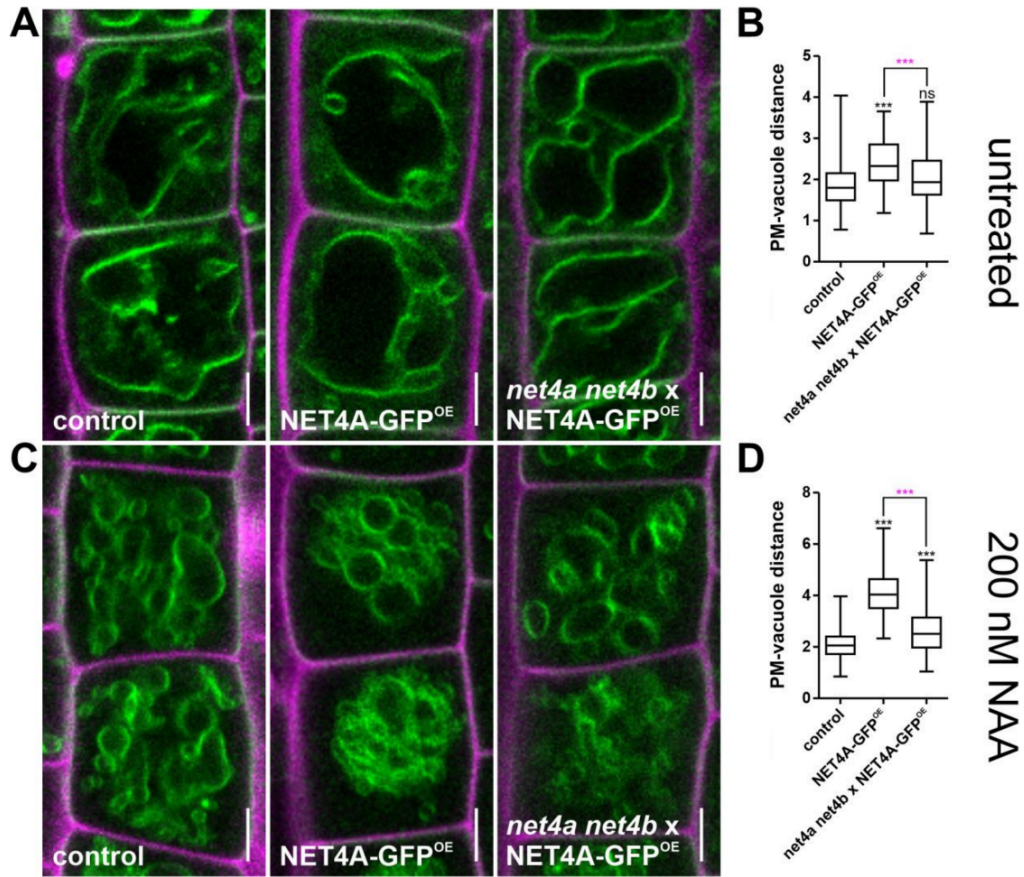
Supplementary Figures



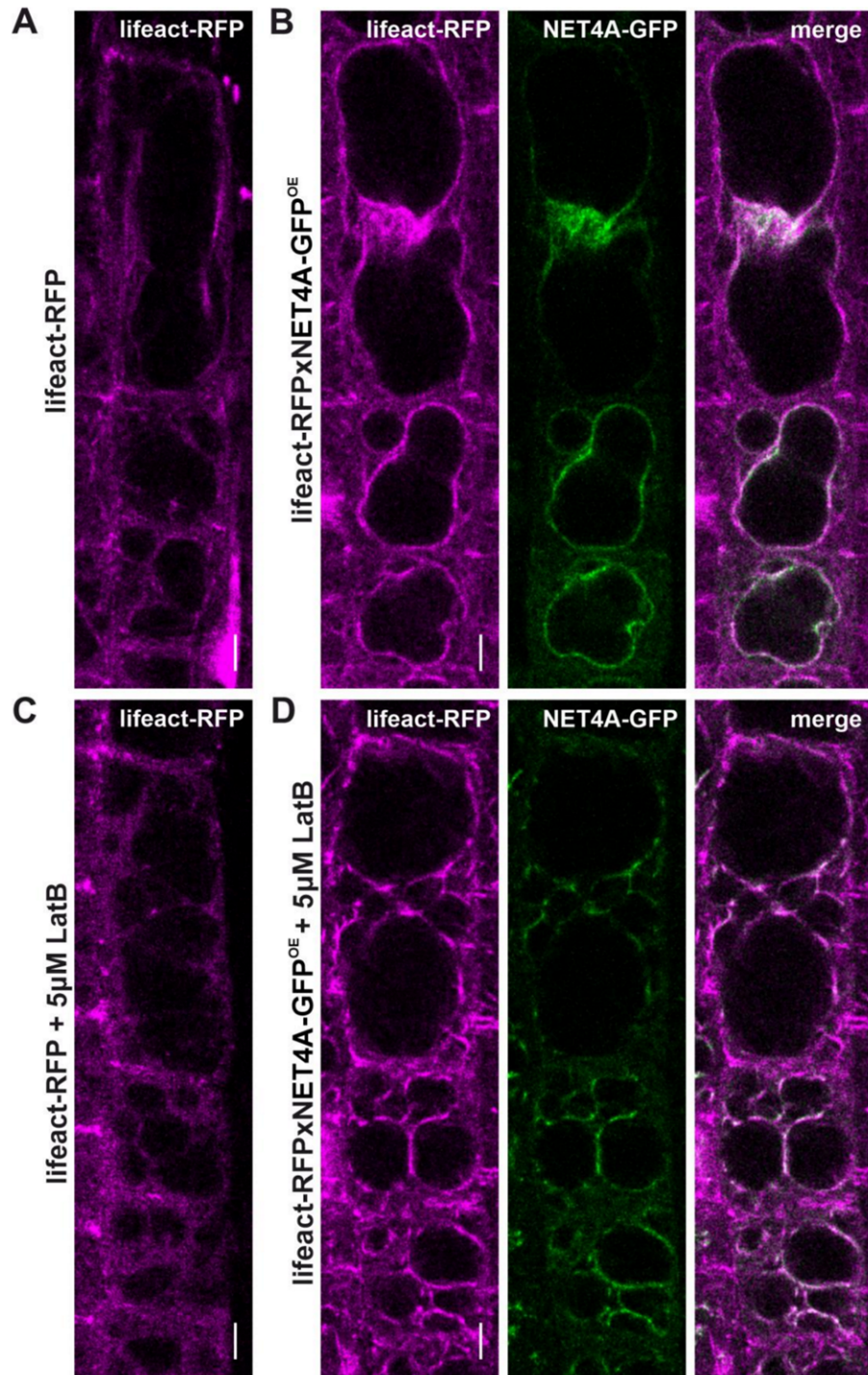
Supplementary Figure S1. NET4B functions similar to NET4A. A, 3D vacuole models of Col-0 wild type control and B, NET4B-mCherry^{OE} epidermal cells from the root meristem. C, Quantification of vacuolar occupancy of the cell (n=7 for each line). D, Root length of NET4B-mCherry^{OE} (n=62) in comparison to the control (n=50). Significant differences were analyzed by Student's t-test, * $P < 0.05$; ** $P < 0.01$. E, Investigation of gene upregulation in NET4B and NET4A overexpression lines by qRT-PCR. F, Subcellular localization of NET4B-GFP (green), expressed under the endogenous promoter. Cell walls (magenta) were stained with propidium iodide (PI). Scale bars = 5 μ m (A, B, F) or 5 mm (D).



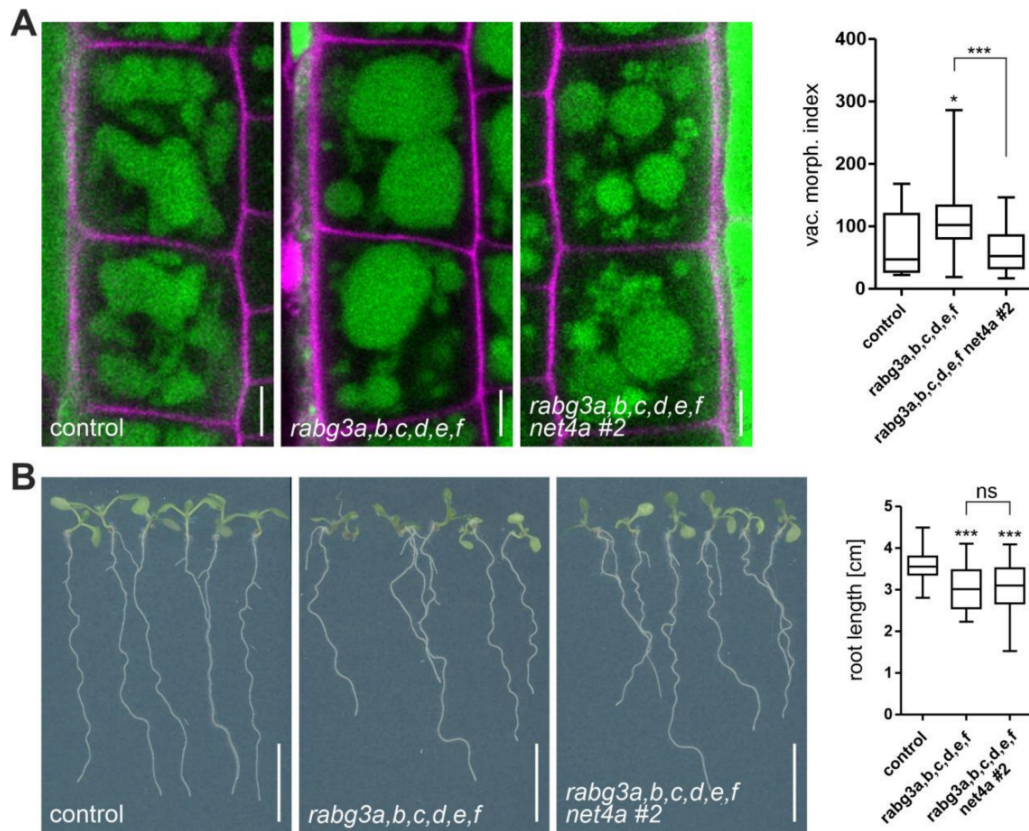
Supplementary Figure S2. NET4A overexpression leads to actin bundling from the cell periphery to the nucleus. A, Actin filaments decorated by lifeact-RFP (magenta) and BCECF stained vacuoles (green) of lifeact-RFP and lifeact-RFP x NET4A-GFP^{OE} for different optical sections starting from the cortex towards the center of the cell. B, Maximum projections of (A). Scale bars = 5 μ m.



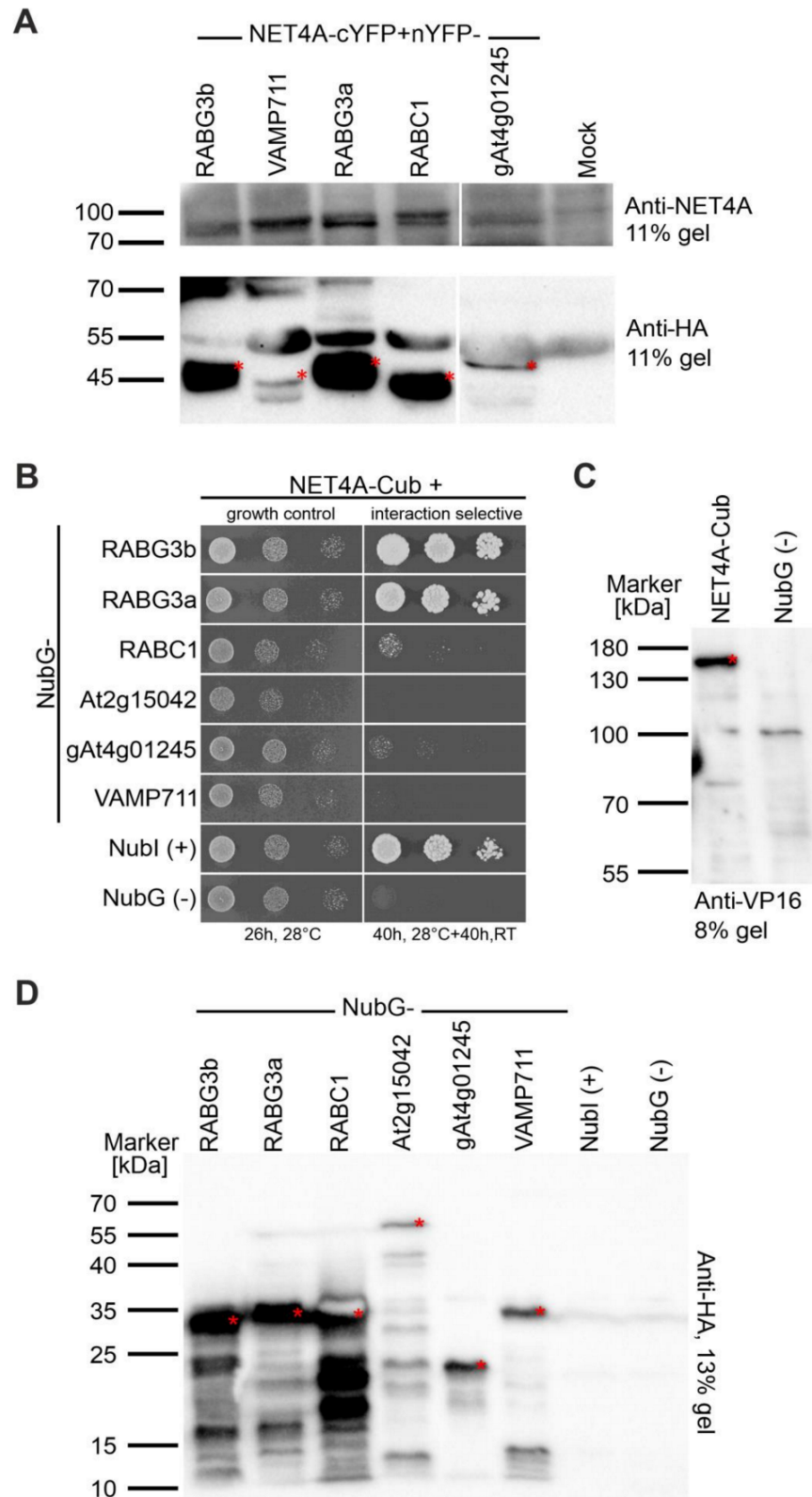
Supplementary Figure S3. Crossing of *net4a net4b* and NET4A-GFP^{OE} complements vacuolar phenotypes. A and B, PM to tonoplast distance of control (n=96), NET4A-GFP^{OE} (n=92) and *net4a net4b* x NET4A-GFP^{OE} (n=96). C and D, Effect of exogenous auxin (NAA) on PM to tonoplast distance (n=92 for each line). Tonoplast was stained with MDY-64, cell walls were stained with propidium iodide (PI). Scale bars = 5 μ m. Box limits in all graphs represent 25th-75th percentile, the horizontal line the median and whiskers minimum to maximum values. Significant differences compared with the wild-type (control) are shown (one-way ANOVA and Tukey post hoc test; ns = not significant; *** $P < 0.001$). Selected differences between lines are highlighted in magenta (based on one-way ANOVA and Tukey post hoc test).



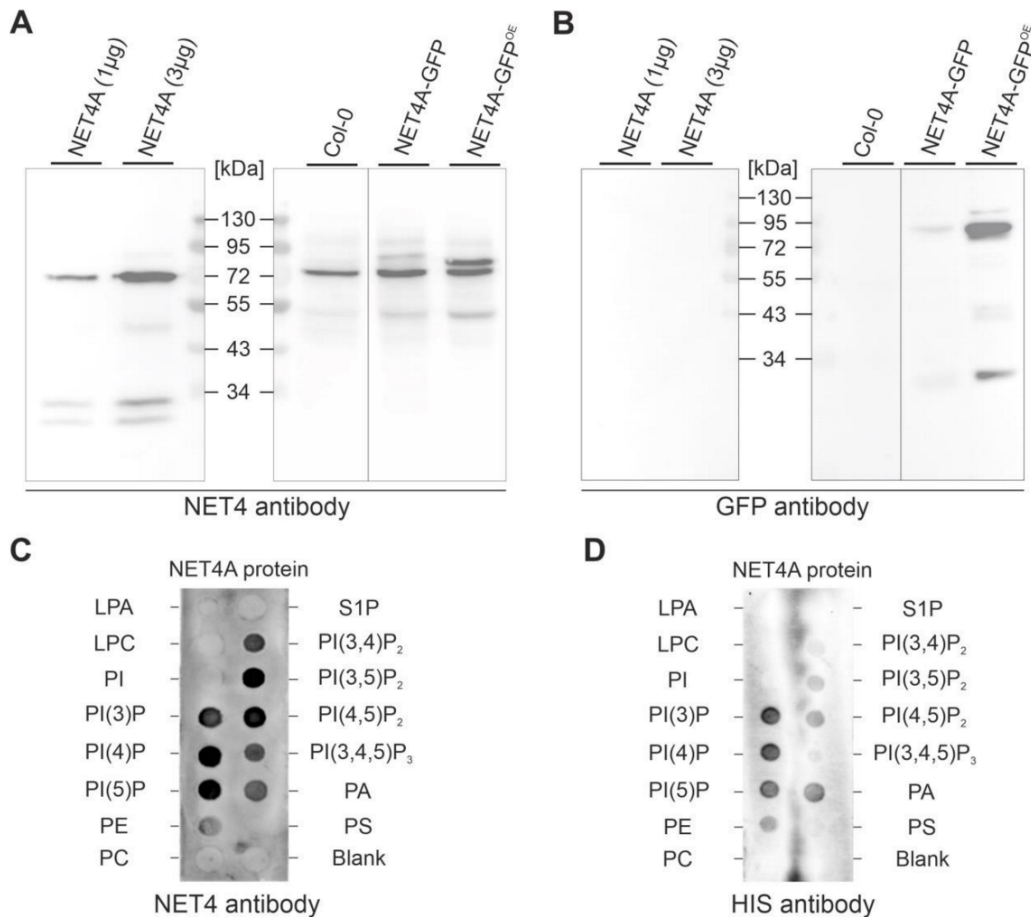
Supplementary Figure S4. NET4A overexpression stabilizes actin filaments. A, lifeact-RFP (magenta) signals in epidermal cells of the root transition zone. B, Transversal optical sections of cells expressing lifeact-RFP and NET4A-GFP^{OE} (green). C, LatB treatment (5 μ M, 5h) of lifeact-RFP. D, Same treatment as in (C) of lifeact-RFP x NET4A-GFP^{OE}. Scale bars = 5 μ m.



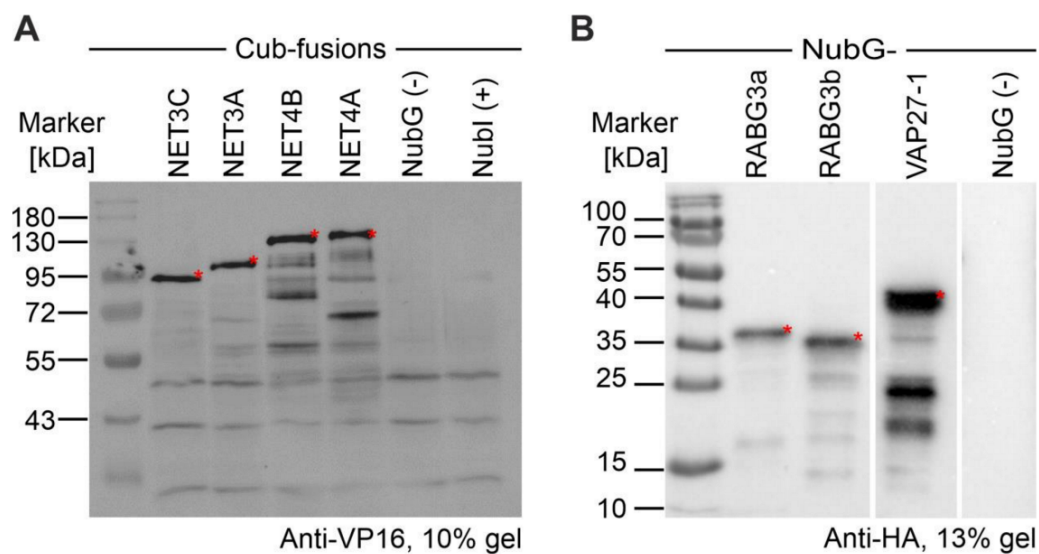
Supplementary Figure S5. *rabg3a,b,c,d,e,f* sextuple and *rabg3a,b,c,d,e,f net4a* septuple mutants show more round vacuoles and inhibited root growth. A, Vacuoles in the *rabg3a,b,c,d,e,f* sextuple (n=28) and the *rabg3a,b,c,d,e,f net4a #2* septuple mutant (n=32) compared to Col-0 wild type control (n=28) and quantification of vacuolar morphology index. B, 6-days old Arabidopsis seedlings. Root length of *rabg3a,b,c,d,e,f* (n=35) and *rabg3a,b,c,d,e,f net4a #2* (n=41) was quantified in comparison to the Col-0 control (n=48). Box limits represent 25th-75th percentile, the horizontal line the median and whiskers minimum to maximum values. Significant differences are shown (one-way ANOVA and Tukey post hoc test; ns = not significant; * $P < 0.05$; *** $P < 0.001$). Scale bars = 5 μ m for (A) and 1 cm for (B).



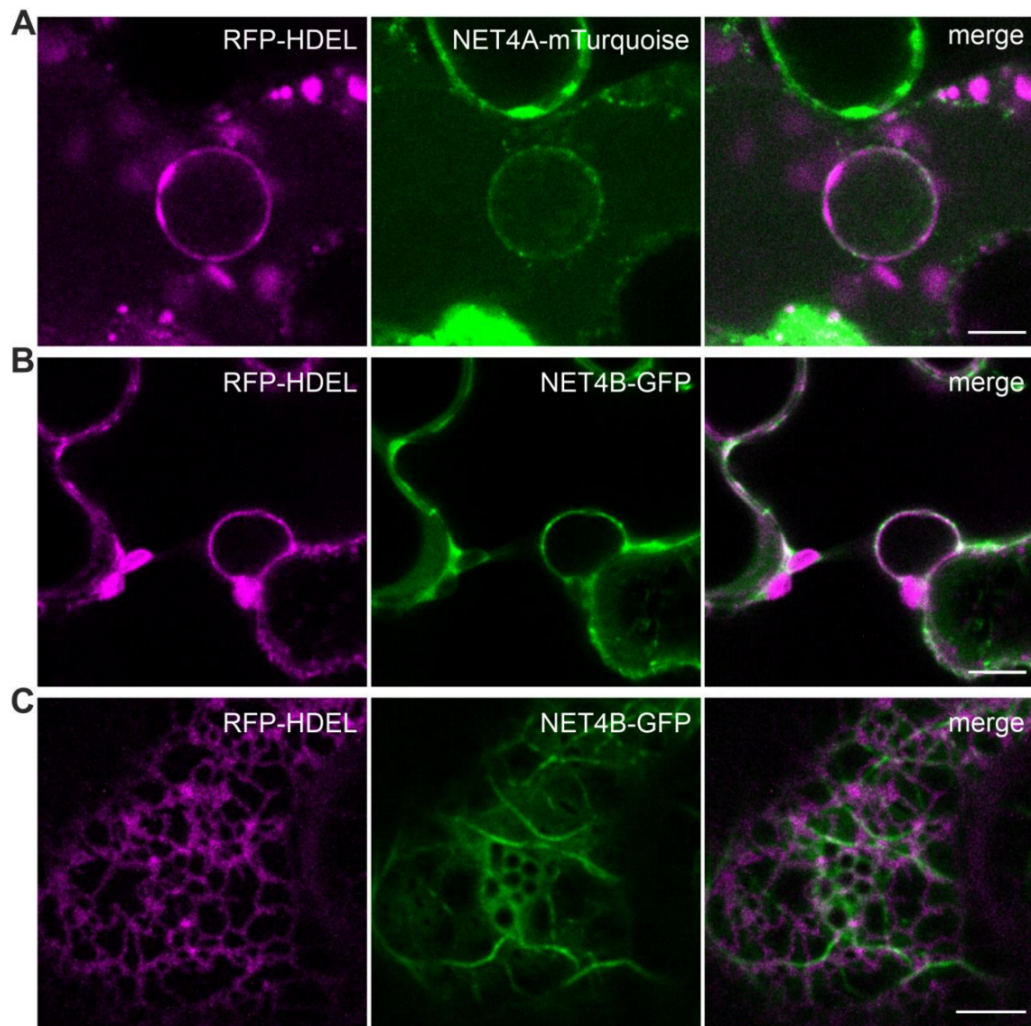
Supplementary Figure S6. Confirmation of NET4A interaction. A, Confirmation of NET4A-cYFP (bait) and interaction partner (nYFP, prey) expression for rBiFC. B, Mating-based Split-Ubiquitin System (mbSUS) growth assays in yeast using NET4A-Cub to test for interaction with NubG-RABG3a, RABG3b, RABC1, At2g15042 and At4g01245. For mbSUS growth assays THY.AP4 (MAT α) yeast strains transformed with Cub-fusions were mated with THY.AP5 (MAT α) strains transformed with NubG-fusions. Growth was assayed in dilution series of OD₆₀₀ from 1 to 0.001 at 28°C on growth control media for 36 h to confirm presence of vector fusion constructs and interaction selective media for 72 h to test for specific interaction dependent activation of the reporter genes. NubG was used as negative, Nubl as positive control. C, Expression control of NET4A by immunological detection. D, Western blot indicating NubG-construct expression. Expected size is highlighted by red asterisks.



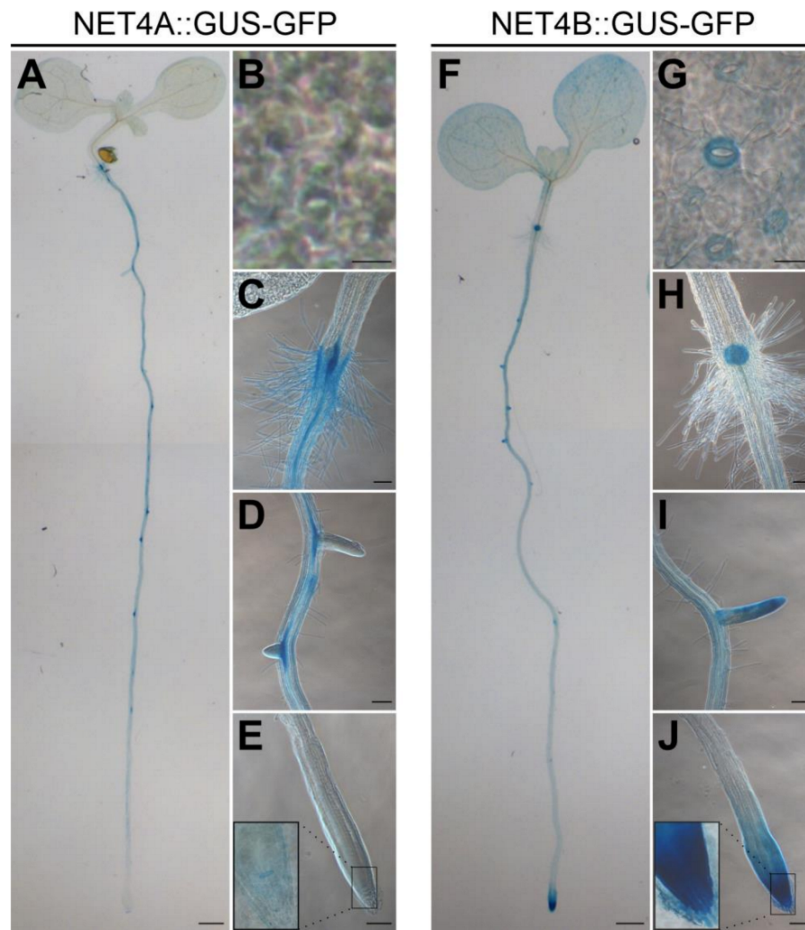
Supplementary Figure S7. Lipid overlay assays (PIP-strips) using NET4 protein. A, Characterization of the NET4 antibody by probing antigen, endogenous NET4A (Col-0) and NET4-GFP expressing lines. B, Probing the same samples as in (A) using a GFP antibody. C, Lipid-overlay-assays (PIP strips) using NET4A protein and the NET4 antibody for detection. D, Same assay as in (C) but using a HIS antibody for detection of HIS-tagged NET4A protein.



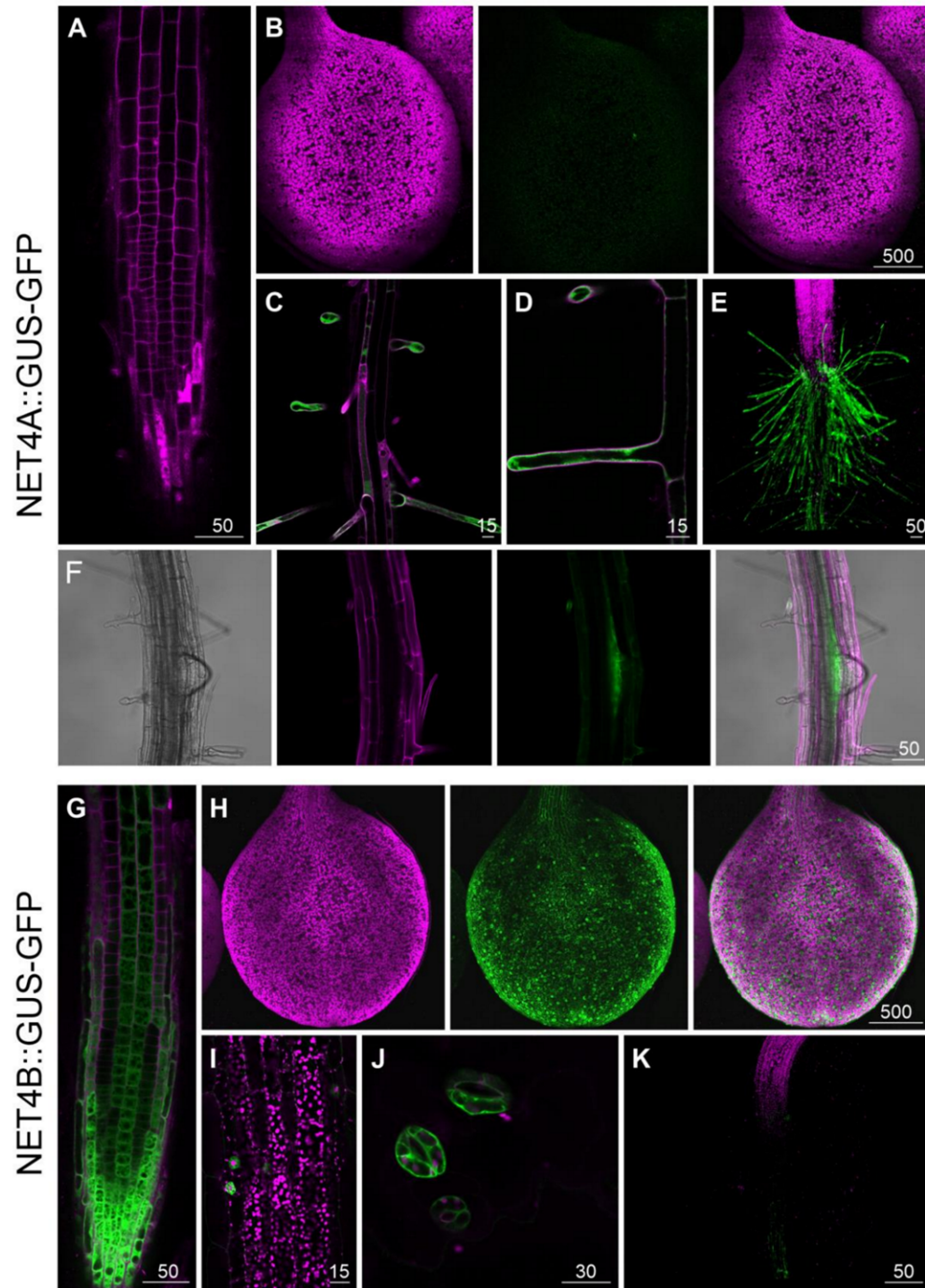
Supplementary Figure S8. Expression control for mbSUS experiments in Fig 6. A, Western blot showing detection of NET4A-, NET4B-, NET3A- and NET3C-Cub. B, Western blot showing detection of NubG-RABG3a and -RABG3b. Expected size is highlighted by red asterisks.



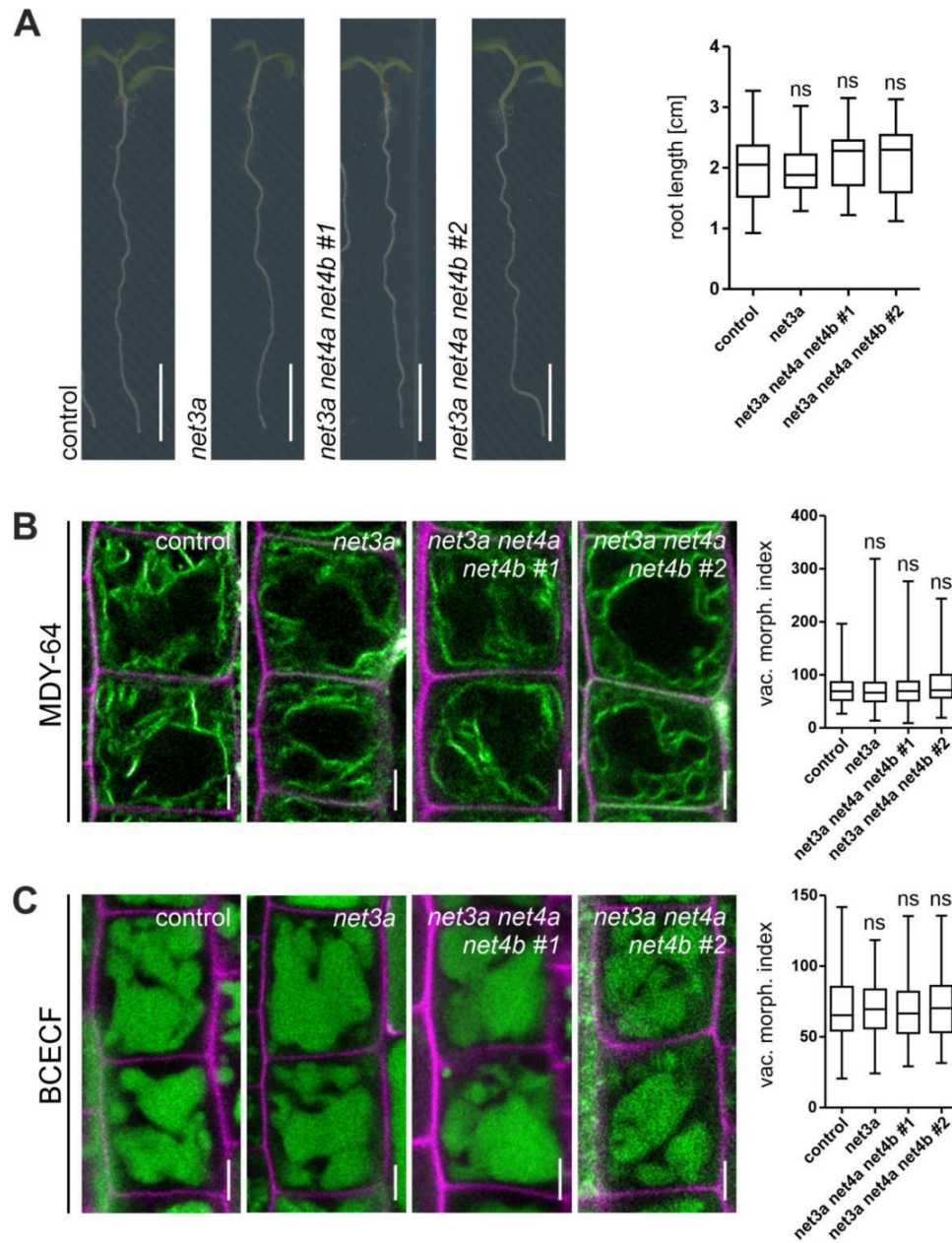
Supplementary Figure S9. NET4A and NET4B both show localization at the nuclear envelope. A-B, Colocalization of NET4A-mTurquoise (A) or NET4B-GFP (B and C) with the ER marker RFP-HDEL at the nuclear envelope upon coexpression in epidermal cells of *N. benthamiana* leaves. C, Cortical view of both markers. Scale bars = 5 μ m.



Supplementary Figure S10. *NET4A* and *NET4B* gene expression in Arabidopsis using promoter-GUS fusions. A, Overview of *NET4A* activity highlighted by GUS-staining in Arabidopsis seedlings. B, Activity in leaf. C, Collet zone. D, Lateral roots. E, Root tip. F, Overview of *NET4B* activity. G, Activity in leaf. H, Collet zone. I, Lateral roots. J, Root tip. Scale bars = 500 μm for A and F; 30 μm for B and G, 100 μm for all others.

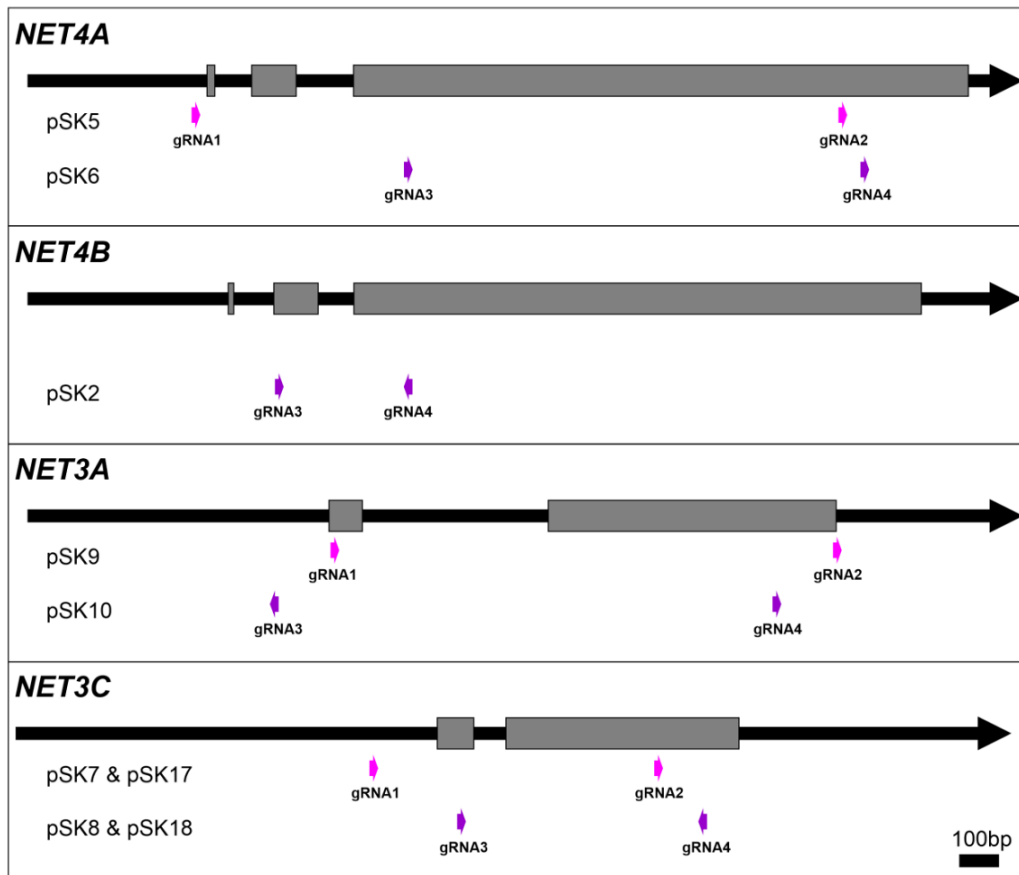


Supplementary Figure S11. *NET4A* and *NET4B* expression using promoter-GFP fusions. A-F, confocal images of *NET4A* activity (green) in the root tip (A), cotyledons (B), root hairs (C and D), the collet region (E), and lateral root founder cells (F). G-K, *NET4B* activity (green) in the root tip, cotyledons (H), the shoot (I), guard cells (J) and the collet region (K). Roots are stained with PI for orientation (magenta). In leaves, autofluorescence is detected (magenta). Scale bars in µm are indicated.



Supplementary Figure S12. Phenotypic characterization of *net3a* and *net4a net4b net3a* mutants.

A, Investigation of root length for lines with CRISPR/Cas9 derived deletion of *NET3A* in Col-0 wild type (n=55) and *net4a net4b* t-DNA mutant (*net3a net4a net4b #1* (n=56) and *net3a net4a net4b #2* (n=61)) compared to Col-0 control (n=150). Scale bars = 0.5 cm. B, Analysis of vacuolar morphology based on the tonoplast dye MDY-64 (n=88 for control, 100 for *net3a*, 108 for *net3a net4a net4b #1* and 88 for *net3a net4a net4b #2*). C, Analysis of vacuolar morphology based on the vacuole dye BCECF (n=96 for control and *net3a*, 100 for *net3a net4a net4b #1* and 108 for *net3a net4a net4b #2*). Box limits represent 25th-75th percentile, the horizontal line the median and whiskers minimum to maximum values. Differences were analyzed by one-way ANOVA and Dunnett's post hoc test; ns = not significant. Scale bars = 5 μ m.



Supplementary Figure S13. Schematic overview of CRISPR/Cas9 derived deletions for *NET4A*, *NET4B*, *NET3A* and *NET3C*. The genomic region of each gene is illustrated as black arrow showing exons as grey bars. The genomic sites of each gRNA pair used to generate CRISPR/Cas9 based deletion mutants are shown as coloured arrows. For each gene, gRNA1 and 2 (pink arrows) or gRNA3 and 4 (violet arrows) were used in combination to delete the genomic area in between the two gRNAs. The generated plasmids, which contain the individual gRNA pairs and are listed in Supplementary Table S7, are given on the left site. Arrow heads of gRNAs mark their direction.

Supplementary Tables

Supplemental Table S1: Primers used for qRT-PCR.

Primer name	Primer sequence	Gene to detect
qRT_NET4A_fw	GCTGGAAGCCAATGTGCGTTATC	NET4A
qRT_NET4A_rev	CGACTTATCTCCGACTCTAGCTCACTC	
qRT_NET4B_fw	CGTCTACGGCTCAGAGCAAG	NET4B
qRT_NET4B_rev	GCTGGATTAACCTCGGGACGTTTC	
qRT_PP2A_fw	TCGTGCAGTATCGCTTCTCG	PP2A (housekeeping)
qRT_PP2A_rev	CACAACCGCTTGGTCGACT	

Supplemental Table S2: List of used expression constructs generated by GreenGate cloning. For all constructs, the destination vector pGGZ003 was used as Module Z. Entry vectors for Module A to F are given for each construct.

Expression construct	Module A (promoter)	Module B (N-terminal tag)	Module C (coding sequence)	Module D (C-terminal tag)	Module E (terminator)	Module F (selection marker)
NET4B-mCherry ^{OE}	pGGA004	pGGB003	pGGC-NET4B	pGGD010	pGGE001	pGGF AllimCherry
NET4B::NET4B-GFP	NET4B promoter (PCR-product)	pGGB003	pGGC-NET4B	pGGD011	pGGE001	pGGF AllimCherry
NET4A ¹⁻¹⁰⁵ -GFP	pGGA004	pGGB003	pGGC-NET4A ¹⁻¹⁰⁵	pGGD011	pGGE001	pGGF AllimCherry
NET4A ¹⁰⁶⁻⁵⁰³ -GFP	pGGA004	pGGB003	pGGC-NET4A ¹⁰⁶⁻⁵⁰³	pGGD011	pGGE001	pGGF AllimCherry
NET4A ⁵⁰⁴⁻⁵⁴² -GFP	pGGA004	pGGB003	pGGC-NET4A ⁵⁰⁴⁻⁵⁴²	pGGD011	pGGE001	pGGF AllimCherry
NET4A ⁵⁰⁴⁻⁵⁵⁸ -GFP	pGGA004	pGGB003	pGGC-NET4A ⁵⁰⁴⁻⁵⁵⁸	pGGD011	pGGE001	pGGF AllimCherry
NET4A-mTurquoise	pGGA006	pGGB003	pGGC-NET4A	pGGD-GSL-mTurquoise	pGGE001	pGGF AllimCherry
NET4A::GUS-GFP	pGGA-NET4A	pGGB003	pGGC051	pGGD011	pGGE001	pGGF AllimCherry
NET4B::GUS-GFP	NET4B promoter (PCR-product)	pGGB003	pGGC051	pGGD011	pGGE001	pGGF AllimCherry

Supplemental Table S3: Primers used for GreenGate cloning. Bases introducing mutations are displayed in red.

Primer name	Primer sequence	Purpose
ggNET4B_fw	AACAGGTCTCAGGCTCAACAATGGCTTCGTC TACGGCTCAG	Amplification of NET4B coding sequence
ggNET4B_rev	AACAGGTCTCTCTGAAGTTGATAAGACCACT ACTCTCTTACTCTTATGTCC	
ggNET4A1/2_FMP	GGGATAGTCATATCGGACTCAAAAATTCTAA GTGGC	mutating internal BsaI site in NET4A coding sequence
ggNET4A1/2_RMP	GCCACTTAGAATTTTTGAGTCCGATATGACT ATCCC	
ggNET4A1/2_fw	AACAGGTCTCAGGCTCAACAATGGATTATGA TCTGCTTCGTTCCAAGAAG	Amplification of full and partial NET4A coding sequences
ggNET4A-NAB_rev	AACAGGTCTCTCTGAAGAGCCTTTTCTCAAC TCTCCGG	
ggNET4A1-tr_fw	AACAGGTCTCAGGCTCAACAATGCCTTTAGA GCTTCAGTCACAGGG	
ggNET4A-tr_rev	AACAGGTCTCTCTGACTTCTCCATCTCCATA GTCCTATCGTC	
ggNET4A-IRQ_fw	AACAGGTCTCAGGCTCAACAATGGAGGTGG AGAAGCAGAGGAGG	
ggNET4A-IRQ_rev	AACAGGTCTCTCTGATATGCGTAGTCTCTTG TATTCGTCTCTGG	

ggNET4A1_rev	AACAGGTCTCTCTGAAGAAGCAAGAATGGAT GATGGTCTTGTG	Amplification of 1900bp upstream of <i>NET4A</i> start codon (promoter region)
gg-pNET4A1_fw	AACAGGTCTCAACCTAGGCTCGTCGTAGTCA TCCAAAG	
gg-pNET4A1_rev	AACAGGTCTCTTGTGGCTGCAAAAATCAAT GGACCTATG	
Esp3I-pNET4B_fw	AACACGTCTCAACCTTGC GGCTCGAAAAAG TTATAGAGG	Amplification of 1900bp upstream of <i>NET4B</i> start codon (promoter region)
Esp3I-pNET4B_rev	AACACGTCTCTTGTGACCGTGGAGTGCAGA G	

Supplemental Table S4: List of entry vectors used for GreenGate cloning.

Plasmid	Description	Source
pGGA000	Empty entry vector for promoter	Lampropoulos, et. al., 2013
pGGA004	35S (Cauliflower mosaic virus) promoter	Lampropoulos, et. al., 2013
pGGA006	UBQ10 (UBIQUITIN10) promoter	Lampropoulos, et. al., 2013
pGGA-NET4A	NET4A (Networked 4A) promoter; 1900bp upstream of start codon	This work
pGGB003	B-dummy (short default random sequence)	Lampropoulos, et. al., 2013
pGGC000	Empty entry vector for coding sequence	Lampropoulos, et. al., 2013
pGGC051	GUS (<i>E. coli</i> β - GLUCURONIDASE)	Lampropoulos, et. al., 2013
pGGC-NET4B	NET4B (Networked 4B) coding sequence	This work
pGGC-NET4A	NET4A (Networked 4A) coding sequence	This work
pGGC-NET4A ¹⁻¹⁰⁵	Partial NET4A coding sequence, aa 1-105	This work
pGGC-NET4A ¹⁰⁶⁻⁵⁰³	Partial NET4A coding sequence, aa 106-503	This work
pGGC-NET4A ⁵⁰⁴⁻⁵⁴²	Partial NET4A coding sequence, aa 504-542	This work
pGGC-NET4A ⁵⁰⁴⁻⁵⁵⁸	Partial NET4A coding sequence, aa 504-558	This work
pGGD010	mCherry	Stührwohltd et al., 2020
pGGD011	mGFP (GREEN FLUORESCENT PROTEIN; A206K)	Lupanga et al., 2020
pGGD-GSL-mTurquoise	mTurquoise with GS linker	Waadt et al., 2017
pGGE001	RBCS terminator (pea)	Lampropoulos, et. al., 2013
pGGF Alli-mCherry	Seed coat selection cassette for mCherry	Stephani et al., 2020

Supplemental Table S5: Primers for amplification of *amiR-vps16* sequence.

Primer name	Primer sequence
Primer A	CTGCAAGGCGATTAAGTTGGGTAAC
Primer B	GCGGATAACAATTTACACAGGAAACAG
I miR-s (vps16)	GATAAGTACTCAGATATCCGCCGCTCTTTTGTATTCCA
II miR-a (vps16)	AGCGGCGGATATCTGAGTACTTATCAAAGAGAATCAATGA
III miR*s (vps16)	AGCGACGGATATCTGTGTACTTTTACAGGTCGTGATATG
IV miR*a (vps16)	GAAAGTACACAGATATCCGTCGCTACATATATTCCTA

Supplemental Table S6: Primers used to generate pHEE-mCherry.

Primer name	Primer sequence
EcoRI-pHEE401E_fw1	caacgaattcgtaatcatgtcatagctg
BsaI-pHEE401E_rev1	aacaggtctctggcaagctgcttagccaatac
BsaI-SCSC_fw	aacaggtctcatgccTTGAAACCAAATTAACATAGGG

Bsal-SCSC_rev	aacaggtctctggggGGTACCCTGGATTTTGG
Bsal-pHEE401E_fw2	aacaGGTCTCacccgaattaattcgcgtaattc
SacII-pHEE401E_rev2	gaaaccgcggtgatcacagg

Supplemental Table S7: Primers used for the generation of CRISPR/Cas9 constructs. Bases of incorporated gRNAs are bold.

Primer name	Primer sequence
gRNA_NET4B_3_FW	ATATATGGTCTCGATT GGAGCAAGAAGCAGTTTAAG TTTTAGAGCTAGAAAT AGC
gRNA_NET4B_4_REV	ATTATTGGTCTCGAAAC CATGTATCGCGCATTGGCTCAATCTCTTAGTCGACTC TAC
gRNA_NET4A_1_FW	ATATATGGTCTCGATT GGTGTTCAGCTTTCCCAT TTTTAGAGCTAGAAATA GC
gRNA_NET4A_2_REV	ATTATTGGTCTCGAAAC CGATTTCGCTCTTCAGCTTCAATCTCTTAGTCGACTC TAC
gRNA_NET4A_3_FW	ATATATGGTCTCGATT GGTACCGTGCTTTGGCAGAG TTTTAGAGCTAGAAAT AGC
gRNA_NET4A_4_REV	ATTATTGGTCTCGAAAC TTCTGCTTAACGTCTCTATCAATCTCTTAGTCGACTC TAC
gRNA_NET3C_1_FW	ATATATGGTCTCGATT GATCGCTCTCAGAATACAAT TTTTAGAGCTAGAAATA GC
gRNA_NET3C_2_REV	ATTATTGGTCTCGAAAC TGTCTAAGAGCTGTTTCCTCAATCTCTTAGTCGACTC TAC
gRNA_NET3C_3_FW	ATATATGGTCTCGATT GGAGCTCCAAACATTCTCAAG TTTTAGAGCTAGAAATA GC
gRNA_NET3C_4_REV	ATTATTGGTCTCGAAAC CCATTCTCTCAAGCAACGCCAATCTCTTAGTCGACTC CTAC
gRNA_NET3A_1_FW	ATATATGGTCTCGATT GGATGGACTCATCAAAATGGG TTTTAGAGCTAGAAAT AGC
gRNA_NET3A_2_REV	ATTATTGGTCTCGAAAC CTCTGTCTCTCTAAAGAGCAATCTCTTAGTCGACTC TAC
gRNA_NET3A_3_FW	ATATATGGTCTCGATT GAATTACCAACCTCGGTGCGG TTTTAGAGCTAGAAAT AGC
gRNA_NET3A_4_REV	ATTATTGGTCTCGAAAC CTTCTTATTACGCCTTGCAATCTCTTAGTCGACTC TAC

Supplemental Table S8: List of used CRISPR/Cas9 constructs for generating deletion mutants. The gRNAs are given without "NGG". Red bases were changed to G (gRNA 1 or 3) or C (gRNA 2 or 4) when incorporated into the primers listed in Supplemental table S6.

Construct	gRNA 1 or 3	gRNA 2 or 4	Base vector
pSK2	A GAGCAAGAAGCAGTTTAAG	C AGCCAATGCGCGATACATG	pHEE401E
pSK5	T GTGTTTCCAGCTTTCCCAT	A AAGCTGAAGAGCGAAATCG	pHEE401E
pSK6	T GTACCGTGCTTTGGCAGAG	C ATAGAGACGTTAAGCAGAA	pHEE401E
pSK17	T ATCGCTCTCAGAATACAAT	G AGGAAACAGCTCTTAGACA	pHEE-mCherry
pSK8	A GAGCTCCAAACATTCTCAA	T GCGTTGCTTGAGAGAATGG	pHEE401E
pSK18	A GAGCTCCAAACATTCTCAA	T GCGTTGCTTGAGAGAATGG	pHEE-mCherry
pSK9	T GATGGACTCATCAAAATGG	A CTCTTTAGAGGAGACAGAG	pHEE401E
pSK10	A AATTACCAACCTCGGTGCG	G CAAGGCGTAATAAGGAAGG	pHEE401E

Supplemental Table S9: List of CRISPR/Cas9 derived deletion mutants. Base lines and constructs used to obtain the specific gene deletions are given for each line. All mutant lines are homozygous for the introduced deletion and lost the integrated CRISPR/Cas9 construct during the screening process.

Deletion mutant	Base line	Construct
<i>net4b</i> (CRISPR mutant)	Col-0	pSK2
<i>rabg3a,b,c,d,e,f net4a</i> #1	<i>rabg3a,b,c,d,e,f</i> (Ebina et al., 2014)	pSK6
<i>rabg3a,b,c,d,e,f net4a</i> #2	<i>rabg3a,b,c,d,e,f</i> (Ebina et al., 2014)	pSK5
<i>net3c</i>	Col-0	pSK18
<i>net3c net4a net4b</i> #1	<i>net4a net4b</i> (T-DNA mutant, Kaiser et al., 2019)	pSK8

<i>net3c net4a net4b</i> #2	<i>net4b</i> (CRISPR mutant, this work)	pSK17 & pSK5
<i>net3a</i>	Col-0	pSK9
<i>net3a net4a net4b</i> #1	<i>net4a net4b</i> (T-DNA mutant, Kaiser et al., 2019)	pSK10
<i>net3a net4a net4b</i> #2	<i>net4a net4b</i> (T-DNA mutant, Kaiser et al., 2019)	pSK9

Supplemental Table S10: Primers used for the generation of rBiFC and mbSUS constructs.

Primer name	Primer sequence	Purpose
attB1_NET4A.FOR	GGGGACAAGTTTGTACAAAAAAGCAGGC TCTATGGATTATGATCTGCTTCGTTCCAA GA	Amplification of sequences for rBiFC constructs (used entry vector: pDONR221- P1P4, used destination vector: pBiFCt-2in1-NC)
attB4-wo_NET4A.REV	GGGGACAACCTTTGTATAGAAAAGTTGGG TGAGAAGCAAGAATGGATGATGGTCTTG	
attB3_RABG3b.FOR	GGGGACAACCTTTGTATAATAAAGTTGCTA TGTCGACGCGAAGACGAAC	Amplification of sequences for rBiFC constructs (used entry vector: pDONR221- P3P2, used destination vector: pBiFCt-2in1-NC)
attB2-ST_RABG3b.REV	GGGGACCACTTTGTACAAGAAAGCTGGG TTCAGCAAGCACAACCTCCTCT	
attB3_RABG3a.FOR	GGGGACAACCTTTGTATAATAAAGTTGCTA TGGCGACGAGAAGACGTAC	
attB2-ST_RABG3a.REV	GGGGACCACTTTGTACAAGAAAGCTGGG TTCAGCAAGCGCAACCACC	
attB3_VAMP711.FOR	GGGGACAACCTTTGTATAATAAAGTTGCTA TGGCGATTCTGTACGCC	
attB2-ST_VAMP711.REV	GGGGACCACTTTGTACAAGAAAGCTGGG TTTAAATGCAAGATGGTAGAGTAGGTCG	
attB3_RABC1.FOR	GGGGACAACCTTTGTATAATAAAGTTGCTA TGGGTCTTCGTCAGGACAAC	
attB2-ST_RABC1.REV	GGGGACCACTTTGTACAAGAAAGCTGGG TCTAAGACGAGCAGCAGTAGCT	
attB3_1245.FOR	GGGGACAACCTTTGTATAATAAAGTTGCTA TGGTGATTCACCTTAGTTCATCTTGTATT CC	
attB2-ST_1245.REV	GGGGACCACTTTGTACAAGAAAGCTGGG TTCATGATGTACAACAAAAGTACCATTGC TG	
attB1_RABG3b.FOR	GGGGACAAGTTTGTACAAAAAAGCAGGC TCTATGTCGACGCGAAGACGAAC	Amplification of sequences for mbSUS prey constructs (used entry vector: pDONR207, used destination vector: pNX35- DEST-1)
attB2-ST_RABG3b.REV	GGGGACCACTTTGTACAAGAAAGCTGGG TTCAGCAAGCACAACCTCCTC	
attB1_RABG3a.FOR	GGGGACAAGTTTGTACAAAAAAGCAGGC TCTATGGCGACGAGAAGACGTAC	
attB2-ST_RABG3a.REV	GGGGACCACTTTGTACAAGAAAGCTGGG TTCAGCAAGCGCAACCACCG	
attB1_RABC1.FOR	GGGGACAAGTTTGTACAAAAAAGCAGGC TCTATGGGTTCTTCGTCAGGAC	
attB2-ST_RABC1.REV	GGGGACCACTTTGTACAAGAAAGCTGGG TCTAAGACGAGCAGCAGTAGCTC	
attB1_1245.FOR	GGGGACAAGTTTGTACAAAAAAGCAGGC TCTATGGTGATTCACCTTAGTTCATCTTG	
attB2-ST_1245.REV	GGGGACCACTTTGTACAAGAAAGCTGGG TTCATGATGTACAACAAAAGTACCATTGC	
attB1_15042.FOR	GGGGACAAGTTTGTACAAAAAAGCAGGC TCTATGGACGCTACCAACTTTGGAC	
attB2-ST_15042.REV	GGGGACCACTTTGTACAAGAAAGCTGGG TTTAACGAGTTGTGCTGCTTGTG	
attB1_VAMP711.FOR	GGGGACAAGTTTGTACAAAAAAGCAGGC TTAATGGCGATTCTGTACGCCCT	
attB2-ST_VAMP711.REV	GGGGACCACTTTGTACAAGAAAGCTGGG TTTAAATGCAAGATGGTAGAGTAGG	
attB1_VAP27-1.FOR	GGGGACAAGTTTGTACAAAAAAGCAGGC TCTATGAGTAACATCGATCTGATTGGGAT GAGTAAC	

attB2-ST_VAP27-1.REV	GGGGACCACTTTGTACAAGAAAGCTGGG TTATGTCCTCTTCATAATGTATCCCAAAA TTAGACC	Amplification of sequences for mbSUS bait constructs (used entry vector: pDONR207, used destination vector: pMETOYC-Dest)
attB1_NET4A.FOR	GGGGACAAGTTTGTACAAAAAAGCAGGC TCTATGGATTATGATCTGCTTCGTTCCAA GA	
attB2-wo_NET4A.REV	GGGGACCACTTTGTACAAGAAAGCTGGG TGAGAAGCAAGAATGGATGATGGTC	
attB1_NET4B.FOR	GGGGACAAGTTTGTACAAAAAAGCAGGC TCTATGGCTTCGCTACGGCTCAG	
attB2-wo_NET4B.REV	GGGGACCACTTTGTACAAGAAAGCTGGG TGAGTTGATAAGACCACTACTCTCTTACT CTTATGT	
attB1_NET3A.FOR	GGGGACAAGTTTGTACAAAAAAGCAGGC TCTATGGTGATGGACTCATCAAATGGTG	
attB2-wo_NET3A.REV	GGGGACCACTTTGTACAAGAAAGCTGGG TGAAGAGTCATGAGCTCTTGGAAGTAG	
attB1_NET3C.FOR	GGGGACAAGTTTGTACAAAAAAGCAGGC TCTATGGTTAGAGAAGAGGAGAAATCGA GATG	
attB2-wo_NET3C.REV	GGGGACCACTTTGTACAAGAAAGCTGGG TGAAGGACCTTGTGCCATCGC	

Supplemental Table S11: List of generated Gateway expression constructs used for rBiFC and mbSUS experiments. The used destination vectors, including tags, as well as the sequences cloned from suitable entry vectors are shown for each construct.

Constructs	N-terminal tag	Coding (or genomic) sequence	C-terminal tag	Destination vector
NET4A-cYFP+nYFP-VAMP711	nYFP-HA	NET4A + RFP + VAMP711	MYC-cYFP	pBiFCt-2in1-NC
NET4A-cYFP+nYFP-RABG3b	nYFP-HA	NET4A + RFP + RABG3b	MYC-cYFP	pBiFCt-2in1-NC
NET4A-cYFP+nYFP-RABG3a	nYFP-HA	NET4A + RFP + RABG3a	MYC-cYFP	pBiFCt-2in1-NC
NET4A-cYFP+nYFP-RABC1	nYFP-HA	NET4A + RFP + RABC1	MYC-cYFP	pBiFCt-2in1-NC
NET4A-cYFP+nYFP-gAt4g01245	nYFP-HA	NET4A + RFP + At4g01245 (genomic)	MYC-cYFP	pBiFCt-2in1-NC
NubG-RABG3b	NubG-2xHA	RABG3b	-	pNX35-DEST-1
NubG-RABG3a	NubG-2xHA	RABG3a	-	pNX35-DEST-1
NubG-RABC1	NubG-2xHA	RABC1	-	pNX35-DEST-1
NubG-At2g15042	NubG-2xHA	At2g15042	-	pNX35-DEST-1
NubG-gAt4g01245	NubG-2xHA	At4g01245 (genomic)	-	pNX35-DEST-1
NubG-VAMP711	NubG-2xHA	VAMP711	-	pNX35-DEST-1
NET4A-Cub	Ost4	NET4A	Cub	pMETOYC-Dest
NET4B-Cub	Ost4	NET4B	Cub	pMETOYC-Dest
NET3A-Cub	Ost4	NET3A	Cub	pMETOYC-Dest
NET3B-Cub	Ost4	NET3B	Cub	pMETOYC-Dest
NubG-VAP27-1	NubG-2xHA	VAP27-1	-	pNX35-DEST-1

Supplemental Table S12: Primers used to clone constructs for recombinant protein expression.

Primer name	Primer sequence
NET4A_fw_BtgZI	aacaGCGATGtctaggacgaCATGGATTATGATCTGCTTCGTTCCAAGAAG
NET4A1/2_rev_XhoI	atctCTCAGAGAAGCAAGAATGGATGATGGTCTTGTTG

Supplemental Table S13: List of Arabidopsis lines obtained by crossing. The parental lines used for crossing and information about the homozygosity are given for each line.

Crossing line	Mother line	Father line	Status
---------------	-------------	-------------	--------

lifeact-RFP x NET4A-GFP ^{OE}	lifeact-RFP	NET4A-GFP ^{OE}	homozygous
<i>xi-k/1/2</i> x NET4A-GFP ^{OE}	<i>xi-k/1/2</i>	NET4A-GFP ^{OE}	homozygous
<i>act7-4</i> x NET4A-GFP ^{OE}	<i>act7-4</i>	NET4A-GFP ^{OE}	homozygous
<i>act2 act8</i> x NET4A-GFP ^{OE}	<i>act2 act8</i>	NET4A-GFP ^{OE}	homozygous
NET4A-GFP ^{OE} x <i>amiR-vps16</i>	NET4A-GFP ^{OE}	<i>amiR-vps16</i>	homozygous
SRβ-mTurquoise x NET4A-GFP ^{OE}	SRβ-mTurquoise	NET4A-GFP ^{OE}	heterozygous
RFP-HDEL x NET4A-GFP	RFP-HDEL	NET4A-GFP	heterozygous

Supplemental Table S14: Primers used for genotyping. For T-DNA insertional mutants, primers were used as described previously in Kandasamy et al., 2009 or designed and used as recommended by the Nottingham Arabidopsis Stock Centre (NASC) (Nottingham University, UK; <http://signal.salk.edu/tdnaprimers.2.html>).

Primer name	Primer sequence	Purpose
GT_amiR-vps16_fw	CACGCTCGGACGCATATTAC	Detection of integrated <i>amiR-vps16</i> construct
GT_amiR-vps16_rev	GCGGCGGATATCTGAGTACTTATC	
GFP_fw	CCTCGTGACCACCTTCACCTAC	Detection of integrated GFP-fusion constructs
GFP_rev	GTGATCGCGCTTCTCGTTGG	
GT_NET4B-A_fw	GGCCGCGTTTCCAATTATC	Screening for CRISPR/Cas9 provoked gene deletions
GT_NET4B-B_rev	GCTAGATTGACGGCGACTC	
GT_NET4A_fw	CACCTGGCCACGTTGAAATTGC	
GT_NET4A_rev	GGCTATGCGTAGTCTCTTGTATTCTG	
GT_NET3C_fw	GGTTGAAGACGAGCGACATGG	
GT_NET3C_rev	GCTAGTGCGCAGTTGTTGTAATTG	
GT_NET3A_fw	CTGAACCTCTCAAGTCCGAAGACAG	
GT_NET3A_rev	CAATCCTATGATATACCTTACGCTAAC	
EC_fw	CGTCTCCAATAGGAGCGCTACTG	Screening for integrated CRISPR/Cas9 constructs
EC_rev	GGGCCGATTAGAATCACTCAGTC	
SALK_067972_LP (<i>myosin XI-k</i>)	GGGTAGCAAGATACTCCTCGG	Screening for T-DNA insertions
SALK_067972_RP (<i>myosin XI-k</i>)	GCAAGAGCAACTCAATTCTGG	
SALK_019031_LP (<i>myosin XI-1</i>)	TCAAAACGTTGAACTAACC GG	
SALK_019031_RP (<i>myosin XI-1</i>)	TTGTTTGGACGGGTATCTCAG	
SALK_055785_LP (<i>myosin XI-2</i>)	TAGGTTTCTGGCTAGGAAGGC	
SALK_055785_RP (<i>myosin XI-2</i>)	CAAAGGATACCTCTGCATTGC	
SALK_LBb1.3	ATTTTGCCGATTTCCGAAC	
ACT2-173S	CTTCTCAATCTCATCTTCTT	
ACT2-AS	CATGACACCATGATGTCTTGGCCT	
ACT2-173S_LBp	GCTCAGGATCCGATTGTCTGTTCCCGC CTT	
ACT8-5'S4	TCGATCAAGATTCAGATCTTTATG	
ACT8-74A	ACACCATGCTCAATAGGGTATTTCAAT	
LB-GABIS1	CCCATTGACGTGAATGTAGACAC	
AAc7S	AGGATTCTTCTCGCTTCTGTCTGATCTCT CGCT	
AAc7-11A	AAATCATGATCAGTAGTCTTACACATGT	
JLB7804	TTGGTAATTACTCTTTCTTTCTCTCCATA TT	

13.4 Article 4

“To Lead or to Follow: Contribution of the Plant Vacuole to Cell Growth”



To Lead or to Follow: Contribution of the Plant Vacuole to Cell Growth

Sabrina Kaiser and David Scheuring*

Plant Pathology, University of Kaiserslautern, Kaiserslautern, Germany

OPEN ACCESS

Edited by:

Eugenia Russinova,
Ghent University, Belgium

Reviewed by:

Gian Pietro Di Sansebastiano,
University of Salento, Italy
Enrique Rojo,
National Center of Biotechnology
(CSIC), Spain

*Correspondence:

David Scheuring
scheurin@rhrk.uni-kl.de

Specialty section:

This article was submitted to
Plant Traffic and Transport,
a section of the journal
Frontiers in Plant Science

Received: 28 February 2020

Accepted: 14 April 2020

Published: 08 May 2020

Citation:

Kaiser S and Scheuring D (2020)
To Lead or to Follow: Contribution
of the Plant Vacuole to Cell Growth.
Front. Plant Sci. 11:553.
doi: 10.3389/fpls.2020.00553

Cell division and cell elongation are fundamental processes for growth. In contrast to animal cells, plant cells are surrounded by rigid walls and therefore loosening of the wall is required during elongation. On the other hand, vacuole size has been shown to correlate with cell size and inhibition of vacuolar expansion limits cell growth. However, the specific role of the vacuole during cell elongation is still not fully resolved. Especially the question whether the vacuole is the leading unit during cellular growth or just passively expands upon water uptake remains to be answered. Here, we review recent findings about the contribution of the vacuole to cell elongation. In addition, we also discuss the connection between cell wall status and vacuolar morphology. In particular, we focus on the question whether vacuolar size is dictated by cell size or *vice versa* and share our personnel view about the sequential steps during cell elongation.

Keywords: vacuole, cell elongation, auxin, cell wall, turgor, cell size, cytoskeleton, actin

INTRODUCTION

The plants largest organelle, the vacuole, occupies up to 90% of the cellular volume in vegetative tissues. Although the name *vacuole* originates from the Latin *vacuus* (= vacuum), implying an empty and potentially functionless space, quite the opposite is true. Vacuoles fulfill a plethora of important and diverse functions in plant cells. Among them are the degradation of cellular waste, the storage of ions and proteins, plant defense against pathogens, pH homeostasis and plant growth. The vacuole's prominent size and the finding that individual cells hold turgor pressure up to 5 bar (Zimmermann et al., 1980) established the believe that vacuoles provide the driving force for plant growth. Here, vacuoles were thought to simply drive cell elongation via turgor pressure (Marty, 1999). While there is no doubt that turgor pressure contributes to cell elongation (Cosgrove, 2018), the precise role of the vacuole in this process remains unclear and has not yet been addressed experimentally. However, restricting the vacuole's dimensions has been shown to inhibit cellular elongation and root organ growth (Löfke et al., 2015; Kaiser et al., 2019). Conversely, increasing vacuolar occupancy of the cell is of eminent importance during elongation (Dünser et al., 2019).

Besides the vacuole, the properties of the plant cell wall represent another crucial component for defining cell size and growth rates. Cell wall acidification and subsequent loosening are long known to be a prerequisite for expansion (Cosgrove, 1993), but the interplay with intracellular changes (vacuolar expansion) are less well understood. Only lately substantial progress was made in understanding the signaling and coordination between extracellular and intracellular changes during cell elongation (Dünser et al., 2019).

CELL WALL LOOSENING AS PREREQUISITE FOR CELL ELONGATION

Since plant cells are sheathed by rigid, shape-giving cell walls, cellular extension cannot be explained by vacuolar expansion alone but must, consequently, also include cell wall modifications. Already in the early 70s of the last century, researchers could show that the elongation of stem and coleoptile cells promoted by the phytohormone auxin was coupled to cell wall loosening (Rayle and Cleland, 1970; Hager et al., 1971). This led to the formulation of the so-called *acid growth theory*, primarily proposing a connection of auxin and acidification of the cell exterior, the apoplast. The current understanding of this hypothesis includes the activation of plasma membrane (PM) H^+ -ATPases by auxin and subsequent acidification of the apoplast and thus the cell wall. Following this, pH-responsive non-enzymatic proteins from the expansin family (McQueen-Mason et al., 1992) are activated, leading to cell wall loosening via xyloglucan slipping (Cosgrove, 2000). Cell elongation is then achieved by water uptake alongside with the deposition of new wall material.

Not long ago, the acid growth theory has been confirmed in shoots (Fendrych et al., 2016) and roots of the model plant *Arabidopsis* (Barbez et al., 2017). In the latter, the model was heavily debated, due to the complex role of auxin in plant development and technical limitations in investigating apoplastic pH at cellular resolution. Depending on the concentration and the cell type, auxin promotes and inhibits growth, respectively. In the physiological concentration range, auxin preferentially induces growth in aerial, and inhibits growth in underground tissues (Evans et al., 1994; Dünser and Kleine-Vehn, 2015). However, Barbez and coauthors showed that cell wall acidification induced cellular expansion and that this is preceded by and dependent on auxin signaling (Barbez et al., 2017). Interestingly, increasing total levels of auxin induced a transient alkalization of the apoplast and reduced cellular elongation. This in turn was dependent on the receptor-like kinase FERONIA (FER) which has been demonstrated to control the elasticity of the cell wall (Höfte, 2015) and functions as a mechano-sensor (Shih et al., 2014).

CONTRIBUTION OF THE VACUOLE TO CELL ELONGATION

It has been shown that auxin does not only affect cell wall loosening but also directly impacts on the vacuole. In the *Arabidopsis* root meristem, the phytohormone induced smaller and more constricted vacuoles (Löfke et al., 2015). Changes of vacuolar morphology in turn directly affected cell-size control and restricted root growth (Löfke et al., 2015). Since this auxin-induced vacuolar phenotype was accompanied by an increased abundance of soluble N-ethylmaleimide-sensitive-factor attachment receptors (SNAREs), especially VTI11, auxin was hypothesized to impact on homotypic vacuolar fusion events (Löfke et al., 2015). Subsequently, auxin-induced constrictions of the vacuole were demonstrated to be dependent on the

actin cytoskeleton (Scheuring et al., 2016). In actin and myosin mutants, auxin-induced changes of vacuolar morphology, cell-size restriction and inhibition of root growth were all largely abolished (Scheuring et al., 2016). In mammalian cells, members of the HOPS (homotypic fusion and protein sorting) complex interact with the actin cytoskeleton (Richardson et al., 2004). This complex mediates homotypic vacuole fusion in plants (Takemoto et al., 2018) and a potential actin interaction here would at least partly explain the actin-dependency of auxin-induced vacuolar changes.

Notably, the tonoplast-localized auxin transporter WALLS ARE THIN1 1 (WAT1) has been identified, facilitating auxin export from the vacuole (Ranocha et al., 2013). Hence, a key role for the vacuole in intracellular auxin homeostasis was suggested. Moreover, WAT1 has been proposed to integrate auxin signaling and secondary cell wall formation of stem fibers in *Arabidopsis* (Ranocha et al., 2010).

Another layer of complexity is added by the presence of different vacuole types in plants. Dependent on their function, vacuoles are classified into protein storage vacuoles (PSVs), predominantly found in seed tissues, and lytic vacuoles (LVs) which are commonly found in vegetative tissue and are primarily discussed in the present mini-review. For both, PSVs and LVs, independent inhibition of trafficking has been demonstrated (Bolte et al., 2004; Park et al., 2005), and thus separate transport routes were assumed. Furthermore, it has been shown that trafficking to these vacuoles requires different members of SNARE proteins. While VTI12 plays an important role in protein transport to PSVs, trafficking to the LV is mainly dependent on VTI11 (Sanmartín et al., 2007). This could indicate that the auxin induced vacuolar changes seen for LVs accompanied by upregulation of VTI11 (Löfke et al., 2015) are unique for LVs, potentially not impacting on PSVs.

To unravel the morphological changes of the lytic vacuole upon exogenous auxin treatment in detail, the combination of state-of-the-art imaging and staining methods were employed. This allowed 3D modeling and quantitative analysis of different parameters such as vacuolar volume and surface area. Markedly, upon auxin application, most vacuolar subvolumina were still connected and together formed one single interconnected organelle (Scheuring et al., 2015, 2016). Based on the reduced cellular space that (auxin-induced) constricted vacuoles occupy, a space-filling function of the vacuole was proposed. This would allow plant cells to elongate without altering the amount of cytosol, thereby massively reducing energy investment (Scheuring et al., 2016; Krüger and Schumacher, 2018). Accordingly, auxin would limit the intracellular occupancy of the vacuole to restrict cell elongation. This is well in accordance with the observation that the size of plant vacuoles correlates with cell size (Owens and Poole, 1979).

Due to the close proximity of the vacuolar membrane (tonoplast) and actin filaments it has been suggested that there might be a direct physical connection (Kutsuna et al., 2003). In a screen for GFP-fusion proteins labeling actin filaments, the plant-specific Networked (NET) family was identified (Deeks et al., 2012). NET proteins possess an actin-binding domain and are membrane-associated, thus linking actin filaments with different

cell organelles. One specific member, NET4A, has been shown to bind actin and overlaps with the tonoplast (Deeks et al., 2012). Recently, it was shown that NET4A localizes to highly constricted regions of the tonoplast and, together with NET4B, modulates vacuolar occupancy. Overexpression led to a decrease, and loss-of-function to an increase of vacuolar occupancy, respectively (Kaiser et al., 2019). As increased vacuolar volume allows for rapid cellular elongation with relatively little *de novo* production of cytosolic content (Dünser et al., 2019); more compact vacuoles induced by NET4A overexpression might explain the accompanied cell size and root length limitations observed in a NET4A overexpressor line (Kaiser et al., 2019). Furthermore, this finding confirms that cell size and vacuole size are tightly linked and that inhibited cell elongation via restricted vacuolar size does not exclusively depend on auxin. Indeed, additional factors, such as blue light and most of the other described phytohormones are also involved in cell size determination (Halliday et al., 2009; Perrot-Rechenmann, 2010).

Naturally, the observed restrictions of vacuolar expansion led to the question of their function apart from restricting cell size. One explanation could be the requirement of increasing cytosol demands during cell division. In agreement with this, vacuolar volume has been reported to decrease by 80% within cell division, increasing the amount of cytosol required to accommodate the forming phragmoplast and associated cell plate-forming structures (Seguí-Simarro and Staehelin, 2006). In line with this, unequal vacuole partitioning during embryogenesis in the *gravitropism defective 2* (*grv2*) mutant resulted in daughter cell formation of unequal size (Silady et al., 2008). It was postulated that the presence of an unusually large vacuole in one daughter cell led to misalignment of the phragmoplast, explaining the observed disturbance of cell division in the mutant (Silady et al., 2008).

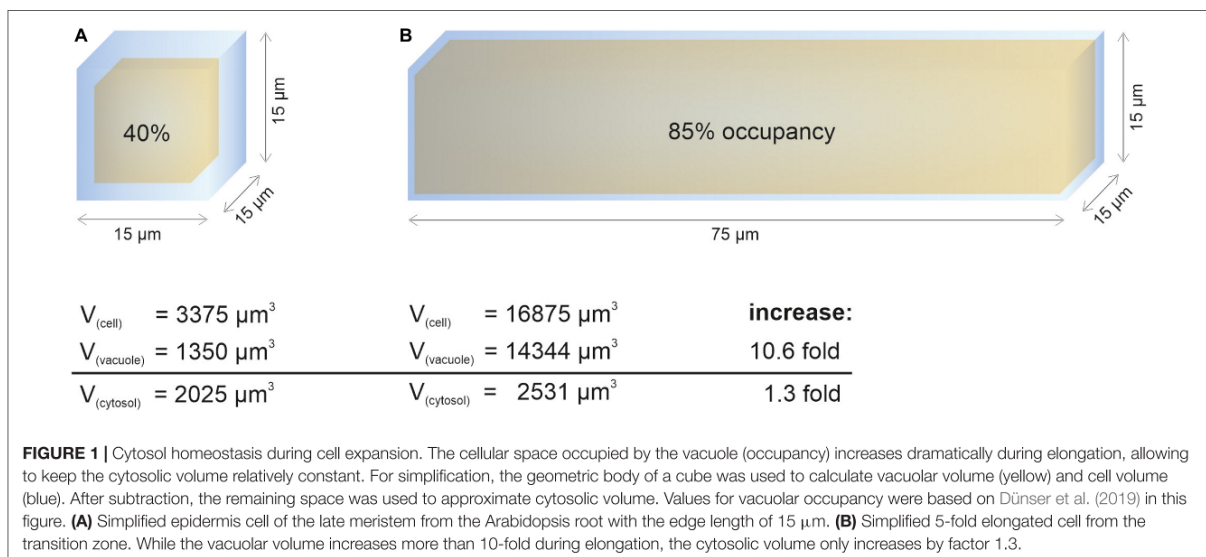
In contrast to vacuole size restriction during cytokinesis, developing cells of the root meristem display gradually larger

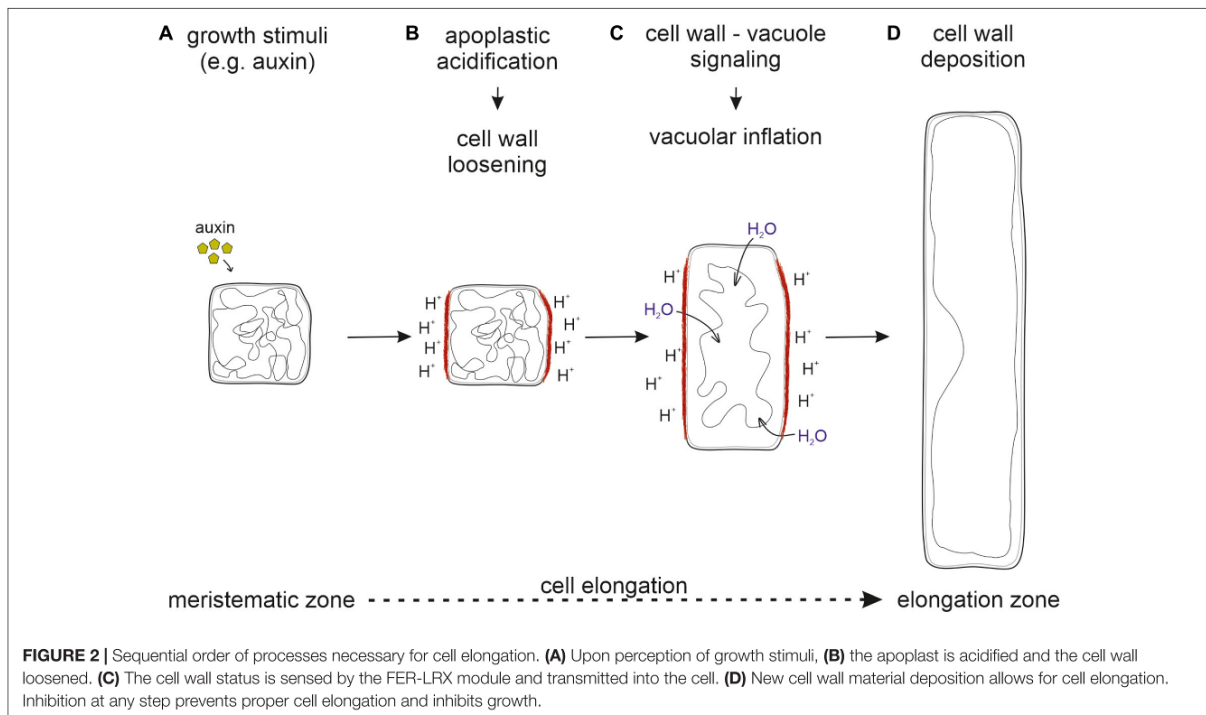
vacuoles as cells transit into the elongation zone. Cells leaving meristematic zones extend their original size 10–1,000-fold (Veytsman and Cosgrove, 1998). To fulfill its space-filling function and to avoid high metabolic costs for the generation of large amounts of cytosolic content, the vacuole must dramatically increase its volume (Figure 1). Indeed, vacuolar occupancy of the cell increases from around 40% in meristematic cells to more than 85% in cells of the late elongation zone (Dünser et al., 2019). Initially, the osmotic potential in the vacuole must be higher than in the cytosol to enable water uptake, but eventually it must reach equilibrium. The tonoplast (unlike the cell wall) has limited tensile strength and cannot withstand significant differences in pressure without rupturing.

DISCUSSION

Obviously, vacuolar expansion and cell wall loosening both are of eminent importance for cell elongation. Thus, the question arises: How are these processes coordinated and is the vacuole indeed the driving force for cell elongation as proposed previously?

Recent data revealed that the receptor-like kinase FER together with extracellular leucine-rich repeat extensins (LRXs) sense cell wall properties (such as loosening) and subsequently impact on the intracellular expansion of the vacuole (Dünser et al., 2019). This module was proposed to integrate the cell wall status with intracellular growth processes, but it remained unclear how precisely LRX/FER signaling at the cell surface leads to the modulation of vacuolar size. One hypothesis involves several transduction steps to regulate the actin cytoskeleton (Dünser et al., 2019). Since the actin cytoskeleton surrounds the vacuole and contributes to the regulation of vacuolar size (Scheuring et al., 2016), this link could in principle explain how extracellular sensing and intracellular control of vacuolar volume are integrated. In agreement, *lrx* and *fer* mutants display





a pronounced enlargement of the vacuolar lumina and a higher vacuolar occupancy of the cell (Dünser et al., 2019). Moreover, these vacuoles are resistant to pharmacological treatments that presumably impact on cell wall properties and normally restrict vacuolar expansion (Dünser et al., 2019). Thus, it is tempting to state that without transmission of the cell wall status, vacuolar changes will not occur. Additionally, in fully elongated cells, the osmotic potential of cytosol and vacuole needs to be equilibrated to prevent membrane rupture. It is conceivable that a high turgor pressure could be build up without the vacuole, albeit with dramatically higher energy investment.

Furthermore, it has been shown that the expression of a specific tonoplast intrinsic protein (γ -TIP), enabling water uptake, is correlated with cell elongation (Ludevid et al., 1992). If the vacuole would be indeed the driving force, one would expect the onset of TIP expression before cell elongation is initiated. In contrast, several TIPs were found to be preferentially expressed in elongating cells but not in the meristematic zone of *Arabidopsis* roots (Gattolin et al., 2009, 2010). This again questions the vacuole's role in leading cell expansion via increasing turgor pressure.

Taken together, it seems likely that cell wall loosening through apoplastic acidification is the driving force for vacuolar expansion. For this, the cell wall status has to be sensed and external signals must be transmitted into the cell to initiate vacuolar expansion. Only then, the space-filling capacity of the vacuole allows the occupation of the emerging space in expanding cells. This ensures that cytosolic content does not become the growth-limiting factor (Figure 2).

Therefore, we believe that vacuolar expansion follows cell wall loosening which marks the onset for cell expansion. Only in concert, both processes jointly grant rapid cell elongation and enable fast plant growth rates. However, the precise relationship between vacuolar expansion, cell wall properties and cell elongation is not fully understood and it will be an exciting future task to identify yet unknown players involved in the coordination of this complex and delicate process.

Another important question that needs to be addressed in future research is the source of membrane material to allow for rapid cell elongation. Due to the enormous increase in cell size, not only the vacuole but also the PM requires new membrane material to adapt their surface area. While the endoplasmic reticulum (ER) is the main synthesis site for lipids destined for the PM (Blom et al., 2011) the source for newly synthesized vacuole membrane is not yet unanimously agreed on. During vacuole biogenesis two seemingly opposing models are controversially discussed. One describes the ER as the main membrane source while the second considers small vacuoles (SV), derived through fusion and maturing of multivesicular bodies (MVBs) which in turn originate from the trans-Golgi network (TGN) as membrane carrier (reviewed in Viotti et al., 2013; Krüger and Schumacher, 2018; Cui et al., 2020). Certainly, rearrangement of the convoluted and constricted tonoplast in meristematic cells will provide some excessive membrane material for gradually expanding vacuoles (Figure 2), but this seems hardly sufficient for full expansion in elongated cells. Therefore, it must not only shed light upon the relationship

between vacuole expansion and cell wall properties, but also investigated how membrane material is delivered to the PM and the tonoplast during cell elongation. In addition, the spatiotemporal coordination of cell wall loosening and vacuole expansion with growing PM surface area remains to be addressed. Understanding the integration of all these processes and the sequential order of events will provide challenging future research tasks.

AUTHOR CONTRIBUTIONS

SK and DS wrote the manuscript and prepared the figures.

REFERENCES

- Barbez, E., Dünser, K., Gaidora, A., Lendl, T., and Busch, W. (2017). Auxin steers root cell expansion via apoplastic pH regulation in *Arabidopsis thaliana*. *Proc. Natl. Acad. Sci. U.S.A.* 114, E4884–E4893. doi: 10.1073/pnas.1613499114
- Blom, T., Somerharju, P., and Ikonen, E. (2011). Synthesis and biosynthetic trafficking of membrane lipids. *Cold Spring Harb. Perspect. Biol.* 3:a004713. doi: 10.1101/cshperspect.a004713
- Bolte, S., Brown, S., and Satiat-Jeuemaitre, B. (2004). The N-myristoylated Rab-GTPase m-Rabmc is involved in post-Golgi trafficking events to the lytic vacuole in plant cells. *J. Cell Sci.* 117(Pt 6), 943–954. doi: 10.1242/jcs.00920
- Cosgrove, D. J. (1993). How do plant cell walls extend? *Plant Physiol.* 102, 1–6. doi: 10.1104/pp.102.1.1
- Cosgrove, D. J. (2000). Expansive growth of plant cell walls. *Plant Physiol. Biochem. PPB* 38, 109–124. doi: 10.1016/s0981-9428(00)00164-9
- Cosgrove, D. J. (2018). Diffuse growth of plant cell walls. *Plant Physiol.* 176, 16–27. doi: 10.1104/pp.17.01541
- Cui, Y., Zhao, Q., Hu, S., and Jiang, L. (2020). Vacuole biogenesis in plants: how many vacuoles, how many models? *Trends Plant Sci.* (in press). doi: 10.1016/j.tplants.2020.01.008
- Deeks, M. J., Calcutt, J. R., Ingle, E. K. S., Hawkins, T. J., Chapman, S., Richardson, A. C., et al. (2012). A superfamily of actin-binding proteins at the actin-membrane nexus of higher plants. *Curr. Biol. CB* 22, 1595–1600. doi: 10.1016/j.cub.2012.06.041
- Dünser, K., Gupta, S., Herger, A., Feraru, M. I., Ringli, C., and Kleine-Vehn, J. (2019). Extracellular matrix sensing by FERONIA and Leucine-Rich Repeat Extensins controls vacuolar expansion during cellular elongation in *Arabidopsis thaliana*. *EMBO J.* 38:e100353. doi: 10.15252/embj.2018100353
- Dünser, K., and Kleine-Vehn, J. (2015). Differential growth regulation in plants—the acid growth balloon theory. *Curr. Opin. Plant Biol.* 28, 55–59. doi: 10.1016/j.pbi.2015.08.009
- Evans, M. L., Ishikawa, H., and Estelle, M. A. (1994). Responses of *Arabidopsis* roots to auxin studied with high temporal resolution: comparison of wild type and auxin-response mutants. *Planta* 194, 215–222. doi: 10.1007/BF00196390
- Fendrych, M., Leung, J., and Friml, J. (2016). TIR1/AFB-Aux/IAA auxin perception mediates rapid cell wall acidification and growth of *Arabidopsis hypocotyls*. *eLife* 5:e19048. doi: 10.7554/eLife.19048
- Gattolin, S., Sorieul, M., and Frigerio, L. (2010). Tonoplast intrinsic proteins and vacuolar identity. *Biochem. Soc. Trans.* 38, 769–773. doi: 10.1042/BST0380769
- Gattolin, S., Sorieul, M., Hunter, P. R., Khonsari, R. H., and Frigerio, L. (2009). In vivo imaging of the tonoplast intrinsic protein family in *Arabidopsis* roots. *BMC Plant Biol.* 9:133. doi: 10.1186/1471-2229-9-133
- Hager, A., Menzel, H., and Krauss, A. (1971). Versuche und Hypothese zur Primärwirkung des Auxins beim Streckungswachstum. *Planta* 100, 47–75. doi: 10.1007/BF00386886
- Halliday, K. J., Martínez-García, J. F., and Josse, E.-M. (2009). Integration of light and auxin signaling. *Cold Spring Harb. Perspect. Biol.* 1:a001586.
- Höfte, H. (2015). The yin and yang of cell wall integrity control: brassinosteroid and FERONIA signaling. *Plant Cell Physiol.* 56, 224–231. doi: 10.1093/pcp/pcu182
- Kaiser, S., Eisa, A., Kleine-Vehn, J., and Scheuring, D. (2019). NET4 modulates the compactness of vacuoles in *Arabidopsis thaliana*. *Int. J. Mol. Sci.* 20:4752. doi: 10.3390/ijms20194752
- Krüger, F., and Schumacher, K. (2018). Pumping up the volume - vacuole biogenesis in *Arabidopsis thaliana*. *Semin. Cell Dev. Biol.* 80, 106–112. doi: 10.1016/j.semcdb.2017.07.008
- Kutsuna, N., Kumagai, F., Sato, M. H., and Hasezawa, S. (2003). Three-dimensional reconstruction of tubular structure of vacuolar membrane throughout mitosis in living tobacco cells. *Plant Cell Physiol.* 44, 1045–1054. doi: 10.1093/pcp/pcg124
- Löfke, C., Dünser, K., Scheuring, D., and Kleine-Vehn, J. (2015). Auxin regulates SNARE-dependent vacuolar morphology restricting cell size. *eLife* 4:e05868. doi: 10.7554/eLife.05868
- Ludevid, D., Höfte, H., Himelblau, E., and Chrispeels, M. J. (1992). The expression pattern of the tonoplast intrinsic Protein gamma-TIP in *Arabidopsis thaliana* is correlated with cell enlargement. *Plant Physiol.* 100, 1633–1639. doi: 10.1104/pp.100.4.1633
- Marty, F. (1999). Plant vacuoles. *Plant Cell* 11, 587–600. doi: 10.1105/tpc.11.4.587
- McQueen-Mason, S., Durachko, D. M., and Cosgrove, D. J. (1992). Two endogenous proteins that induce cell wall extension in plants. *Plant Cell* 4, 1425–1433. doi: 10.1105/tpc.4.11.1425
- Owens, T., and Poole, R. J. (1979). Regulation of cytoplasmic and vacuolar volumes by plant cells in suspension culture. *Plant Physiol.* 64, 900–904. doi: 10.1104/pp.64.5.900
- Park, M., Lee, D., Lee, G.-J., and Hwang, I. (2005). AtRMR1 functions as a cargo receptor for protein trafficking to the protein storage vacuole. *J. Cell Biol.* 170, 757–767. doi: 10.1083/jcb.200504112
- Perrot-Rechenmann, C. (2010). Cellular responses to auxin: division versus expansion. *Cold Spring Harb. Perspect. Biol.* 2:a001446. doi: 10.1101/cshperspect.a001446
- Ranocha, P., Denancé, N., Vanholme, R., Freydis, A., Martínez, Y., Hoffmann, L., et al. (2010). Walls are thin 1 (WAT1), an *Arabidopsis* homolog of *Medicago truncatula* NODULIN21, is a tonoplast-localized protein required for secondary wall formation in fibers. *Plant J. Cell Mol. Biol.* 63, 469–483. doi: 10.1111/j.1365-3113X.2010.04256.x
- Ranocha, P., Dima, O., Nagy, R., Felten, J., Corratgé-Faillie, C., Novák, O., et al. (2013). *Arabidopsis* WAT1 is a vacuolar auxin transport facilitator required for auxin homeostasis. *Nat. Commun.* 4:2625. doi: 10.1038/ncomms3625
- Rayle, D. L., and Cleland, R. (1970). Enhancement of wall loosening and elongation by Acid solutions. *Plant Physiol.* 46, 250–253. doi: 10.1104/pp.46.2.250
- Richardson, S. C. W., Winistorfer, S. C., Poupon, V., Luzio, J. P., and Piper, R. C. (2004). Mammalian late vacuole protein sorting orthologues participate in early endosomal fusion and interact with the cytoskeleton. *Mol. Biol. Cell* 15, 1197–1210. doi: 10.1091/mbc.e03-06-0358
- Sanmartín, M., Ordóñez, A., Sohn, E. J., Robert, S., Sánchez-Serrano, J. J., Surpin, M. A., et al. (2007). Divergent functions of VTI12 and VTI11 in trafficking to storage and lytic vacuoles in *Arabidopsis*. *Proc. Natl. Acad. Sci. U.S.A.* 104, 3645–3650. doi: 10.1073/pnas.0611147104

FUNDING

This work was supported by grants to David Scheuring from the German Research Foundation (DFG; SCHE 1836/4-1) and the *BioComp* Research Initiative from the state Rhineland-Palatinate, Germany.

ACKNOWLEDGMENTS

We would like to thank Kai Dünser for critical reading of the manuscript. We apologize to researchers whose work could not be included in this manuscript due to space constraints.

- Scheuring, D., Löffke, C., Krüger, F., Kittelmann, M., Eisa, A., Hughes, L., et al. (2016). Actin-dependent vacuolar occupancy of the cell determines auxin-induced growth repression. *Proc. Natl. Acad. Sci. U.S.A.* 113, 452–457. doi: 10.1073/pnas.1517445113
- Scheuring, D., Schöller, M., Kleine-Vehn, J., and Löffke, C. (2015). Vacuolar staining methods in plant cells. *Methods Mol. Biol.* 1242, 83–92. doi: 10.1007/978-1-4939-1902-4_8
- Seguí-Simarro, J. M., and Staehelin, L. A. (2006). Cell cycle-dependent changes in Golgi stacks, vacuoles, clathrin-coated vesicles and multivesicular bodies in meristematic cells of *Arabidopsis thaliana*: a quantitative and spatial analysis. *Planta* 223, 223–236. doi: 10.1007/s00425-005-0082-2
- Shih, H.-W., Miller, N. D., Dai, C., Spalding, E. P., and Monshausen, G. B. (2014). The receptor-like kinase FERONIA is required for mechanical signal transduction in *Arabidopsis* seedlings. *Curr. Biol. CB* 24, 1887–1892. doi: 10.1016/j.cub.2014.06.064
- Silady, R. A., Ehrhardt, D. W., Jackson, K., Faulkner, C., Oparka, K., and Somerville, C. R. (2008). The GRV2/RME-8 protein of *Arabidopsis* functions in the late endocytic pathway and is required for vacuolar membrane flow. *Plant J. Cell Mol. Biol.* 53, 29–41. doi: 10.1111/j.1365-313X.2007.03314.x
- Takemoto, K., Ebine, K., Askani, J. C., Krüger, F., Gonzalez, Z. A., Ito, E., et al. (2018). Distinct sets of tethering complexes. SNARE complexes, and Rab GTPases mediate membrane fusion at the vacuole in *Arabidopsis*. *Proc. Natl. Acad. Sci. U.S.A.* 115, E2457–E2466. doi: 10.1073/pnas.1717839115
- Veytsman, B. A., and Cosgrove, D. J. (1998). A model of cell wall expansion based on thermodynamics of polymer networks. *Biophys. J.* 75, 2240–2250. doi: 10.1016/S0006-3495(98)77668-4
- Viotti, C., Krüger, F., Krebs, M., Neubert, C., Fink, F., Lupanga, U., et al. (2013). The endoplasmic reticulum is the main membrane source for biogenesis of the lytic vacuole in *Arabidopsis*. *Plant cell* 25, 3434–3449. doi: 10.1105/tpc.113.114827
- Zimmermann, U., Hüskens, D., and Schulze, E. D. (1980). Direct turgor pressure measurements in individual leaf cells of *Tradescantia virginiana*. *Planta* 149, 445–453. doi: 10.1007/BF00385746

Conflict of Interest: The authors declare that the research was conducted in the absence of any commercial or financial relationships that could be construed as a potential conflict of interest.

Copyright © 2020 Kaiser and Scheuring. This is an open-access article distributed under the terms of the Creative Commons Attribution License (CC BY). The use, distribution or reproduction in other forums is permitted, provided the original author(s) and the copyright owner(s) are credited and that the original publication in this journal is cited, in accordance with accepted academic practice. No use, distribution or reproduction is permitted which does not comply with these terms.